

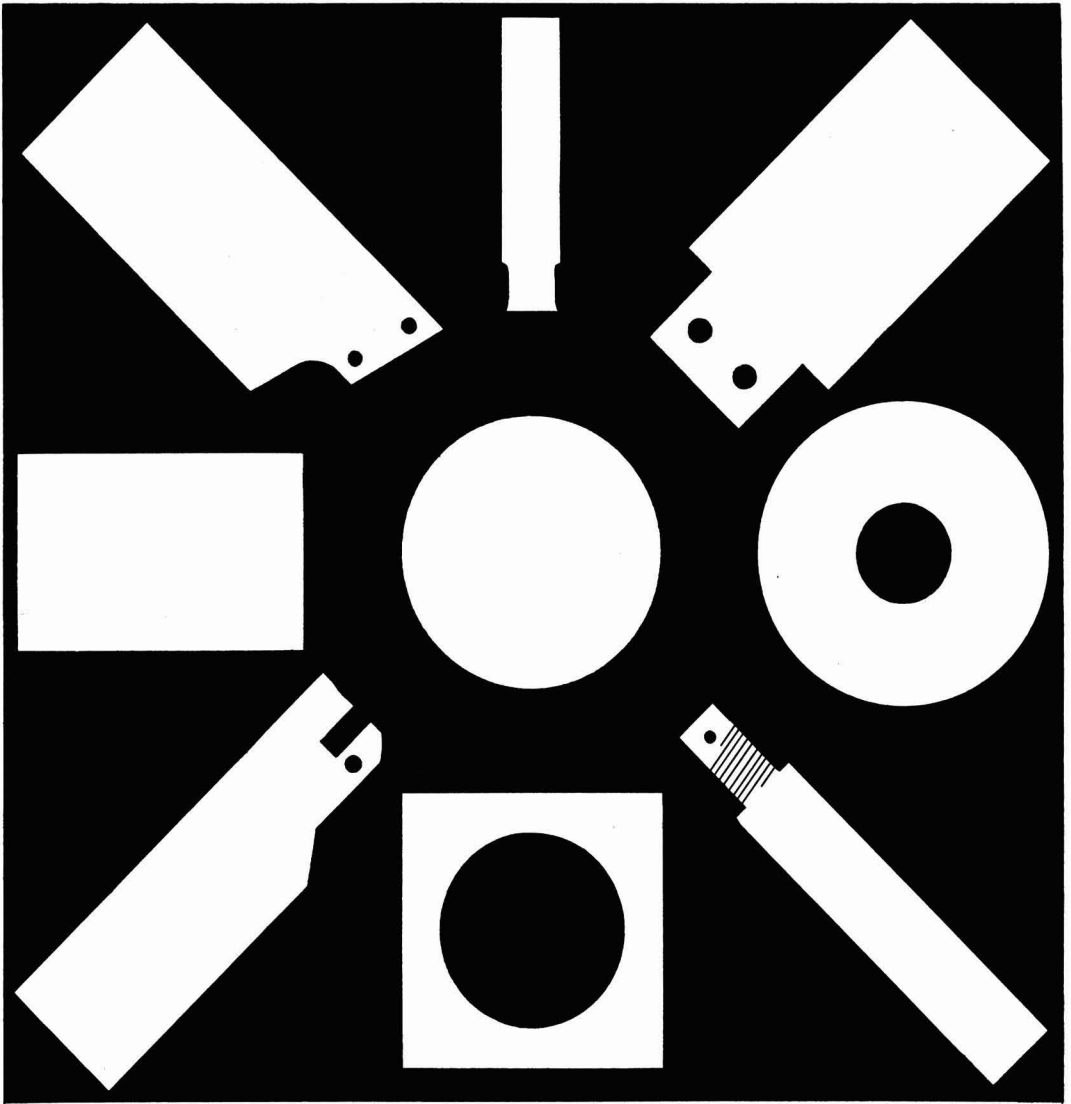
JOURNAL OF THE

Electrochemical Society

Vol. 112, No. 5

May 1965





GLC ANODES:

**delivering unmatched dependability to
chlor-alkali producers everywhere**

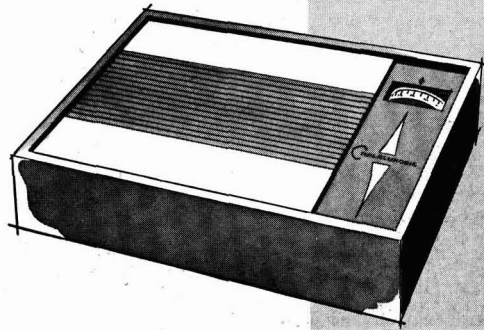


GREAT LAKES CARBON CORPORATION

18 East 48th Street • New York, N. Y. 10017
OFFICES AND AGENTS IN PRINCIPAL CITIES AROUND THE WORLD

*Great Lakes Carbon Corporation
is one of the world's largest
manufacturers of graphite for
electrochemical and electro-
thermic processes—and for
aerospace, nuclear, metallurgical
and other industrial uses.*

**IN EVERYTHING
FROM RADIOS
TO ROCKETS...**



WEBRIL[®]

NON-WOVEN FABRICS

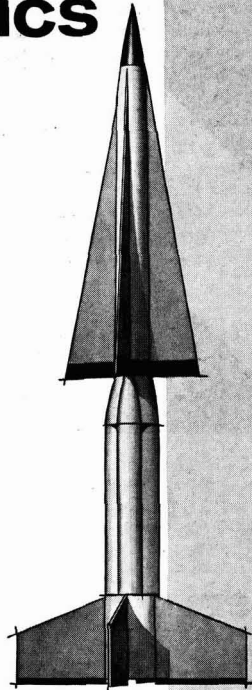
MAKE IDEAL SEPARATOR-ABSORBERS TO IMPROVE BATTERY PERFORMANCE

Both primary and secondary battery systems perform much more reliably because these remarkable fabrics can do the following:

- 1, Inhibit dendrite growth and passage.
- 2, Permit free ionic passage.
- 3, Remain unaffected by acid or alkali.
- 4, Minimize loss of active plate material.
- 5, Assure electrolyte contact with plates.

WEBRIL *non-woven* Fabrics have been performance-tested over millions of hours in mercury, silver-zinc, silver-cadmium, lead-acid, cuprous-chloride, and nickel-cadmium systems.

The unusually broad WEBRIL product line gives you greater design flexibility . . . even in fuel cells. You can choose from polypropylene, Dynel*, nylon, highly purified cotton, modified cellulose, and other fibers. Find out more today. Write to: ELECTRICAL SPECIALTIES DEPT.



KENDALL

THE KENDALL COMPANY, FIBER PRODUCTS DIVISION, WALPOLE, MASS. 02081

*Union Carbide Corp. trademark for its modacrylic fiber

MAY 1965

C. L. Faust, Chairman, Publication Committee
R. A. Kolbe, Manager of Publications

EDITORIAL STAFF

Cecil V. King, Editor
Norman Hackerman, Technical Editor
Ruth G. Sterns, Managing Editor
H. W. Salzberg, Book Review Editor
Daniel J. Immediato, Assistant Editor

DIVISIONAL EDITORS

W. C. Vosburgh, Battery
Paul C. Milner, Battery
G. A. Marsh, Corrosion
A. C. Makrides, Corrosion
Morris Cohen, Corrosion
Harry C. Gatos, Corrosion—Semiconductors
Newton Schwartz, Electric Insulation
Seymour Senderoff, Electrodeposition
Ephraim Banks, Electronics
Simon Larach, Electronics
Charles S. Peet, Jr., Electronics—Semiconductors
F. A. Trumbore, Electronics—Semiconductors
P. Wang, Electronics—Semiconductors
Sherlock Swann, Jr., Electro-Organic
Stanley Wawzonek, Electro-Organic
John M. Blocher, Jr., Electrothermics & Metallurgy
J. H. Westbrook, Electrothermics & Metallurgy
Scott Lynn, Industrial Electrolytic
C. W. Tobias, Theoretical Electrochemistry
A. J. deBethune, Theoretical Electrochemistry
R. M. Hurd, Theoretical Electrochemistry
M. W. Breiter, Theoretical Electrochemistry

ADVERTISING OFFICE

ECS

30 East 42 St., New York, N. Y., 10017

ECS OFFICERS

Lyle I. Gilbertson, President
207 Dogwood Lane,
Berkeley Heights, N. J.
E. B. Yeager, Vice-President
Western Reserve University,
Cleveland, Ohio
H. J. Read, Vice-President
Dept. of Metallurgy
Pennsylvania State University
University Park, Pa.
H. C. Gatos, Vice-President
Depts. of Met. & Electrical Engng.,
Massachusetts Institute of Technology,
Cambridge, Mass., 02139
R. A. Schaefer, Treasurer
The Electric Storage Battery Co.,
Yardley, Pa.
Ivor E. Campbell, Secretary
220 Gentry Rd.,
Coraopolis, Pa.
Ernest G. Enck, Executive Secretary
National Headquarters, The ECS,
30 East 42 St., New York, N. Y., 10017
Robert A. Kolbe, Assistant Executive Secretary
The ECS, 30 East 42 St., New York, N. Y., 10017

EDITORIAL

C. V. King
... 117C
Salty Waters

TECHNICAL PAPERS

J. A. Shropshire
... 465
The Catalysis of the Electrochemical Oxidation of
Formaldehyde and Methanol by Molybdates

K. E. Gubbins and
R. D. Walker, Jr.
... 469
The Solubility and Diffusivity of Oxygen in Electro-
lytic Solutions

D. Caplan and
M. Cohen
... 471
Scaling of Fe-26Cr Alloys at 870°-1200°C

J. P. Pemsler
... 477
Studies on the Oxygen Gradients in Oxidizing Met-
als, III. Kinetics of the Oxidation of Zirconium at
High Temperatures

F. Vratny and
D. J. Harrington
... 484
Tantalum Films Deposited by Asymmetric A-C
Sputtering

J. G. Rabatin and
G. R. Gillooly
... 489
Vapor Transport Reactions Related to Halophosphate
Phosphor Formation

A. Dreeben
... 493
Microstructures in CdS:Au Single Crystals

T. O. Sedgwick
... 496
Bourdon Gauge Determination of Chemical Equilib-
rium in the Ge-Cl₂ System

K. E. Haq
... 500
Deposition of Germanium Films by Sputtering

J. Klerer
... 503
On the Mechanism of the Deposition of Silica Py-
rolytic Decomposition of Silanes

B. D. Lichter and
M. A. Bredig
... 506
Solid and Liquid Phase Miscibility of Calcium
Metal and Calcium Fluoride

C. E. Price and
I. H. Warren
... 510
Some X-Ray and Thermoelectric Studies on Cubic
Th₃X₄ Compounds

ELECTROCHEMICAL SOCIETY

VOL. 112 • NO. 5

R. P. Frankenthal and H. W. Pickering
... 514
Some Considerations on the Use of Platinum Electrodes in Chloride Solutions

L. H. Jenkins and U. Bertocci
... 517
On the Equilibrium Properties of Single Crystalline Copper Electrodes

V. Markovac and B. Lovrecek
... 520
Studies of the Electrochemical Kinetics of Indium, II. System Indium + Indium Sulfate at Higher C.D.

TECHNICAL NOTES

R. L. Every
... 524
Preparation of Transition Metal Oxide-Metal Electrodes

R. Jasinski
... 526
Cobalt Phthalocyanine as a Fuel Cell Cathode

A. B. Kuper and E. H. Nicollian
... 528
Effect of Oxide Hydration on Surface Potential of Oxidized P-Type Silicon

D. O. Johnston and P. A. D. de Maine
... 530
The Minimum in Molar Conductance of CdCl_2 in Water-Methanol

S. Eisner
... 532
Observation of Active Areas in Thin Films of Palladium

BRIEF COMMUNICATIONS

S. Nielsen
... 534
Recrystallization of Thin Films of Germanium and Silicon

J. D. Filby and S. Nielsen
... 535
Low-Temperature Epitaxy of Silicon by Sublimation onto Thin Alloy Layers

J. B. Story and R. D. Wales
... 536
Microampere Multiple Constant Current Power Supply

CURRENT AFFAIRS

... 121C-126C

Manuscripts submitted to the Journal should be sent, in triplicate, to the Editorial Office at 30 East 42 St., New York, N. Y., 10017. They should conform to the revised instructions to Authors published on pp. 366-45C of the Mar. issue. Manuscripts so submitted become the property of The Electrochemical Society and may not be published elsewhere, in whole or in part, unless permission is requested of and granted by the Editor.

The Electrochemical Society does not maintain a supply of reprints of papers appearing in its Journal. A photoprint copy of any particular paper, however, may be obtained by corresponding direct with the Engineering Societies Library, 345 E. 47 St., New York, N. Y., 10017.

Inquiries re positive microfilm copies of volumes should be addressed to University Microfilms, Inc., 313 N. First St., Ann Arbor, Mich.

Walter J. Johnson, Inc., 111 Fifth Ave., New York, N. Y., 10003, have reprint rights to out-of-print volumes of the Journal, and also have available for sale back volumes and single issues, with the exception of the current calendar year. Anyone interested in securing back copies should correspond direct with them.



Published monthly by The Electrochemical Society, Inc., at 215 Canal St., Manchester, N. H.; Executive Offices, Editorial Office and Circulation Dept., and Advertising Office at 30 East 42 St., New York, N. Y., 10017, combining the JOURNAL and TRANSACTIONS OF THE ELECTROCHEMICAL SOCIETY. Statements and opinions given in articles and papers in the JOURNAL OF THE ELECTROCHEMICAL SOCIETY are those of the contributors, and The Electrochemical Society assumes no responsibility for them.

Claims for missing numbers will not be allowed if received more than 60 days from date of mailing plus time normally required for postal delivery of JOURNAL and claim. No claims allowed because of failure to notify the Circulation Dept., The Electrochemical Society, 30 East 42 St., New York, N. Y., 10017, of a change of address, or because copy is "missing from files." Subscription to members as part of membership service; subscription to non-members \$24.00 plus \$1.50 for postage outside U.S. and Canada. Single copies \$1.70 to members, \$2.25 to nonmembers. © 1965 by The Electrochemical Society, Inc. Entered as second-class matter at the Post Office at Manchester, N. H., under the act of August 24, 1912. Postage paid at Manchester, N. H.

Report from

**BELL
LABORATORIES**

SUPERCONDUCTING MAGNET FOR MASERS PROVIDES UNIFORM FIELD, ADJUSTABLE BANDWIDTH

For efficient operation, a low-noise traveling-wave maser needs a very low-temperature environment such as that of liquid helium (4.2°K) and a uniform magnetic field which determines the maser's operating frequency. These requirements suggest using a superconducting magnet for providing the field.

A compact maser amplifier based on this concept has been developed at Bell Laboratories. It incorporates an 8-pound superconducting magnet immersed in liquid helium, replacing an earlier

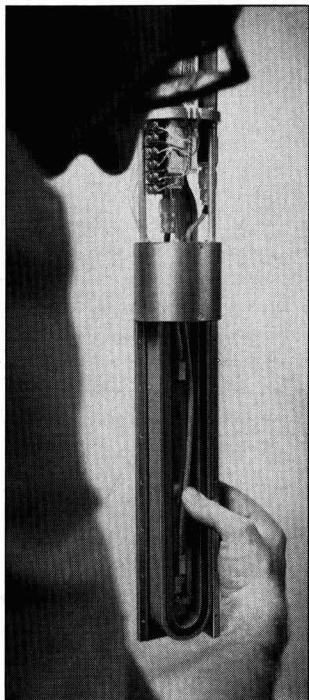
500-pound Alnico magnet mounted outside the dewar. This maser also provides the desirable feature of an adjustable bandwidth of amplification.

As shown in the illustrations, the uniform field is obtained with a superconducting solenoid enclosed in a close-fitting box of high-permeability iron. Adjustable bandwidth is obtained with an auxiliary superconducting trimmer coil which overlays one half the solenoid cross section. This coil modifies the main field, creating two discrete and individually uni-

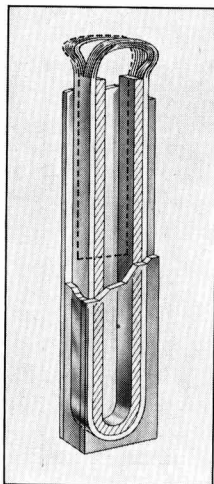
form field regions. Changing the current in the coil adjusts the "step" between the two fields and thereby changes the bandwidth.

The two fields are each uniform to one part per thousand near 3300 gauss, and the maser bandwidth can be adjusted smoothly from 14 to 55mc centered at an operating frequency near 4170mc.

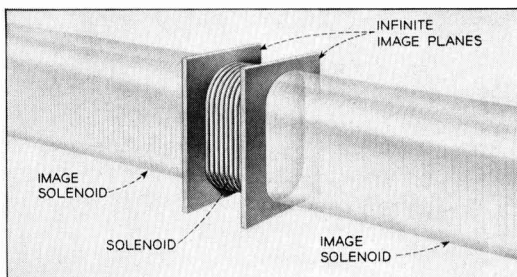
At the broadest band, its gain is 34db with an effective noise temperature of 5°K. The maser has demonstrated stable low-noise performance in a variety of satellite communications experiments.



New maser magnet (left) has front and left side of enclosure removed to expose superconducting solenoid. Drawing (center) corresponds to photograph and shows solenoid inside box enclosure. Solenoid is wound on U-shaped nonmagnetic form and is spread apart at top to permit insertion of the maser. Dotted line indicates position of trimmer coil. Drawing at right indicates how front and rear plates of enclosure act as "image planes." These high-permeability plates are made to appear very large by the magnetic return paths provided by the sides of the box. The resulting magnetic field approximates the ideal uniform field of a solenoid of infinite length.



Bell Telephone Laboratories
Research and Development Unit of the Bell System





Salty Waters

WE should all be aware of the governmental program for obtaining potable water from salt and brackish water. Does it hold great promise for the future, or is it just another way for Washington to redistribute the national wealth?

In 1952 Congress authorized the Department of the Interior to use \$2 million over a five-year period to study methods of desalting water, and the Office of Saline Water (OSW) was set up to administer the program. In 2 or 3 years it was evident that there was no easy breakthrough to cheap desalted water, and the program and the funds were extended upwards. As we know, when a small temporary government program is set up, it is very likely to become permanent, ever-expanding, and more costly. For 1966 some \$29 million is requested for OSW with an expected expenditure of \$200 million during the next 5 years. When water is desalted on a truly large scale, as it surely will be eventually, will it pay for itself or will it be government-subsidized?

Large-scale distillation plants could even now supply fresh water for the personal needs of the inhabitants of large cities, at not unreasonable expense, provided salt water could be distributed for other uses. Many industrial plants could get by with careful planning and re-use of the purified water. There seems no possibility in the near future at least, of using desalted water for crop irrigation except on the smallest scale, as for greenhouse and hydroponics projects. We can then envisage new cities built in near-desert regions, with limited industry and most food imported from areas with more rainfall.

It is becoming apparent that economy could be achieved by combining large-scale nuclear power production with water desalination. Endless political problems arise: private industry will shy away from the desalting program, fight tooth-and-nail against government power production in such plants. Because of such squabbles the Hanford plutonium project was never able to use its own heat for power production.

Fresh water can be made by freezing, too, since salts are not incorporated in the ice crystals. A most intriguing variation of the freezing method, and probably more economical, is the *clathrate* method. Ice is less dense than water due to the directional fixing of hydrogen bonds throughout the crystals. An open structure results, with cavities large enough to accommodate certain molecules such as those of propane and isobutane. In the presence of a "help gas" the crystal may be slightly modified and stabilized, with cavities of two sizes all or partly occupied by the larger and smaller "guest" molecules. For example, water, carbon tetrachloride, and xenon form a triple clathrate which can be a solid at 13°C and normal pressure. Sea water salts are excluded, although the crystals must be washed to remove adhering salt water. Recovery of pure water from the organic solvents is not difficult; the liquids are hardly miscible.

For the near future, except for special localities, our greatest development in the use of water will lie in improved impounding and distribution of rain water, and in the protection of usable waters from pollution. When desalinated water is added regularly to public water supplies, we trust that someone will remember to add suitable minerals to protect the users from "Diener's disease." There is a story, true or not, that European laboratory servants suffered mineral deficiencies from years of drinking only distilled water.

—CVK



Important books in the electrochemical field for your reference table. Examine them now, on approval.

DOUBLE LAYER AND ELECTRODE KINETICS

Edited by PAUL DELAHAY. The only book in English that covers in detail the fundamentals of the electrical double layer and electrode kinetics, and shows in detail the correlation between these two areas.

CONTENTS: PART I: THE ELECTRICAL DOUBLE LAYER. Thermodynamics of the Ideal Polarized Electrode. Structure of the diffuse double layer in the absence of specific adsorption. Structure of the double layer with specific adsorption. Adsorption at an ideal polarized electrode. The electrical double layer

for other systems than the Mercury—Aqueous solution interface. PART II: ELECTRODE KINETICS. Kinetics of simple electrode processes without specific adsorption or chemisorption. Kinetics of electrode processes involving more than one step. Correlation between electrode kinetics and double layer structure in the absence of significant specific adsorption of reactants and products. Kinetics of electrode processes with potential—dependent adsorption of reactants and/or products. 1965. Approx. 320 pages. Prob. \$14.00

ADVANCES IN ELECTROCHEMISTRY AND ELECTROCHEMICAL ENGINEERING, VOL. 3: ELECTROCHEMISTRY

Edited by PAUL DELAHAY. The latest volume in the Interscience Series edited by Paul Delahay and Charles W. Tobias. The series gives authoritative reviews of electrochemical phenomena and bridges the gap between electrochemistry and electrochemical engineering. **CONTENTS:** The interface between interface electrolyte solutions and the gas phase.

Thermogalvanic cells. Metal deposition and electrocrystallization. Anodic films. Hydrogen overvoltage and adsorption phenomena. 1963. 397 pages. \$15.00. Vol. 1: Electrochemistry. 1961. 348 pages. \$12.00. Vol. 2: Electrochemical Engineering. 1962. 300 pages. \$12.00

ALTERNATING CURRENT POLAROGRAPHY AND TENSAMMETRY

By B. BREYER and H. H. BAUER. Vol. 13 of the Interscience Chemical Analysis Series. Here is the first comprehensive, detailed account of the subject. The book acquaints the reader with the essentials of new techniques that can be applied usefully in both analytical work and the study of electrochemical processes.

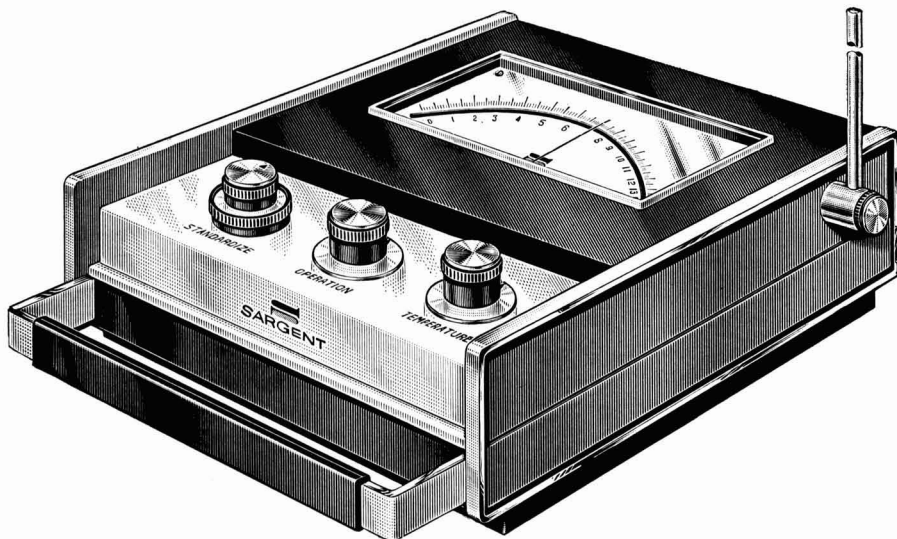
CONTENTS: Classes of Polarographic procedures. Electrodes in alternating current polarography. Development of Tensammetry. Recti-

fying properties of electron-transfer reactions. Electrodes and electrode processes. The A. C. Polarographic wave. Rectification effects. Tensammetry. Instrumentation for analytical purposes. Specialized instrumentation. Analytical applications—methodology. A. C. polarography of organic compounds. Tensammetric investigation of non-reducible substances. Elucidation of electrode processes. 1963. 288 pages. \$12.00

JOHN WILEY & SONS, INC.

605 THIRD AVENUE, NEW YORK, N. Y. 10016

A new concept in pH meters ...



Interchangeable power supplies for laboratory and field.

Accuracy and stability found heretofore only in the highest-priced meters.

Rugged construction for use in any environment under field conditions.

SARGENT

■ **Relative Accuracy** ■ for the most exacting purposes, readable to 0.02 pH, with meter accuracy of ± 0.03 pH within 4 pH of the standardized point, and ± 0.05 pH anywhere on the scale.

MODEL PB—with modular mercury cell power source providing over 6 months of normal usage in the field.

MODEL PL—with modular Zener reference line power source for continuous use in the laboratory.

■ **Stability** ■ for long term use without need for readjustment, eminently suitable for recording, with circuit drift less than 0.02 pH per hour after short initial warm-up.

■ **Rugged Construction** ■ for use in any locale, any climate; moisture-proofed, transistorized circuitry, shock-proof case.

MODEL PB Cat. No. S-30007 with batteries, buffers and electrodes . . . \$255.00

Cat. No. S-30007-10 with batteries only, for use with any electrodes . . . \$215.00

MODEL PL Cat. No. S-30008 with line power source, buffers and electrodes . . . \$295.00

Cat. No. S-30008-10 with line power source only, for use with any electrodes . . . \$255.00

Power Supplies Cat. No. S-30007-15 Zener Line Source for substitution in Model PB meters . . . \$60.00

Cat. No. S-30008-15 Mercury Cell Source for substitution in Model PL meters . . . \$20.00

For complete information write for bulletin pHP.



SARGENT®

SCIENTIFIC LABORATORY INSTRUMENTS • APPARATUS • SUPPLIES • CHEMICALS

E. H. SARGENT & CO., 4647 W. Foster Ave., Chicago, Ill. • Anaheim, Calif. • Birmingham • Dallas • Denver • Detroit • Springfield, N. J. • Toronto, Canada

Stackpole Anodes *last longer...* **COST LESS**

Stackpole GraphAnodes[®] have "long life" built-in. Controlled manufacturing insures structural uniformity. Careful inspection of anode surfaces assures perfect cell alignment. Such care produces anodes that wear evenly, last longer and produce less cell contamination. Special Stackpole impregnants lengthen diaphragm life and reduce cell maintenance.

GraphAnodes are supplied with holes, slots, threads, bevels, and other features to meet individual needs. For those doing their own finishing, unmachined anodes within commercial tolerances can be supplied.

Whether you have diaphragm cells or mercury cells, Stackpole offers the shapes you require in a wide range of strength, porosity and resistance characteristics. For more information on how long-lasting, economical Stackpole GraphAnodes can cut costs for you, write: Stackpole Carbon Company, Carbon Division, St. Marys, Pa. Phone: 814-834-1521 TWX: 814-826-4808.



STACKPOLE
CARBON DIVISION



The Catalysis of the Electrochemical Oxidation of Formaldehyde and Methanol by Molybdates

J. A. Shropshire

Process Research Division, Esso Research and Engineering Company, Linden, New Jersey

ABSTRACT

The electrooxidation of formaldehyde and methanol on platinum has been shown to be catalyzed in sulfuric acid solution by the presence of molybdates. Decreased polarization has been shown to result from a cycle involving chemical reaction of the fuels with an oxidized molybdate species with subsequent electrooxidation of the reduced molybdate. The process requires the adsorption of molybdate at the electrode surface throughout the entire cycle.

The existence of catalytic currents during the electrochemical reaction of a variety of substances is well known (1). Catalytic currents in general arise when the product of an electrochemical reaction reacts with another species in solution in a subsequent chemical step, thus to regenerate the original form. The net observed result is an increase in the effective concentration of the electroactive species near the electrode and a corresponding increase in the observed current due to its reaction. In many cases this unique feature has been found useful in improving the polarographic determination of trace constituents in solution (1, 2).

An interesting variation of this principle has been investigated in the course of a recent study of the electrochemical oxidation of low molecular weight alcohol and aldehyde fuels for fuel cell use. This variation involves the catalytic reaction of HCHO or CH₃OH with a molybdate species at a platinum black electrode in H₂SO₄. In this case the molybdate species apparently is adsorbed and remains adsorbed at the electrode surface during both the electrochemical and chemical reaction steps.

This "surface redox" reaction, as it will be referred to hereafter, has been of particular interest in fuel cell studies on HCHO and CH₃OH. Through its use the electrochemical oxidation of these fuels to CO₂ may be carried out at a considerable decrease in polarization over that normally found on platinum based electrodes. A series of studies has been carried out to define the advantages and limitations of this system and to determine if in fact a catalytic mechanism is responsible for the observed improvements.

Experimental Techniques and Equipment

All electrochemical measurements in these systems were carried out in conventional glass "H" cells with anode and cathode compartments separated by glass frits. Voltage measurements were made against commercial saturated calomel reference electrodes through Luggin capillaries containing H₂SO₄ of concentration equal to that in the cell proper. All measurements were made using Keithley 610 A or 610 electrometers. Acid solutions were prepared from reagent grade 96% H₂SO₄ and deionized water of conductivity < 10⁻⁶ mho/cm. Due to the practical necessity of high conductivity for fuel cell electrolytes, studies were carried out in 3.7M H₂SO₄, a solution exhibiting near-optimum conductivity. Absolute methanol and sodium molybdate were reagent grade chemicals. Formaldehyde was obtained as USP Formaldehyde solution (37% in water with a small amount of CH₃OH added for stabilization). Due to the higher reducing activity of HCHO no effect of the added CH₃OH was ever observed.

Electrodes used in this study were of two types. For performance studies (polarization-log current) of CH₃OH and HCHO in molybdate-containing electro-

lytes, the electrodes were prepared by pressing powdered platinum black into platinum screens. The platinum, prepared by the reduction of H₂PtCl₆ by NaBH₄ in aqueous solution, was found to have high surface area and to provide high activity for this purpose. In the chronopotentiometric studies on this system, small platinized platinum electrodes of about 0.25 cm² apparent area were used.

In one phase of this study oscilloscopic chronopotentiograms were obtained on the 0.25 cm² platinized electrode. Constant current for these transients was obtained from a 30v regulated d-c supply through a high series resistance. Transients were displayed on a Tektronix 545 A oscilloscope with type-D plug-in preamplifier and photographed with the aid of a Dumont type-453 A Polaroid attachment. Potentiostatic studies, where indicated, were carried out using the Duffers Model 600 potentiostat. Other pertinent experimental details will be found in the text where necessary. All polarizations in this study are referred to a hydrogen electrode in the same acid solution (NHE) or to the saturated calomel electrode (SCE), measured difference in these reference voltages being 0.194v at 25°C in the systems involved.

Oxidation of CH₃OH and HCHO on Pt in the Presence of Molybdate

The electrochemical oxidation of CH₃OH or HCHO on platinum black in strong acid media is a highly irreversible process. Passage of practical currents with either fuel is accompanied by polarizations up to 0.6v from the thermodynamically calculated potentials. Both fuels react at about the same potential level on platinum despite a computed difference of about 0.14v in theoretical potential ($E^{\circ}_{25}\text{CH}_3\text{OH} = +0.03\text{v}$, $E^{\circ}_{25}\text{HCHO} (\text{g}) = -0.11\text{v}$ vs. NHE). This behavior has led to widespread belief that oxidation of both fuels involves a common slow step. The product of the oxidation of either fuel in acid has been shown by several investigators to result in essentially 100% production of CO₂ at steady state (3-5). Typical measured performances of 1M CH₃OH and 1M HCHO on NaBH₄-reduced platinum black in 3.7M H₂SO₄ at 82°C are shown in Fig. 1. Tafel slopes of about 0.06 v/decade are commonly found for oxidation of these fuels on platinum catalysts.

The addition of Na₂MoO₄ to the electrolyte before fuel addition results in a significant alteration of the performance curves (Fig. 1). The polarization at low current densities decreases by as much as 0.3v from that observed with platinum alone. Furthermore, the similarity of HCHO and CH₃OH performance largely disappears with HCHO in this system capable of sustaining currents 100 times as great as CH₃OH at the improved voltage. Also, neither fuel shows evidence of a well-defined Tafel behavior. Instead, the low polarization region exhibits a limiting current, beyond

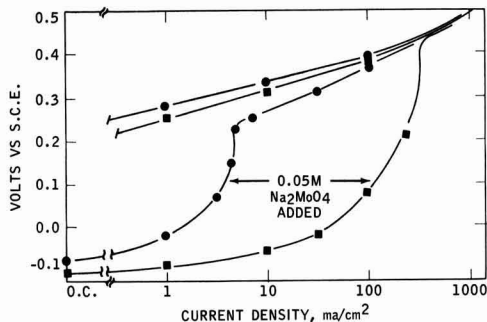


Fig. 1. Effect of Na_2MoO_4 on oxidation of CH_3OH and HCHO on Pt black (NaBH_4 reduced); $3.7\text{M H}_2\text{SO}_4$, 82°C ; \bullet , $1\text{M CH}_3\text{OH}$; \blacksquare , 1M HCHO .

which polarization increases in both cases approximately to the level of the original platinum system. It was found that, if current was decreased following severe polarization of the system, the voltage followed the behavior found on platinum black in the absence of molybdate. This hysteresis was not evident until the limiting current of the initial plateau was exceeded. Thereafter, anodization of the electrode in fresh electrolyte without fuel was necessary to restore activity. It is significant to note that decreased polarization requires that the molybdate be added before the fuel is present. This point will be discussed in a later section.

An activation energy was obtained for the electrode reaction using 0.05M molybdate and 1M HCHO fuel at $+0.10\text{v}$ vs. SCE using potentiostatic control. This voltage level lies in the region of the curve near the initial reaction limit, but not yet in a region where the normal reaction of HCHO on platinum black would be expected (see Fig. 1). Currents were measured at constant voltage in the temperature range $25^\circ\text{--}90^\circ\text{C}$. The activation energy (Fig. 2) was about 11.4 kcal/mole , much too high to be indicative of a mass transport limitation.

Chemical Reaction of Molybdate with CH_3OH and HCHO

With these early indications of catalytic currents, it was discovered with some surprise that the chemical reaction between molybdate and these hydrocarbon fuels required a catalyst. It was found that with no catalyst present no significant reaction occurred between molybdate and CH_3OH or HCHO in $3.7\text{M H}_2\text{SO}_4$. In the presence of platinum, however, reaction appeared to occur readily with the formation of a product which colored the strong acid solution red-brown. The molybdate equivalent in the reaction with CH_3OH was determined by monitoring the CO_2 production during the complete reaction of 0.025 moles of Na_2MoO_4 with CH_3OH in the presence of 0.42g of Pt black powder (82°C , $3.7\text{M H}_2\text{SO}_4$). The CO_2 produced from the reaction was carried by a fixed flow of nitrogen to the absorption cell of a Liston-Becker Model 15A IR analyzer calibrated at a fixed wavelength for CO_2 analysis. The continuous record of CO_2 production versus reaction time is reproduced in Fig. 3. The peak CO_2 production corresponds roughly to a current of 14 ma/cm^2 on the type of electrode discussed previously. Although this value is undoubtedly subject to some error caused by lag in the nitrogen carry-over system, it indicates a rough rate to be expected from the initial system. Integration of the entire CO_2 production vs. time curve was used to establish the moles of molybdate required to produce 1 mole of CO_2 . This value was found to be about six, indicating

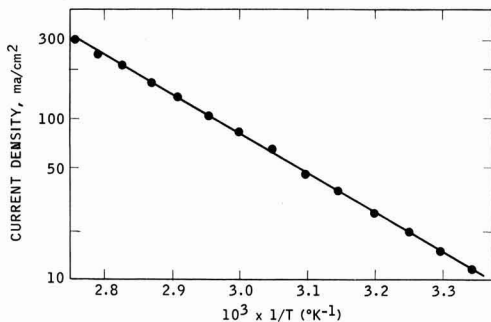


Fig. 2. Effect of temperature on reaction of HCHO on Pt black in presence of Na_2MoO_4 , 1M HCHO ; $0.05\text{M Na}_2\text{MoO}_4$; $3.7\text{M H}_2\text{SO}_4$; $E = 0.1\text{v}$ vs. SCE; $\Delta E^\ddagger = 11.4\text{ kcal/mole}$.

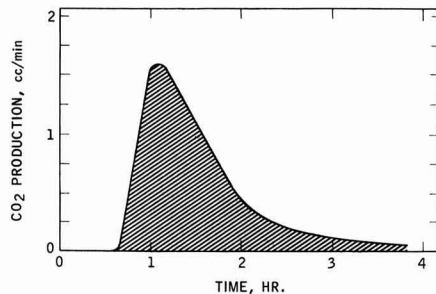


Fig. 3. Chemical reaction of CH_3OH with Na_2MoO_4 in presence of Pt black. $1\text{M CH}_3\text{OH}$, 82°C ; initial $\text{Na}_2\text{MoO}_4 = 0.025$ mole; 0.42g Pt black catalyst; total $\text{CO}_2 = 0.0045$ mole.

a valence change of one for the reacting molybdate, in view of the six electron oxidation of CH_3OH to CO_2 .

Although a similar complete curve was not recorded and analyzed for the reaction of molybdate with HCHO , the peak CO_2 production at the start of that reaction corresponded to about one half the value found for CH_3OH . In view of the greater reducing power of HCHO , this observation would seem inconsistent. An explanation of this result will be reserved to a later section.

Coulometry

As mentioned earlier, the product of the molybdate chemical reaction with fuel in $3.7\text{M H}_2\text{SO}_4$ forms a red-brown solution. It was found that solutions identical in appearance were formed by electroreduction of an acid solution containing Na_2MoO_4 at a platinum electrode at 0.0 vs. SCE. (This voltage is about 0.2v negative to $E_{1/2}$ recorded in Fig. 4.) Since the chemical equivalent of molybdate to CH_3OH determined in the previous section would be wrong if CO_2 were not the sole product in the chemical reaction, an independent test of the valence change was made. Two coulometric determinations were carried out for reduction of the molybdate in $3.7\text{M H}_2\text{SO}_4$ to equilibrium on a platinum basket held at 0.0v vs. SCE. This voltage level was fixed by means of a potentiostat and current vs. time recorded from the voltage drop across a fixed precision resistor in the auxiliary electrode lead. Auxiliary electrode was segregated using an agar plug to minimize bulk mixing of the electrolyte compartments. The data obtained leaves no doubt that a one electron reduction of the molybdate takes place.

Run	Coulombs calc. for 1 electron	Coulombs observed
1	571	573
2	398	390

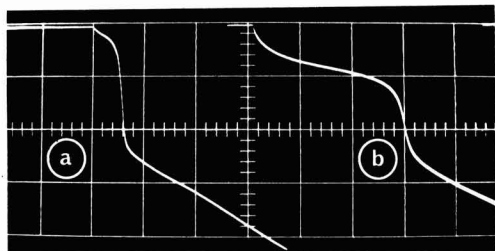


Fig. 4. Chronopotentiograms on platinumized Pt in (a) 3.7M H_2SO_4 ; (b) 3.7M H_2SO_4 -0.05M Na_2MoO_4 . Top line, 0.0v vs. SCE, 300 mv/div (positive downward), 1 sec/div (left to right), 40 ma/cm², 25°C.

An attempt was made to confirm the equivalence value in run No. 1 by complete reoxidation of the reduced molybdate at potentials up to +0.8v vs. SCE. Such attempts were completely unsuccessful, however, resulting in very low current production over long periods of time. It appears that the pentavalent species is combined in solution in some relatively inert form, and reoxidation currents are limited by a slow release of the electroactive species.

Chronopotentiometry on Platinumized Platinum

A typical anodic chronopotentiogram for a platinumized platinum micro-electrode (0.25 cm² apparent area) in 3.7M H_2SO_4 -0.05M Na_2MoO_4 at 25°C is shown in Fig. 4b. The electrode was polarized to 0.0v vs. SCE immediately prior to recording the voltage transient produced by impressing a constant current of 40 ma/cm² on the electrode. Under the conditions observed here, a well-defined wave is formed, with $E_{1/2} \approx 0.2\text{v}$ vs. SCE (one-quarter wave). Formation of platinum oxide is evident when the voltage reaches +0.7v vs. SCE.

Since it was apparent that the over-all reaction of CH_3OH and molybdate involved other than a free molybdate species in solution, an attempt was made to use this well-defined transient to study the factors involved in molybdate adsorption on platinumized platinum. Information on both molybdate and formaldehyde adsorption was obtained at 25°C by the anodic stripping technique originally used by Pavela (6). In this method, the preconditioned electrode was placed in the solution of adsorbate for a desired interval, removed rapidly to a 3.7M H_2SO_4 rinse solution to remove excess bulk solution, then placed in a cell containing 3.7M H_2SO_4 and the (anodic) stripping transient recorded. While this technique suffers the drawback of permitting determination of only the material strongly adsorbed, it nonetheless allows the separation of the independent factors in molybdate and fuel adsorption.

The 0.25 cm² platinumized electrode used for this study was preconditioned by evolving H_2 and O_2 successively

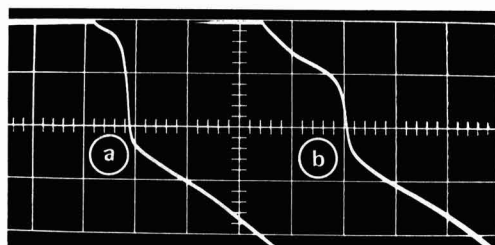


Fig. 5. Chronopotentiograms on platinumized platinum in 3.7M H_2SO_4 (a) blank; (b) following 2-min dip in 0.05M Na_2MoO_4 -3.7M H_2SO_4 and subsequent rinse in 3.7M H_2SO_4 . Coordinates and conditions as in Fig. 4.

a few times (in H_2SO_4 solution) with final equilibration at 0.0v vs. SCE before removal to adsorbate solutions. Adsorbate solutions referred to in the following paragraphs are 1M HCHO in 3.7M H_2SO_4 and 0.05M Na_2MoO_4 in 3.7M H_2SO_4 in all cases not otherwise noted. Anodic transients, with the exception of Fig. 9, were recorded in pure 3.7M H_2SO_4 .

It was found that a second immersion of this platinumized electrode in 3.7M H_2SO_4 -0.05M Na_2MoO_4 with no fuel present was sufficient to produce a tenaciously held layer of molybdate, yielding about 40 millicoulombs/cm² in the subsequent anodic stripping, Fig. 5b. The blank transient, also shown in Fig. 5a, clearly shows the initial regions of pseudocapacitance from oxidation of chemisorbed hydrogen atoms, the steep so-called double layer region, followed by platinum oxide formation at more positive voltages. By comparison, the electrode with adsorbed molybdate retained much of the initial pseudocapacitance of oxidation of adsorbed hydrogen, indicating that the adsorbed molybdate is not seriously blocking hydrogen sites. This single chemisorbed layer of molybdate was found to be sufficient to produce steady-state performance in a subsequent test with HCHO fuel, in 3.7M H_2SO_4 , provided excessive polarization was avoided.

Immersion of the platinumized electrode in 3.7M H_2SO_4 -1M HCHO with no molybdate results in the rapid formation of a layer of tightly bound HCHO with an oxidation transient as shown in Fig. 6. Oxidation of this strongly held HCHO appears to occur only at or near voltages at which platinum oxidation occurs. Note the marked decrease in double layer capacity in the presence of this adsorbed HCHO , as evidenced by the very steep rise of voltage between 0.0 and +0.3v vs. SCE compared to the blank in Fig. 6. Absence of hydrogen pseudo-capacitance is taken as an indication that formaldehyde occupies the majority of the surface, including sites normally held by adsorbed hydrogen atoms. While HCHO was used as the fuel in this and subsequent studies of transients on platinum, the observations made apply in a general way to CH_3OH as well. Due to a stronger adsorption of HCHO , however, effects with that fuel are somewhat more pronounced and therefore have been used to illustrate the behavior.

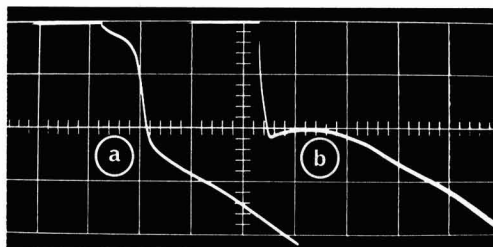


Fig. 6. Chronopotentiograms on platinumized platinum in 3.7M H_2SO_4 (a) blank; (b) after 2-min dip in 1M HCHO -3.7M H_2SO_4 and rinse. Coordinates and conditions as in Fig. 4.

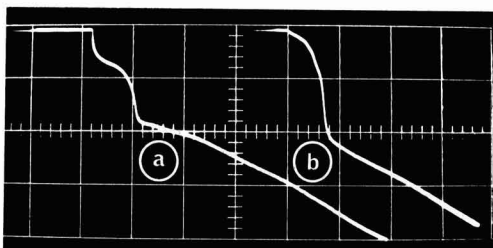


Fig. 7. Chronopotentiograms on platinumized platinum in 3.7M H_2SO_4 (a) after 2-min dip in acid-molybdate solution, rinse, 2-min dip in acid-formaldehyde solution and rinse; (b) first subsequent transient on same electrode.

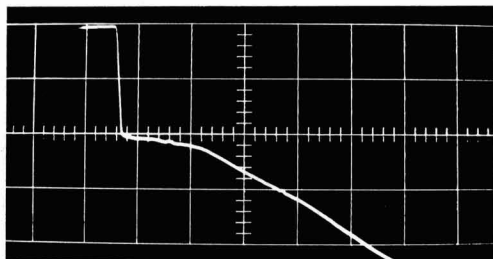


Fig. 8. Chronopotentiogram on platinumized platinum in 3.7M H_2SO_4 following 2-min dip in acid-formaldehyde solution, rinse, 2-min dip in acid-molybdate solution, rinse. Coordinates and conditions as in Fig. 4.

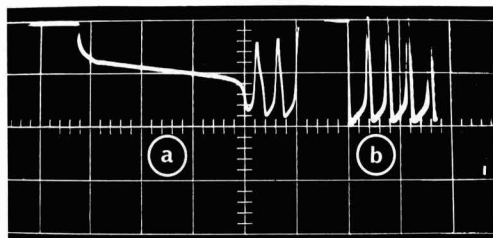


Fig. 9. Chronopotentiograms on platinumized platinum in 1M HCHO-3.7M H_2SO_4 (a) after 2-min dip in acid-molybdate and rinse (3.7M H_2SO_4); (b) first subsequent transient on same electrode. Coordinates as in Fig. 4 except 2 sec/div (left to right).

If the electrode is immersed in molybdate solution, rinsed, and then immersed in formaldehyde, both components occupy the surface simultaneously as evidenced by the presence of both characteristic waves in the transient of Fig. 7a. The quantity of molybdate adsorbed appears to be only slightly less than that adsorbed in the previous case of Fig. 5, and absence of adsorbed hydrogen pseudocapacitance makes it seem probable that the strongly adsorbed formaldehyde is present on the hydrogen-type sites not occupied by molybdate.

It is important to recognize in this sequence that the molybdate oxidation wave is not catalytically enhanced through interaction with the HCHO that is strongly adsorbed on the surface. This is evidenced by the fact that the adsorbed HCHO remains on the surface until electrooxidized (Fig. 7a). As shown in Fig. 7b, however, a single anodic transient here serves to eliminate essentially all molybdate as well as formaldehyde.

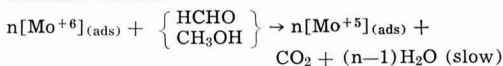
If the electrode is treated in the reverse order (i.e., contacted with HCHO first) no chemisorbed molybdate is found on the electrode (Fig. 8). The preadsorbed HCHO layer is apparently completely impervious to replacement by molybdate. (This is not completely true in the case of CH_3OH .) Thus, once the formaldehyde layer is formed at the platinum surface in a formaldehyde-containing solution, the electrode must be removed to a plain acid solution and adsorbed HCHO anodized off before the electrode once more is active for molybdate adsorption.

In contrast, anodic stripping of the preadsorbed molybdate layer in the presence of the 1M HCHO- H_2SO_4 solution at 25°C results in a sevenfold increase in transition time before voltage increases to the oscillatory level characteristic of constant current oxidation of HCHO on platinum in these solutions at 25°C (4, 7). This catalytic enhancement of the molybdate oxidation wave is shown in the transient of Fig. 9a. The second transient, Fig. 9b, shows no trace of remaining molybdate, only the oscillating trace of HCHO electrooxidation.

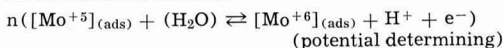
Proposed Mechanism

Based on the foregoing observations, the Pt-molybdate-HCHO (CH_3OH) interaction in H_2SO_4 would seem best summarized as follows:

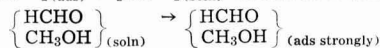
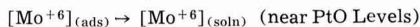
Chemical reaction:



Electrochemical reaction:



Irreversible failure (to normal Pt levels)



Thus, this reaction differs from a normal catalytic current-producing reaction in that the active intermediate must be fixed at the surface in order to be effective. This characteristic has given rise to the designation "surface redox" or "immobilized redox."

In this scheme no pretense of knowledge is made as to the exact nature of the adsorbed molybdate species. Based on the decrease in transition times for coadsorbed HCHO, however, it appears that strongly held molybdate occupies less than half the electrode surface, primarily those sites not involved in the (most anodic) hydrogen atom adsorption. Fuel on the other hand, especially HCHO, is capable of occupying the entire surface, blocking molybdate adsorption.

Based on the lack of Tafel behavior and dissimilarity of CH_3OH and HCHO performance, the slow step in this catalytic mechanism would seem to arise in some phase of the chemical reaction. Recalling that strongly adsorbed HCHO does not appear to react with adsorbed molybdate, it would seem that the observed rates are determined by the chemical reaction of adsorbed molybdate and nonadsorbed fuel. The high (limiting) activation energy is in accord with this reasoning. In this connection, adsorbed fuel refers to that fuel strongly chemisorbed and does not eliminate the possibility that a weaker, perhaps physical, state of adsorption exists for reactive fuel molecules. Mass transport considerations are eliminated by the fact that the molybdate can be fixed at the electrode, and HCHO (CH_3OH) diffusion is capable of supporting much higher currents (as shown by the subsequent reaction on Pt alone). The difference in performance, then, of HCHO and CH_3OH reflects the true difference in reducing power toward molybdate in the chemical step. If the Nernst equation can be assumed to apply to the surface species involved here, it would appear that Mo^{+5} concentration on the surface is very high during this reaction. Thus, for example, in order to operate at 0.0v vs. SCE with $E_{1/2} = 0.2\text{v}$, a Nernst ratio for $\text{Mo}^{+5}/\text{Mo}^{+6}$ of over 1000 would be required.

It would seem possible, since all molybdate is removed during anodization in the presence of fuel solutions, that the irreversible failure step might involve complexing surface molybdate with a product formed during the direct electrooxidation of HCHO (CH_3OH). Alternatively the adsorbed molybdate layer may be forced off by formation of platinum oxides as the potential moves in a positive direction. In any event, once molybdate is lost from the surface, rapid and essentially irreversible replacement by the organic molecule occurs. Thus, as pointed out in a previous section, the sequence of contacting the electrode with molybdate and fuel becomes all important.

The proposed mechanism makes it apparent that the chemical reaction rate observed between fuel and molybdate need have no relation to the electrochemical rates which may be achieved in the "surface redox" process. Thus, the observed chemical reaction requires the desorption of reduced (pentavalent) molybdate in order to perpetuate the reaction, while

the electrochemical cycle does not. If this desorption process is slow, or re-adsorption of fuel in preference to molybdate occurs, the rates may differ widely. Thus, as pointed out previously, the low apparent chemical rate for reaction of HCHO with molybdate is not inconsistent with the mechanism, but indicates high coverage of the surface with formaldehyde and the inability of molybdate to replace it at a reasonable rate. In the case of CH₃OH this displacement does occur more readily and higher apparent rates are observed.

Summary

The use of molybdates as cocatalysts in the complete oxidation of HCHO and CH₃OH on platinum in acid electrolyte can result in a higher efficiency of this reaction. This improvement has been shown to arise from the catalytic chemical reaction of the fuel with an adsorbed (oxidized) molybdate species with subsequent electrooxidation of its reduced form. To remain operative the molybdate species must remain adsorbed at the electrode surface. Molybdate is lost from the surface under conditions of excessive polarization where HCHO is directly electrooxidized and performance subsequently is characteristic of the levels found with platinum alone. Strong adsorption of fuel under these operating conditions makes the failure irreversible.

The molybdate-fuel-platinum interaction outlined here is probably of little interest for a practical fuel cell system since HCHO is not at present a practical fuel and current densities for CH₃OH reaction are too low to be of interest. The surface redox concept, however, may have broad implications in the search for new fuel cell catalysts. Thus, other compounds may

exist which would undergo this same type of redox reaction with fuel and whose adsorption at the electrode interface is not irreversible in the sense described above.

Acknowledgments

The work reported in this paper was made possible by the support of the Advanced Research Projects Agency under Order No. 247 through the U.S. Army Electronics Laboratories (Contract No. DA 36-039 SC-89156). Permission to publish is gratefully acknowledged. The author wishes to thank H. E. Frew for carrying out much of the experimental work.

Manuscript received Oct. 30, 1964. This paper was presented at the Washington Meeting, Oct. 11-15, 1964.

Any discussion of this paper will appear in a Discussion Section to be published in the December 1965 JOURNAL.

REFERENCES

1. P. Delahay, "New Instrumental Methods in Electrochemistry," p. 100, Interscience Publishers, New York (1954).
2. I. M. Kolthoff and J. J. Lingane, "Polarography," 2nd. ed., Vol. I, Chap. XV, Interscience Publishers, New York (1952).
3. H. Krupp, H. Rabenhorst, G. Sandstede, and G. Walter, *This Journal*, **109**, 553 (1962).
4. B. L. Tarmy, *et al.*, Report No. 1, Contract DA 36-039 SC-89156, Esso Research and Engineering Co., 1 Jan. 1962-30 June 1962.
5. M. J. Schlatter, Preprint of the Div. of Petroleum Chemistry, ACS 6 B-149 (1961).
6. T. O. Pavela, *Ann. Acad. Sci. Fennicae, Ser. A*, **2**, 59 (1954).
7. R. P. Buck and L. R. Griffith, *This Journal*, **109**, 1005 (1962).

The Solubility and Diffusivity of Oxygen in Electrolytic Solutions

Keith E. Gubbins and Robert D. Walker, Jr.

Department of Chemical Engineering, University of Florida, Gainesville, Florida

ABSTRACT

Measurements of the solubility of oxygen in sulfuric acid, phosphoric acid, and potassium hydroxide are reported, together with values of the diffusivity of oxygen in potassium hydroxide solutions at 25°C. It is shown that for the electrolyte concentrations commonly employed in fuel cells the solubility and diffusivity of oxygen may each be reduced to as little as 2% of their corresponding values for pure water.

It seems probable that in some cases the current obtainable from fuel cells is limited by diffusion of the reacting gas through the liquid (electrolyte) phase to active sites on the surface of the electrode. Under these conditions it follows from Fick's law that the limiting current that may be drawn from a given electrode will depend on the concentration of the gas in the bulk electrolyte and on its diffusivity. In order to enable calculations concerning the performance of such electrodes to be made experimental measurements of solubilities and diffusivities of oxygen in fuel cell electrolytes have been carried out.

Experimental

Solubility.—Gas chromatography was used to determine the solubilities; a diagram of the apparatus is shown in Fig. 1. A sample of electrolyte was equilibrated with oxygen in a constant temperature bath controlled to $\pm 0.1^\circ\text{C}$. A sample of known volume was withdrawn by means of a syringe and injected into a glass gas stripping cell. This cell contained a medium porosity glass frit and had a volume of about 7 ml; it was also equipped with an injection point consisting of a rubber serum cap. The sample size used was 5 ml. Helium carrier gas passed through the reference side of the thermal conductivity detector and into the sam-

ple cell; dissolved gases were rapidly and completely removed from solution by the dispersed carrier gas, and the gas mixture passed through drying tubes before entering the molecular sieve column. Since there was only one component to be analyzed the separating column was not really necessary; however it was included as an experimental convenience in providing a

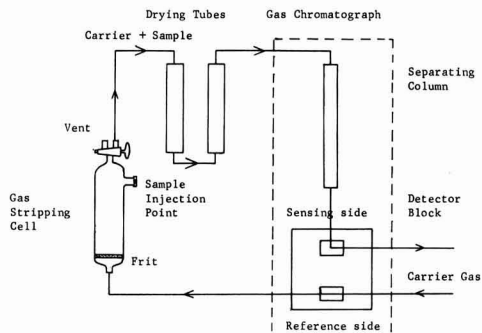


Fig. 1. Apparatus for measurement of solubility

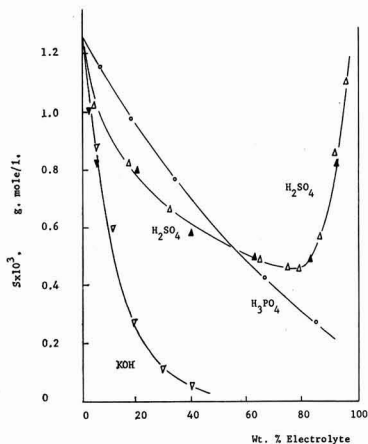


Fig. 2. Solubility of O_2 at $25^\circ C$: \circ , experimental results for H_3PO_4 ; Δ , experimental results for H_2SO_4 ; ∇ , experimental results for KOH; \blacktriangle , results of Bohr for H_2SO_4 (corrected to 1 atm assuming Henry's law); \blacktriangledown , results of Geffcken for KOH.

suitable time interval between sample injection and the arrival of the peak. The peaks obtained by this method were somewhat broader than normal, but there was no excessive "tailing." The gas chromatograph was calibrated for oxygen by injecting a sample of pure water saturated with oxygen at $25^\circ C$. The solubility in this case has been accurately determined by chemical methods.

Diffusivity.—The diffusivity of oxygen in potassium hydroxide solutions was obtained by a polarographic method involving measurement of the limiting current during the reduction of the oxygen to hydrogen peroxide at the dropping mercury electrode. The apparatus was similar to that used by Lingane and Laitinen (7). A well-defined limiting current region was observed over the voltage range -0.2 to -1.0 v vs. a saturated calomel electrode; this wave corresponds to reduction of oxygen to hydrogen peroxide. The second oxygen wave, corresponding to the reduction of hydrogen peroxide to hydroxyl ion, was less well-defined; in addition the mass flow rate and drop-time vary fairly rapidly with change in voltage in this region. The diffusivity (D) was therefore calculated from measurements made on the first wave, using the modified Ilkovic equation (8, 11)

$$i_d = 607 n D^{1/2} C m^{2/3} t^{1/6} \left(1 + \frac{A D^{1/2} t^{1/6}}{m^{1/3}} \right)$$

where A is a constant; n the number of electrons in-

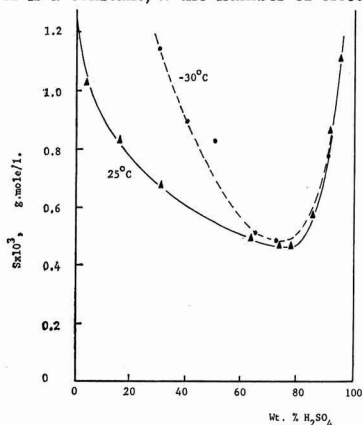


Fig. 3. Solubility of O_2 in H_2SO_4 at 25° and $-30^\circ C$

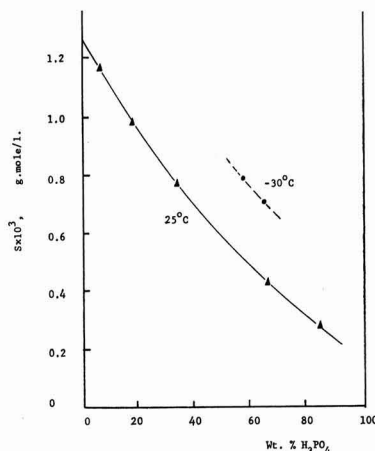


Fig. 4. Solubility of O_2 in H_3PO_4 at 25° and $-30^\circ C$

involved in reaction = 2; i_d the limiting diffusion current, μa ; C the concentration of oxygen, millimoles/liter; m the mass flow rate of mercury electrode, mg/sec; t the drop time of mercury electrode, sec.

The limiting current depends on both the solubility and the diffusivity. However, since the solubility was known from independent measurements, the diffusivity could be calculated from measurements of the limiting current. Different workers have given somewhat different values for the constant A . Strehlow and von Stackelberg (11) predicted the value 17 theoretically and claimed that this value was supported experimentally; Lingane and Loveridge (8) predicted a value of 39 from theory and found values of 31.7 and 33.5 by experiment. Meites and Meites (9) give the value of 31.5. Since experimental evidence supports the higher values for A (5) the value 31.5 given by Meites and Meites was used. Under normal experimental conditions the value obtained for D is not highly sensitive to changes in the value of A ; thus changing the value of A from 31.5 to 39 produces a change in the value of D obtained of only about 4%. Jordan (4) has used polarography to determine the diffusivity of oxygen in glycerol-water mixtures and aqueous sucrose solutions

Results

Solubility.—The solubility of oxygen in sulfuric acid, phosphoric acid, and potassium hydroxide solutions has been determined. The results for $25^\circ C$ are shown in Fig. 2. The solubility values plotted are gram moles of oxygen per liter for a solution equilibrated with oxygen gas at 1 atm pressure (i.e., excluding water vapor pressure). The reproducibility of these results was of the order $\pm 2\%$.

Figure 2 shows that the solubility of oxygen falls off rapidly and continuously with increasing concentration of potassium hydroxide or phosphoric acid. The solubility in sulfuric acid solutions shows a pronounced minimum at about 75 w/o (weight per cent) H_2SO_4 , however. Bohr (1) has reported data for the solubility of air in sulfuric acid at $21^\circ C$; these data also show a minimum solubility in the range 70-80% H_2SO_4 , and the values are in good general agreement with those shown in Fig. 2. Geffcken (2) has presented data on the solubility of oxygen in dilute solutions of potassium hydroxide (up to $2N$); these results are in quite good agreement with those shown in Fig. 2.

Figure 3 compares solubilities in sulfuric acid at -30° with values at $25^\circ C$; at concentrations less than about 35% or greater than 90%, solid freezes out of solution at $-30^\circ C$. Figure 4 shows the solubility in phosphoric acid at -30° compared with values at $25^\circ C$. Some additional experimental difficulties occurred at low temperatures owing to the high viscosity of the

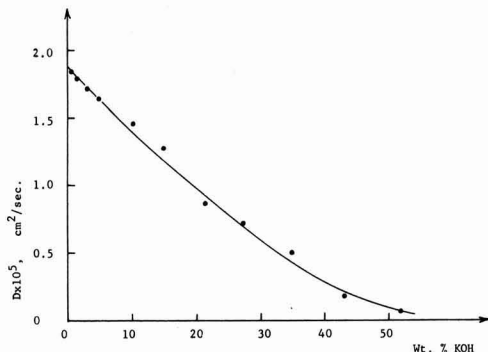


Fig. 5. Oxygen diffusivity in KOH at 25°C

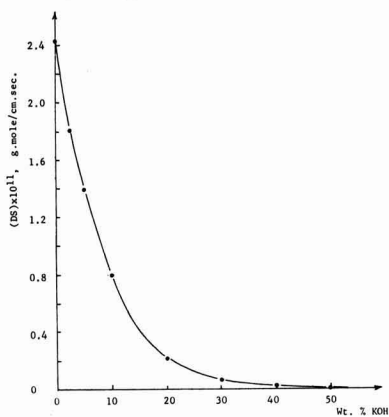


Fig. 6. Rate of diffusion, KOH at 25°C

solutions; this caused difficulty in saturating the solution with the gas and in transferring solution by means of a syringe.

Diffusivity.—Figure 5 presents diffusivity values for oxygen in potassium hydroxide at 25°C. Extrapolation of the curve back to zero concentration gives a value of 1.90×10^{-5} cm²/sec for the diffusivity of oxygen in water at 25°C. This is in good agreement with values determined by other workers (3); thus Kreuzer (6) gives 1.90×10^{-5} , Semerano (10) gives 1.87×10^{-5} , and Jordan (4) gives 2.12×10^{-5} . Taking into consider-

ation the uncertainty in the value of constant *A*, and experimental errors in the measurement of the variables in the Ilkovic equation, it is estimated that the maximum error of the diffusivity values reported is about $\pm 6\%$.

Discussion

Figures 2 and 5 indicate that both the solubility and diffusivity of oxygen in potassium hydroxide decrease rapidly with increase in concentration. The rate of mass transport of dissolved oxygen to an electrode is proportional to the product of the diffusivity and the solubility. Figure 6 shows this product for potassium hydroxide at 25°C. From this figure it is seen that for a 35% KOH electrolyte the oxygen mass transport rate is less than 2% of that obtainable in pure water. Calculations of the current expected from a mass transport-limited fuel cell in which data for pure water are assumed will therefore give current values that are much too high.

Acknowledgments

The authors wish to express their appreciation to the Harry Diamond Laboratories, U. S. Army Materiel Command, for sponsoring the work reported here. The encouragement and suggestions of Mr. Nathan Kaplan of the Harry Diamond Laboratories, and the assistance of co-workers in this laboratory are also gratefully acknowledged.

Manuscript received Nov. 9, 1964; revised manuscript received Jan. 16, 1965. This paper was presented at the Washington Meeting, Oct. 11-15, 1964.

Any discussion of this paper will appear in a Discussion Section to be published in the December 1965 JOURNAL.

REFERENCES

1. C. Bohr, *Z. Physik. Chem.*, **71**, 47 (1910).
2. G. Geffcken, *ibid.*, **49**, 17 (1904).
3. D. M. Himmelblau, "Diffusion of Gases in Aqueous Solutions," Final Report, March 1, 1963, University of Texas, Austin, Texas.
4. J. Jordan, E. Ackerman, and R. L. Berger, *J. Am. Chem. Soc.*, **78**, 2979 (1956).
5. I. M. Kolthoff and J. J. Lingane, "Polarography," Vol. 1, 75, Interscience Publishers, Inc., New York (1952).
6. F. Kreuzer, *Helv. Physiol. et Pharmacol. Acta*, **8**, 505 (1950).
7. J. J. Lingane and H. A. Laitinen, *Ind. Eng. Chem., Anal. Ed.*, **11**, 504 (1939).
8. J. J. Lingane and B. A. Loveridge, *J. Am. Chem. Soc.*, **72**, 438 (1950).
9. L. Meites and T. Meites, *ibid.*, **73**, 395 (1951).
10. G. Semerano, L. Riccoboni, and A. Foffani, *Gazz. Chim. Ital.*, **79**, 395 (1949).
11. H. Strehlow and M. von Stackelberg, *Z. Elektrochem.*, **54**, 51 (1950).

Scaling of Fe-26Cr Alloys at 870°-1200°C

D. Caplan and M. Cohen

Division of Applied Chemistry, National Research Council, Ottawa, Ontario, Canada

ABSTRACT

The oxide layers formed on Fe-26Cr alloy are wrinkled, porous, and blistered, and the metal/oxide interface markedly roughened. This is interpreted as evidence that compressive stresses are generated continuously in the growing oxide, hence that anion diffusion participates in the growth process. Smooth oxidation curves are observed if the wrinkled scale is adherent, even though non-uniform. However, when blistering and cracking occurs, as with electropolished specimens, the weight-gain/time curves are irregular. Similar irregularities occur with Fe-26Cr-0.5 Si, Fe-26Cr-1Mn, type 446 and pure Cr. Manganese decreases oxidation resistance.

An earlier publication (1) described the oxidation of Cr at 980°, 1090°, and 1200°C. In this paper the oxidation of an Fe-26Cr alloy is examined under the same experimental conditions in a continuing program to investigate the physical nature and mechanism of growth of protective oxide scales. Also included are some experiments with Fe-26Cr containing additions of Mn or Si and with a 26% Cr commercial alloy.

The literature on the oxidation of Fe-Cr alloys has been reviewed recently by Seybolt (2, 3), Kubaschewski and Hopkins (4), Lai *et al.* (5), and most extensively by Wood (6). It is evident that a large effort has gone into investigating this system, but the accumulated information is in many cases contradictory and poorly reproducible. A wide range of scaling rates and a variety of oxide phases is observed. The reviewers

Table I. Composition of specimen materials (weight per cent, w/o)

	Fe-Cr	Fe-Cr-Si	Fe-Cr-Mn	Type 446
C	0.022	0.022	0.012	0.18
Mn	0.003	0.004	1.00	0.75
Si	0.02	0.55	0.01	0.86
Ni	0.02	0.02	0.02	0.32
Cr	26.2	26.2	25.7	25.9

see two main causes. One is the complexity created by experimental variations including alloy composition, impurities, specimen shape, specimen preparation, atmosphere, and procedure in carrying out the oxidation runs. The other is mechanical and structural: pores, blisters, cracks and plastic flow due to stress, local attack and non-uniform scales, phase changes caused by selective oxidation and loss of adhesion are superimposed on the scaling process and obscure the effect of the variables being investigated.

The particular object of the present work was to compare the results to the scaling of unalloyed Cr already carried out and thus disentangle the effects of composition variations in metal and oxide. Further, it was hoped to reduce confusion by using a high-purity Fe-26Cr alloy, oxidizing in purified oxygen, and giving considerable attention to surface preparation and experimental procedure. Since the only oxide formed on Fe-26Cr is Cr₂O₃ containing a small amount of Fe₂O₃ in solution, oxidation behavior similar to that of Cr metal is to be expected; spinel does not form unless surface metal were to become depleted below 13% Cr (2).

As will be seen, clarification was achieved only in part. The structural-mechanical factors are an intrinsic part of Cr alloy scaling and cannot be eliminated. Metallographic cross sections demonstrated their nature and permitted an interpretation of their origins.

Experimental

A high-purity, vacuum-melted Fe-26Cr alloy was used for most of the work. In addition, two similar alloys containing 0.5% Si or 1% Mn and a 26% Cr type 446 commercial steel were oxidized at 1090° only. Table I shows the composition of the four specimen materials. Rectangular specimens 1.1 x 0.5 x 4 cm were machined from 1.3 cm diam rolled rods. A few runs were made with cylindrical specimens 0.6 cm diam x 4 cm long and sheet specimens 1.1 x 0.035 x 5 cm, machined or rolled from the same rods.

The specimens were smoothed by abrading through 600 grit SiC paper and a 10 μ layer of metal electropolished off in glacial acetic-70% perchloric acid (20 to 1) to remove surface contamination. They were then annealed for structural stability at 1100°C in purified argon at 20 Torr and electropolished to remove a further 10 μ layer of metal. The second polish removed the Cr-depleted surface layer caused by preferential evaporation of Cr and any contaminant that formed during annealing; a precipitate of Cr carbide that apparently nucleated at the surface during cooling also was removed. Some specimens were not annealed, in which case the second electropolish was omitted. After electropolishing, the specimens were either rinsed in water and methanol and blotted dry or immediately etched for 15 sec in 1.38N HF (7), or in deoxygenated 4N HCl for 45 sec with the specimen polarized cathodically at 10 μ A/cm² (1).

The oxidation runs were carried out at 870°, 980°, 1090°, and 1200°C in a vertical tube furnace in flowing oxygen from which CO₂ and moisture had been removed (1). Details of the experiments are included in Table II. For experiments in wet oxygen the gas was saturated with moisture at 25°C corresponding to a P_{H₂O} of 24 Torr. Weight increase was recorded continuously on an automatic balance. The open-insertion method was used in which the cold prepared specimen is lowered quickly into the hot reaction tube with oxygen flowing. Specimens required 0.5-3 min to reach temperature depending on cross section, and weight recording began at about 0.5 min. It is of prime importance to make an accurate estimate of the specimen weight at zero time. This differs from its weight in still air at room temperature by a factor involving convection, buoyant force, a piston effect, and a magnetic correction. It cannot be predicted and may take as long as 5 min to reach a steady state. The weight recording is most uncertain at the very beginning when, unfortunately, the weight is changing most rapidly. Satisfactory correction factors, accurate to 0.01 mg/cm², could be obtained from facsimile experiments with nonoxidizing specimens and by other means (1). Different correction factors were obtained if the specimen hung inside a Cr₂O₃ baffle crucible which was sometimes used at the higher temperatures to minimize volatilization of Cr oxide (1, 8).

After removal from the furnace the specimens were observed microscopically as they cooled under argon

Table II. Summary of oxidation runs

Run	Alloy	Temp, °C	Surface prep.	Time, hr	Oxidation curves		Early waves in curves	
					Fig. No.	Plotting symbol	Time of breaks, hr	Wt gain at breaks, mg/cm ²
1	Fe-26Cr	870	Etch	97	1a	—	—	—
2	Fe-26Cr	980	Etch	29	1a	—	—	—
3	Fe-26Cr	980	Etch	50	1a	○	—	—
4	Fe-26Cr	980	Etch	93	1a	○	—	—
5	Fe-26Cr	980	Etch	94	1a	●	—	—
6	Fe-26Cr	1090	Etch	0.4	1a	—	—	—
7	Fe-26Cr	1090	Etch	23	1a	—	—	—
8	Fe-26Cr	1090	Etch	100	1a	—	—	—
9	Fe-26Cr	1090	Etch	100	1a, 9a	—	—	—
10	Fe-26Cr	1090	Etch	136	1a	—	—	—
11	Fe-26Cr	1200	Etch	70	1a	—	—	—
12	Fe-26Cr	980	E.P.	4	1b	—	—	—
13	Fe-26Cr	980	E.P.	4	1b	—	0.8, 2.0	0.2, 0.4
14	Fe-26Cr	980	E.P.	23	1b	—	1.2, 1.7	0.3, 0.4
15	Fe-26Cr	980	E.P.	24	1b	—	1.7, 3.1	0.3, 0.7
16	Fe-26Cr	1090	E.P.	0.4	1b	—	0.2	0.4
17	Fe-26Cr	1090	E.P.	20	1b	—	0.2, 0.6	0.3, 0.7
18	Fe-26Cr	1090	E.P.	64	1b	—	0.3, 0.6	0.4, 0.7
19	Fe-26Cr	1090	E.P.	100	1b, 9b	—	0.2, 0.6	0.4, 0.8
20	Fe-26Cr	1200	E.P.	0.6	1b	—	0.2, 0.4	0.9, 1.6
	Cr	980	Etch	99	1a	—	—	—
	Cr	1090	Etch	100	1a, 9a	—	—	—
	Cr	1200	Etch	42	1a	—	—	—
	Cr	980	E.P.	96	1b	—	—	—
	Cr	1090	E.P.	21	1b, 9b	—	—	—
	Cr	1200	E.P.	1.2	1b	—	—	—
21	Fe-26Cr-0.5Si	1090	Etch	363	9a	—	—	—
22	Fe-26Cr-1Mn	1090	Etch	20	9a	—	—	—
23	446	1090	Etch	166	9a	—	—	—
24	Fe-26Cr-0.5Si	1090	E.P.	92	9b	—	—	—
25	Fe-26Cr-1Mn	1090	E.P.	20	9b	—	—	—
26	446	1090	E.P.	191	9b	—	—	—
Runs in wet oxygen								
27	Fe-26Cr	980	Etch	43	—	—	—	—
28	Fe-26Cr	980	E.P.	24	—	—	1.2, 3.7	0.3, 0.6
29	Fe-26Cr	1090	Etch	140	—	—	—	—

and then examined by x-ray diffraction, chemical analysis, and metallographically in cross section.

Results

Figure 1(a) summarizes the oxidation data for 11 etched Fe-26Cr specimens in 1 atm dry oxygen at 870°, 980°, 1090°, and 1200°C, and Fig. 1(b) the data for 9 electropolished specimens at 980°, 1090°, and 1200°C. The dashed lines are the oxidation curves for pure Cr metal at 980°, 1090°, and 1200°, etched or electropolished, repeated from an earlier publication (1).

Comparison of Fig. 1(a) and 1(b) shows that electropolished Fe-26Cr oxidized more rapidly than the etched alloy. [Cr had shown the same E.P. effect to an even greater degree (1). The etched alloy oxidizes as fast or faster than Cr; after electropolishing, Cr oxidizes faster than the alloy.] The etched specimens yield smooth oxidation curves but those of electropolished specimens all show irregularities near the beginning of the runs as evident in the sub-plot inset in Fig. 1(b). Usually, two such early waves occur between 0.2 and 2 hr. In general, the weight gain before the breaks increases and the time at which they occur decreases with increasing temperature (last two columns of Table II).

Scale structure on etched Fe-26Cr.—Figures 2 to 5 show the structure of the scale formed on the etched Fe-26Cr alloy. The outer surface is wrinkled and the metal surface very roughened, sometimes scalloped in high-crested waves; e.g., compare Fig. 3(c) or 4(d) with the smooth metal as prepared for oxidation [Fig. 2(b)]. The oxide layer is blistered and porous and contains islands of metal [Fig. 3(b), 3(c), and

5(b)] that give the appearance of having been dragged from the metal surface. [The thin scale formed at 870° (Fig. 2) has developed only some of these characteristics and that at 1200° (Fig. 5) is incomplete, much of it having spalled during cooling after the run.] The rugged metal/oxide interface cannot be the result of local or intergranular attack since the oxide is too thin in the metal troughs in relation to the trough depth; it is often thicker over the metal projections instead of where least metal remains. A related phenomenon is shown in Fig. 5: at temperatures and run durations great enough to develop thick scale, the edges of

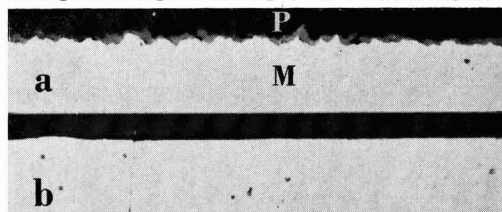


Fig. 2. Metallographic cross section of etched Fe-26Cr alloy oxidized for 97 hr at 870° (curve 1). P is mounting plastic; M is metal. Photograph (b) is a cross section of the etched alloy as prepared for scaling to show the contrast in roughness of the metal surface before and after scaling. Magnification 800X.

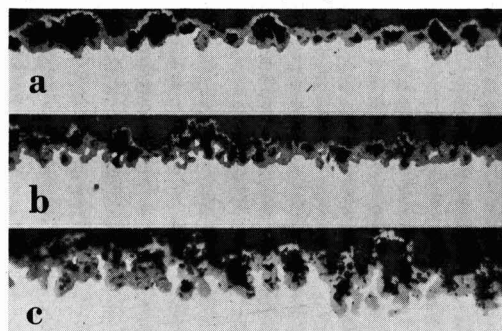


Fig. 3. Section through etched Fe-26Cr oxidized for 94 hr at 980° (curve 5). (a) and (b) magnification 400X; (c), Magnification 800X.

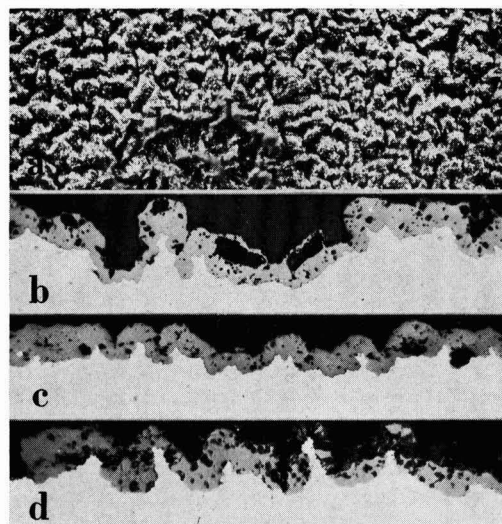


Fig. 4. Etched Fe-26Cr oxidized at 1090°. (a) Outer surface of oxide after 100 hr run (curve 9); (b) cross section after 136 hr (run 10); (c) and (d) cross section after 100 hr (run 8). Fragmentation and some porosity in (d) is artifact. Magnification: (a), 80X; (b) and (c), 400X; (d), 600X.

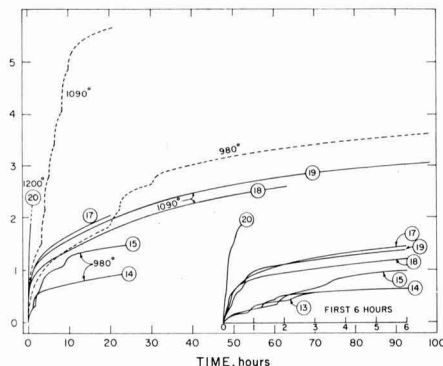
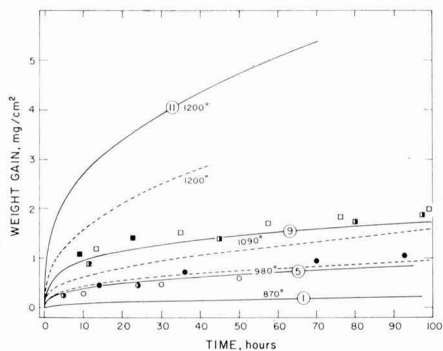


Fig. 1. Oxidation of Fe-26Cr alloy in 1 atm dry oxygen. Fig. 1a. Etched. Curves, 1, 5, 9, and 11 are at 870°, 980°, 1090°, and 1200°C, respectively; symbols half dark circle, open circle, and dark circle represent duplicate runs 2, 3, and 4 at 980°; symbols dark box, half dark box and, open box represent duplicate runs 7, 8, and 10 at 1090°. Fig. 1b. Electropolished. Runs 13, 14, and 15 at 980°; 17, 18, and 19 at 1090°; run 20 at 1200°. In the sub-plot of the first 6 hr the time scale is expanded to illustrate the early waves. Dashed lines in (a) and (b) show Cr oxidized at 980°, 1090°, and 1200°, repeated from Fig. 2 and 3 of ref. (1).

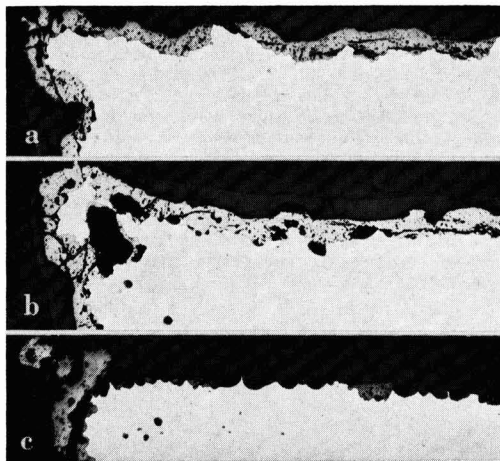


Fig. 5. Section through etched Fe-26Cr oxidized 70 hr at 1200° (curve 11). Scale layer not complete; approximately 50% lost by spalling during cooling at end of run. Magnification 120X.

the rectangular specimens showed a sharply peaked ridge of oxide. In cross section, the metal of the corners also may show a peak [Fig. 5(a)], whereas before oxidation the corners had been smoothly rounded by electropolishing. Measurements of the diagonal distance of the metal core after scaling showed an increase over the original dimension rather than the decrease expected due to metal having been consumed; e.g., in run 11, the diagonals increased by 75 μ while, on the average, 32 μ of metal were oxidized. It follows from these observations that oxide and metal have been subjected to considerable lateral plastic flow, probably as a result of compressive stresses generated in the oxide layer by the growth process.

Scale structure on electropolished Fe-26Cr.—The scales formed on electropolished Fe-26Cr at 980°, 1090°, and 1200° are illustrated in Fig. 6 to 8. All show an outer separated layer and a more solid inner layer. The early waves in the weight-gain/time curves appear to be related to the outer blistered layer. Usually only one blistered layer is observed even though the oxidation curves show two waves; presumably the two sides of the specimen fail at different times. Figure 6(a) is a plan view of the oxide formed in 0.8 hr at 980°; the layer is poorly adherent and wrinkled or blistered but has not yet failed since no irregularity has occurred in the oxidation curve. Figure 6(b) and (c) are sections through the scale formed in 24 hr under the same conditions; the second layer of adherent, nonblistered scale formed when gaseous oxygen

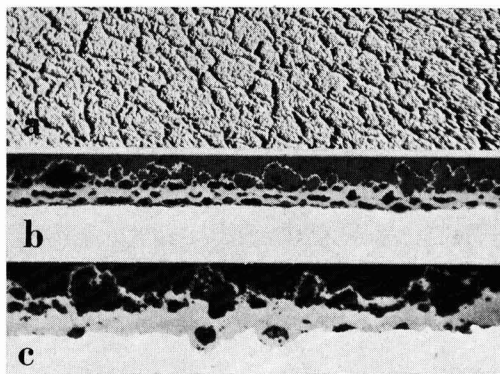


Fig. 6. Electropolished Fe-26Cr oxidized at 980°. (a) Outer surface of oxide after 0.8 hr (run 12); (b) and (c) cross section after 24 hr (curve 15). Some pores next to metal may be artifact. Magnification (a), 80X; (b), 400X; (c), 800X.

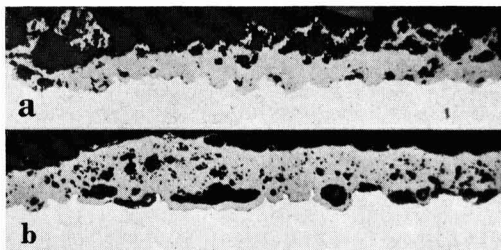


Fig. 7. Section through electropolished Fe-26Cr oxidized at 1090°. (a) Curve 17, 20 hr; (b) curve 19, 100 hr. Pores probably enlarged by polishing. Magnification 400X.



Fig. 8. Section through electropolished Fe-26Cr oxidized 0.6 hr at 1200° (curve 20). Magnification 400X.

was admitted to the bare metal by failure of the outer, wrinkled, first-formed layer at 1.7 (or 3.1) hr. At 1090° the outer blistered layer is less evident, especially after 100 hr [Fig. 7(b)], even though the weight gain before the break was no less than at 980° (last column of Table II); this might be accounted for by the increased sintering and evaporation of oxide (8) that would occur at the higher temperature and longer time. In the 0.6 hr run at 1200° (Fig. 8) the outer ballooned layer is much in evidence, consistent with the greater weight gain before the break and too short a time for significant sintering and evaporation to have occurred.

X-ray diffraction of Fe-26Cr.—The only oxide detected by x-ray diffraction was $(\text{Cr,Fe})_2\text{O}_3$. Thermodynamically, a spinel is possible if the surface metal were to become depleted in Cr below 13% (2). Attempts to induce spinel by scaling for short times at high temperatures, under which conditions the reaction rate and hence Cr depletion would be greatest, were unsuccessful; no spinel was detected. The lattice parameter of the oxide corresponded to pure Cr_2O_3 which signifies an Fe_2O_3 content of less than 3% [based on the 0.01% accuracy of the x-ray method used and the known lattice parameter of the $\text{Fe}_2\text{O}_3\text{-Cr}_2\text{O}_3$ solid solution (9)].

Chemical analysis of Fe-26Cr.—The Fe_2O_3 content found by chemical analysis ranged from 0.4 to 2.5%, consistent with the x-ray result. There was a tendency for oxide formed at more rapid rates (electropolished, high temperatures, and short times) to contain more iron, but this could not be confirmed because of the difficulty of sampling thin oxide layers without contamination by the substrate metal.

Moisture.—Three runs were carried out in wet oxygen as duplicates to dry oxygen runs, etched and electropolished at 980° and etched at 1100° (see Table II). The oxidation curves were little different from the dry oxygen runs except at the higher temperature after the first several hours. The presence of moisture increases the rate of evaporation of Cr oxide (8) which decreases the weight gain but increases the consumption of metal. As the rate of weight gain slows due to increasing oxide thickness, the loss in weight caused by evaporation of Cr_2O_3 becomes relatively important especially if not suppressed by use of the Cr_2O_3 baffle crucible. Hence, the curve of the last 80 hr of run 29 was essentially flat and the final weight gain only half that of run 10 in dry oxygen.

Other alloys.—Figure 9 compares the 1090° oxidation curves of the Fe-26Cr alloy, etched and electropolished, with the three other Fe-26Cr alloys, the compositions of which are shown in Table I. The 1090° curves for Cr are included for reference.

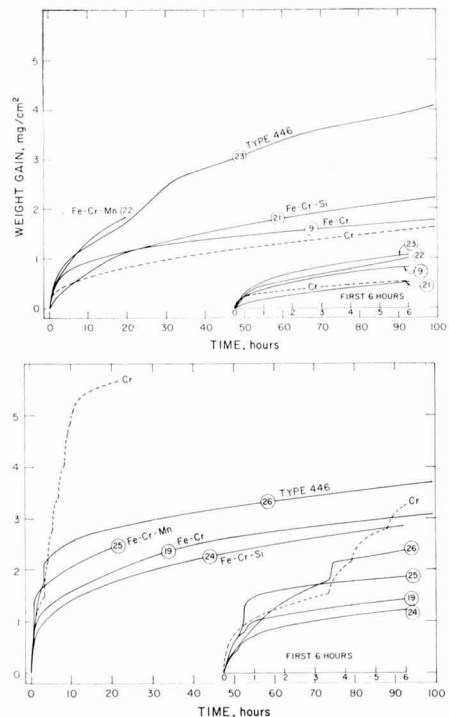


Fig. 9. Oxidation of Fe-26Cr, Fe-26Cr-0.5Si, Fe-26Cr-1Mn, type 446, and pure Cr at 1090° in 1 atm dry oxygen; (a) etched; (b) electropolished.

The increase in rate of oxidation due to electropolishing, which was observed with Cr and Fe-26Cr binary alloy, also occurs with Fe-26Cr-0.5Si, Fe-26Cr-1Mn, and type 446. For all five materials the initial reaction rate is faster after electropolishing than after etching, and all five show early breaks or waves after electropolishing [Fig. 9(b) inset] but not after etching [Fig. 9(a) inset]. The two alloys containing Mn oxidize faster than the others.

Scale structures are shown in Fig. 10. Highly irregular layers are formed. The multiple layers of Cr_2O_3 in Fig. 10(a) correspond directly to the segments of the Cr oxidation curve of Fig. 9(b). In the Fe-26Cr-0.5Si alloy, Si oxidizes preferentially to form silica islands or subscale [Fig. 10(b)] below the outer layer of $(\text{Cr,Fe})_2\text{O}_3$. Mn also oxidizes preferentially but forms a $\text{MnO} \cdot \text{Cr}_2\text{O}_3$ spinel (10) [Fig. 10(c), 10(d)] at the expense of some of the $(\text{Cr,Fe})_2\text{O}_3$.

Discussion

The general oxidation behavior of the Fe-26Cr alloy is similar to that of Cr in regard to scaling rate and general topography of the scale.¹ Both of these are markedly affected by stress formation in the oxide and the prior chemical preparation of the surface, particularly electropolishing. All five specimen materials show a faster initial oxidation rate after electropolishing. [Pure Fe, on the contrary, oxidizes at the same rate

¹ It is not unreasonable that Cr and Fe-26Cr should exhibit similar oxidation behavior since the 74% Fe content changes the system surprisingly little. The alloy is a substitutional solid solution, b.c.c. like Cr, and of nearly identical lattice parameter. The only oxide phase formed is the solid solution of rhombohedral $(\text{Fe,Cr})_2\text{O}_3$ containing less than 3% Fe_2O_3 and indistinguishable in lattice parameter from the rhombohedral Cr_2O_3 on Cr. A spinel phase would develop between metal and $(\text{Fe,Cr})_2\text{O}_3$ if preferential oxidation were to deplete the surface metal below 13% Cr (2) but no spinel was detected by x-ray diffraction. Attempts to produce spinel in short runs at high temperature, where depletion might be a maximum, were unsuccessful. In one instance spinel did form after a very long, hot run (500 hr at 1200°) when no baffle crucible was used to suppress volatilization of Cr oxide; boils of spinel as large as 3 mm were found at the bottom (upstream) corners where Cr depletion would be greatest.

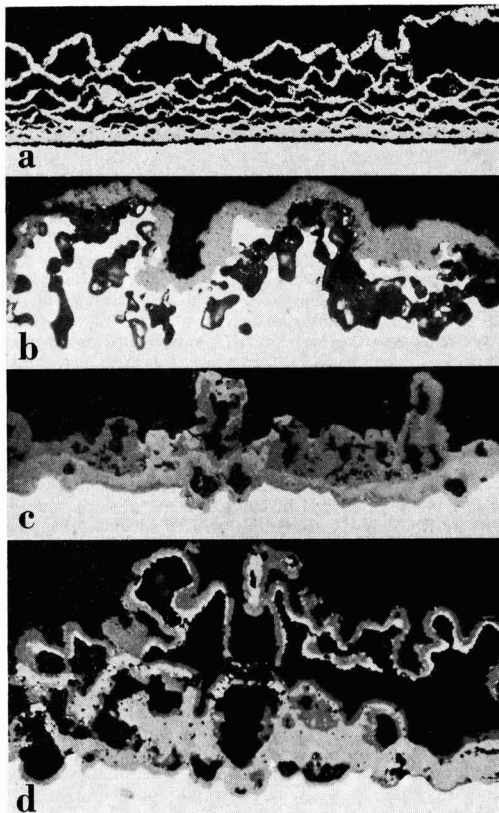


Fig. 10. Sections through Cr, Fe-26Cr-0.5Si and Fe-26Cr-1Mn oxidized at 1090°, illustrating irregular scale structures. (a) electropolished Cr, 21 hr. (Black gap between metal and scale is artifact.) Magnification 200X. (b) etched Fe-26Cr-0.5Si, 117 hr; islands of internal oxide in metal are mainly silica. Magnification 800X. (c) etched Fe-26Cr-1Mn, 20 hr (curve 22). Darker oxide is spinel; lighter oxide is Mn_2O_3 . Magnification 800X. (d) electropolished Fe-26Cr-1Mn, 20 hr (curve 25). Darker oxide is spinel; lighter oxide is Mn_2O_3 . Magnification 800X.

whether electropolished or etched (11).] The compressive stress generated in the oxide leads to wrinkling and separation of the scale and to distortion and roughening of the surface metal.

Scaling Mechanism

The scaling mechanism proposed for Fe-26Cr is closely allied to that deduced for the oxidation of Cr. To account for the observed compressive flow it appears necessary to infer, as with Cr, that oxygen diffusion participates in film growth causing oxide to form below the oxide/gas boundary. Since evidence exists that Cr diffuses in the rhombohedral oxide on Fe-Cr alloys (2), it is assumed that both cations and anions participate in the diffusion process. Thus the zone of oxide formation is within the body of the growing oxide, reasonably accounting for the observed compressive stress.

Plastic flow of the oxide layer on the etched specimens induces extensive deformation in the adherent surface metal. The consequent rugged oxide/metal interface is observed at temperatures as low as 870° (Fig. 2) and at 1200° the effect is sufficient to cause gross deformation of the specimen (Fig. 5). With pure Cr, adhesion between oxide and metal appeared to be weaker since less flow of the metal surface was observed. The explanation for this is not known but some speculations are possible. The hot strength of

metal and oxide will be decreased by the presence of Fe. This will not only make the metal more readily deformable but will facilitate subsidence of the oxide on to the retreating metal to lessen loss of adhesion. Adhesion would be improved further by collapse of pores via plastic flow of the oxide and annihilation of cation vacancies at suitable sinks, e.g., by dislocation climb. The effect of Fe on the defect structure of the oxide is unknown. If anion diffusion becomes relatively favored, as in α -Fe₂O₃, the zone of stress generation would shift toward the oxide/metal interface. Greater metal creep would then be expected. Whatever the reason, the result observed is a very rugged metal surface and peaked edges.

With the alloy, enhancement of diffusivity due to stress and continuing plastic strain is not directly apparent as was the case with Cr where nodule formation was explained in this way. Nevertheless, it is reasonable to assume its existence because the oxides are similar and stress so apparent. The effect of enhanced diffusivity on reaction kinetics should be a maximum initially and decrease progressively as the reaction rate slows.

The early waves in the E.P. oxidation curves can also be explained by the development of compressive stress. The fastest oxidation rate, hence the highest rate of stress generation, is with an electropolished specimen at the start of a run. Stress relief by creep normal to the surface will then be least effective and the stress can come to exceed the force of adhesion between oxide and metal. As a result, the oxide layer blisters away from the metal. A contributing or perhaps alternative cause of loss of adhesion is the higher rate of arrival at high oxidation rate of cation vacancies at the metal/oxide interface which may decrease adhesion by condensing into pores. The scaling process can continue in spite of separation between oxide and metal by transfer of Cr at points of contact and as vapor through the vacuum of the gap (1). Whereas with Cr the blistered layer could persist unbroken for 100 hr or more, with Fe-26Cr it fails in 2 hr or less, creating the early waves. The earlier failure might be because the oxide has lower hot strength than pure Cr₂O₃ or because the vapor pressure of Cr for the alloys is too low, especially after the metal surface becomes depleted in Cr. When the blistered layer perforates at some point, oxygen at 1 atm rushes into the vacuum gap and a second layer of oxide begins on the bare metal; the second layer does not blister because the surface on which it forms is no longer electropolished. The cause of the E.P. effect is believed to be related to the prior oxide produced during electropolishing having a higher concentration of lattice defects or of leakage paths for easy diffusion. This same speculation was proposed for pure Cr.

Oxidation Kinetics

The electropolished specimens are not considered because of the mechanical failure of the blistered first layer. The photomicrographs have shown that the oxide formed on the etched specimens is highly irregular with a rough outer surface, nonuniform thickness, rugged oxide/metal interface and containing blisters, pores and islands of metal. The effective area differs from the geometric area, not all the oxide participates in the protective process, and these factors change nonsystematically with time. As a result, meaningful analysis of the oxidation kinetics is not possible. It is surprising that the oxidation curves, at least of the etched specimens, are so smoothly well-behaved and the reproducibility as good as it is; apparently, despite so many processes operating simultaneously, local events are on a fine enough scale not to perturb the weight-gain/time record perceptibly.

Plotted on parabolic coordinates, (weight)² vs. time, the oxidation curves generally are concave downwards. Possible reasons for this type of deviation from normal parabolic behavior are some oxide being non-

participating, increasing cavity formation, loss of Cr oxide by volatilization, and improvement of the barrier by sintering; if, as postulated previously, plastic deformation resulting from compressive stress enhances diffusion, the effect would decrease as the reaction slows with time.

Double log plots of the oxidation data (log *W* vs. log *t*) yield good straight lines, in some cases over the entire time period of 0.1 to 100 hr, with slopes indicating values of *n* (in the relation $W^n = kt$) usually less than 3 and as low as 2.3 ($n - 2$ for parabolic). Nevertheless, this treatment has even less significance than the parabolic plot. The markedly nonideal character of the barrier layer precludes a systematic treatment and renders derivation of rate constants and consequent activation energies pointless. With Cr it was possible to estimate a local rate constant from areas on the metallographic cross sections where short lengths of ideal barrier layer could be found (1); no such areas of smooth, single-layer, nonporous oxide appeared on the alloy.

Moisture

The companion runs in wet oxygen demonstrate as with Cr that moisture does not significantly change the protectiveness of the M₂O₃ scale. This is in contrast to earlier observations on commercial stainless steels where gross increases and decreases were found depending on alloy type (12, 13). Much of the differences were due to mechanical factors: the huge breaks were obviously the result of separation and cracking of the barrier layer. Certainly moisture can be expected to change the sinterability of the oxide and hence affect plastic deformation and cracking. But increased plasticity cannot explain all the results. The moisture effect still is unexplained.

Other Alloys

In the ternary alloys, Si and Mn both oxidize preferentially and form second oxide phases. The silica formed under the (Cr,Fe)₂O₃ scale on the Fe-26Cr-0.5Si alloy does not develop into a continuous layer and for this reason has no appreciable effect on oxidation resistance. The protectiveness of the (Cr,Fe)₂O₃ layer is not affected. If the Si content were higher or the experimental conditions different, a continuous layer could form and isolate the Cr oxide from the substrate (12). The oxidation resistance would be increased temporarily until mechanical failure of the isolated layer occurred and rapid oxidation resumed.

The Fe-26Cr-1Mn ternary and the 446 stainless alloy, also containing Mn and 26% Cr, scale more rapidly than Cr, Fe-26Cr and Fe-26Cr-0.5Si. The Mn·Cr₂O₃ spinel forms as a continuous layer, in part replacing the (Cr,Fe)₂O₃. The reaction rate is higher because diffusion is faster in the spinel (10) and also because Mn promotes excessive blistering, hence nonparticipating oxide.

Summary

The wrinkled and blistered oxide layers, peaked corners and roughened metal surface indicate that compressive stresses develop continually in the growing oxide. This points to anion diffusion as one of the processes contributing to film growth, resulting in a zone of formation of new oxide within the oxide layer. The consequent compressive stress causes the oxide and metal to deform plastically, creating highly irregular structures and mechanical failure of the barrier layer.

The nonuniformity of the scale structure interferes with the analysis of the reaction kinetics even when smooth oxidation curves are obtained. No rate constants or activation energies were deduced. The several complicating factors, including porosity, nonparticipating oxide, unknown effective area and varying oxide thickness, themselves change nonsystematically with time. If diffusion is enhanced by the continuing plastic flow, as is believed, diffusion coefficients in the oxide also would slow with time.

The oxide formed on Fe-26Cr is the same as the Cr_2O_3 formed on Cr except for a minor Fe content, and the oxidation rates are similar. Addition of 0.5% Si to Fe-26Cr leads to the formation of silica islands under the $(\text{Fe,Cr})_2\text{O}_3$ layer but has no appreciable effect on the oxidation resistance. Fe-26Cr-1Mn and type 446, both containing Mn, form spinel layers as well as Mn_2O_3 and show greater weight gains. Mn is apparently deleterious in oxidation-resistant Fe-Cr alloys.

The oxidation of Fe-26Cr is highly sensitive to surface preparation. The initial rate is especially rapid after electropolishing. The three other Fe-26Cr alloys and Cr behave similarly. As a result the oxide layer blisters away from the metal surface, fails mechanically and a second layer forms below. Corresponding irregularities appear in the oxidation curves.

Moisture appears to have no effect on the oxidation resistance of Fe-26Cr except that it enhances the volatilization of Cr oxide thus thinning the layer and decreasing the weight gain but increasing the amount of metal consumed.

For best results in the utilization of high temperature alloys which rely on Cr for oxidation resistance it should be advantageous to prepare the metal surface carefully, arrange moderate oxidation conditions for the first exposure, and avoid gas flows that would aggravate oxide evaporation. Mn should be avoided; no doubt certain other alloying additives would be beneficial.

Acknowledgment

The authors are grateful to Mrs. Alma Harvey for skillful assistance with the oxidation experiments and Mr. P. E. Beaubien for the metallography.

Manuscript received Dec. 14, 1964. This paper was presented at the Washington Meeting, Oct. 11-15, 1964.

Any discussion of this paper will appear in a Discussion Section to be published in the December 1965 JOURNAL.

REFERENCES

1. D. Caplan, A. Harvey, and M. Cohen, *Corrosion Science*, **3**, 161 (1963).
2. A. U. Seybolt, *This Journal*, **107**, 147 (1960).
3. A. U. Seybolt, *Advan. Phys.*, **12**, 1 (1963).
4. O. Kubaschewski and B. E. Hopkins, "Oxidation Metals and Alloys," p. 236, Butterworths, London (1962).
5. D. Lai, R. J. Borg, M. J. Brabers, J. D. MacKenzie, and C. E. Birchenall, *Corrosion*, **17**, 357t (1961).
6. G. C. Wood, *Corrosion Science*, **2**, 173 (1962).
7. D. Caplan, A. Harvey, and M. Cohen, *This Journal*, **108**, 134 (1961).
8. D. Caplan and M. Cohen, *ibid.*, **108**, 438 (1961).
9. R. K. Di Cerbo and A. U. Seybolt, *J. Am. Ceram. Soc.*, **42**, 430 (1959).
10. D. Caplan, P. E. Beaubien, and M. Cohen, submitted to the Metallurgical Society of AIME (1964).
11. D. Caplan and M. Cohen, *Corrosion Science*, **3**, 139 (1963).
12. D. Caplan and M. Cohen, *J. Metals*, **4**, 1057 (1952).
13. D. Caplan and M. Cohen, *Corrosion*, **15**, 141t (1959).

Studies on the Oxygen Gradients in Oxidizing Metals

III. Kinetics of the Oxidation of Zirconium at High Temperatures

J. P. Pemsler

Ledgemont Laboratory, Kennecott Copper Corporation, Lexington, Massachusetts

ABSTRACT

The oxidation of zirconium was studied in the temperature range 840°-1100°C. Film growth and oxygen solution processes were separated experimentally. Oxygen solution obeys diffusion kinetics and remains parabolic for sufficiently thick samples. Film growth does not obey normal rate laws; an exceedingly rapid initial rate is followed by a period of slower growth. The over-all weight gain curve is explained in terms of the separate film growth and oxygen solution processes. At temperatures $\geq 975^\circ\text{C}$ voids form in the oxide; they act as diffusion blocks and promote formation of a duplex layer. The mechanism of void formation is discussed in terms of a condensation of oxygen vacancies. The effect of orientation, pressure, surface preparation, and initiation temperature are discussed.

The kinetics of the oxidation of zirconium has been extensively investigated over a wide range of temperatures. Authors variously report the rate as cubic transforming to linear or parabolic transforming to linear. There are relatively few measurements at high temperatures where oxygen dissolution in the metal represents a significant quantity of the total oxygen absorbed. The high-temperature data are for the most part of short duration and exhibit poor reproducibility from sample to sample. High-temperature studies have in general relied on thin coupons which are not amenable to long term observation of the kinetics for two reasons: (i) Spalling and cracking at the edges after relatively short times prevents accurate assessment of the weight gains; and (ii) the meeting of the oxygen gradients in the center of the sample alters the rate of dissolution of oxygen in the metal, so that the kinetic curve is dependent on the thickness of the sample.

There has been only one group of investigators which has attempted to separate quantitatively the contributions of film thickness and oxygen dissolution to the kinetics of the high-temperature process. Wallwork, Smeltzer, and Rosa (1) oxidized 2 mm-thick zirconium coupons for times up to 200 hr at 850°C. They report that both the oxide film and over-all weight gain conform to parabolic kinetics. Rosa and Smeltzer (2) oxidized similar samples for times up to 100 hr at 950°C. They report that after an initial deviation both

oxide film thickness and total weight gain conform to parabolic kinetics.

In a recent investigation (3) the author has shown that the oxygen gradient beneath the oxide film on zirconium oxidized at high temperatures may be measured experimentally and is in good agreement with values from a theoretical expression involving the diffusivity, time, and oxide film thickness. Furthermore, it was noted that with coarse grained samples the oxide film thickness at 850°C did not conform to a parabolic rate of growth, but rather grew at a very rapid rate for the first several hours, and thereafter, at a greatly reduced rate.

It is the purpose of this work to attempt: (i) to obtain accurately and reproducibly kinetic data for the oxidation of zirconium at high temperatures for long periods of time; (ii) to separate quantitatively the film growth and oxygen dissolution processes; and (iii) to investigate the mechanism of the film growth process.

Experimental

The zirconium used in this investigation was obtained in the form of 1.9 cm diameter rod, and the analysis is given in Table I. Spheres of 1.74 cm diameter were machined from the rod with a tolerance of 25μ on the diameter. The spherical shape was chosen to eliminate the effects of edges and corners as a source of initiation of oxide failure and spalling. Furthermore, the spherical shape enables precise calcula-

Table I. Analysis of zirconium rod

Element	ppm
C	115
N	30
O	850
Fe	480
Cu	13
Ni	7
Cr	95
Mn	6

Table II. Vendor's analysis of oxygen

Element	ppm
Ar	15
CH ₄	15
Kr	10
Xe	4
CO ₂	7
H ₂ O	6
N ₂	2

tion of the quantity of oxygen dissolved in the metal; the situation is far more complex with other sample shapes such as parallelepipeds where gradients from different directions overlap.

Spheres were etched in an aqueous solution of 50% nitric and 5% hydrofluoric acids, rinsed, dried, and suspended by a thin platinum wire in an Ainsworth continuous recording semi-microbalance of 0.01 mg sensitivity and 400 mg weight gain capacity. The balance was evacuated, and the sphere was annealed for 1 hr at the temperature at which the oxidation was to take place. After annealing, the furnace was removed and the sample allowed to cool to room temperature. High-purity grade oxygen whose analysis is given in Table II was then admitted to the sample tube and the furnace repositioned around the sample tube. A continuous record of the weight gain was obtained throughout the course of the oxidation. In the two runs of less than 1 hr at 910°C, the oxygen was admitted while the sample was at temperature in order to define the exposure time more precisely. At the conclusion of the oxidation run spheres were removed from the balance, imbedded in bakelite mounts, and machined to within 0.25 mm of the diameter. A final polish for 60 sec on a napless cloth was used to prevent rounding of the oxide film. Photographs of the oxide film were taken at suitable magnification at eight areas equidistant around the circumference of the circle of polish. The thickness of the oxide film at each area was obtained from the photographs by measuring the area of the oxide film with a planimeter.

Since the diffusion coefficient of oxygen in zirconium is highly temperature dependent, and at the temperatures under consideration in this study the quantity of oxygen dissolved in the metal represents a considerable portion of the total oxygen absorbed, it is necessary to control and measure the temperature accurately. The initial experiments at 840°C were per-

formed using a rate-proportioning galvanometer controller. In this instance the temperature varied by $\pm 2.5^\circ$ from the control point. In subsequent experiments at higher temperatures, a 1 mv potentiometric controller with an external solid-state zero suppression reference together with a proportioning current adjuster were used to control the temperature of the furnace. A calibrated measuring thermocouple placed

Diffusion Equations

Below α/β transformation.—Calculation of the oxygen gradients beneath the film on oxidized metals necessitates the solution of a moving interface diffusion problem with the oxidation rate as a boundary condition. The solution to this problem for the case of alpha zirconium has been derived elsewhere (3, 4).

The oxygen concentration C at a distance x from the oxide/metal interface is given by the expression

$$C = C_s \frac{\operatorname{erfc}(x/2\sqrt{D_\alpha t})}{\operatorname{erfc}(s/2\sqrt{D_\alpha t})} \quad [1]$$

where C_s is the oxygen concentration in zirconium coexisting with ZrO_2 , D_α is the diffusion coefficient of oxygen in zirconium at the experimental temperature, s is the distance of the oxide/metal interface from the position of the initial surface, and $x = x' + s$.

Integration of Eq. [1] gives the total quantity of oxygen present in the metal beneath the oxide film

$$M = 2C_s\sqrt{D_\alpha t} \left[\frac{\exp(-s^2/4D_\alpha t)}{\sqrt{\pi} \operatorname{erfc}(s/2\sqrt{D_\alpha t})} - \frac{s}{2\sqrt{D_\alpha t}} \right] \quad [2]$$

where M is the quantity of oxygen dissolved in the metal per unit area of surface.

The use of spherical samples necessitates the solution of the above case in spherical coordinates. In a sphere of radius a with an initial oxygen concentration of zero, the boundary conditions are

$$C = 0 \text{ at } r > 0, t = 0 \quad [3]$$

and

$$C = C_s \text{ at } r = a - s \quad [4]$$

where s is defined as above.

The concentration C at a distance r from the center of the sphere is given by

$$C = C_s \left[1 + \frac{2a}{\pi r} \sum_{n=1}^{\infty} \frac{(-1)^n}{n} \sin\left(\frac{n\pi r}{a}\right) \exp\left[-\frac{D_\alpha n^2 \pi^2 t}{a^2}\right] \right] \\ 1 + \frac{2a}{\pi(a-s)} \sum_{n=1}^{\infty} \frac{(-1)^n}{n} \sin\frac{n\pi(a-s)}{a} \exp\left[-\frac{D_\alpha n^2 \pi^2 t}{a^2}\right] \quad [5]$$

Integration of Eq. [5] gives the total quantity of oxygen contained in the metal sphere of radius $a-s$ beneath the oxide film.

$$M = C_s \left[\frac{4}{3}\pi(a-s)^3 + \sum_{n=1}^{\infty} 8\pi(-1)^n \left(\frac{a}{n\pi}\right)^3 \left(\sin\frac{n\pi(a-s)}{a} - \frac{n\pi(a-s)}{a} \cos\frac{n\pi(a-s)}{a} \right) \exp\left[-\frac{D_\alpha n^2 \pi^2 t}{a^2}\right] \right] \\ 1 + \frac{2a}{\pi(a-s)} \sum_{n=1}^{\infty} \frac{(-1)^n}{n} \sin\frac{n\pi(a-s)}{a} \exp\left[-\frac{D_\alpha n^2 \pi^2 t}{a^2}\right] \quad [6]$$

formed using a rate-proportioning galvanometer controller. In this instance the temperature varied by $\pm 2.5^\circ$ from the control point. In subsequent experiments at higher temperatures, a 1 mv potentiometric controller with an external solid-state zero suppression reference together with a proportioning current adjuster were used to control the temperature of the furnace. A calibrated measuring thermocouple placed

The necessity of performing summations makes the equation most conveniently evaluated by computer methods.

The diffusion coefficient of oxygen in alpha zirconium has been measured by the author (5) and subsequently by several additional authors (6-9). The value in the alpha phase is considered to be known with high accuracy and expressed by

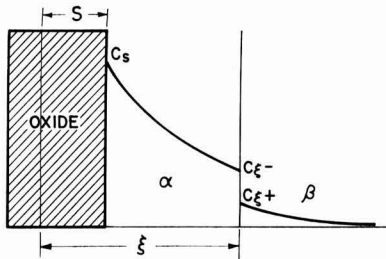


Fig. 1. Schematic diagram of zirconium oxidized at temperatures above the α/β transition temperature.

$$D_{\alpha} \text{ cm}^2/\text{sec} = 5.2 \exp\left[(-50,800 \pm 870)/RT\right] \quad [7]$$

The saturation value of oxygen in alpha zirconium coexisting with zirconia was taken as $C_s = 0.456 \text{ g/cm}^3$ (10, 11). The quantity of metal s consumed in generation of an oxide film of thickness l was taken as $s = 0.666l$.

For spheres of 1.74 cm diameter oxidized at 840°C , the value of M calculated for a sphere from Eq. [6] was about 4% less than values for a semi-infinite sample as calculated from Eq. [2].

Above α/β transformation.—Oxygen is a strong alpha stabilizer and at temperatures above the α/β transformation (862°C) a more complex situation exists, as shown in Fig. 1. Beneath the oxide film there exists a solution of oxygen in alpha zirconium for a distance ξ from the original metal interface, until an oxygen concentration of $C_{\xi-}$ is reached. At this position there is a plane of discontinuity where the concentration falls to $C_{\xi+}$, the saturation value of oxygen in the body centered cubic β zirconium. Thereafter, the concentration falls to a value of C_0 , the initial oxygen content of the metal. The boundary conditions for a semi-infinite sample are expressed as

$$C = C_0 \text{ at } x > 0 \text{ } t = 0 \quad [8]$$

$$C = C_s \text{ at } x = s \text{ } t > 0 \quad [9]$$

$$C = C_{\xi+} \text{ at } x = \xi - 0 \quad [10]$$

$$C = C_{\xi-} \text{ at } x = \xi + 0 \quad [11]$$

The particular integrals satisfying Eq. [8] through [11] are

$$C_{\alpha} = C_s + \frac{(C_s - C_{\xi-}) \left[\operatorname{erf}\left(\frac{s}{2\sqrt{D_{\alpha}t}}\right) - \operatorname{erf}\left(\frac{x}{2\sqrt{D_{\alpha}t}}\right) \right]}{\operatorname{erf}\left(\frac{\xi}{2\sqrt{D_{\alpha}t}}\right) - \operatorname{erf}\left(\frac{s}{2\sqrt{D_{\alpha}t}}\right)} \quad [12]$$

and

$$C_{\beta} = \frac{C_{\xi+} \left[\operatorname{erfc}\left(\frac{x}{2\sqrt{D_{\beta}t}}\right) \right]}{\operatorname{erfc}\left(\frac{\xi}{2\sqrt{D_{\beta}t}}\right)} \quad [13]$$

The mass flow across the boundary ξ is given by

$$(C_{\xi-} - C_{\xi+}) \frac{d\xi}{dt} = -D_{\alpha} \left(\frac{\partial C}{\partial x} \right)_{\xi-0} + D_{\beta} \left(\frac{\partial C}{\partial x} \right)_{\xi+0} \quad [14]$$

where D_{α} is the diffusion coefficient of oxygen in alpha zirconium and D_{β} is the diffusion coefficient in beta zirconium.

Setting $\gamma = \xi/2\sqrt{Dt}$ and $\phi = D_{\alpha}/D_{\beta}$, and integrating Eq. [14] we obtain

$$C_{\xi-} - C_{\xi+} = \frac{C_s - C_{\xi-}}{\left(\operatorname{erf}\gamma - \operatorname{erf}\frac{s}{2\sqrt{D_{\alpha}t}} \right) \gamma \sqrt{\pi}} \exp[-\gamma^2] - \frac{C_{\xi+} - C_0}{\gamma \sqrt{\pi} \phi \operatorname{erfc}(\gamma \phi^{1/2})} \exp[-\gamma^2 \phi] \quad [15]$$

from whence ξ can be calculated.

The total quantity of oxygen contained in the alpha and beta phases are obtained by integrating Eq. [12] and [13], respectively.

$$M_{\alpha} = C_s(\xi - s) + \frac{C_s - C_{\xi-}}{\operatorname{erf}\left(\frac{\xi}{2\sqrt{D_{\alpha}t}}\right) - \operatorname{erf}\left(\frac{s}{2\sqrt{D_{\alpha}t}}\right)} \left[(\xi - s) \operatorname{erf}\left(\frac{s}{2\sqrt{D_{\alpha}t}}\right) - \xi \operatorname{erf}\left(\frac{\xi}{2\sqrt{D_{\alpha}t}}\right) - \frac{2\sqrt{D_{\alpha}t}}{\sqrt{\pi}} \exp\left[-\frac{\xi^2}{4D_{\alpha}t}\right] + s \operatorname{erf}\left(\frac{s}{2\sqrt{D_{\alpha}t}}\right) + \frac{2\sqrt{D_{\alpha}t}}{\sqrt{\pi}} \exp\left[-\frac{s^2}{4D_{\alpha}t}\right] \right] \quad [16]$$

$$M_{\beta} = \frac{C_{\xi+} 2\sqrt{D_{\beta}t}}{\sqrt{\pi}} \frac{\exp\left[-\frac{\xi^2}{4D_{\beta}t}\right]}{\operatorname{erfc}\left(\frac{\xi}{2\sqrt{D_{\beta}t}}\right)} - C_{\xi+} \xi \quad [17]$$

The increase in the quantity of oxygen in the metal during oxidation is then equal to the amount of oxygen in the alpha phase plus the amount in the beta phase minus the initial oxygen content.

$$M = M_{\alpha} + M_{\beta} - \frac{4}{3} \pi a^3 C_0 \quad [18]$$

No attempt was made to solve Eq. [16] directly for the spherical case. The oxygen content of the alpha phase M_{α} was evaluated for a semi-infinite sample from Eq. [16] and the result decreased by 4% (see above) to correct for spherical geometry. The evaluation of M_{β} for the sphere is analogous to the evaluation of M according to Eq. [6], where now s is replaced by ξ , and computer methods used.

Values of C_s , D_{α} , and s are obtained as in the preceding section. Values of D_{β} are obtained from the work of Mallett *et al.* (6).

$$D_{\beta} = 0.0453 \exp\left[(-28,200 \pm 2400/RT)\right] \quad [19]$$

and are known only to within about a factor of two.

Values of $C_{\xi-}$ were estimated from the phase diagram (10, 11) and are probably correct to within a 30% error. Since it was difficult to estimate values of $C_{\xi+}$ from the phase diagram, it was determined experimentally at one temperature. A cylinder 0.5 cm in diameter \times 1.5 cm long was oxidized at 967°C for 64 hr, after which the oxygen concentration at the center was calculated to be $0.69C_{\xi+}$. The oxide film and alpha phases were machined from the sample and the remaining transformed β -phase analyzed for oxygen. The value of $C_{\xi+}$ at 967°C was obtained in this manner, and values at the other temperatures were estimated by assuming that values of $C_{\xi+}$ are linear with temperature near the transformation temperature (in agreement with the shape of the phase diagram). Values of D_{β} , $C_{\xi+}$, and $C_{\xi-}$ are listed in Table III.

Table III. Values used in diffusion calculations

Temp, $^\circ\text{C}$	D_{β} , cm^2/sec	$C_{\xi+}$, g/cm^3	$C_{\xi-}$, g/cm^3
910	2.80×10^{-7}	0.0105	0.0435
975	5.22×10^{-7}	0.0210	0.0790

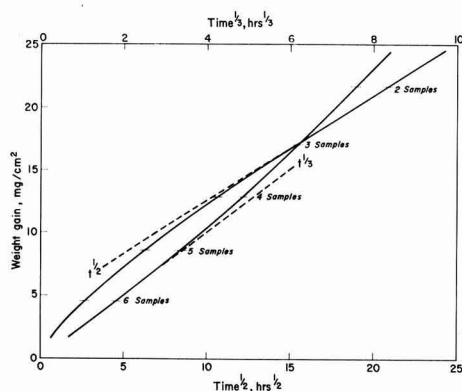


Fig. 2. Total weight gain of zirconium oxidized at 840°C

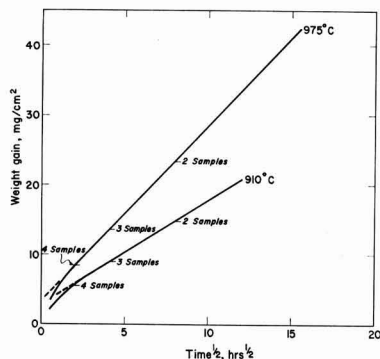


Fig. 3. Total weight gain of zirconium oxidized at 910° and 975°C

Results and Discussion

Weight gain.—Data for the total weight gain at 840°, 910°, and 975°C are given in Fig. 2 and 3. Data at 840°C are presented in the form of both parabolic and cubic plots. Solid lines indicate the continuous weight gain curves, and dashed lines represent extrapolation of parabolic and cubic portions. The reproducibility of the data was excellent, and all sample points fall within the breadth of the line representing the data. Since samples were to be used for further measurements, separate experiments were concluded at varying periods of time; therefore, the data presented in Fig. 2 are derived from seven samples for a duration of 7 hr, six samples for a duration of 40 hr, etc., as indicated on the figure. It is apparent from examination of this figure how a discrepancy may arise in reporting high-temperature kinetic data in terms of parabolic and cubic rates. The rate conforms quite well to a cubic relationship up to about 80 hr after which it bends off toward the ordinate, indicating that the weight gain rate is now more rapid than that represented by a cubic relationship. It should be noted that the cubic curve extrapolates well through the origin. Furthermore, if the data are plotted on logarithmic coordinates, which by their nature emphasize the early time data, a straight line is obtained whose slope equals 0.375, close to the cubic value. Investigators who performed experiments for times not far beyond 80 hr at this temperature would be inclined to report their data as conforming to a cubic relationship.

Examination of the parabolic plot indicates that there is a rapid initial weight gain which does not conform to the parabolic law, and only after about 150 hr does the weight gain increase parabolically. One would have to ignore a large initial portion of the curve

Table IV. Oxide film thickness for various times at 840°, 910°, and 975°C

	Time, hr	$\Delta x_a \pm d_a, \mu$	Min-Max, μ
840°C	7.0	20.1 ± 0.7	18-21
	40.0	29.8 ± 0.8	28-31
	113.0	38.0 ± 1.2	35-40
	234.0	44.9 ± 1.0	44-47
	435.0	52.7 ± 1.1	52-56
	601.5	59.8 ± 0.8	58-63
910°C	0.25	10.9 ± 0.3	9-13
	0.75	13.9 ± 0.3	12-15
	4.0	19.3 ± 0.3	17-21
	17.0	25.8 ± 0.4	23-28
	63.7	35.1 ± 0.5	33-38
	146.0	43.7 ± 0.7	42-47
975°C	4.0	25.9 ± 0.5	21-35
	16.7	30.7 ± 1.2	26-39
	63.7	42.8 ± 1.7	36-49
	237.5	67.1 ± 5.9	60-71

Δx_a is average oxide thickness; d_a is average deviation from mean; Min is minimum oxide thickness; Max is maximum oxide thickness.

to conclude that the weight gain data obeys a parabolic behavior. In any case further analysis will show that the total weight gain curve has little theoretical significance since the total weight gain curve is the sum of the film growth and oxygen dissolution processes which themselves have different rate behaviors.

Data at 910° and 975°C are also highly reproducible and are presented in Fig. 3 as parabolic plots. At these temperatures the region of conformity to cubic kinetics is small so that no cubic plot is given. After relatively short times, representing however considerable weight gains, the total weight gain curves conform closely to parabolic rates. The reason for this will become clear in the following sections where the separate processes are analyzed.

Oxidation behavior was also investigated at 1025°, 1050° and 1100°C, but no total weight gain curves were obtained since the capacity of the continuous weighing balance was exceeded after relatively short periods of time.

Film thickness.—Data for the growth of oxide films at 840°, 910°, and 975°C are presented in Table IV and Fig. 4. At 840° and 910°C the films are of relatively uniform thickness, differing by a maximum of 3-5 μ at different areas. At 975°C the oxide/metal interface becomes irregular and the films differ in thickness by 10-15 μ from point to point (see section on Metallography). Very little difference exists between the rate of growth of oxide at 840° and 910°C; however, at 975°C the film grows appreciably more rapidly than at 910°C.

Data at the two lower temperatures where the oxides appear dense and pore-free are presented in parabolic cubic, and quartic form in Fig. 5. The parabolic plot is inadequate at both short and long times; conformity begins at about 4 hr and ends at about 100 hr at these temperatures. The cubic plot fits the data quite well except for times less than about 4 hr. The quartic

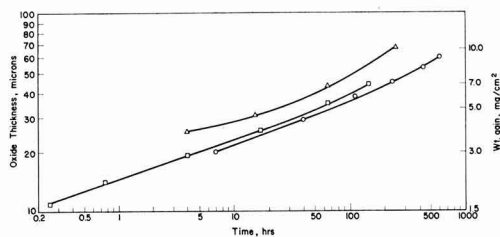


Fig. 4. Logarithmic plot of the oxide film growth on zirconium oxidized at 840° (O), 910° (□), and 975° (Δ).

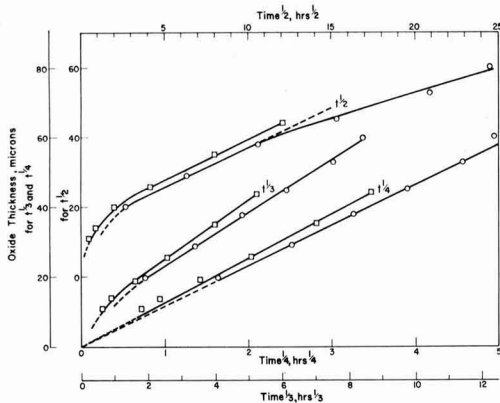


Fig. 5. Parabolic, cubic, and quartic plot of oxide film growth on zirconium oxidized at 840° (○) and 910°C (□).

plot appears to conform to the data rather well even at very short times with the exception of the last point at 840°C for 600 hr, which is slightly above the line. Figure 5 should however at this time remain an exercise in curve fitting, since quantitative information on the structure and transport properties through the oxide is necessary in order to understand, rather than rationalize, the data which does not conform to any established rate law. A qualitative explanation for the rapid initial growth followed by a slower growth will be offered in the section on Mechanism.

Data for growth at 1025°, 1050°, and 1100°C are presented in Table V. The rate of film growth continues to increase greatly at these higher temperatures. At 1025°C the oxide/metal interface becomes highly irregular and the oxide thickness varies by a factor of two to three from place to place. Little additional growth is observed between 16 and 77 hr. At 1050°C after the first 5 hr the film is of fairly uniform thickness, and irregularity commences by 18 hr. At 1100°C there was widespread localized attack in the vicinity of the platinum support wires. The thickness of the unaffected areas was relatively uniform.

Oxygen in the metal.—A knowledge of the total weight gain and measurement of the oxide film thickness enables the computation of the quantity of oxygen dissolved in the metal substrate beneath the oxide film. Furthermore, the latter quantity can be calculated according to Eq. [6] for temperatures below the α/β transformation and by Eq. [16], [17], and [18] above the α/β transformation. Calculated and experimental data for oxygen dissolved in the metal below the α/β transformation are plotted as a function of the square root of time in the lower curve in Fig. 6. Here the solid line represents calculated values, and separate experimental points are indicated in the figure. At 840°C

Table V. Oxide film thickness for various times at 1025°, 1050°, and 1100°C

	Time, hr	$\Delta x_{\text{max}}, \mu$	$\Delta x_{\text{min}}, \mu$
1025°C	4.0	90	45
	16.3	125	45
	77.2	125	60
1050°C	5.3	190	180
	18.5	380	250
	64.0	630	250
1100°C	31.0	650	610

Δx_{max} is maximum oxide thickness; Δx_{min} is minimum oxide thickness.

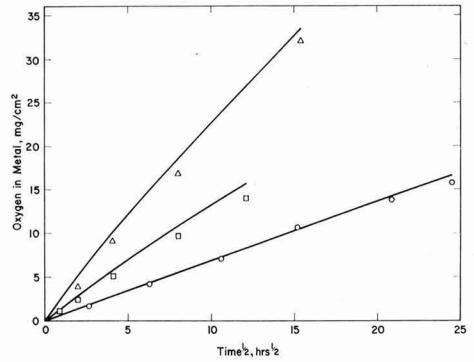


Fig. 6. Oxygen in solution in zirconium oxidized at 840° (○), 910° (□), and 975°C (△).

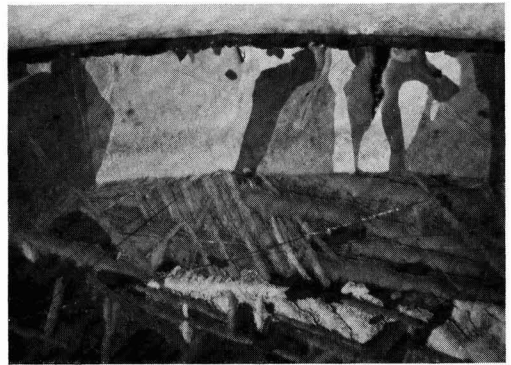


Fig. 7. Zirconium sphere oxidized for 17 hr at 975°C showing α/β phase boundary. Magnified approximately 60X; polarized light.

there is excellent agreement between calculated and observed oxygen content of the metal. Data are parabolic as demanded by diffusion theory.

Metallographic examination of samples oxidized above the α/β transition temperature clearly reveals the position of the α /transformed β boundary (Fig. 7). Measurement of the distance of the α /transformed β boundary from the oxide/metal interface and the previously evaluated oxide thickness enables calculation of the parameter ξ . It is also possible to calculate ξ from Eq. [15]. However, uncertainties in the values of $C_{\xi+}$, $C_{\xi-}$, and D_{β} do not permit the calculation of ξ with great accuracy, and a comparison of observed and calculated values of ξ is not too rewarding. For example, examination of a sample oxidized for 64 hr at 910°C gave an observed value of $\xi = 5.54 \times 10^{-2}$. Calculation using maximum and minimum estimates of $C_{\xi+}$, $C_{\xi-}$, and D_{β} gives values ranging from 4.88×10^{-2} to 5.60×10^{-2} .

Agreement between calculated and experimental data at 910° and 975°C as shown in Fig. 6 are not as good as at 840°C. This may be due to two factors: (a) As discussed above there are appreciable uncertainties in the values of the solubility parameters at the α/β interface and the diffusion coefficient of oxygen in the β -phase; and (b) the formation of voids at the metal/oxide interface (see section on Metallography) may act as discontinuities in the Zr/ZrO_2 diffusion couple so that the flow of oxygen to the metal is interrupted.

The calculated curve at 910°C is initially linear when plotted against $t^{1/2}$, and then curves downward toward the abscissa. This is due to the fact that after about 50 hr the gradients in the β -phase meet at the center of the sphere, thereafter slowing down the rate of ab-

sorption of oxygen into the β -phase. The calculated curve at 975°C is again initially linear with $t^{1/2}$ representing a maximum rate of diffusion. After a few hours at this temperature, the gradients begin to meet in the center of the sphere causing the line to bend toward the abscissa. Shortly thereafter, the β -phase becomes saturated with oxygen, and the rate again becomes parabolic representing the increase of oxygen in the α -phase.

Kinetics.—Having previously examined the film growth and oxygen diffusion kinetics, we are now in a position to understand the over-all weight gain curves as a summation of the two separate processes. In the initial stages the rapid film growth coupled with oxygen dissolution gives rise to an approximately cubic rate of growth. As the reaction proceeds, the rate of film growth decreases markedly, and the relative quantity of oxygen in the metal compared with oxygen in the film increases. Since the oxygen dissolution process is parabolic, it is not surprising that at longer times the over-all kinetics tends toward a parabolic process. Furthermore, the activation energy for the dissolution process is much higher than for oxide growth so that at the higher temperatures the oxygen dissolution process represents a larger part of the over-all weight gain. Consequently, the time necessary to approach parabolic kinetics decreases with increasing temperature.

It must be borne in mind that the depth of oxygen penetration into the sample is quite appreciable at these temperatures and the thickness and geometry of the specimen are exceedingly important in determining the shapes of the kinetic curves. A thin sample may rapidly become saturated with oxygen, and the film growth will then be paramount in determining the kinetics. Conversely, a thick sample will continue to dissolve oxygen at a parabolic rate, while the film growth will proceed comparatively slowly.

At the temperatures under consideration in this study the over-all kinetic curve is of little theoretical significance. The oxygen dissolves in the metal according to diffusion theory, and its contribution to the over-all kinetics is entirely predictable according to equations previously discussed. It remains then to understand the film growth law in terms of the structure and transport properties of the film.

Metallography.—The film formed at 840°C appears dense and adherent and exhibits a fine, columnar structure. In all samples except the one with the longest exposure time there was no evidence of cracking in the oxide or accelerated growth. However, the sample exposed for 601.5 hr developed several thin lines of white oxide around the circumference of the sphere. The fine cracks probably develop due to the accumulation of stresses caused by the oxide growth. This process may be enhanced by thermal cycling, and a specimen with a thick oxide film which has been rapidly cooled and reheated to temperature in oxygen shows a network of such cracks around the sample.

Careful examination of the structure of the sound film formed at 840°C indicates some difference in the structure of the oxide near the oxide/metal interface compared with the oxide further out toward the oxide/gas interface. In order to reveal this more clearly it is necessary to polish perpendicular to the fine columnar grains so that they are viewed in the direction of growth. This is best achieved on a spherical sample by polishing at the circumference through the oxide film until the metal is just reached. In addition, appreciable magnification of the oxide is achieved since this technique is similar to polishing a flat oxide at a low angle. Examination of the sample prepared in this manner indicates that the outer oxide consists of a somewhat coarser structure than the fine inner oxide.

The oxide film formed on samples exposed at 910°C is quite similar to that observed on the samples formed at 840°C. The oxide again appears dense and adherent.

Differences in structures of the outer and inner oxide are more pronounced at 910°C than at 840°C.

At 975°C the duplex nature of the scale becomes more pronounced than at lower temperatures. After the initial exposure (4 hr), voids are visible at the oxide/metal interface; at later times they become buried in the oxide by further growth, while new voids continue to originate at the metal/oxide interface (Fig. 8-11). These voids act as diffusion blocks preventing further oxidation of metal below them and necessitate that further oxidation occur around them. Voids also appear to enhance the tendency toward formation of the duplex oxide layer. Beyond the voids toward the oxygen/oxide interface, there are ovals of oxide with a milky white appearance under polarized light; the fine columnar structure is retained between the void and oxide/metal interface. The whitening of the oxide may be logically explained by the action of the void in preventing access of the oxide above it to the demand for oxygen from the oxide and metal below it. The non-stoichiometric oxide would then tend to be oxidized toward the stoichiometric composition by oxygen from the gas phase.

The presence of second phase particles in the metal enhances the formation of voids, and a Zr-0.5 w/o (weight per cent) B alloy containing particles of ZrB₂ exhibits void formation at temperatures as low as 840°C. At higher temperatures voids selectively nucleate at the second phase particles.

At 1025°C after the first exposure time of 4 hr the film is highly irregular and contains many voids. The duplex oxide layer becomes quite pronounced. By 16 hr the oxide whitens appreciably, and by 77 hr the entire oxide appears milky white.

At 1050°C after the first exposure of 5 hr, the film is quite uniform in thickness. There appears to be a distribution of fine voids throughout the oxide, but it

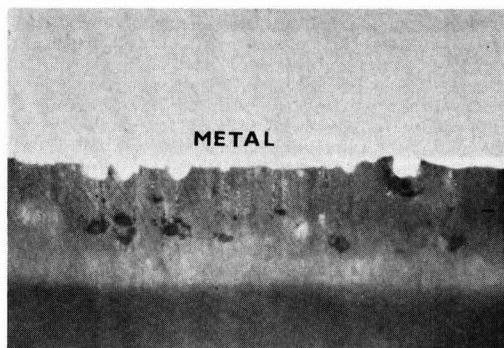


Fig. 8. Zirconium sphere oxidized for 64 hr at 975°C showing voids at metal/oxide interface and in the oxide. Magnified approximately 525X; bright light.

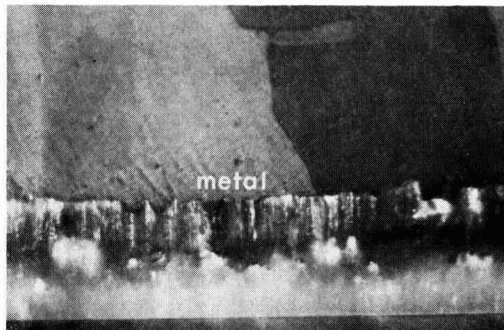


Fig. 9. Same as Fig. 8 but viewed under polarized light.

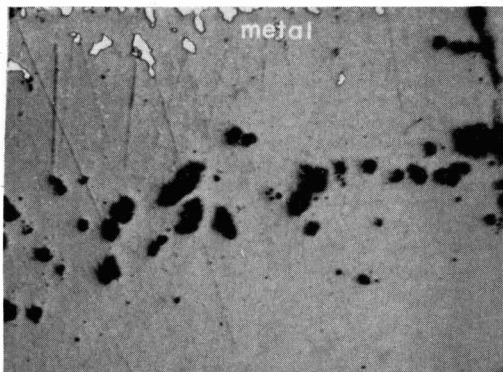


Fig. 10. Perpendicular taper section of sample in Fig. 8. Bright light. Areas of metal near the top of the picture are due to an irregular metal/oxide interface combined with a tapering polish.

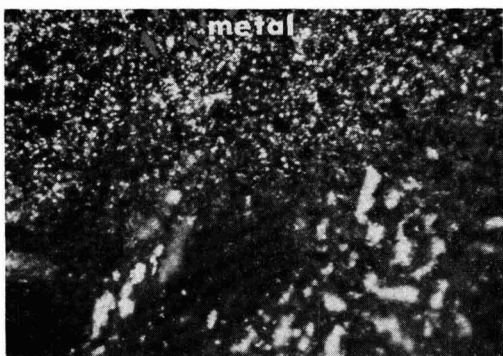


Fig. 11. Same as Fig. 10 but viewed under polarized light

is difficult to be certain of this due to the tendency of the columnar grains of oxide to be pulled out during polishing. There is no evidence of the development of the larger voids or the duplex layer characteristic of samples oxidized at lower temperatures. However, by 18.5 hr the oxide has become irregular, larger voids are forming at the metal/oxide interface, and there is a tendency toward the formation of a duplex layer. Several areas of accelerated oxidation due to gross cracking of the oxide were observed. After 64 hr areas of accelerated oxidation were widespread. In other areas the oxide consisted of a duplex oxide containing voids.

At 1100°C after an exposure of 31 hr, accelerated attack occurred in those areas where the sample was in contact with the platinum support wire. In other areas the oxide was uniform in thickness and as yet showed no tendency toward large void formation or a duplex layer.

Various authors have noted that the onset of accelerated oxidation at high temperatures is accompanied by the formation of a duplex layer. It appears on the basis of this work that the development of the duplex layer is gradual and dependent on time and temperature. At 840° and 910°C for the times investigated in this study, the duplex layer appears to be developing slowly. Voids are not observed, but their presence on a micro scale is not precluded and may even be inferred by the early stages of duplex layer development as observed. Accelerated corrosion at these temperatures appears to be due to gross cracks developing in the oxide film. At higher temperatures and simultaneous with the appearance of voids in the oxide film, the duplex layer undergoes a more rapid development. The development of stoichiometric ZrO_2 as an outer

Table VI. Effect of pressure on oxide thickness on $\frac{1}{2}$ in. spheres oxidized for 64 hr at 910°C

Pressure, Torr	Average thickness and deviation, μ	Maximum, μ	Minimum, μ
1	35.5 \pm 0.6	36.5	34.8
14	35.1 \pm 0.6	36.0	34.0
100	36.3 \pm 1.0	38.5	35.2
730	37.3 \pm 0.7	39.2	35.9
730*	35.1 \pm 0.5	36.0	34.4

* $\frac{3}{4}$ -in. sphere.

layer is accompanied by an accelerated growth of the total oxide. It therefore appears that the outer stoichiometric layer becomes nonprotective.

Orientation effect.—The thickness of the oxide film formed on coarse grained zone refined zirconium oxidized at 910°C for 64 hr was found to vary somewhat from grain to grain. The variation of the oxidation rate of zirconium with orientation has been reported previously (3). Its persistence to the thick film region is noted in this study. Variation of thickness with orientation is much less pronounced for zirconium than for hafnium (12). In the latter case wide deviations from stoichiometry have been noted in those grains oxidizing more slowly. Thus, the oxidation rates may involve unequal rates of formation of vacancies from crystal faces of different orientations. This phenomenon is under further investigation in this laboratory using single crystal material.

Pressure.—One-half inch diameter spheres were oxidized at 910°C for 64 hr at pressures ranging from 1 to 730 Torr. Results of the oxide thickness measurements are given in Table VI which includes the average value, average deviation, and maximum and minimum values at each pressure. For comparison, data from the $\frac{3}{4}$ in. diameter sphere is listed. The variation in thickness from sample to sample appears to be within the experimental reproducibility, so that pressure in the range investigated does not affect the oxidation rate.

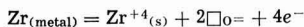
Surface preparation.—In order to determine the effect of surface preparation on film growth and total weight gain, spherical samples were oxidized in both the as-machined condition and as shot-blasted with fine-grit sand. Samples were oxidized at 840°C for 24 hr. The weight gain curve paralleled those of the chemically polished samples, but the ordinate was displaced higher by several per cent. Metallographic examination indicated that, with the exception of small protrusions at the surface, the oxide thickness was identical with that observed on chemically polished samples. The differences in weight gain must then be due to the small protrusions from the irregular surface which were oxidized during the initial stages of the oxidation. Therefore, at 840°C for times beyond the initial stages of the reaction, it does not appear that the surface treatment has any effect on the kinetics. However, the possibility cannot be excluded that at much later stages of oxidation the surface irregularities may act as sites for initiation of cracks in the film.

Initiation temperature.—Experiments were performed to determine whether there is an effect of exposing the sample to oxygen while at temperature as opposed to the technique used in nearly all of these experiments of allowing the sample to cool before admitting oxygen. At 840°C beyond the very early stages of the reaction (~ 15 min), the weight gain curves were identical.

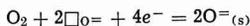
Mechanism.—Zirconium dioxide exhibits a complex dependence of conductivity on oxygen partial pressure (13, 14). Conduction is considered to be largely ionic with n-type conductivity predominating at low oxygen partial pressures ($< 10^{-20}$ atm) such as would exist within a sound oxide film growing on the metal substrate. Oxygen vacancies and possibly interstitials

are believed to be the mobile species. At higher oxygen partial pressures ($>10^{-8}$ atm) such as would be encountered in a cracked ZrO_2 film, the p-type oxide may predominate (14), and cation migration cannot be excluded.

The oxidation process is generally pictured as occurring by the formation of an oxygen ion vacancy at the metal/oxide interface



where $Zr_{(metal)}$ represents a zirconium atom in the metal lattice, $Zr^{+4}_{(s)}$ represents a Zr^{+4} ion on a lattice site in the oxide, and $\Box_{O=}$ represents an oxygen ion vacancy in the oxide lattice. The electrons may be bound to the oxygen vacancy, present as a defect associated with $Zr^{+3}_{(s)}$ ions, or mobile in the lattice. In order for oxidation to proceed, $\Box_{O=}$ and electrons must diffuse through the oxide to the oxygen/oxide interface where they are consumed in the reaction



where $O^{=}_{(s)}$ is an oxygen ion in the oxide lattice.

It is suggested here that the formation of voids at the metal/oxide interface encountered during oxidation at the higher temperatures of this study ($\approx 975^{\circ}C$) may be considered to result from a condensation of oxygen vacancies. It is also possible that at 840° and $910^{\circ}C$ voids are forming on a microscale too fine to be viewed with optical microscopy. These voids may act as diffusion blocks preventing the access of oxygen ions to the metal/oxide interface, thereby retarding the oxidation rate.

In the initial phase of oxidation the film is forming at an exceedingly rapid rate, leading to a highly defect-rich oxide. As time passes, the oxygen vacancies may cluster and eventually condense to form voids. This may occur most readily at the oxide/metal interface or at an inclusion if it is present to aid the nucleation. One then may consider oxidation to occur through an oxide containing blocked diffusion paths. At the higher temperatures where the voids occur on a gross scale, oxidation of the outer oxide toward the stoichiometric value becomes more complete, and the duplex layer more pronounced. The near stoichiometric outer layer is apparently nonprotective. This may be due to the fact that a p-n junction may develop within the oxide

at the meeting of the two oxide layers. The outer scale may then allow migration of Zr^{+4} ions which could account for its lack of protectiveness.

Any theory explaining the oxidation of zirconium and hafnium must account for the orientation dependence of the oxidation rate in the thick film region. For this reason, studies using single crystal material have been initiated in this laboratory. Further work on the structure and transport within the oxide films is also in order.

Acknowledgment

The author is again indebted to J. K. Litchfield for experimental assistance and suggestions through the course of this study; thanks are expressed to E. J. Moreau for extensive metallography. Valuable discussions on the diffusion equations were held with Drs. A. L. Loeb, S. H. Gelles, and G. Kemeny, and on nonstoichiometry with Dr. G. G. Libowitz.

Manuscript received Nov. 12, 1964. This paper was presented at the Washington Meeting, Oct. 11-15, 1964.

Any discussion of this paper will appear in a Discussion Section to be published in the December 1965 JOURNAL.

REFERENCES

1. G. R. Wallwork, W. W. Smeltzer, and C. J. Rosa, *Acta Met.*, **12**, 409 (1964).
2. C. J. Rosa and W. W. Smeltzer *ibid.*, **13**, 55 (1965).
3. J. P. Pemsler, *This Journal*, **111**, 381 (1964).
4. J. P. Pemsler, *J. Nuclear Materials*, **7**, 16 (1962).
5. J. P. Pemsler, *This Journal*, **105**, 315 (1958).
6. M. W. Mallett, W. M. Albrecht, and P. R. Wilson, *ibid.*, **106**, 181 (1959).
7. M. Davis, K. R. Montgomery, and J. Standing, *J. Inst. Metals*, **89**, 172 (1961).
8. G. Sainfort, R. Jacquesson, and P. Laurent, "Colloquium on Diffusion in the Solid State," C. E. N. Saclay (1958), North Holland Publishing Co.
9. J. N. Chirigos, "The Use of Microhardness in the Determination of the Diffusivity of Oxygen in Alpha Zirconium," Report WAPD-TM-306 (1962).
10. R. F. Domagala and D. J. McPherson, *Trans. AIME*, **200**, 238 (1954).
11. E. Gebhardt, H.-D. Seghezzi, and W. Dürschnabel, *J. Nuclear Materials*, **4**, 255 (1961).
12. J. P. Pemsler, *This Journal*, **111**, 1339 (1964).
13. P. Kofstad and D. J. Ruzicka, *ibid.*, **110**, 181 (1963).
14. N. M. Tallan, *J. Am. Ceram. Soc.*, **47**, 635 (1964).

Tantalum Films Deposited by Asymmetric A-C Sputtering

F. Vratny and D. J. Harrington

Bell Telephone Laboratories, Incorporated, Murray Hill, New Jersey

ABSTRACT

The new technique of asymmetric a-c sputtering has been evaluated for the deposition of tantalum films in argon, oxygen-argon, and nitrogen-argon gas mixtures. This method utilizes a lower sputtering potential on the tantalum substrate holder every half cycle compared to the potential on the tantalum cathode. At an optimum current ratio, tantalum films of three to five times that of bulk resistivity are obtained compared to twenty to forty times bulk resistivity for normal d-c glow discharge sputtering. The reactive sputtering experiments confirm that the normal high resistivity of sputtered tantalum films are caused by impurities gettered during the deposition and that the greater tolerance to reactive gas pressure with asymmetric a-c sputtering may be due to ion and electron bombardment during deposition. Further work is required to confirm this latter supposition.

Present methods for the deposition of tantalum films rely upon evaporation methods (1,2), i.e., electron beam evaporation, or d-c sputtering from a tantalum cathode (3-6). With some exceptions, the sputtering technique when used with initial background pressures of 10^{-6} Torr produces films with specific resistivities

of 100 to 300 μ -ohm-cm and temperature coefficients of resistance in the range of ± 200 ppm/ $^{\circ}C$ (7). The high resistivity in sputtered films is indicative of 5-10 a/o (atomic per cent) of oxygen impurity (6) assuming the latter is the prime component gettered during deposition. Evaporated films have been obtained with

values of $15 \mu\text{-ohm-cm}$ and $+3000 \text{ ppm}/^\circ\text{C}$ (1, 2, 3, 8) under conditions of ultra high vacuum and/or very high deposition rates. By careful control over sputtering variables it has been possible to obtain sputtered films with resistivities of only $50 \mu\text{-ohm-cm}$ and temperature coefficients of $+1500 \text{ ppm}/^\circ\text{C}$ (4, 6) although the basic criteria for obtaining such films routinely have not been rigorously established.

The advent of asymmetric a-c sputtering (9-11) offers the possibility of obtaining routinely tantalum films of high purity without the necessity of ultra high vacuum techniques. Frerichs (9-11) reported that superconducting tantalum films were obtained with a transition region from 4.45° to 4.3°K , compared to a value of 4.38°C for bulk tantalum. The purity of the film was ascribed to argon bombardment of the surface of the sample and a decrease in rate of incorporation of residual gases from the vacuum system.

The sputtering of tantalum has provided an important method of preparing thin film components and integrated circuits (12-14) especially when utilized with reactive gases to deposit a tantalum nitride film. The asymmetric a-c sputtering technique could provide a means of obtaining relatively pure films which would serve as a reproducible starting material for reactive sputtering, provided reactive gas molecules can be incorporated in the film under asymmetric a-c deposition conditions. A comparison of the properties of films prepared by reactive sputtering both with a normal d-c and the asymmetric a-c method should provide a pertinent test of the proposed method of purification.

Method

Asymmetric a-c sputtering is performed by applying a partially rectified 60 cycle a-c potential to two identical tantalum electrodes. The substrate is placed on the electrode with the lower bombarding potential. In analogy with the geometry used for film deposition in normal d-c sputtering, the latter electrode, the substrate electrode, will be designated the anode in this paper. With a completely symmetrical voltage wave form, the anode and cathode collect equal numbers of energetic argon ions, and no net deposition occurs. However, by using a smaller average potential (E_2) at the substrate electrode (see Fig. 1) more tantalum arrives from the cathode than can be removed by ion bombardment at the anode. Concurrent with the ion motion in the plasma there is also electron transport. This is indicated by curve C which represents the inverse of curve B. Thus, if curve B represents the field affecting the ion density at the substrate and B' represents the field affecting the ion density at the cathode, then curve C represents, respectively, the field affecting the electron density at the cathode while C' represents the field affecting the electron density at the substrate. Frerichs (9) reported that a favorable degree of asymmetry is a cathode to anode current ratio of five to ten. To obtain a wide range of anode to cathode current ratio a supply was used with silicon rectifiers and a variable resistance (R) in one arm of a bridge network (Fig. 2). The output from a high-voltage transformer is placed across the anode and the current limiting network which in turn is connected to the cathode. The cathode current I_c , is controlled by the

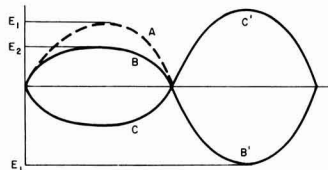


Fig. 1. A typical cathode wave form: (A) normal; (B) asymmetric, cathode potential, E_2 less E_1 ; (C) substrate potential.

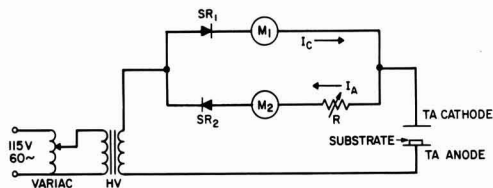


Fig. 2. Asymmetric a-c power supply. SR1, SR2, high voltage diodes; M1, Mw, milliammeter; R, variable resistance 2K to 1 meg; HV, high voltage transformer 10 kv.

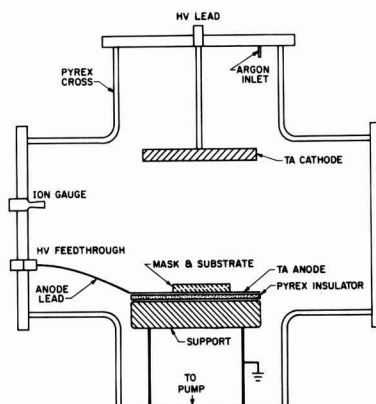


Fig. 3. Schematic of the sputtering chamber

plasma impedance and a small resistive drop across the diodes while the anode current, I_A , is diminished further by the resistance, R. By varying the resistance, R, a range of anode to cathode current ratios (I_A/I_c) is obtained of approximately 0.05 to 0.35.

The cathode and anode were high-purity tantalum plates 4 in. in diameter and $\frac{1}{4}$ in. thick. These were mounted in a 6 in. ID "Pyrex-cross" sputtering chamber (Fig. 3). The cathode was suspended from a high voltage feedthrough while the anode was mounted on a Pyrex spacer. All experiments were performed at a cathode potential of 4 kv and a cathode current density of 0.25 ma/cm^2 at an argon pressure of 20×10^{-3} Torr. Tantalum was deposited on 1 by 3 in. Corning 7059 glass through mechanical masks covered by a thin layer of tantalum. These substrates were cleaned by a succession of washes in detergents, water, hydrogen peroxide, and deionized water. They were dried in a nitrogen stream at 110°C and placed in the vacuum chamber. The system was evacuated by means of a 300 l/sec diffusion pump with a liquid nitrogen cooled baffle. An ultimate pressure of 2×10^{-6} Torr and a nominal leak rate of 0.05 l atm/sec are typical for this machine. Tantalum films with specific resistivities of $150\text{-}200 \mu\text{-ohm-cm}$ and temperature coefficients of resistance of $\pm 200 \text{ ppm}/^\circ\text{C}$ are conventionally produced by d-c sputtering in this system

Results

In the process of asymmetric a-c sputtering argon ion bombardment occurs at both the cathode and anode. If we consider the two extreme cases, it is evident that for an identical potential at both electrodes there will be no deposition at the anode, yet due to the high intensity of ion bombardment this condition will produce the maximum cleaning at the surface. Correspondingly, for normal d-c cathode sputtering the deposition rate will be large at the anode, yet due to minimal bombardment, the substrate will be ineffectively cleaned. Between these two extremes there is a compromise of effective deposition and cleaning. To

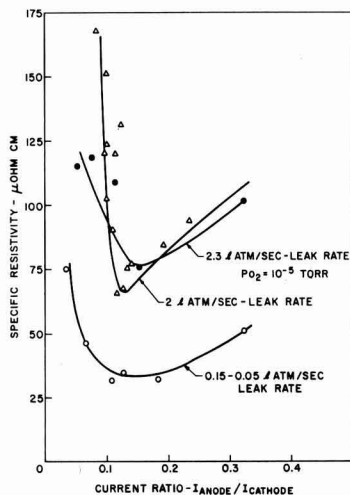


Fig. 4. Specific resistivity as a function of current ratio

explore this method of sputtering, the deposition rate, resistivity, and temperature coefficient of tantalum films were evaluated as a function of the current ratio to determine the optimum conditions. Due to the direct correlation between resistivity and impurity level (6) the specific resistivity can also be used as an indication of the purity of the deposited film.

The measured deposition rate, using a constant cathode potential of 4 kv (rms) was a direct function of the current asymmetry ratio. The sputtering pressure was 20μ while the pressure before sputtering was typically $\sim 2 \times 10^{-6}$ Torr. At an anode to cathode current ratio of 0.25 the deposition rate was ~ 30 A/min, and at a current ratio of 0.1 it was ~ 60 A/min. Further data indicated that a linear correlation exists between the deposition rate and the difference in power (Δw , in watts) supplied to the cathode and anode (Eq. [1]).

$$\text{Deposition rate (A/min)} = 5.1 (\pm 0.6) (\Delta w) - 100 (\pm 10) \quad [1]$$

This equation shows that for a constant flux of tantalum atoms arriving from the cathode, less tantalum remains deposited on the substrate with increasing power supplied to the anode. This result tends to confirm that bombardment-sputtering occurs at the anode with increasing current ratio.

The increased bombardment at the anode reflects itself in increased purity of the resultant tantalum film as manifested in the resistivity and temperature coefficient of resistance despite the lower deposition rate. The resistivity drops to a minimum value with increasing current ratio from 0 to 0.15 (Fig 4) while further anode current beyond a ratio of 0.15 causes an increase in resistivity. The resistivity change at a background pressure of $\sim 2.5 \times 10^{-6}$ Torr (0.05 to 0.15 liter-atm/sec virtual leak) from $200 \mu\text{-ohm-cm}$ for d-c sputtering to a minimum of $\sim 37 \mu\text{-ohm-cm}$ represents a change from ~ 10 a/o oxygen to ~ 3 a/o oxygen if the change in resistivity is due to this impurity (6). The increase in resistivity with anode current ratio above 0.15 will be discussed later.

The change in resistivity with increasing current ratio to ~ 0.15 exhibits a sensitivity to residual impurities in the vacuum system. At a leak rate of residual gases of ~ 2 liter-atm/sec the resistivity minimum corresponds to $\sim 65 \mu\text{-ohm-cm}$ while a deliberate oxygen leak rate of 10^{-5} Torr (2.3 liter-atm/sec) gives a nearly identical current ratio profile with a resistivity minimum at $\sim 75 \mu\text{-ohm-cm}$. The temperature coefficient of resistance of these films similarly exhibits a

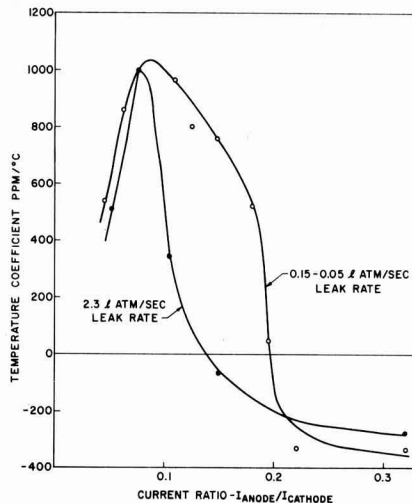


Fig. 5. Temperature coefficient of resistance as a function of current ratio.

sensitivity to the current ratio and gaseous impurity (Fig. 5). It is noteworthy that the maxima in the temperature coefficient curve occur at a lower current ratio than the minima in the resistivity curve. This difference indicates that the film properties that determine the resistivity and temperature coefficient have a different dependence on the anode-cathode current ratio.

It is evident that the ability to obtain low resistivity films by this technique is a function of the level of the residual gases in the system during sputtering. Thus, it is possible to sputter reactively by this method. The main advantage of this technique is that it provides a reproducible low resistivity film as a starting point for the controlled modification of its electrical properties. During reactive sputtering it would have the effect of diluting the contribution of undesired reactive gases in the system. An evaluation of the process of reactive sputtering and a study of the quality of the resultant film components have been carried out. Gerstenberg (6) and Pendergast (15) have prepared tantalum nitride and tantalum oxide films. The tantalum oxide films exhibit a monotonic increase in resistivity with increasing oxygen content and a monotonic decrease in the temperature coefficient. The tantalum nitride films have a specific resistivity of $200 \mu\text{-ohm-cm}$ which is nearly independent of the nitrogen partial pressure over a pressure range corresponding to the formation of the compound Ta_2N and TaN . In the same nitrogen partial pressure range, the temperature coefficient of resistance has a value of -50 to -100 ppm/°C. Due to the inherent leak rate of vacuum systems and other d-c deposition variables it has not been possible to completely reproduce the exact pressure dependence reported by Gerstenberg (6) although the Ta_2N and TaN phases always occur with approximately the same electrical properties.

Experiments were performed at varying nitrogen and oxygen partial pressure in argon to assess the suitability of the asymmetric a-c process for controlled deposition by reactive sputtering. Reactive sputtering was carried out at a current ratio of 0.13, a cathode potential of 4 kv and cathode current of 20 ma (~ 0.25 ma/cm²) at an argon pressure of 20μ . Sputtering in oxygen-argon gas mixtures produced an increase in resistivity with increasing oxygen partial pressure (Fig. 6) for both the a-c and d-c technique. However, the resistivity is always lower at a given oxygen pressure in the a-c sputtering technique. As an example, at a background pressure of 2×10^{-6} Torr there is a re-

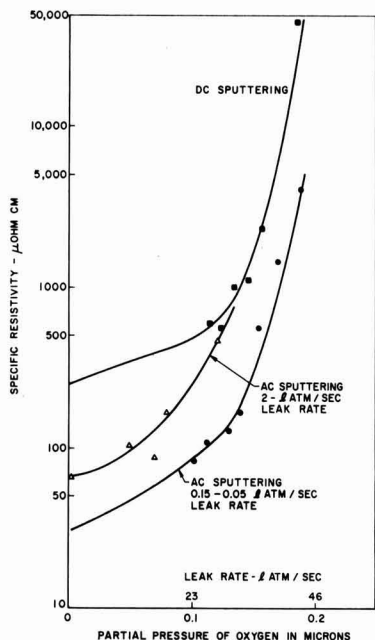


Fig. 6. Specific resistivity as a function of oxygen partial pressure

sistivity differential of $\sim 200 \mu\text{-ohm-cm}$. This constitutes a decreased sensitivity to oxygen of 4-7 a/o (6). At higher oxygen pressures the curves tend to merge. This difference is also apparent in the temperature coefficient of resistance for these films. They are generally higher by 600 to 800 ppm/ $^{\circ}\text{C}$ for the asymmetric a-c method (Fig. 7). Correspondingly, it was possible to sputter in argon-nitrogen gas mixtures and reproduce d-c results which were obtained only by using extreme care to control sputtering parameters and residual gases (see Fig. 8 and 9).

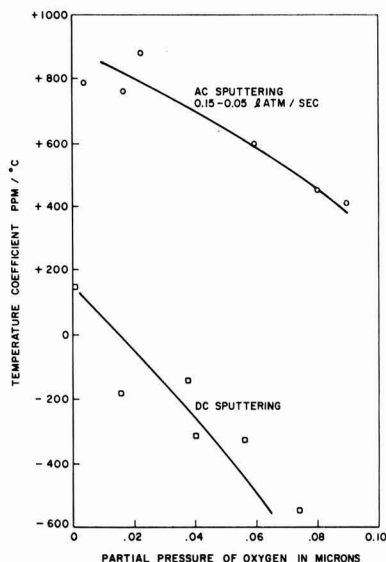


Fig. 7. Temperature coefficient of resistance as a function of oxygen partial pressure.

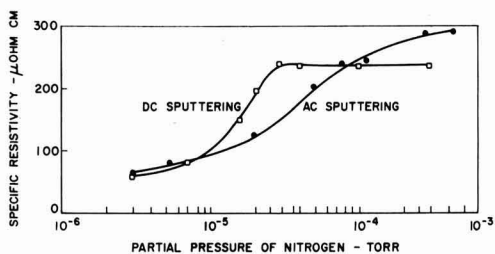


Fig. 8. Specific resistivity as a function of nitrogen partial pressure

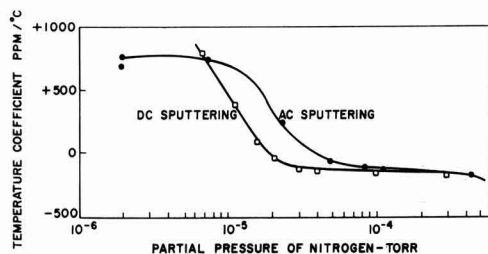


Fig. 9. Temperature coefficient of resistance as a function of nitrogen partial pressure.

Discussion

The basic model employed by Frerichs (9-11) to explain purification of films deposited by the asymmetric a-c sputtering technique is the argon ion bombardment of the film during deposition. The degree of cleaning given the depositing film on the anode is determined by the degree of current asymmetry. The latter factor establishes the ion flux to the surface while the energy and flux density of incident ions determines the probability of removal of matter from the film. An additional feature which we will consider below is the effect of electron bombardment of the substrate.

In considering a model of film cleaning by argon ion bombardment it is necessary to evaluate three factors: the probability of collision between the individual incident ions and impurity atoms; the fraction of energy available to an impurity atom as a result of collision; and the probability of desorption of an impurity atom. If we assume that an impurity atom has the same cross section as a tantalum atom, we can calculate the probability of collision between the incident ions and atoms on the surface. In this way we can obtain an estimate of the probability of reducing an impurity level (excluding secondary processes).

When tantalum is deposited at a rate of 50 $\text{\AA}/\text{min}$, the arrival rate or the collision rate of tantalum is $\sim 6 \times 10^{14}$ at./sec/cm 2 while the impurity level at a background pressure of 10^{-6} Torr and 300 $^{\circ}\text{K}$ is 3.6×10^{13} molecules/sec/cm 2 (taken for the case of oxygen 1) with a sticking coefficient of 0.1. Although it is known that sticking coefficients can be as large as 1.0 for fresh reactive surfaces (17) and as small as 10^{-5} for dirty surfaces (18) or physically adsorbed states at high temperatures (19). For physically adsorbed states at modest temperatures or clean surfaces a sticking coefficient of 0.1 is a reasonable approximation (17,19). For this sticking coefficient, the impurity level corresponds to about 12 a/o of monatomic oxygen which will be incorporated in the film. Thus, the total flux corresponds to 88% tantalum and 12% impurity. Since an impurity atom (as oxygen) which is present at low surface coverage will probably sit on a

1 It is recognized that many residuals exist in conventional vacuum systems. In the system under consideration it is estimated that the residuals are made up of 20% oxygen, 60% nitrogen, 5% carbon as CH_4 and CO , 15% others. During deposition the oxygen level drops to a very low level, nitrogen drops by about 20% and the hydrogen level increases to $\sim 10^{-6}$ Torr (18).

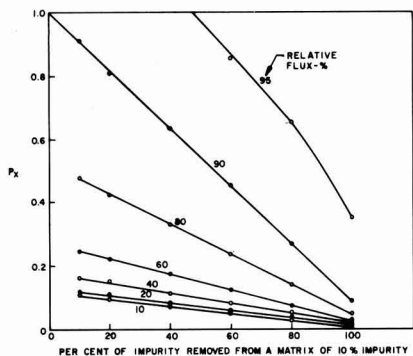


Fig. 10. Probability of surface cleaning as a function of relative incident flux.

tantalum lattice site there will be an equal probability of collision between an argon ion and either tantalum or oxygen assuming equal cross section. With the initial assumption that an impurity atom is the same size as a tantalum atom and occupies a random tantalum lattice site the probability of collision between an argon ion and surface impurity was calculated for a variable argon ion flux and for a constant surface density of 10% impurity atoms and 90% tantalum atoms (Fig. 10). The probability of collision between the argon ion flux and the surface density of impurity flux is large above a relative ion flux of 92% while the probability drops appreciably at lower flux densities. If the collision probability is interpreted in terms of removal then the probability of removal of 10% of the impurities, i.e., reducing the total level from 10 to 9% is appreciable in the range of 95-100% relative ion flux, but decreases rapidly as the flux density decreases.

In addition to the collision probability it is necessary to consider the relative size of the impurity atom and tantalum as well as the probability of their removal. It is known that the relative cross section of oxygen and tantalum is quite different and that the cross section may vary with the energy of the incident ion (20). It may be estimated that at rest energy an oxygen ion has a larger relative cross section than tantalum by 5.45 (21). As a result, the collision probability would be larger by a proportionate factor. On impact, an argon ion is able to impart $\sim 98\%$ of its energy to an oxygen molecule while tantalum will receive roughly 59% of the energy of the incident argon ion as a result of momentum conservation in a diatomic collision. However, this energy is distributed in the lattice. It can be approximated that tantalum has a sputtering threshold between 25 and 30v (22) with reported values as large as 120v (23-25). The lattice surface displacement energy is ~ 4.79 ev (26) while oxygen on tantalum has a dissociation energy of roughly 9 ev (27). If the lattice energies and momentum conservation processes are interpreted in terms of sputtering yields, we can combine energy transfer and surface desorption effects and estimate (28) a relative sputtering ratio (S_O/S_{Ta}) of 0.78 with a range of 0.35 to 1.5 depending on the upper and lower limits of the threshold. If we include the relative cross section of oxygen and tantalum (5.45), we obtain a sputtering ratio S_O/S_{Ta} of 4.25 with a range from ~ 2.1 to 8.5, i.e., oxygen desorption is more probable. When this is applied to the collision probability (Fig. 10) we may see that a 60% relative ion flux corrected by the above sputtering ratio will be as effective as 92% relative flux i.e., a single projectile will be 4.25 times as productive on oxygen as on tantalum.

In establishing an argon ion flux to the sample, it is evident that argon can respond to the 60 cycle changes in the anode-cathode potential as it is able to

traverse 8-16 cm (29-34) between these changes. The measured current ratio of anode current to cathode current then gives an indication of the relative degree of surface bombardment. In Fig. 4 we initially have 10 a/o impurities at a zero current ratio and 2-3 a/o at the resistivity minima or 70 to 80% removal of impurities. At this point the argon flux is $\sim 1.5-3 \times 10^{14}$ or 25-50% of the deposition flux. This corresponds to a collision probability with a 10% surface impurities coverage of $\sim 0.1-0.42$. When modified by the difference in sputtering yield this represents a probability of at least 0.2 but no more than 3 with a mean value of 0.8. This is a marginal proof of effective cleaning by argon bombardment for the most probable yield is less than one. Further, this model also requires a continuous improvement in resistivity at a higher asymmetry current ratio due to the enhancement of the argon ion density. However, we obtain an increase in the film resistivity at a higher anode current as seen by the rise in resistivity above a current ratio of 0.15.

Because of these anomalies we feel this deposition mechanism is inadequate. This may suggest a coexisting mechanism of argon incorporation at high argon ion flux density, for it is known that a bombarding particle will have an effective penetration depth from about 2 to 200 Å/kev (35). This produces incorporation of the neutralized species at a rate of 10^{14} to 10^{15} at./cm²/kev (36) or between 1 and 10% of the deposition flux. Films analyzed for argon place the argon content in this range (37). This will reduce the effective electron mean free path and thus increase the resistivity and reduce the temperature coefficient. These factors are insufficient to explain the ability of the incident argon ion flux to clean the sample to the implied degree exhibited by the resistivity current-ratio profile of Fig. 4. An additional mechanism we wish to propose is the clean up by the presence of an intense electron flux at the substrate surface. It should be noted in Fig. 1 that as the potential alternates between the cathode and substrate the argon ion and electron flux density to the substrate also change. In the first half of the potential cycle, the argon ion flux to the substrate is low while the electron flux to the cathode is also low. In the latter half of the potential cycle the electron flux to the substrate is large while the argon ion flux to the cathode is also large. It is felt that the electron flux to the substrate contributes to an additional degree of cleaning. This phenomena has been observed by Peterman (38), Moore (39), and Redhead (40). Further work is in progress to clarify the deposition mechanism in asymmetric a-c sputtering (41).

Conclusions

Our results agree with earlier work which has demonstrated that deposition of thin films by asymmetrical a-c sputtering can lead to an improvement in film purity as demonstrated by the lower resistivity and higher temperature coefficients of resistance.

It was also pointed out that the background pressure has a pronounced effect on the ultimate purity of the deposited film. This was demonstrated by the variation in resistivity and temperature coefficient of resistance as a function of doping conditions.

It was proposed that the removal of these impurities is due to argon ion bombardment. This is suggested by the reduction in deposition rate which occurs at high anode currents. Secondary mechanisms are proposed to expand on this mechanism. One proposal was that the increase in resistivity at higher asymmetry ratio I_A/I_C is due to argon incorporation. A further proposal is that electrons which are generated in the plasma play a significant role in the deposition process.

It has been shown that deposition of thin films by a-c asymmetric sputtering can offer a reproducible base for controlled reactive sputtering. Evaluation of passive components prepared by this technique is presently in progress and appears to be favorable.

Manuscript received Sept. 29, 1964. This paper was presented at the Pittsburgh Meeting, April 15-18, 1964.

Any discussion of this paper will appear in a Discussion Section to be published in the December 1965 JOURNAL.

REFERENCES

- J. F. Marchand and F. A. Venema, *Phillips Res. Repts.*, **14**, 427 (1959).
- D. Gerstenberg and P. Hall, *This Journal*, **111**, 936 (1964).
- R. W. Berry and D. J. Sloan, *Proc. IRE*, **47**, 1070 (1959).
- C. Altman, 9th Proc. Amer. Vacuum Society (1962).
- N. W. Silcox and L. I. Maisel, *This Journal*, **109**, 1151 (1962).
- D. Gerstenberg and C. J. Calbick, *J. Appl. Phys.*, **35-2**, 402 (1964).
- Landolt-Boernstein, *Elektrische Eigenschaften I*, Vol. II, No. 6, p. 4, Springer Verlag, Berlin (1959).
- C. A. Neugebauer and R. A. Ekvall, *J. Appl. Phys.*, **35**, 547 (1964).
- R. Frerichs, *ibid.*, **33**, 1898 (1962).
- R. Frerichs and C. J. Kircher, Proc. 8th International Conf. on Low Temperature Physics, London, September, 1962.
- C. J. Kircher, Late News Paper presented at the Pittsburgh Meeting of the Society, April, 1963; R. Frerichs and C. J. Kircher, *J. Appl. Phys.*, **34**, 3541 (1963).
- D. A. McLean, *Wescon Conf. Proc.* 1959.
- R. W. Berry and N. Schwartz, *Proc. Natl. Conv. Mil. Elect.*, **1960**, p. 214.
- D. Gerstenberg and E. H. Mayer, *Proc. Elect. Comp. Conf.*, **1962**, p. 57.
- W. Pendergast, Paper presented at the Pittsburgh Meeting of the Society, April 1963; Extended Abstracts.
- J. Sosniak, Private communication
- A. E. J. Eggleton, F. C. Tompkins, and D. W. B. Wanford, *Proc. Roy. Soc.*, **A213**, 266 (1952).
- I. Langmuir, *J. Am. Chem. Soc.*, **37**, 1139 (1915).
- Buritz, Varnerin, *Trans. Faraday Soc.*, **284** (1961).
- J. B. Hasted, *Proc. Roy. Soc.*, **A205**, 421 (1951).
- L. Pauling, "Nature of the Chemical Bond," Cornell University Press, (1959); *J. Am. Chem. Soc.*, **49**, 765 (1927); W. H. Achariassen, *Z. Krist.*, **80**, 137 (1931); M. L. Neuberger, *ibid.*, **83**, 1 (1936).
- G. K. Wehner, Proc. 5th International Conf. on Ionization Phenomena in Gases, p. 1141 (1961).
- G. K. Wehner, *Phys. Rev.*, **93**, 633 (1954).
- G. K. Wehner, Sputtering Yield Data in the 100 to 600 e.v. Energy Range, General Mills Rept. #2309, July 15, 1962.
- E. B. Henschke, *Phys. Rev.*, **121**, 1286 (1961).
- R. L. Eager and D. B. Langmuir, *ibid.*, **89**, 911, (1953).
- B. W. M. Trapnell, "Chemisorption P100," W. E. Garner, Editor, Butterworth (1957).
- R. S. Pease, *Scuola Intern. Fisica Corso, XIII SETT*, 151 to 165 (1959).
- M. A. Biondi and L. M. Chanin, *Phys. Rev.*, **94**, 910 (1954).
- J. A. Hornbeck, *ibid.*, **84**, 615 (1951).
- R. A. Nielsen, *ibid.*, **50**, 950 (1936).
- L. Colli and U. Facchini, *Rev. Sci. Instr.*, **23**, 39 (1952).
- H. D. Hagstrum and J. T. Tate, *Phys. Rev.*, **59**, 354 (1941); J. T. Tate and P. T. Smith, **39**, 270 (1932).
- G. H. Kinchin and R. S. Pease, *Repts. Prog. in Phys.*, **18**, 1 (1955).
- B. Johnson, J. L. Lineweaver, and J. T. Kerr, *J. Appl. Phys.*, **31**, 51 (1950).
- J. S. Colligan, *Vacuum*, **11**, 5/6, 272 (1961).
- Analysis performed by W. Guldner of this Laboratory, see: *Anal. Chem.*, **35**, 1744 (1963); Proc. 1964 Electronic Comp. Conf., p. 9-13, Washington, D. C., May 1964, Bell Telephone Monograph 4803.
- L. A. Peterman, *Nuovo Aimento*, 1-2 suppl., p. 201 (1963); *Trans. Amer. Vac. Soc.* (1962).
- G. E. Moore, *Trans. Amer. Vac. Soc.*, **16** (1959); *J. Appl. Phys.*, **32**, 124 (1961).
- P. A. Redhead, *Appl. Phys. Letters*, **4-9**, 166 (1964); *Can. J. Phys.*, **42**, 886 (1964).
- F. Vratny and N. Schwartz, Deposition of Tantalum Films by Substrate Electrode Bias Sputtering, 11th National Symposium of the American Vacuum Society, October 1, 1964.

Vapor Transport Reactions Related to Halophosphate Phosphor Formation

Jacob G. Rabatin and George R. Gillooly

Luminescent Materials Laboratory, General Electric Company, Cleveland, Ohio

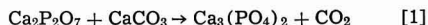
ABSTRACT

A double crucible technique has demonstrated that the principal phosphor forming reactions may involve particle-particle interaction between $\text{Ca}_2\text{P}_2\text{O}_7$ and CaF_2 leading to direct formation of apatite and POF_3 . The POF_3 , or vapors of similar composition, react with CaCO_3 also forming apatite. The transport of vapors containing fluorine, phosphorus, oxygen, and antimony has been demonstrated. Activation of the phosphor above 1000°C occurs by a reaction of Sb_2O_4 vapor with apatite.

The ease of formation of apatites from solid-state reactants commonly used in the preparation of halophosphate phosphors belies the complexity of the system from which these products are derived. Some general reactions of the usual starting materials, investigated by the use of differential thermal analyses and thermogravimetric analyses, have been reported along with isolated chemical and x-ray diffraction studies (1-6). These data reveal such a multiplicity of possible intermediate reactions as to preclude interpretation of the kinetics or mechanism of apatite formation. Thus it is sometimes assumed that apatite formation and activation proceed by solid-state diffusion processes (7, 4).

Based on earlier studies (8, 9) it has been postulated that, with the usual starting material, CaHPO_4 , CaCO_3 , CaF_2 , CaCl_2 , etc., halophosphates form by a two-step

solid-state process. In the first step, $\text{Ca}_3(\text{PO}_4)_2$ is formed by the reaction



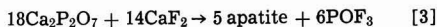
It is further assumed that CaCO_3 dissociates to CaO before reaction [1] begins. The subsequent apatite-forming reaction is also a solid-solid type, namely;



Mixed apatites can be obtained by varying any of the above ingredients (8, 9).

The possibility of vapor transport as a mechanism accelerating apatite formation was first indicated by the work of Daubree (10) who obtained apatite by passing vapor of phosphorus trichloride over red-hot lime. More recently, Montel (11) has studied in detail

the reaction between $\text{Ca}_2\text{P}_2\text{O}_7$ and CaF_2 showing that apatite and the vapor, POF_3 , are the two products according to the reaction



Since both $\text{Ca}_2\text{P}_2\text{O}_7$ (formed by low-temperature decomposition of CaHPO_4) and CaF_2 are normally employed as solids in the manufacture of halophosphate phosphors, the presence of POF_3 or a vapor of similar composition may play a role during the synthesis. The present study further indicates that the vapor transport of P, O, Sb, and halogens does play an important part in the formation of halophosphate phosphors.

Methods

Two simple techniques were used for the studies reported herein. The first involved the use of a small crucible placed inside a larger covered crucible as is illustrated in Fig. 1. Firings were made at various temperatures and for several times. Appropriate mixtures were placed in each crucible, thus permitting reaction between crucible contents only by vapor transport mechanisms. As indicated by undisturbed surfaces, there was no evidence in any case of solid material transfer by gas entrainment. Further, in most cases no evidence for a liquid phase was found; thus any possibility of liquid creep from one vessel to another can be discounted.

After firing, the contents of each crucible were identified by standard x-ray diffraction methods using an XRD-5 GE x-ray diffraction apparatus. ASTM x-ray data file together with comparisons of original x-ray patterns were used to identify the various phases present. Although this technique is qualitative, since some vapor may escape, the appropriate choice of reactants and trapping materials enables definitive demonstration of vapor transport from one crucible to the other. Relative line intensities of the x-ray diffraction patterns were used to estimate the amounts of the products present.

The second technique makes use of a quartz tube with a constriction at the center which allows the flow of gas from one compartment to the other. A quartz wool plug was also placed in the constriction. Appropriate materials were placed in each compartment; then the tube was evacuated and sealed. Firings were also performed for various times and temperatures. After firing, the products were examined by x-ray diffraction and chemical methods. Since this is a closed system, quantitative data can be obtained about vapor transport and mechanisms.

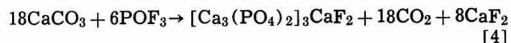
Results and Discussion

Apatite Forming Reactions

Reaction of $\text{Ca}_2\text{P}_2\text{O}_7$ with CaF_2 .—In order to confirm Montel's (11) work, several proportions of $\text{Ca}_2\text{P}_2\text{O}_7$ and CaF_2 were blended and fired at temperatures from 700° to 1100°C. The major product in every case was fluorapatite. When excess $\text{Ca}_2\text{P}_2\text{O}_7$ was used over that shown in reaction [3], x-ray diffraction showed the presence of $\text{Ca}_2\text{P}_2\text{O}_7$. When CaF_2 was used in excess

of that shown in reaction [3], CaF_2 was present in the product.

To show the presence of POF_3 (or vapors of similar composition) as one of the products of reaction [3] the following double crucible experiment was performed: The outer crucible contained Montel's mixture (reaction [3]); the inner crucible contained CaCO_3 . After firing at 1000°C for 1 hr, the product in the outer crucible was fluorapatite. The products of the inner crucible were fluorapatite and CaF_2 . It can be readily concluded that F, O, and P were all transported to the inner crucible where the most probable reaction was



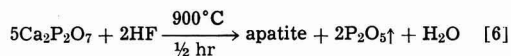
The product of the outer crucible was fluorapatite as expected from Montel's reaction (reaction [3]). If reactions [3] and [4] are combined and divided by 6 the following equation results.



Reaction [5] has the usual proportions of reactants used in phosphor formulations.

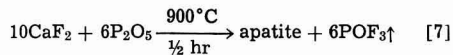
When the mixture for reaction [5] was placed in the outer crucible and CaCO_3 was placed in the inner crucible, on heating 1 hr at 1000°C, the products in the inner crucible were CaO and a trace of CaF_2 . These results indicate that, in an intimate mixture of the reactants, the vapors liberated by the solid-solid reaction of $\text{Ca}_2\text{P}_2\text{O}_7$ with CaF_2 will react quickly and completely with the nearest CaCO_3 . Thus no vapor escapes to react with the CaCO_3 in the inner crucible.

Reaction of HF with $\text{Ca}_2\text{P}_2\text{O}_7$.—Since hydrolysis of POF_3 may occur to some extent and, thus, free HF and P_2O_5 may be reactants, the following double crucible experiment was performed. $\text{Ca}_2\text{P}_2\text{O}_7$ was placed in the outer crucible, and in the inner inverted crucible NH_4HF_2 (as a source of HF) was placed. The crucibles were heated for ½ hr at 900°C, and the products of the outer crucible were examined (the inner crucible was empty because of the volatility of NH_4HF_2). Both unreacted $\text{Ca}_2\text{P}_2\text{O}_7$ and fluorapatite were present. The following reaction is proposed.



Vapor-solid reactions of this type would be expected to lead to a more rapid and complete dispersion of reactants than the usual solid-solid diffusion processes.

Reaction of P_2O_5 with CaF_2 .—When the outer crucible containing CaF_2 and inner inverted crucible containing $(\text{NH}_4)_2\text{HPO}_4$ (as source of P_2O_5) were heated ½ hr at 900°C, the products of the outer crucible were fluorapatite and some unreacted CaF_2 . The reaction leading to apatite formation is in balanced form



This reaction along with [4] and [6] is of the gas-solid type. The liberation of POF_3 by this reaction would lead to a further repeat of reaction [4] wherever POF_3 came in contact with CaCO_3 . The fact that a gaseous phosphorus-fluoride product did form according to reaction [7] was demonstrated by the use of a third small crucible containing CaCO_3 placed in the crucible setup mentioned above. After heating at 900°C for ½ hr, this third crucible now contained CaF_2 and $\text{Ca}_2\text{P}_2\text{O}_7$ with some apatite again illustrating the vapor transport of P and F.

Reaction of POF_3 with $\text{Ca}_3(\text{PO}_4)_2$.—Since there is a possibility that in a phosphor mix some $\text{Ca}_2(\text{PO}_4)_2$ may form according to reaction [1], the following double crucible experiment was performed. The outer crucible contained a mixture of $\text{Ca}_2\text{P}_2\text{O}_7$ and CaF_2 as a source of POF_3 (reaction [3]). The inner crucible con-

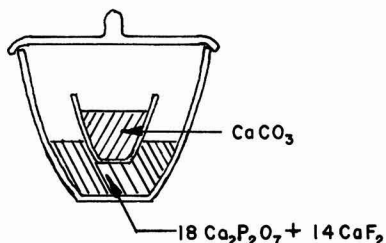


Fig. 1. Double crucible arrangement for vapor transport experiments

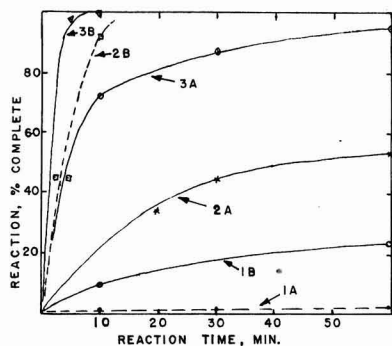
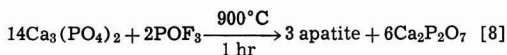


Fig. 2. Rate of formation of products at A, 800°C; B, 900°C for the reactions.

1. $\text{Ca}_2\text{P}_2\text{O}_7 + \text{CaCO}_3 \rightarrow \text{Ca}_3(\text{PO}_4)_2$
2. $3\text{Ca}_3(\text{PO}_4)_2 + \text{CaF}_2 \rightarrow \text{apatite}$
3. $18\text{Ca}_2\text{P}_2\text{O}_7 + 14\text{CaF}_2 \rightarrow 5 \text{apatite}$

tained $\text{Ca}_3(\text{PO}_4)_2$. The setup was heated 1 hr at 900°C. The products of the inner crucible were fluorapatite and $\text{Ca}_2\text{P}_2\text{O}_7$. The probable reaction is



These results once again illustrate the great tendency toward apatite formation whenever the ions Ca^{+2} , P^{+5} , O^- , and F^- are present.

Reaction Rates for Apatite Formation

It may be argued that reactions [3], [4], [6], [7], and [8] occur only under very special conditions, but that in actual practice apatite forms only by a stepwise process involving reactions [1] and [2]. To answer this more definitely, kinetic studies were performed on mixtures according to reactions [1], [2], and [3] at 800° and 900°C. Samples were heated in 5 ml crucibles at these temperatures for the desired times. The products were analyzed by standard x-ray diffraction techniques involving the measurement of line intensities. The completely reacted product line intensities were used for the 100% values of apatite for reactions [2] and [3], and $\beta \text{Ca}_3(\text{PO}_4)_2$ for reaction [1]. Although some error will arise due to line broadening for very small crystallites formed during the initial stages of reaction, the results are sufficiently accurate to determine relative rates of formation. Results are presented in Fig. 2. The data could not be fitted to either first order or parabolic rate curves. Thus only qualitative estimates of relative rates are indicated in the discussion.

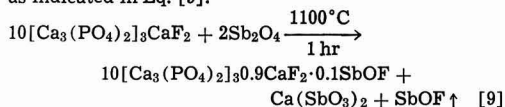
The results demonstrate that at 800°C apatite formation by reaction [3] is much more rapid than its formation by the stepwise process involving reactions [1] and [2] since reaction [1] [formation of $\beta \text{Ca}_3(\text{PO}_4)_2$] is a relatively sluggish rate-determining step. Reaction [3] is several times more rapid than reaction [2] and about 100 times more rapid than reaction [1]. Even at 900°C reaction [3] is still the most rapid. Thus it can be concluded that in apatite mixtures reaction [3] would be the dominant reaction.

Other Vapor Reactions

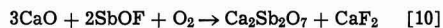
Reaction of apatite with Sb_2O_4 .—During the formation of fluorescent apatites, solid solution of Sb^{+3} ions occurs in the apatite structure. To determine how apatite might react with antimony compounds, the following double crucible experiment was performed. The inner crucible contained a mixture of 10 fluorapatite + $2\text{Sb}_2\text{O}_4$. Antimony tetroxide was chosen because of its low volatility at high temperatures. The outer crucible contained CaCO_3 . The system was heated at

1100°C for 1 hr and the products analyzed. The inner crucible contained a luminescent apatite (indicating the solid solution of Sb^{+3} ions in fluorapatite) plus a minor phase of $\text{Ca}(\text{SbO}_3)_2$. The outer crucible (originally CaCO_3) now contained CaF_2 , $\text{Ca}_2\text{Sb}_2\text{O}_7$, and CaO . The proposed sequence of reactions to explain these results is as follows, (assuming a solid solution of 0.1 mole Sb^{+3} per mole of apatite).

The solid solution of antimony in apatite appears to require the removal of F^- and Ca^{+2} ions from apatite. The Ca^{+2} ions react with Sb_2O_4 to give $\text{Ca}(\text{SbO}_3)_2$. The F^- ions form an antimony halide, perhaps SbOF , as indicated in Eq. [9].

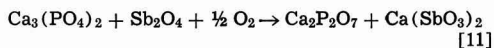


The outer crucible trapped this vapor to give (in air)

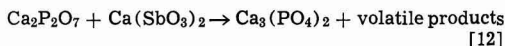


Reaction of $\text{Ca}_2\text{P}_2\text{O}_7$ with $\text{Ca}(\text{SbO}_3)_2$.—According to Butler *et al.* (3) the Sb_2O_3 usually used as the starting antimony compound rapidly reacts to form $\text{Ca}(\text{SbO}_3)_2$. To determine how $\text{Ca}(\text{SbO}_3)_2$ may enter into phosphor formation, the system $\text{Ca}_2\text{P}_2\text{O}_7 + \text{Ca}(\text{SbO}_3)_2$ was studied at several temperatures together with the reaction of $\text{Ca}_3(\text{PO}_4)_2$ with Sb_2O_4 . The results are as follows.

1. Below about 1100°C (in air)



2. Above 1100°C (open crucibles)



Presumably Sb_2O_4 is the volatile product. Kinetic studies were performed on mixtures according to reaction [12] at temperatures of 1000°, 1100°, and 1200°C. Results are presented in Table I.

The theoretical weight loss for reaction [12] is 49.0%. Thus the results in Table I confirm that this reaction did occur above 1100°C. Since Sb_2O_4 is a product of this reaction, presumably as a vapor, it can now react according to reaction [9] leading to solid solution of Sb^{+3} in apatite.

Vapor transport of F and Cl from apatites.—To determine if high-temperature vapor transport of F^- and Cl^- ions may occur, possibly by means of a water cycle, the following sealed tube experiments were performed. Chlorapatite was placed in one compartment, fluorapatite in another. The systems were evacuated, sealed, and heated at 1200°C for 20 and 72 hr, respectively. Chemical analysis for chlorine was made on the products of each compartment. X-ray diffraction analyses of the products after 72 hr firings show the product of each compartment were fluorchlorapatites of almost identical patterns. The chloride analyses are listed in Table II. The results lead to the conclusion that both Cl^- and F^- ions were involved in a vapor transport mechanism, possibly through a water cycle as indicated.

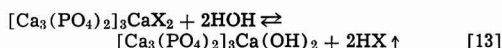


Table I. Weight losses for reaction of $\text{Ca}_2\text{P}_2\text{O}_7 + \text{Ca}(\text{SbO}_3)_2$

Reaction time, hr	% Wt loss			Product at 1200°C
	1000°C, %	1100°C, %	1200°C, %	
1	0	1.5	4.9	$\beta \text{Ca}_3(\text{PO}_4)_2 + \text{Ca}_2\text{P}_2\text{O}_7 + \text{Ca}(\text{SbO}_3)_2$
2	0	3.0	12.0	$\beta \text{Ca}_3(\text{PO}_4)_2 + \text{Ca}_2\text{P}_2\text{O}_7 + \text{Ca}(\text{SbO}_3)_2$
23	3.0	5.2	50.0	$\beta \text{Ca}_3(\text{PO}_4)_2$

Table II. Chloride content of sealed tubes fired at 1200°C

Compartment	Chloride Content Wt %	
	20 hr	72 hr
Fluorapatite	1.8	2.9
Chlorapatite	5.3	2.5

Table III. Decomposition of CaCO₃ at high pressures of CO₂

Mixture	Pressures of CO ₂ , psi	Temp., °C	% Wt loss	Theory wt loss %
CaCO ₃	90	1100	15.0	44.0
CaCO ₃	120	1000	1.2	44.0
6CaHPO ₄ + 3CaCO ₃ + CaF ₂	120	700	15.2	15.6

By simple gaseous diffusion the hydrogen halides could diffuse to the opposite chamber resulting in the mixed fluorchlorapatites. At 1200°C the equilibration by direct vapor transport of CaCl₂ and CaF₂ might also be considered.

Vapor transport of CaF₂.—Measurable vapor pressure of CaF₂ at 1200°C has been reported (12). To determine if this vapor may react with β Ca₃(PO₄)₂, a sealed tube experiment was performed at 1200°C. One compartment contained CaF₂ and the other β Ca₃(PO₄)₂. After heating the system for 20 hr, the products were examined by x-ray diffraction. The Ca₃(PO₄)₂ compartment now contained a major phase of fluorapatite plus minor unreacted phases of Ca₃(PO₄)₂ and CaF₂. These results confirm that a vapor transport of F did occur. Although these results may be only of passing interest to the study of the usual processes for apatite formation, they do illustrate once again that unusual vapor transport phenomena can exist at high temperatures.

Apatite Formation under CO₂ Pressures

A pressure vessel similar to that previously described for DTA (13) was used to study the effect of pressure of CO₂ on the tendency for apatite formation. If it is assumed that the two-step process of apatite formation occurs according to reactions [1] and [2], then reaction [1] should be greatly depressed in a CO₂ atmosphere if free CaO is essential to the process as has been assumed by other authors (2, 6). Various mixtures were placed in the pressure vessel and heated for 1 hr at the indicated pressure and temperatures. Weight losses were determined on the cooled samples. The results are presented in Table III. The results in Table III clearly indicate that CaCO₃ dissociation can be greatly depressed in CO₂ even at 1100°C, yet apatite formation is essentially complete even at 700°C. It is highly unlikely therefore that the usual dissociation of CaCO₃ to CaO is necessary to apatite formation. This is additional evidence that the principal apatite forming reaction is pressure insensitive as would be expected from the reaction of Ca₂P₂O₇ with CaF₂ (reaction [3]). The second most important apatite forming reaction is between POF₃ and CaCO₃ (reaction [4]), which can be considered an acid-base-type reaction and therefore insensitive to CO₂ pressure.

High-Temperature X-ray Diffraction Studies of Halophosphate Mixes

Phosphor mixes composed of CaHPO₄, CaCO₃, CaF₂, CaCl₂, Sb₂O₃, and MnCO₃ in proportions used for phos-

phor manufacture were examined by high-temperature x-ray diffraction methods using the GE-XRD-5 unit together with a Tem-Press furnace assembly. X-ray diffractometer traces were made at various temperatures. The results are in general agreement with the thermogravimetric data of Wanmaker and Verheyke (2) namely that:

- beginning at about 450°C
 $2\text{CaHPO}_4 \rightarrow \gamma\text{Ca}_2\text{P}_2\text{O}_7$
- beginning at about 500°C
 $\text{Sb}_2\text{O}_3 + \frac{1}{2}\text{O}_2 \rightarrow \text{Sb}_2\text{O}_4$
- beginning at about 650°C, fluorchlorapatite forms.

In no cases were any diffraction lines detected for Ca₃(PO₄)₂ to indicate its presence even in small amounts. These results also tend to indicate that in phosphor mixes apatite formation probably occurs primarily by reactions [3] and [4].

Summary

The present studies have permitted a simplification of the potential reactions involved in the preparation of halophosphate phosphors from the usual starting materials (CaHPO₄, CaCO₃, CaF₂, Sb₂O₃). The principal apatite forming reaction involves the interaction of Ca₂P₂O₇ particles with CaF₂ particles beginning at about 600°–700°C leading directly to formation of the apatite plus a vapor phase of POF₃ (11). The second most important apatite forming reaction is between POF₃ and CaCO₃ which also proceeds by a direct reaction that does not require free CaO, thus being pressure insensitive. These studies demonstrate that vapor transport plays a dominant role in the formation and activation of halophosphate phosphors.

Acknowledgments

The authors greatly appreciate the helpful comments and criticisms of Dr. H. C. Froelich and Dr. E. F. Apple.

Manuscript received Sept. 14, 1964; revised manuscript received Dec. 22, 1964. This paper was presented at the Toronto Meeting, May 3–7, 1964.

Any discussion of this paper will appear in a Discussion Section to be published in the December 1965 JOURNAL.

REFERENCES

- W. L. Wanmaker, A. H. Hoekstra, and M. G. A. Tak, *Phillips Research Repts.*, **10**, 11 (1955).
- W. L. Wanmaker and M. L. Verheyke, *ibid.*, **11**, 1 (1956).
- K. H. Butler, M. J. Bergin, and V. M. B. Hannaford, *This Journal*, **97**, 117 (1950).
- J. L. Ouweltjes and W. L. Wanmaker, *ibid.*, **103**, 160 (1956).
- D. Robbins, ECS Electronic Division Extended Abstracts, **11**, 31 (1962).
- S. Kamiya, *Electrochemistry, Japan*, **31**, 246 (1963).
- W. L. Wanmaker and C. Bakker, *Proc. Symp. React. Solids*, 709 (1960).
- G. Chaudron and R. Wallaelys, *Soc. Chim. France Bull. fasc.*, 3–4 mars-avril, pp. 132–134 (1949).
- G. Chaudron and R. Wallaelys, *Compt. rend.*, **230**, (1950).
- A. Daubree, *ibid.*, **32**, 625 (1851).
- G. Montel, Silicium, Schwefel, Phosphate, Colloq. Sek. Anorg. Chem. Intern. Union Reine U. Angew. Chem., Munster, 1954, pp. 178–183 (1955).
- D. Schulz and A. Searcy, *J. Phys. Chem.*, **67**, 103 (1963).
- J. Rabatin and C. Card, ECS Electronic Division Extended Abstracts, Abstract 90, 222–224 (1957).

Microstructures in CdS:Au Single Crystals

Arthur Dreeben

RCA Laboratories, Radio Corporation of America, Princeton, New Jersey

ABSTRACT

The incorporation of gold in CdS crystals grown from the vapor phase results in the formation of two types of precipitates. Type I, probably a CdAu phase, consists of small ($2.5\text{--}7\mu$) hexagonally shaped platelets throughout the crystal oriented to reflect the CdS crystal symmetry. Type II are much larger hexagons (160μ) apparently of elemental gold in localized positions, and with an orientation rotated 30° with respect to the small ones. Type I precipitates have been found to decorate a unique, highly symmetrical network of dislocations associated only with Type II hexagons. The dislocations are generated in a critical strain field developed around hexagons of sufficient size. Strain birefringence has been observed around these hexagons in polarized light.

In a previous investigation (1), it was demonstrated that extraneous phases precipitate in CdS crystals containing the acceptor elements Cu, Ag, or Au. The precipitates involving Cu and Ag were thought to be sulfide phases, whereas gold was found to segregate as the element together with a CdAu phase. It was shown that each of the precipitates had a characteristic shape and crystallographic orientation. The sulfides formed needles, rods, or disks, but the gold phases formed hexagonal platelets.

In this paper, additional results of direct optical observations of precipitates in CdS:Au crystals are presented. The principal findings include the identification of two kinds of hexagonal platelets, which differ in size and crystallographic orientation, and the observation of a unique, decorated imperfection network associated with the larger hexagons.

Experimental

The crystals used in this work were cut from large boules of CdS:Au which were grown from the vapor phase, oriented, and polished as previously described (1). The powder charge from which the boules were produced, contained 5 mole % of gold as gold (III) sulfide prepared by precipitation from a solution of chloroauric acid, trihydrate. With this amount of gold, globules of the metal, formed by thermal decomposition of the sulfide during crystal growth, are found in contact with the boule. During growth, therefore, molten gold is present, and this condition promotes its incorporation in the crystal. The polished samples were examined under the polarizing microscope using transmitted, incident and dark field illuminations.

Observations

As previously noted (1), discrete hexagonal platelets lying in a (0001) basal plane had been found to segregate in CdS:Au crystals. In the present samples, the average size of this species (hereafter called type I) ranges from about 2.5 to 7μ . However, in Fig. 1A, some giant hexagons (hereafter called type II) up to 160μ across can also be seen in localized sites which are at various distances below the surface of the crystal. Transmitted polarized light disclosed a strain birefringence around these large precipitates clearly seen as the white areas radiating outward from the type II hexagons in Fig. 1B. The "specks" in these photomicrographs are the smaller, type I precipitates.

In addition to their size, type II hexagons are also distinguished by a surrounding array of unique, highly symmetrical, decorated dislocations. This network in the CdS crystal consists of two distinct patterns as seen in Fig. 2. One of these is superimposed over the hexagon in the form of an asterisk whose arms are directed through and extend beyond the vertices of the large hexagon. The other decoration is a peripheral, open hexagonal array with sides paralleling those of

the precipitate at a distance of about $40\text{--}45\mu$. The asterisk and the peripheral hexagon both consist of many individual, aligned type I precipitates.

The photomicrograph in Fig. 2 was taken with the aperture diaphragm of the microscope condenser stopped-down to increase the depth of field, thereby showing all features of the arrays together. However, the type II hexagon and the two decorated patterns are not coplanar, the composite consisting of the separate parts shown in Fig. 3. In this typical crystal, 0.7 mm thick, incipient formation of the asterisk is visible close to the surface (Fig. 3A), but the fully developed pattern is first seen at 0.17 mm below the surface of the crystal. The asterisk continues in a three-dimensional array and is still clearly seen at a depth of 0.25 mm where distinct outlines of the peripheral, open hexagon also appear (Fig. 3B). In fact at this focus, elements of an inner pattern (I in 3B) and outer pattern (O in 3B) can be seen. The peripheral hexagon is at last sharply defined at a depth of 0.32 mm, while the decoration forming the asterisk is beginning to diminish (Fig. 3C). Both patterns essentially terminate at about 0.47 mm below the surface. Finally, the type II hexagonal precipitate is brought into focus at a depth of 0.57 mm (Fig. 3D). Below this hexagon, there is a somewhat less distinct repeat pattern of the peripheral figure and the asterisk.

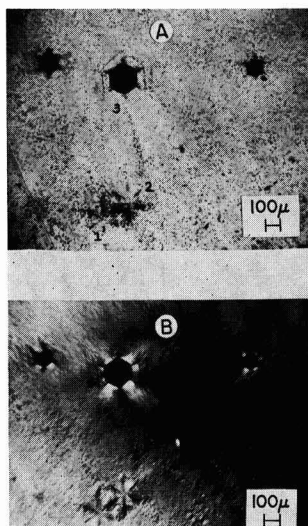


Fig. 1. Photomicrograph of CdS:Au single crystal showing (A) giant hexagons in transmitted light and (B) strain birefringence around the hexagons in polarized light.

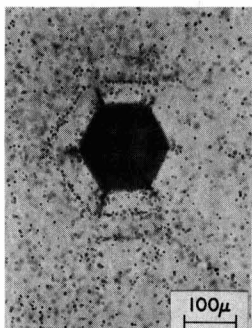


Fig. 2. Decorated dislocation arrays around hexagon No. 3 in Fig. 1

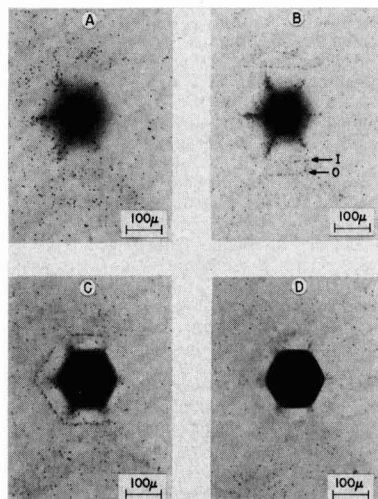


Fig. 3. Separate parts of the decorated array in Fig. 2, (A) near the crystal surface; (B) asterisk and outlines of peripheral rings, 0.25 mm below surface; (C) sharply defined ring, 0.32 mm below surface; and (D) type II hexagon, 0.57 mm below surface.

The interesting formation of the decorations above and below another type II hexagon is shown in Fig. 4. In this specimen, the asterisk and the peripheral hexagon (Fig. 4A) are seen above and essentially around the left side of the type II precipitate (Fig. 4B), while below the large hexagon, the patterns are around its right side (Fig. 4C). In Fig. 4D, a different portion of the peripheral hexagon appears at a level 0.07 mm below the position in Fig. 4C and also further away from the sides of the type II hexagon.

In the lower central portions of each illustration in Fig. 1, two asterisks (labelled 1 and 2 in 1A) can be seen without accompanying type II hexagons. Found at the surface of the crystal, they are the remnants of the typical systems already shown, but from which the other parts were removed during polishing. One of these is seen in greater detail in Fig. 5, which also clearly shows that these decorations consist of arrays of individual type I hexagons.

Crystallography of Precipitates

In (0001) planes, type I precipitates observed in many crystal slices from different boules always have the same orientation. They are bounded by $\{10\bar{1}0\}$ planes of the CdS with the a -axes directed through the vertices of the hexagons which have the same orientation as etch pits in the basal plane. This correspondence is shown in Fig. 6.

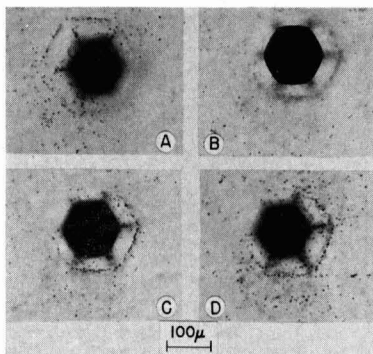


Fig. 4. (A) Dislocation array above hexagon; (B) type II hexagon; (C) dislocation array below hexagon; (D) 0.07 mm below field in (C), note outward displacement of peripheral ring.

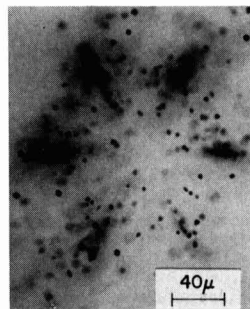


Fig. 5. Dislocation array after hexagon is removed. Note that decoration consists of individual type I hexagons.

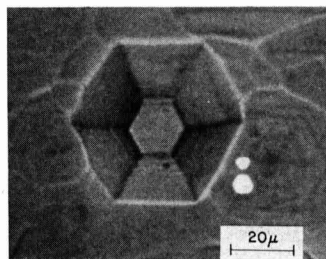


Fig. 6. Photomicrograph in incident light showing orientation of type I hexagons and etch pits in basal plane.

The large type II hexagons also have a self-consistent orientation, but it is different from that of type I. In Fig. 7, the outlines drawn around several of the type I precipitates make it readily apparent that the type II hexagon is rotated 30° with respect to the small ones. The relationship between the precipitates and the decorated dislocations with respect to the basal plane of CdS is summarized schematically in Fig. 8.

In all of the preceding photomicrographs, the precipitates have been seen as they are arranged in a basal plane. In Fig. 9 the arrangement in a $(10\bar{1}0)$ plane is shown in transmitted, dark-field illumination. Type I hexagons appear as the short bright lines, while type II are the longer ones. X-ray methods established that the CdS C -axis ($[0001]$ direction) is perpendicular to the lines in the plane of the picture and that the a -axis $[\bar{1}2\bar{1}0]$ is parallel to them. This illustration also shows arrays from asterisks and peripheral hexagons above and below the type II precipitates. However, the clear, undecorated regions directly around the pre-

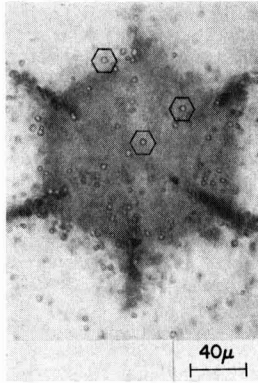


Fig. 7. Photomicrograph showing different orientations of type I (small) and type II hexagons.

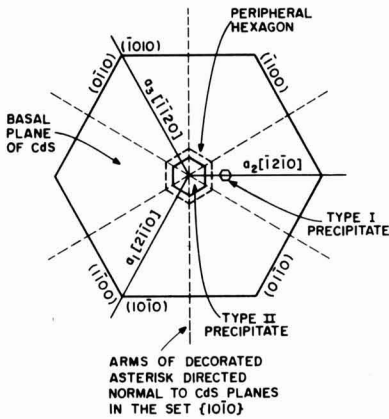


Fig. 8. Orientations of precipitates and decorated arrays with respect to the basal plane of CdS.

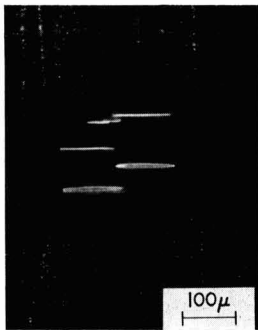


Fig. 9. Dark field illumination of hexagonal platelets in a $\{10\bar{1}0\}$ plane of CdS. C-axis perpendicular and a-axis parallel to hexagonal "lines."

precipitates confirm the earlier observation that the decoration patterns terminate at some distance from the large hexagons.

Other Decorations

In addition to the dislocation arrays surrounding the type II precipitates, there are often decorated lines that emanate from the type II precipitates, one of which can be seen in Fig. 1A between the positions labelled 2 and 3. Similar lines are also shown in Fig. 10 where it will be noted that many type I precipitates

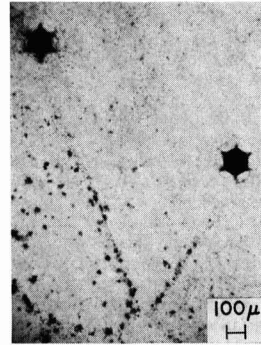


Fig. 10. Decorated boundaries emanating from type II hexagons

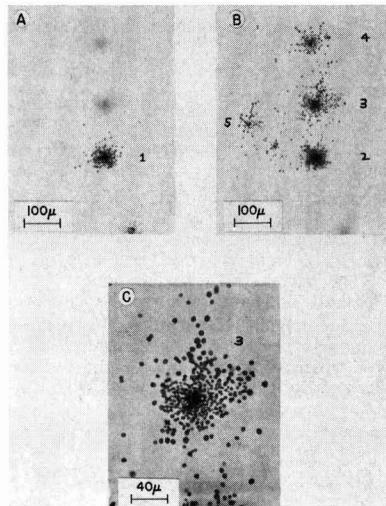


Fig. 11. Clusters of type I hexagons along boundaries shown in Fig. 10.

are grouped in clusters along and near the lines. The clusters, seen at higher magnification in Fig. 11, are arranged in a three-dimensional network. For example, group 1 in Fig. 11A is about 0.2 mm below the crystal surface, and the defocused outlines of other groups can also be seen. These appear in the same field, but at a depth of 0.4 mm as shown in Fig. 11B where the shadow of group 1 can be seen over group 2. Formations of this type are often associated with sub-boundaries.

Discussion

The two respective orientations of type I and type II precipitates suggest that they may be different chemical species. This is consistent with electron diffraction data indicating the presence of Au and CdAu phases in the CdS crystal. Gold has a face-centered cubic lattice and some CdAu phases have a hexagonal structure (2). In view of these structural differences, it is reasonable to expect the precipitates to have dissimilar epitaxial arrangements in the hexagonal CdS lattice. At present it has not been possible to obtain selected area electron or x-ray diffraction patterns of the precipitates. However, it is likely that the CdAu hexagonal structure would adopt the orientation bounded by the low index $\{10\bar{1}0\}$ planes of hexagonal CdS and thereby reflect the crystal symmetry in the same way as the etch pits and type I precipitates shown in Fig. 6. On the other hand, the cubic Au, with $\{111\}$ close packed planes, may well prefer the other ob-

served orientation of type II precipitates which are rotated at a 30° angle with respect to type I (see Fig. 7).

The different crystallographic orientations, and the probable separate identities of each precipitate, together with the fact that the dislocation arrays and boundaries are decorated with type I precipitates, suggest that different precipitation mechanisms are operating. One possible sequence for precipitation and decoration consistent with the observations is the following. Type II precipitates nucleate and grow at localized sites during the formation of the CdS boule while it is still at a high temperature. When these hexagons are sufficiently large, a critical strain field is established, and the symmetrical dislocation network is generated. In this connection it can be pointed out that the networks have never been observed around the small type I precipitates. In addition, the peripheral hexagonal loop is either very weakly defined or missing from type II precipitates well within the crystal, but which are less than about 100 μ in size compared with 140 μ for those associated with a complete array.

The CdAu phase, on the other hand, appears to have a greater solubility and remains in solution at or near the crystal growth temperature of CdS. As the crystal cools, type I hexagons precipitate randomly and on preferred sites for nucleation provided by the dislocations.

The decoration of sub-boundaries in the crystals was pointed out earlier (see Fig. 10 and 11). The other prominent dislocations in these crystals comprise the symmetrically decorated arrays around type II precipitates. The peripheral hexagons appear to be decorated prismatic loops (3) whose sides are on traces of (11 $\bar{2}$ 0) planes in the basal plane. It is also possible that the loop is part of a helical dislocation, an arrangement which could account for the displacement of the sides of the peripheral hexagon with respect to

the type II precipitate as shown in Fig. 3B, 4C, and 4D. Two observations are of particular interest. One is that the network consisting of the precipitate, the asterisk, and the peripheral hexagon is not coplanar; the other is the situation shown in Fig. 4, wherein parts of hexagonal loops exist on opposite sides above and below a type II precipitate. The mechanisms leading to these formations are not yet completely known. However, the source of the dislocation network appears to be a type II precipitate of sufficient size to develop around it, a critical strain field which is observable in polarized light. The dislocation loops once formed may glide away from the source thereby tending to relieve the stresses and leave the precipitate relatively isolated (4).

Acknowledgment

The author is indebted to M. S. Abrahams for helpful discussions. W. M. Anderson ably assisted in preparing the materials, and G. Neighbor performed the x-ray analyses.

The research reported in this paper was sponsored by the Department of Defense, Advanced Research Projects Agency, Materials Sciences Office, under Contract No. SD-182.

Manuscript received Sept. 22, 1964. This paper was prepared for delivery before the San Francisco Meeting, May 9-13, 1965.

Any discussion of this paper will appear in a Discussion Section to be published in the December 1965 JOURNAL.

REFERENCES

1. A. Dreeben, *This Journal*, **111**, 174 (1964).
2. V. G. Rivlin, W. Hume-Rothery, and B. Ryder, *Acta Met.*, **10**, 1143 (1962).
3. F. Seitz, *Phys. Rev.*, **79**, 723 (1950).
4. K. B. Harvey, *Phil. Mag.*, **8**, 435 (1963).

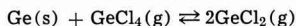
Bourdon Gauge Determination of Chemical Equilibrium in the Ge-Cl₂ System

T. O. Sedgwick

Thomas J. Watson Research Center, International Business Machines Corporation, Yorktown Heights, New York

ABSTRACT

Bourdon gauge pressure measurements of samples of GeCl₄(g) and GeCl₄(g) plus Ge(s) have been made in the temperature range 300°-1300°K. The pressure change of pure GeCl₄ as a function of temperature indicates that it does not dissociate up to 1300°K. The pressure vs. temperature behavior of GeCl₄(g) plus Ge(s) is described by the equilibrium

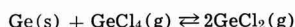


The standard enthalpy, ΔH° , and entropy, ΔS° , of reaction at 723°K were found to be 34.9 kcal and 46.7 eu, respectively.

In contrast to the Ge-H₂-I₂ and Si-H₂-Cl₂ epitaxial growth systems (1, 2) for which complete thermodynamic analyses have been made, there is insufficient thermodynamic data currently available for a similar analysis of the Ge-H₂-Cl₂ system. A complete thermodynamic description of this system would, for example, obviate the present speculation regarding the gas phase composition in GeCl₄ epitaxial growth and etching processes (3-5). As a first step toward this goal, the present work describes a quantitative determination of the equilibrium in the Ge-Cl₂ system using a Bourdon gauge.

As early as 1887 Nilson and Pettersson (6) noted the thermal stability of GeCl₄. By measuring the vapor density of GeCl₄ vapor they found that it was essen-

tially undecomposed up to 1012°K at atmospheric pressure. In contact with solid Ge, however, it has been repeatedly postulated that an equilibrium with the dichloride obtains (3, 4, 7, 8)



Although both Dennis and Hunter (7) and Schwarz and Baronetzky (9) have obtained a solid reaction product with a Cl/Ge ratio of 2 from the action of gaseous GeCl₄ on solid Ge, it does not necessarily follow that the vapor phase species has either the same stoichiometry or the same degree of polymeric character (monomer vs. dimer, etc.). This is particularly true since it appears that the solid (GeCl₂)_x phase is polymeric (10).

Although related Group IVA halide systems, *i.e.*, Si-Cl₂, Ge-I₂, Ge-Br₂, exhibit disproportionation type equilibria (11-13), there was the possibility that species other than GeCl₂ and GeCl₄ might be important in the present system. For example, both Ge₂Cl₆ and GeCl have been produced under nonequilibrium conditions in this system (9, 14-16).

Experimental

Bourdon gauge, pressure control, and measurement.

—The Bourdon gauge (12) and furnace used in the present studies are shown in Fig. 1. Flag movements caused by pressure changes modulate a light beam passing through the light pipes. The resultant optical signal is used to actuate automatically the valves to both pressure and vacuum sources which control the pressure in the equalizing chamber to "null" the flag. The details of this automatic pressure control system have been described previously by Hochberg (17).

The pressure in the equalizing chamber was measured with a model FA 129 Wallace and Tiernan dial-type manometer which had been calibrated with a 13 mm diameter Hg manometer. Both the pressure control and accuracy are within ± 0.2 mm Hg. The zero pressure point was checked frequently and, although its variation was normally within the above limits, an occasional deviation of 1-2 mm Hg was observed.

Chemical purity.—Sylvania "Special High Purity" semiconductor grade GeCl₄ was distilled under vacuum to remove all inert gases and transferred to the gauge in an all glass apparatus. Since 1-mg quantities of GeCl₄ were used, the glass apparatus was carefully cleaned and baked out before transfer of the GeCl₄. In sample 1, a 36 ohm-cm undoped Ge wafer was used. In samples 2 and 3, small wafers of 16 ohm-cm Ga doped Ge were used as the Ge solid phase. The wafers were etched in "white etch" and rinsed with deionized water and ethanol before use. The Bourdon gauge and wafer were baked out at 450°-700°C for more than 12 hr at a final pressure of 2×10^{-7} mm Hg (at the pump). The bake out tube (to vacuum) and the sample delivery tube were subsequently removed from sample chamber and are not shown in Fig. 1.

Experimental procedure.—The pressure of a total of four different samples was measured as a function of

temperature. The pressure readings were taken over several cycles of increasing and decreasing temperatures. In the temperature region where a chemical reaction took place, it was necessary to wait for $\frac{1}{2}$ hr ($T > 800^\circ\text{K}$) to several days ($T < 600^\circ\text{K}$) before chemical equilibrium was achieved, and no further change in pressure occurred as a function of time. The temperature was measured with a Pt-Pt 10 Rh or a Chromel-Alumel thermocouple both at the Ge wafer in the bottom of the sample chamber and at the top of the thermocouple well. The temperature in the furnace was adjusted so that the top of the Bourdon gauge was 2-10°C higher than the bottom (position of Ge wafer) to avoid condensation of solids on the spoon.

Results and Discussion

Thermal stability of GeCl₄(g).—The pressure of a sample of gaseous GeCl₄ (59 mm Hg at 300°K) at constant volume was found to be a linear (within <1%) function of the temperature up to 1300°K. It was therefore concluded that GeCl₄ does not dissociate significantly over this range of temperature and pressure.

Equilibrium in the GeCl₄-Ge system.—The pressure vs. temperature data for three different samples of GeCl₄(g) plus Ge(s) spanning a fivefold range in total pressure are shown in Fig. 2. In each sample the number of moles of solid Ge used was at least a factor of ten greater than the number of moles of gaseous GeCl₄. The presence of an excess Ge solid phase was confirmed visually up to $\sim 800^\circ\text{K}$. During the measurements no solid phase other than Ge was observed with one exception.¹

In all three samples the initial linear portion of the curves (up to $\sim 570^\circ\text{K}$) is attributed to an ideal gas law pressure increase of GeCl₄ gas. From $\sim 570^\circ$ - 950°K the increasing slope shows an increase in the number of gas molecules. In samples 1 and 3 the second linear region above $\sim 950^\circ\text{K}$ has a slope, P/T , twice the slope

¹In one experiment using a different furnace arrangement, the sample temperature was dropped rapidly by cooling the bottom of the gauge with an air stream. In this case a yellow-green-gray solid was condensed on the chamber walls and the final pressure read 36 mm Hg instead of the expected 54 mm Hg. Presumably the color was due to a condensed chlorine containing phase similar to that described by Schwarz and Baronetzky (9). On recycling the system at a uniform temperature, the condensed phase disappeared, and the pressure returned to the expected value.

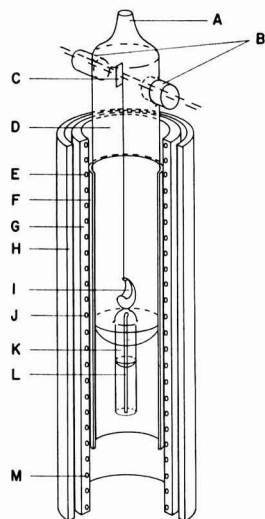


Fig. 1. Bourdon gauge and furnace arrangement: A, to pressure control; B, light pipes; C, flag; D, equalizing chamber; E, M, end windings; F, nickel pipe; G, quartz furnace; H, Morganite heat reflector; I, asymmetric spoon; J, center winding; K, sample chamber; L, thermocouple well.

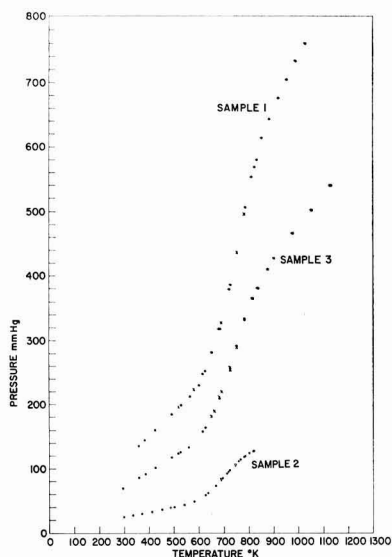


Fig. 2. Pressure vs. temperature data for three samples of GeCl₄(g) plus Ge(s) at constant volume.

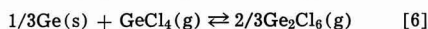
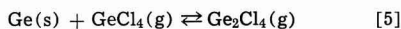
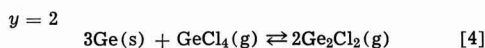
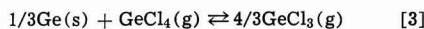
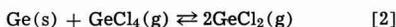
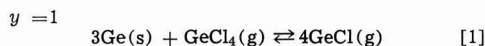
Table I. Slope of pressure vs. temperature curves for samples of $\text{GeCl}_4(\text{g}) + \text{Ge}(\text{s})$

	(P/T) for $T < 570^\circ\text{K}$	(P/T) for $T > 950^\circ\text{K}$	(P/T) for $T > 950^\circ\text{K}$
			(P/T) for $T < 570^\circ\text{K}$
Sample I	0.375 ± 0.001 [7]	0.742 ± 0.001 [4]	1.98
Sample II	0.240 ± 0.001 [8]	0.477 ± 0.001 [3]	1.98

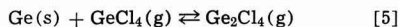
The numbers in brackets indicate the number of data points averaged.

of the respective low temperature linear regions as indicated in Table I.

Postulation of an equilibrium model.—As possible models, we have considered all equilibria involving $\text{GeCl}_4(\text{g})$, $\text{Ge}(\text{s})$, and the species $(\text{GeCl}_x)_y$ where $x = 1, 2, 3$ and $y = 1, 2$.



The observed doubling of the number of gas molecules in passing from low to high temperatures (see Table I), indicates that only the equilibria Eq. [2] and [4] are adequate models. In addition, there is a model involving two simultaneously operative equilibria, i.e., Eq. [5] and [7], which is consistent with the observed doubling of molecules as discussed above.



Although the three models Eq. [2], [4], and [5] and [7] are indistinguishable on the basis of Bourdon gauge measurements alone, the latter two models are considered unlikely since neither the species Ge_2Cl_4 , Ge_2Cl_2 , nor their analogs for any Group IVA-halide (carbon excepted) combination have ever been observed (18, 19). In the $\text{Ge}-\text{I}_2$ system, for instance, the complementary Bourdon gauge measurements of Lever (12) and weight-loss measurements of Jona *et al.* (13) specifically rule out the possibility that Ge_2I_2 and Ge_2I_4 are major constituents of the vapor phase. In the $\text{Ge}-\text{Cl}_2$ system Haq (20) has been able to observe only a single species which persists over the whole temperature range $473^\circ\text{--}873^\circ\text{K}$ (presumed to be GeCl_2). In the present study the onset of Ge etching has been observed visually to coincide with a measurable pressure increase, which indicates qualitatively that there is at most only a small concentration of Ge_2Cl_4 present. For the above reasons the model involving GeCl_2 has been chosen as the most probable description of the system, and the following analysis will be made on the basis of Eq. [2].

Test of the model.—In order to test the validity of the proposed model, Eq. [2], the functional dependence of the equilibrium constant, K_p , on temperature and pressure was determined.

$$K_p = \frac{P_{\text{GeCl}_2}^2}{P_{\text{GeCl}_4}} \quad [8]$$

The partial pressures of GeCl_2 and GeCl_4 were calculated by noting that

$$P_{\text{total}} = P_{\text{GeCl}_4} + P_{\text{GeCl}_2} \quad [9]$$

and since no chlorine containing solid phase was observed, the molecular conservation of chlorine in the vapor phase requires that

$$\frac{N_{\text{Cl}}RT}{V} = 4P_{\text{GeCl}_4} + 2P_{\text{GeCl}_2} \quad [10]$$

where N_{Cl} is the total number of moles of chlorine atoms in the gas phase.

Simultaneous solutions of Eq. [9] and [10] yield

$$P_{\text{GeCl}_4} = \frac{N_{\text{Cl}}RT}{2V} - P_{\text{total}} \quad [11]$$

$$P_{\text{GeCl}_2} = 2P_{\text{total}} - \frac{N_{\text{Cl}}RT}{2V} \quad [12]$$

The quantity $N_{\text{Cl}}R/V$ is a constant for each sample and was calculated from Eq. [11] for $T > 950^\circ\text{K}$ where P_{GeCl_4} is essentially zero and from Eq. [12] for $T < 570^\circ\text{K}$ where P_{GeCl_2} is essentially zero (see Table I).

The standard enthalpy ΔH° , and entropy, ΔS° , of reaction were obtained by the second law treatment using the relation

$$\log K_p = \frac{\Delta H^\circ}{-2.303RT} + \frac{\Delta S^\circ}{2.303R} \quad [13]$$

where ΔH° and ΔS° are assumed independent of temperature.

Calculated values of $\log K_p$ vs. $1/T$ are shown in Fig. 3. The constancy of K_p with varying pressure at constant temperature and the linearity of the $\log K_p$ vs. $1/T$ are confirmation that the model Eq. [2] is a satisfactory description of the system. If significant quantities of GeCl , GeCl_3 , or Ge_2Cl_3 were present, \log

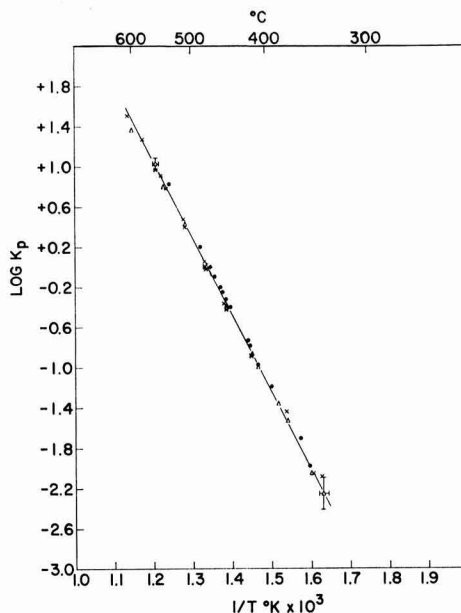


Fig. 3. $\log K_p$ vs. $1/T$ for the postulated equilibrium $\text{Ge}(\text{s}) + \text{GeCl}_4(\text{g}) \rightleftharpoons 2\text{GeCl}_2(\text{g})$. X, Sample 1; ●, sample 2; Δ, sample 3.

Table II. Calculated thermodynamic properties of the reaction

	Ge(s) + GeCl ₄ (g) ⇌ 2GeCl ₂ (g)	
	ΔH° _{722°K} (kcal)	ΔS° _{722°K} (eu)
Sample 1	34.1	45.6
Sample 2	35.5	47.7
Sample 3	35.0	46.7
Avg	34.9 ± 0.5	46.7 ± 0.7

Standard state 1 atm

K_p would not be constant with varying total pressure nor would it in general be linear with $1/T$.

Calculated values of ΔH° and ΔS° for each sample based on a least squares fit of Eq. [13] to the data are presented in Table II.

As a check on the experimentally determined value of ΔS° , the entropy of reaction was calculated at 700°K from entropy values of Ge(s) and GeCl₄(g) listed by Kelley (21, 22) and from a computed entropy of GeCl₂(g) from estimated molecular constants and spectroscopic data described in Appendix I.

$$\begin{aligned}\Delta S_{700}^\circ &= 2S_{\text{GeCl}_2(\text{g})}^\circ - S_{\text{Ge}(\text{s})}^\circ - S_{\text{GeCl}_4(\text{g})}^\circ \\ \Delta S_{700}^\circ &= 2 \times 80.7 \pm 2 - 12.6 \pm 0.1 - 103.8 \pm 0.8 \\ \Delta S_{700}^\circ &= 45.0 \pm 4 \text{ eu} \quad [14]\end{aligned}$$

The calculated value of 45.0 eu is in excellent agreement with the measured value of 46.7 eu and is well within the uncertainties in the entropy values indicated.

Acknowledgment

The author wishes to thank A. Reisman, R. Lever, and H. Leonhardt for many helpful discussions. He is particularly indebted to B. Agule who made most of the experimental measurements and calculations, and to G. Cheroff and F. Hochberg who designed, built, and tested the automatic pressure control system. This work was supported in part by AFCRL Contract No. AF19(628)-2468.

Manuscript received Nov. 2, 1964. This paper was presented at the Toronto Meeting, May 3-7, 1964.

Any discussion of this paper will appear in a Discussion Section to be published in the December 1965 JOURNAL.

REFERENCES

- A. Reisman and S. A. Alyanaky, *This Journal*, **111**, 1154 (1964).
- R. F. Lever, *IBM J. Res. & Dev.*, **8** #[4], 460 (Sept. 1964).
- J. J. Grossman, *This Journal*, **110**, 1065 (1963).
- E. I. Giurgizov, *Fiz. Tverdogo Tela*, **5**, 1150 (1963).
- K. J. Miller and M. J. Grieco, *This Journal*, **111**, 1099 (1964).
- L. F. Nilson and D. Pettersson, *Z. Physik. Chem.*, **1**, 27 (1887).
- L. M. Dennis and H. L. Hunter, *J. Am. Chem. Soc.*, **51**, 1151 (1929).
- O. H. Johnson, *Chem. Rev.*, **51**, 441 (1952).
- R. Schwarz and E. Baronetzky, *Z. anorg. u. allgem. Chem.*, **275**, 1 (1954).
- C. W. Moulton and J. G. Miller, *J. Am. Chem. Soc.*, **78**, 2702 (1956).
- H. Schafer and J. Nickl, *Z. anorg. u. allgem. Chem.*, **274**, 250 (1953).
- R. F. Lever, *This Journal*, **110**, 775 (1963).
- F. Jona, R. F. Lever, and H. R. Wendt, *ibid.*, **111**, 413 (1964).
- D. Shriver and W. L. Jolly, *J. Am. Chem. Soc.*, **80**, (1958).
- W. L. Jolly, C. B. Lindahl, and R. W. Kopp, *Inorgan. Chem.*, **1**, 958 (1962).
- Jevons, Bashford, and Biscoe, *Proc. Phys. Soc. (London)*, **49**, 532 (1937).
- F. Hochberg, Paper presented at the New York Meeting of the Society, Sept. 29-Oct. 3, 1963, Abstract 139.
- T. Moeller, "Inorganic Chemistry," Chap. 16, John Wiley & Sons, Inc., New York (1952).
- C. Eaborn, "Organosilicon Compounds," Chap. 3, Academic Press, New York (1960).
- K. E. Haq and W. von Muench, Paper presented at the New York Meeting of the Society, Sept. 29-Oct. 3, 1963, Abstract 140.
- K. K. Kelley and E. G. King, *Bur. Mines Bull.* **592**, U. S. Gov't. Printing Office, Washington, D. C. (1961).
- K. K. Kelley, *Bur. Mines Bull.* **584**, U. S. Gov't. Printing Office, Washington, D. C. (1961).
- "Tables of Interatomic Distances and Configuration in Molecules and Ions," Special Publication No. 11, The Chemical Society, London (1958).
- R. K. Asundi, M. Karim, and R. Samuel, *Proc. Roy. Soc.*, **A50**, 581 (1938).
- G. C. Sinke, "Thermodynamic Properties of Combustion Products," Dow Chemical Co., Midland, Mich. (April 1959).
- G. Herzberg, "Molecular Spectra and Molecular Structure," p. 131, Van Nostrand, New York (1945).
- "JANAF Thermochemical Data," Dow Chemical Co., Midland, Mich.

APPENDIX I

Calculation of the Entropy of GeCl₂(g)

The bond length of 2.1 Å was taken to be essentially equal to the Ge-Cl bond length in GeCl₄(g) (23). There is electron diffraction (23) and spectroscopic (24) evidence that the Group IV A dihalides are nonlinear. The bond angle of GeCl₂ was assumed to be the same as for SiCl₂ which was estimated by Sinke (25). The symmetric valence vibration frequency, ω_1 , and the deformation vibration frequency, ω_2 , for GeCl₂ were estimated by averaging the corresponding vibrational frequencies of SnCl₂ and SiCl₂ as measured by Asundi, Karim and Samuel (24). The asymmetrical valence vibrational frequency, ω_3 , was estimated to be equal to 1.12 ω_1 since the nonlinear XY₂ molecules listed by Herzberg (26) in Table 37 exhibit on the average the property $\omega_3 \approx 1.12 \omega_1$.

Table III. Summary of the estimated and calculated molecular constants

Molecular weight	143.5g
Ge-Cl bond length	2.1 Å
Cl-Ge-Cl angle	110°
Product of moments of inertia I _A I _B I _C	1.308 × 10 ⁻¹¹³ g ³ cm ⁶
Symmetry number	2
Vibrational levels [multiplicities]	
ω_1	450 cm ⁻¹ [1]
ω_2	185 cm ⁻¹ [1]
ω_3	505 cm ⁻¹ [1]

The entropy was calculated from the data in Table III using the formulas given in the JANAF tables (27). Only the ground electronic state was assumed to be occupied in analogy to SnCl₂ and SiCl₂ (24, 25), and the usual assumptions of a rigid rotator and harmonic oscillator were made.

$$\begin{aligned}S_{\text{total}}^\circ &= S_{\text{electronic}}^\circ + S_{\text{translation+rotation}}^\circ + S_{\text{vibration}}^\circ \\ &= 0 + 72.6 + 8.1 \\ S_{\text{total}}^\circ &= 80.7 \pm 2 \text{ eu} \quad [15]\end{aligned}$$

Deposition of Germanium Films by Sputtering

K. E. Haq

Thomas J. Watson Research Center, International Business Machines Corporation, Yorktown Heights, New York

ABSTRACT

Both n and p-type germanium films were deposited epitaxially by using asymmetric a-c sputtering. The quality of the films was found to be strongly dependent on the substrate temperature and the voltages during both the cleaning and the sputtering cycles. It was demonstrated that when the sputtering parameters were properly adjusted, the films deposited from n-type source material showed n-type conductivity, even when they were polycrystalline, indicating that the p-type conductivity observed previously in sputtered films was primarily due to impurities. Further, epitaxial films of the same type and conductivity and of approximately the same carrier concentration as the source material were deposited with substrate temperatures as low as 350°C.

There have been continuing efforts in the deposition of single crystal films of semiconducting materials epitaxially on various substrates. Considerable success has been achieved in obtaining good quality films by the halogen transport process. Although germanium and silicon films were deposited epitaxially by vacuum evaporation and sputtering techniques (1-5), the films, with the exception of a few cases, showed p-type conductivity, even though the source materials were heavily doped with n-type impurities. In those few instances (4-5) where the authors reported success in depositing n-type silicon films, the evaporations were conducted at a vacuum of 10^{-9} Torr. As for germanium there have been no reports of successful deposition of n-type films by either sputtering or evaporation. There has been considerable discussion in the literature as to why the films generally showed p-type conductivity (6-7). Some authors attributed this result to impurities, while others considered it to be due to imperfection in the crystalline structure of the films. Recently, it has been demonstrated in the case of silicon that the p character in conductivity is not entirely due to structural defects but due partially to contamination.

Frerichs (8) has reported that good quality superconducting metal films can be deposited by using asymmetric a-c sputtering. In the present investigation the same technique has been successfully used for the deposition of single crystal germanium films. It has been observed that even with the use of a system capable of obtaining vacuum in the high 10^{-6} range, both n- and p-type germanium films can be deposited on either type of germanium substrate, if the sputtering conditions are properly adjusted. In the present paper detailed conditions for depositing such films by sputtering and their properties will be reported.

Experimental

Apparatus.—The experimental apparatus consisted of a 14 in. glass bell jar system with a 2-in. oil diffusion pump and a liquid nitrogen trap. After overnight pumping, the system reached an ultimate vac-

uum of 7×10^{-6} mm Hg. The electrode geometry was as shown in Fig. 1. The electrodes were made of $\frac{1}{4}$ in. stainless steel rods surrounded with stainless steel shields. A spacing of 1/16 in. was maintained between the rod and the shield. A disk of polycrystalline germanium approximately 2 in. in diameter was used as a source material. It was prepared by casting pure germanium with a known amount of impurity. The disk rested on a molybdenum stage screwed to the top of the lower electrode. This arrangement precluded the use of any clips or screws for holding the source, and thus eliminated the problem of sputtering of undesirable impurities along with the source material. The germanium substrate was held with clips to a molybdenum disk which was screwed to the upper electrode with the substrate facing down towards the source.

One geometrical feature of the shields surrounding the source and the substrate should be pointed out. In the case of the source, the shield protruded approximately 1/16 in. beyond the level of the source. This arrangement confined the bombardment to the source alone, due to the repulsion of the positive ions by the shield. The substrate, on the other hand, protruded about the same distance beyond its shield. This configuration insured uniform bombardment of the substrate by the positive ions during the cleaning cycle.

The substrate heater consisted of a hollow doughnut shaped structure attached to the shield that surrounded the substrate holder. The heating of the substrate was accomplished by radiation. The temperatures of the substrate were determined in the following way: In an auxiliary experiment the temperatures of the substrate holder corresponding to different temperatures of the heater were measured by attaching one thermocouple to the heater and another to the substrate holder. A calibration curve was then plotted. During the actual run, the temperature of the heater was monitored. Using the calibration curve, the temperature of the substrate was determined.

An asymmetric 60 cycle a-c voltage was used for sputtering. The characteristics of the voltages applied to the source, the substrate, and the shields are shown in Fig. 2. Several features of the voltages should be

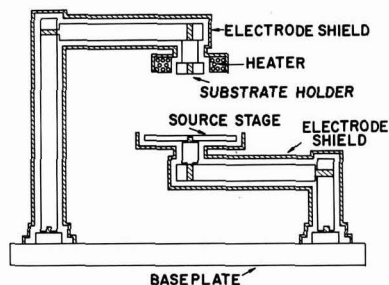


Fig. 1. Electrode geometry used for deposition of germanium film by sputtering.

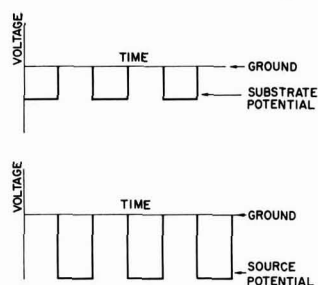


Fig. 2. Characteristics of voltages appearing on the source, substrate, and the shields during sputtering.

pointed out. First, the wave forms of the voltages appearing on the electrodes were square rather than sinusoidal. Second, when the source became negative, the substrate and the shields were at the ground potential. Similarly, when the substrate became negative, the source and the shields were at the ground potential. In this way, during sputtering the bombardment of all the undesirable parts of the system by positive ions was prevented. In the rest of the discussion, the negative voltages appearing on the source and the substrate will be referred to as the sputtering voltage and the cleaning voltage respectively.

Operational Procedure

The following procedure was used for the deposition of films. Germanium wafers, cut from a single crystal ingot, were first mechanically polished, and given a 5 min etch with CP₄. The wafer was then rinsed several times with deionized water and stored under alcohol until ready to be mounted. The source material was cleaned in the same way as the substrates. No further cleaning was done to the source between runs. After the source and the substrate were mounted, the system was evacuated to 7×10^{-6} Torr. The substrate heater was then turned on. Sufficient time was allowed for the substrate to come to a predetermined temperature equilibrium. A dynamic equilibrium pressure of approximately 45μ was then established in the bell jar by bleeding in ultra high purity argon through a needle valve, with the system open to the mechanical pump through a liquid nitrogen trap. It is essential that a cold trap be used between the bell jar and the mechanical pump to prevent the back-streaming of oil vapor from the mechanical pump. Experience has shown that unless such a precaution is taken, the properties of the film are adversely affected.

After the establishment of the argon pressure in the bell jar, both the source and the substrate were cleaned for 5 min with 1000v ions. At the end of the cleaning period, the source voltage was raised, while the substrate voltage was lowered to some predetermined values. The run was continued for a period of several hours, at the end of which time the system was opened to the diffusion pump and allowed to cool under vacuum before the film was exposed to air.

Results and Discussion

Since there has been considerable discussion in the literature as to why the evaporated and sputtered germanium films showed only p-type conductivity, part of the present investigation was devoted to determining the various deposition parameters which gave either n- or p-type films when n-type source material was used. After determining the conditions that gave reproducible n-type films, several such films were deposited on p-type substrates. The characteristics of the films and the p-n junction were then investigated. Germanium films were deposited on germanium substrates under various growth conditions. In all experiments the source to substrate distance was maintained constant at $2\frac{1}{2}$ in. X-ray diffraction techniques were used to determine whether or not the films were epitaxial. The thickness of the films was determined by an interferometric method. The type of conductivity of the films was established from thermoelectric voltage measurements.

It has been observed that films deposited from a n-type source material show p-type conductivity unless several precautions are taken. First, after the system is pressurized with clean argon to a predetermined value, the sputtering must be immediately initiated. Second, the ion bombardment should be confined between the source and the substrate. Otherwise, impurities released from the electrodes and the fixtures during sputtering are incorporated in the film. Finally, the geometry of the electrodes should be such that

uniform bombardment of the substrate during the cleaning cycle is insured. Otherwise, part of the film may show n-type conductivity, whereas the rest may be p-type. This phenomenon was observed during the early part of the investigation when proper precautions were not taken.

As the run proceeds the system slowly becomes heated and as a result, outgassing of the apparatus increases. If the run is continued for too long, the contamination from outgassed impurities may be so severe that the type of conductivity of the film may vary through the deposit thickness. It will be instructive, perhaps, to describe the result of a particular run, since it illustrates such an effect; and moreover, it gives an indication as to what might have been the chief reason for the general occurrence of p-type conductivity of sputtered and evaporated films deposited from n-type source material.

The experiment was designed to obtain a thick n-type film on a p-type substrate, therefore the run was continued for 8 hr, instead of the usual 3-4 hr. When examined, the film unexpectedly showed p-type conductivity. After a few upper layers were removed by flash etching, the film underneath was found to be n-type, indicating that the p-type impurity was incorporated in the layers that were deposited in the latter part of the run. We interpret this to be associated with system outgassing as the temperature of the supporting structures increases. This result would also imply that the chief cause of the generally observed p-type conductivity in films prepared by evaporation and sputtering from n-type sources is due to impurity rather than crystal defects. It should be noted that several of the deposited films during the present investigation showed n-type conductivity, even though they were found to be polycrystalline by x-ray analysis.

The crystalline quality of the films was found to be strongly dependent on sputtering parameters, namely substrate temperature, deposition rate (*i.e.*, the sputtering voltage) and the cleaning voltage. For a particular temperature of the substrate and cleaning voltage, the film may be epitaxial, polycrystalline, or amorphous, depending on the growth rate. At a low growth rate the film is epitaxial, while at an increasing growth rate the film becomes first polycrystalline and then amorphous. Similar dependence of crystalline properties of deposited films on substrate temperature and deposition rate was observed by Krikorian (9) in the case of d-c sputtering.

Films deposited from p-type source always showed p-type conductivity, whether or not the films were single crystal. On the other hand, the films deposited from an n-type source material showed p-type conductivity, unless the temperature and the voltage applied during the cleaning cycle were consistent with the sputtering voltage (*i.e.*, deposition rate). For example the films deposited with the substrate at 400°C and the cleaning voltage of 250v showed p-type conductivity when the sputtering voltage was 3000v. However, when the sputtering voltage was reduced to 2000v, the films deposited at the same substrate temperature and cleaning voltage showed n-type conductivity. Table I shows the highest sputtering volt-

Table I. Highest sputtering voltages at which n-type Ge films were obtained on p-type $\langle 111 \rangle$ oriented Ge substrates at various substrate temperatures and cleaning voltages

Substrate temp, °C	Cleaning voltage	Sputtering voltage	Deposition rate, μ/hr	Crystallinity
500	500	3700	1.0	Single
400	250	2000	0.32	Single
400	600	3000	1.1	Single
350	600	3000	0.9	Single
325	600	3000	1.5	Poly
300	600	3000	1.4	Poly

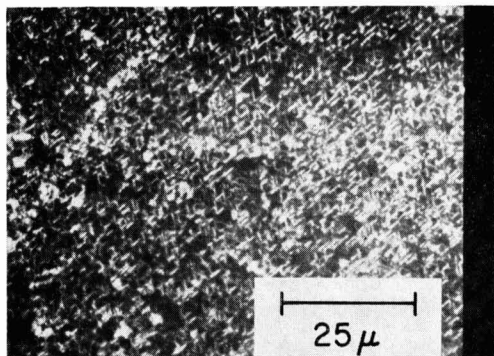


Fig. 3. Photograph of the "as grown" surface of the germanium epitaxial layer deposited by sputtering.

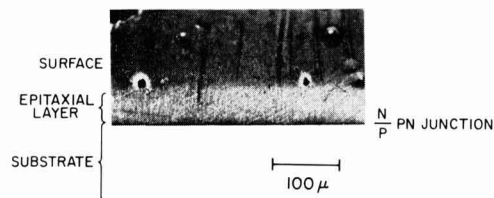


Fig. 4. Appearance of the junction after it was angle lapped and stained with copper.

ages at which n-type films were obtained at various substrate temperatures and cleaning voltages.

The films were examined in several ways to evaluate their properties. To do that, a polycrystalline n-type source doped with $2-3 \times 10^{17}$ atoms/cc of antimony was prepared. Using this source, single crystal n-type films were deposited on p-type substrates.

Under microscopic examination, films deposited on substrates oriented in the $\langle 111 \rangle$ direction showed triangular pyramids, as can be seen in Fig. 3. From an n-type layer deposited on a p-type substrate containing $7-9.4 \times 10^{18}$ atoms/cc of impurity, diodes were fabricated by mesa etching. The current voltage characteristics and the differential capacitance of the diodes were measured. A plot of $1/C^2$ vs. voltage showed a straight line indicating that the junction was abrupt. Further, from the slope of the straight line, the carrier concentration was estimated at $1.04 \times 10^{17}/\text{cc}$, which was approximately the doping level of the source material. The reverse bias breakdown voltage also agreed with the value calculated from the carrier concentration. To further examine the nature of the junction, a sample was angle lapped and stained with copper. The appearance of the junction at 250X, exhibited in Fig. 4, shows that the junction was fairly sharp. To determine the concentration and the mo-

bility of the carriers, a sample was prepared by depositing n-type film on a 40 ohm/cm p-type germanium substrate oriented in the $\langle 111 \rangle$ direction. The previously described source material was used here also. The sputtering voltage, 3000v; substrate temperature, 360°C; cleaning voltage, 600v were used for deposition. A 100 mil square chip of the deposit was diced and contact was made at the four corners. The resistivity and the Hall voltage were measured at liquid nitrogen temperature by using the Van der Pauw method. The mobility and the carrier concentration, calculated from the above measurements were as follows:

$$\mu = 1930 \text{ cm}^2/\text{v sec}$$

$$N = 3 \times 10^{17}/\text{cc}$$

Thus the carrier concentration of the film is approximately equal to the doping level of the source material. This would indicate that in the sputtering process the transfer of material from source to substrate takes place without change of composition.

Fritzsch (10) made Hall voltage and resistivity measurements at liquid nitrogen temperatures on bulk samples with various carrier concentrations. The mobilities calculated from his data for carrier concentrations $2.7 \times 10^{17}/\text{cc}$ and $1.3 \times 10^{17}/\text{cc}$ are 1810 $\text{cm}^2/\text{v sec}$ and 3230 $\text{cm}^2/\text{v sec}$, respectively, showing that the mobility of the carriers in the sputtered films is similar to that of the bulk material for the same range of carrier concentration. This would indicate that the films obtained by sputtering have fairly good crystal-line quality.

Acknowledgment

The author expresses his appreciation to M. Cowher for making the Hall voltage and resistivity measurements and to Dr. F. Fang for differential capacitance data. He also thanks Dr. A. Reisman for his critical reading of the manuscript.

Manuscript received Dec. 2, 1964.

Any discussion of this paper will appear in a Discussion Section to be published in the December 1965 JOURNAL.

REFERENCES

1. G. A. Kurov, S. A. Semiletov, and Z. G. Pinsker, *Kristallografiya*, **2**, 59 (1957).
2. O. Weinreich, G. Dermitt, and C. Tufts, *J. Appl. Phys.*, **32**, 1170 (1961).
3. F. Reizman and H. Basseches, "Metallurgy of Semiconducting Material," J. B. Schroeder, Editor, Interscience Publishers, New York (1961).
4. E. T. Handelman and E. I. Povilonis, *This Journal*, **11**, 201 (1964).
5. I. G. Ptushinskii and I. A. Lupan, *Ukrain. Fiz. Zhur.*, **4** [1], 125 (1959).
6. G. A. Kurov, *Fiz. Tverdogo Tela*, **3**, No. 6 (1961).
7. D. S. Campbell, *Brit. J. Appl. Phys.*, **15**, (1964).
8. R. Frerichs, *J. Appl. Phys.*, **33**, 1898 (1962).
9. E. Krikorian and R. J. Sneed, *Vac. Trans. Symposium* 1963.
10. H. Fritzsch, *J. Phys. Chem. Solids*, Pergamon Press, Vol. 6 (1958).

On the Mechanism of the Deposition of Silica by Pyrolytic Decomposition of Silanes

Julius Klerer

Bell Telephone Laboratories, Incorporated, Murray Hill, New Jersey

ABSTRACT

The mechanism of formation of silica films produced by the thermal decomposition of ethyltriethoxysilane has been studied. It is proposed that the thermal decomposition of the silane results in the production of complex silicon-alkyl radicals which become chemisorbed on a hot surface and suffer further decomposition in order to form a silica film. Recombination of these radicals on a cold surface leads to the formation of organic polymers of silicon. A new technique for the production of thick silica films is also presented.

Thermal decomposition of organo-oxy-silanes has been reported to provide a method for the deposition of thin silica films. Jordan (1) used ethyltriethoxysilane vapor which was passed with argon as a carrier gas into a furnace at $\approx 700^\circ\text{C}$ to accomplish film formation on a sample contained in the furnace at the same temperature. This is a closed tube technique. Klerer (2), utilizing the same experimental arrangement and conditions, allowed the gases from the furnace to contact a sample outside of the furnace in an open tube technique and obtained a film claimed to be silica.

The mechanism of formation of these films has been formulated and their properties measured. It is shown that the films produced by the technique of Jordan are probably pure silica and that those produced by the technique of Klerer are organic polymers of silicon.¹ A new technique for producing silica films is also presented.

Materials and Methods

Ethyltriethoxysilane was obtained from Union Carbide Silicones Division and redistilled to obtain the purified silane. This product was then used as the starting material for all of the investigations. Mass spectrographic analysis of the gases exiting from the furnace during the thermal decomposition of the silane was performed. Gases evolved on heating of the polymer film were also examined by the mass spectrograph. Infrared transmission spectra of both types of films were obtained. Density and refractive index of the films were determined by ellipsometric techniques.

Experiments and Results

Furnace films.—Utilizing the closed tube technique, argon was passed through ethyltriethoxysilane at 1 CFH and then through a furnace maintained at $725 \pm 5^\circ\text{C}$. A gas sampling tube was placed at the exit end of the furnace, and gases were allowed to pass through it for a period of 15 min; then the tube was sealed off. The composition of the gases were determined by the mass spectrograph. The principal gases observed and their relative amounts normalized to C_2H_4 were $\text{CH}_2 = \text{CH}_2$ [1], CH_4 [0.75], CO [1], and H_2 [0.49]. Trace amounts of C_2H_6 and C_3H_8 [0.02] were also noted, and essentially no evidence of water was found.

Samples of chemically (CP-4) polished silicon (100 ohm-cm), when placed in the furnace at 725°C , were coated with a film. The infrared transmission spectra of these films were comparable to silica films produced by thermal (1200°C , dry O_2) and steam (975°C) oxidation of similar silicon wafers.

The furnace films, when heated to 825°C in air or in argon, appeared to become denser as evidenced by

an increase in refractive index from 1.430 to 1.450. Similar results were reported by Pliskin *et al.* (3). Deposition of the furnace films at 825°C resulted in a silica film with a refractive index of 1.450, and further heat-treatment at 900°C did not result in any further change in the refractive index. Deposition of furnace films above 825°C resulted in cloudy films initially which were followed by whitish and grayish appearing films as the temperature was raised to 950°C .

One deficiency of the furnace films is that, unless they are properly annealed, cracking or crazing of the film occurs when the thickness exceeds 15,000-20,000Å (3). A new technique for depositing silica films was developed to overcome this difficulty. Wafers of silicon were placed on a hot stage at 900°C and ethyltriethoxysilane vapor, carried in a stream of nitrogen, was allowed to impinge on the heated silicon. Formation of a silica layer occurred. The refractive index was determined to be 1.455.

Further heating at higher temperatures did not change this value, and the infrared spectra agreed closely with that of thermally oxidized silicon. At a nitrogen flow rate of 2 CFH and a surface temperature of 800°C , 2000Å of silica were formed per minute. Clear and continuous layers up to 200,000Å have been formed which withstood temperature cycling from 900°C to liquid nitrogen temperature.

Polymer films.—A reinvestigation of the films produced by the open tube technique was initiated in order to characterize them with respect to the other silane decomposition techniques.

Table I. Infrared absorption bands of polymer films

Frequency, cm^{-1}	Intensity	Provisional assignment	Effect of heating on intensity, 300°C , air
3600	W	Free—OH	Appears on heating
3380	S	H_2O , Silanol, —OH	Diminishes
2960	M	$=\text{CH}_2$, $\text{CH}_2 = \text{CH}_2$	No change
2880	W	$-\text{CH}_2$, $\text{O}-\text{CH}_2$	Diminishes
2240	M	$\text{Si}-\text{H}$	Diminishes
1637	VW	$\text{CH}_2 = \text{CH}_2$, Opal	No change
1460	W	$\text{R}-\text{CH}_2$, CH Bend	Diminishes
1415	VW	$\text{R}-\text{CH}_2$, CH Bend	Diminishes
1395	VW	$\text{R}-\text{CH}_2$, CH Bend	Vanishes
1255	W	$\text{Si}-\text{CH}_3$, $\text{Si}-\text{C}$ Bend	Diminishes
1170	SSH	$=\text{Si}-\text{O}-\text{R}$, Opal	No change
1065	VS	$\text{Si}-\text{O}$ stretch, Opal	No change
1013	WSh	$\text{Si}-\text{O}-\text{Si}$	No change
965	W	—OH deformation	Diminishes
940	W	—OH deformation	Vanishes
880	S	$\text{Si}-\text{C}$ stretch	Diminishes
		$\text{Si}-\text{OH}$ deformation	
770	M	$\text{Si}-\text{O}-\text{C}$	Diminishes and shifts to 800 cm^{-1}
		$\text{Si}-\text{CH}_3$	

VW, very weak; W, weak; M, medium; S, strong; VS, very strong; Sh, shoulder.

References: L. J. Bellamy, "The Infra-red Spectra of Complex Molecules" John Wiley & Sons, Inc., New York (1954); G. J. Janz and Y. Mikawa, *Bull. Chem. Soc. Japan*, 34, 1504 (1961); K. E. Lawson, "Infra-red Absorption of Inorganic Substances," Reinhold Publishing Corp., New York (1961); R. S. McDonald, *J. Phys. Chem.*, 62, 1188 (1958); F. A. Miller and C. H. Wilkins, *Anal. Chem.*, 24, 1253 (1952); M. Randic, *Spectrochim. Acta*, 18, 115 (1962); N. Wright and M. J. Hunter, *J. Am. Chem. Soc.*, 69, 803 (1947).

¹ Jordan's silica films will henceforth be called "Furnace" films and the films produced by Klerer will be called "Polymer" films.

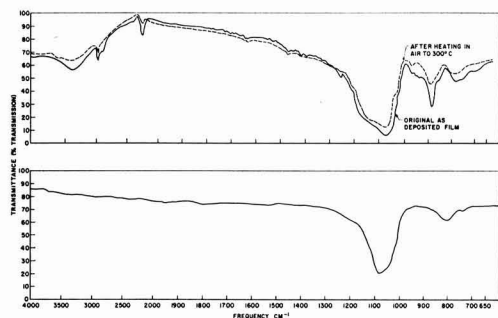


Fig. 1. Infrared spectra of polymer film before and after heat treatment (top) and typical spectra for a furnace produced (750°-825°C) film of silica. Perkins-Elmer model 221 with NaCl prism. Films were deposited on 100 μ -ohm-cm silicon wafers of 0.010 in. thickness. Film thickness was approximately 15,000Å.

Films produced by the open tube process in thicknesses below 3000Å had exhibited infrared transmission spectra similar to the furnace films (2). However, on examination of 15,000Å polymer films, absorption bands were readily observed indicating the presence of $\equiv\text{Si}-\text{CH}_3$, $\equiv\text{Si}-\text{OCH}_3$, $\equiv\text{Si}-\text{OCH}_2\text{CH}_3$, $\equiv\text{Si}-\text{O}-\text{Si}=\text{Si}$, $\equiv\text{SiOH}$, $\equiv\text{Si}-\text{H}$, and $\equiv\text{Si}-\text{CH}=\text{CH}_2$ groups as well as bands similar to those in silica gel or opal. Heating of the polymer films above 175°C caused a decrease in magnitude of the absorption bands of $\equiv\text{Si}-\text{OH}$, $\equiv\text{Si}-\text{OCH}_3$, $\equiv\text{Si}-\text{OCH}_2\text{CH}_3$, $\equiv\text{Si}-\text{H}$ and $\equiv\text{Si}-\text{CH}_3$ with the appearance of some free $-\text{OH}$ groups, the remainder of the infrared band structure being unaffected.

Table I lists the principal infrared absorption band positions and provisional assignments together with the change in intensity of the bands on heating of the polymer film to 300°C in air. The particular bands listed appear most frequently in the spectra of polymer films prepared under slightly differing conditions of gas flow and temperature. The principle changes in the spectra are in the different fine structure observed. Figure 1 presents the infrared absorption spectra of a typical polymer film (prepared at 720°C and gas flow of 1 CFH) before and after heat treatment as compared to the spectra obtained from a furnace deposited oxide.

Gases evolved on heating the polymer films were analyzed by the mass spectrograph. The principal gases found were $\text{CH}_3\text{CH}_2\text{OH}$, H_2 , $\text{CH}_3\text{CH}_2\text{CH}_3$, and H_2O . The relative amounts of these gases varied from film to film. Since these gases differed from the thermal decomposition products obtained from the closed tube process, the question arose as to the influence of room air on the polymer film.

A long furnace tube was prepared in which a series wafer was placed from the center of the furnace (725°C) out to the cold exit end (95°C). To prevent back diffusion, the exit from the tube was arranged to bubble through silicone oil. On admitting the ethyltriethoxysilane and argon mixture, film formation was observed on those wafers in the temperature zone between 600°-725°C and on those wafers in the zone between 250°-95°C. The films formed at 600°-725°C were identical to the furnace films, and the films formed between 150° and 95°C were found similar to the polymer films by means of infrared spectral analysis and dissolution behavior in hydrofluoric acid solution. No film formation was observed on substrates in the temperature range between 250° and 600°C. The formation of polymer films in this controlled atmosphere indicated that the gases evolved on heating of the polymer film come from the structure of the film rather than the environment of deposition.

The effect of substrate temperature on the film formed utilizing the open tube technique was investigated. An open furnace was set up so that the gases exiting from the tube would impinge on substrates mounted on a hot stage. During the course of these experiments, the gas flow and temperature in the furnace were constant at 1 CFH and 720°C. Films were deposited on silicon wafers at room temperature to 700°C in 50° steps. No film deposition occurred in the temperature range 250° to 500°C. In addition, the rate of growth of the films decreased as the temperature of the substrate was raised to 250°C, no growth of the film occurred between 250° and 500°C, and then the rate of growth increased from 500° to 700°C. The films deposited in the range of room temperature to 250°C were identical to the polymer film, and the films deposited from 500° to 700°C were similar to the furnace coating.

One of the characteristics of the polymer film in contrast with the furnace film is that in thicknesses $> 20,000\text{Å}$ it will crack or spall off silicon or germanium surfaces when heated to $\approx 250^\circ\text{C}$. This can be attributed to a change in density and bonding characteristics upon heating the film to 250°C. Table II presents the results obtained on these films before and after heating together with data obtained for silica films produced by the different techniques.

Discussion of Results

Thermal Decomposition Mechanism

The thermal decomposition of metal alkyls of the type MR_x has been shown to result in the production of free radicals (6). In some cases, besides the normal formation of alkyl radicals, metal alkyl radicals have been proposed to explain the order of the reaction and to justify the end products of the decomposition. One such example is the thermal decomposition of silicon tetramethyl, $\text{Si}(\text{CH}_3)_4$, in which free radicals such as $\text{Si}(\text{CH}_3)_3$ and $\text{Si}(\text{CH}_3)_3\text{CH}_2$ have been proposed in the reaction mechanism.

A tentative mechanism for the thermal decomposition of ethyltriethoxysilane can be arrived at by a consideration of both the bond structure of the silane, $(\text{CH}_3\text{CH}_2)_3\text{Si}(\text{OCH}_2\text{CH}_3)_3$, and the gaseous products evolved during the decomposition; namely, C_2H_4 , CO , CH_4 , H_2 , and traces of C_3H_8 and C_2H_6 . The bond energies involved in the ethyltriethoxysilane would be as follows: $\text{Si}-\text{O}$ (108 kcal); $\text{Si}-\text{C}$ (60 kcal); $\text{C}-\text{O}$ (86 kcal); $\text{C}-\text{C}$ (83 kcal); $\text{C}-\text{H}$ (96 kcal) (7). As the temperature is raised, it would be expected that initial bond rupture would occur in the group $\equiv\text{Si}-\text{CH}_2\text{CH}_3$ followed by attack on the group $\equiv\text{Si}-\text{OCH}_2\text{CH}_3$ to give the following possibilities:

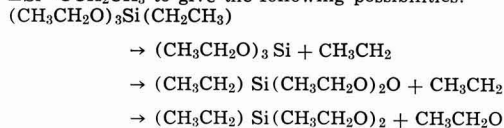


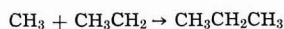
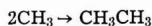
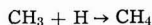
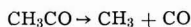
Table II. Properties of silica films prepared by different techniques*

Technique	Refractive index	Density	Dissolution rate in 1.8M HF, Å/sec
Thermal (dry O ₂)	1.450	2.23 ± 0.02	3.3
Steam (high pressure)	1.475	2.32 ± 0.02	3.7
Anodic	1.362	1.80 ± 0.05	360.0
Furnace	1.430	2.14 ± 0.07	48.0
Furnace (after heating to 825°C)	1.450		12.0
Polymer	1.430	1.63 ± 0.04	550.0
Polymer after heating at 250°C	1.390	1.9 ± 0.02#	1200.0

* Measurements made by R. J. Archer and Miss R. E. Cox of these Laboratories.

Calculated from observed volume decrease of 30.6 ± 1.5% and weight decrease of 12.8 ± 4.1%.

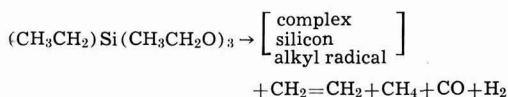
Other conceivable reactions could, and quite possibly do, occur, but these shown are sufficient to justify the final products observed. The alkyl free radicals produced from the proposed reactions can then react further in the following well-known manner (6):



Although the formation of the gaseous products observed can be explained by these equations, the relative amounts found did not fit any stoichiometric relations that could be derived from these free radical processes.

The radicals such as R_3Si or $\text{R}_2\text{-Si-O}$ where R can be $\text{CH}_3\text{CH}_2\text{-}$ or $\text{CH}_3\text{CH}_2\text{O-}$ should exist in the gas phase. These can combine with the radicals previously proposed or with themselves to condense out on cooler portions of the apparatus to form polymer films. This can be illustrated in the experiments, where a series of wafers were placed in the closed furnace. Polymer coatings were obtained at the cooler exit end of the furnace tube. In the hot zone of the furnace, the radicals were further decomposed, forming a silica coating.

The over-all reaction for the thermal decomposition of ethyltriethoxysilane can be simply stated as



Mechanism of Furnace Film Formation

In the hot zone of the furnace ($600^\circ\text{-}850^\circ\text{C}$) the complex silicon alkyl radicals in the gas phase can now proceed to build up silica layers. Radicals such as R_3Si or $\text{R}_3\text{Si-O}$ can associate with a metal surface by attachment of the $-\text{O}$ atom to the metal, or through the $-\text{Si}$ atom coupling to a surface oxide by bonding with an oxygen atom. The organic fractions of the radical then can be thermally cracked to form new bonds to repeat the process, and film formation would continue to occur.

The changes in refractive index and etch rate of these films on heating suggest the presence of organic groups in the film. For films formed below 825°C , these groups can be removed by heating to $>825^\circ\text{C}$. Deposition of the film at 825°C appears to result in organic free silica coatings. The presence of these organic groups in the silica films deposited below 825°C probably cause the crazing of the thicker films ($>15,000\text{\AA}$), since they can alter the bonding characteristics and/or structural arrangement of the film. This can thus result in poor stress or strain release leading to discontinuous films. The thermal treatment of the film *in situ* ($>825^\circ\text{C}$) results in producing thick craze-free films and is attributed to densification of the film (3).

The question of whether organic groups are occluded in the film or really part of the structure can be resolved by observations made on films which were deposited on the hot stage at $\cong 800^\circ\text{C}$. The hot stage technique illustrates direct thermal surface decomposition, with minimum chance for entrapment of gases. At temperatures below 800°C on the hot stage, films containing organic grouping were produced, imply-

ing that these organic groups are not occluded or entrapped in the film but are still attached to the silicon atom. If this is the case, it would lend supporting evidence to the existence of radicals such as those mentioned earlier in this section.

Mechanism of Polymer Film Formation

It is not surprising that the mechanism of film formation of the furnace and polymer films should differ. In one case, the silane is being thermally decomposed with simultaneous deposition on a hot surface, and in the other case the silane is being thermally decomposed and then deposited on a relatively cold surface. The difference in properties of these films is shown in Table II.

The behavior of the deposition rate of the polymer film on surfaces which were at different temperatures can be explained by the following mechanism.

The ethyltriethoxysilane is decomposed in the furnace to organic gas residues and the complex silicon alkyl radical. This radical emerges from the furnace tube and contacts a surface. There it undergoes physical adsorption and when another radical attachment occurs in its proximity, crosslinking can occur. Repetition of this process would lead to thicker and thicker layers. This process requires a finite time for the radical to remain on the surface until another radical approaches. As the temperature of the surface is raised, more kinetic energy is imparted to these radicals, and they tend to spend a shorter time on the surface, thus decreasing the probability of crosslinking with another radical landing nearby. Since there is probably a Boltzmann distribution of energy in the particles emerging from the open furnace, there should be a decrease in deposition rate as the temperature of the surface is raised because the more energetic particles spend less time on the surface. Ultimately, when the temperature is raised to a point such that the hot surface imparts sufficient kinetic energy to the least energetic radicals, sufficient physical adsorption on the surface cannot occur and deposition ceases. This situation remains in effect until 500°C is reached.

At this and higher temperatures, it is proposed that a chemisorption mechanism is initiated since there is now enough energy available so that bonding between the radical and the surface can occur. Initially, the more active sites on the surface react and then as the temperature is raised, more sites come into play until rapid formation of a coating occurs. After the first monolayer is complete, the other radicals can link up with this monolayer, etc. These coatings are similar to the furnace films, and essentially the same mechanism occurs there, namely, radical attachment to the surface and subsequent cracking of the radical to produce new bonds for further growth of the oxide.

The film layers deposited at the lower temperature must be organic polymers of silica. From the proposed mechanism presented on the thermal decomposition of ethyltriethoxysilane, the formation of a complex silicon alkyl radicals plus radicals such as CH_3CH_2 , $\text{CH}_3\text{CH}_2\text{O}$, H , CH_3 , and CH_3CO occurs in the heated zone of the furnace. As these radicals exit from the furnace, they can recombine on cooling on surfaces to form bonds such as $\equiv\text{Si-CH}_3$, $\equiv\text{SiOCH}_3$, $\equiv\text{Si-OH}$ and also to cross link on the surface to form polymers of varying lengths and linkages intermixed with small silica groupings. The low density and high dissolution rate of the polymer film demonstrates a fairly open network in the film. Its refractive index indicates that SiO_2 groupings are present in large concentration.

On heating, the film undergoes a shrinkage and rearrangement leading to a higher density. This shrinking and rearrangement are due to condensation and elimination reactions between neighboring silane groupings to eliminate H_2O , $\text{CH}_3\text{CH}_2\text{OH}$, H_2 , and $\text{CH}_3\text{CH}_2\text{CH}_3$. The higher dissolution rate is due probably to increased porosity with change in structure. The decrease in refractive index serves to demon-

strate that a more open network was present. The films, however, remain coherent on heating at thicknesses less than 15,000Å, and their similarity in chemical properties to silica makes them an attractive coating for use in applications where high-temperature processing is not a factor.

Summary

It has been proposed that the thermal decomposition of ethyltriethoxysilane on a hot surface to form a continuous, amorphous, silica film is essentially a free radical process, involving an initial chemisorption on the surface. The chemisorbed radical suffers further thermal decomposition resulting in the formation of new bonds for attachment to other radicals, thus building up the layer.

Recombination of thermally produced radicals on a cold surface results in an organic polymer of silicon, which exhibits some of the properties of pure silica.

Thermal decomposition of silanes on a hot surface in air has been demonstrated and leads to a technique for growing thick films of pure silica.

Acknowledgment

Acknowledgment is due E. E. Francois for the mass spectrographic determinations and Miss D. M. Dodd for the infrared spectra measurements.

Manuscript received Nov. 10, 1964.

Any discussion of this paper will appear in a Discussion Section to be published in the December 1965 JOURNAL.

REFERENCES

1. E. Jordan, *This Journal*, **108**, 478 (1961).
2. J. Klerer, *ibid.*, **108**, 1070 (1961).
3. W. A. Pliskin and H. S. Lehman, Paper presented at the Toronto Meeting of the Society, Abstract No. 76, May 1964.
4. "Free Radicals," The Catholic University of America Press, Washington (1958).
5. R. B. Sosman, *Trans. Brit. Ceram. Soc.*, **54**, 655 (1955).
6. E. W. R. Steacie, "Atomic & Free Radical Reactions," Reinhold Publishing Co., New York (1954).
7. T. L. Cottrell, "The Strengths of Chemical Bonds," Butterworths Scientific, London (1953).

Solid and Liquid Phase Miscibility of Calcium Metal and Calcium Fluoride¹

Barry D. Lichter² and M. A. Bredig

Chemistry Division, Oak Ridge National Laboratory, Oak Ridge, Tennessee

ABSTRACT

The solubility of Ca in solid CaF₂ was determined by vapor phase equilibration in the temperature range 1060°–1265°C in which it rises from 0.4 to approximately 2 mole %. This solubility is considered in an analysis of the melting point depression of CaF₂, which suggests that the ionization, $\text{Ca}^{++} = + 2e^-$, takes place in dilute solution. The equilibrium $2\text{Ca}^{++} + 2e^- \rightleftharpoons \text{Ca}_2^{++}$ is shifted toward the right, i.e., molecule ion formation, by increasing metal concentration. Literature data for liquid solutions are reinterpreted in terms of complete miscibility of Ca and CaF₂ in the liquid state.

In studies of the phase equilibria and electrical conductance of one type of molten metal halide-metal system, the assumption has been made (1) that in dilute solutions the metal dissolves by being ionized in the ionic medium according to $M = M^{z+} + ze^-$. At higher concentrations, evidence was found (1, 2) in some systems of association of the electrons to form molecules or molecule ions such as Na₂ or (Ca₂)²⁺. The latter species was thought by Rogers, Tomlinson, and Richardson (3) to exist even in dilute solutions of Ca in CaF₂; but in order to support this hypothesis, a heat of fusion of CaF₂ as high as 10 kcal/mole rather than 7.1 kcal/mole measured calorimetrically (4), as well as insolubility of calcium and of NaF (5) in solid CaF₂, has to be assumed. Since evidence for a rather unexpectedly high solubility of Ca in solid CaF₂ existed in the literature (6), determination of the true extent of such solid solution was made the objective of the work reported below.

Experimental Procedures and Results

Materials.—Calcium fluoride was in the form of large, high-purity, optical quality crystals (Harshaw).

Calcium metal (Nelco Metals, Inc.) was in the form of redistilled pellets (metallic impurities in ppm: 800 Mg, 5 Fe, 6 Mn, 40 Ni, and 10 Al). The calcium was kept under argon in a metal can with a tight-fitting lid. Attempts were made to select pellets having a minimum of surface oxide.

Armco iron crucibles (impurities in ppm: 80 C, 260 S, 90 P, 500 O, and 6 N) were used to contain Ca and CaF₂ during experimental runs.

High-temperature equilibration.—Experiments consisted of high-temperature annealing of CaF₂ crystals in an atmosphere of Ca vapor, followed by moderately rapid quenching to room temperature (100° min⁻¹ initial cooling rate). The pressure of the Ca vapor was established as the equilibrium calcium vapor pressure of a saturated solution of CaF₂ in molten Ca metal at the experimental temperature.

Figure 1 shows the arrangement of materials in the iron crucible. The bottom compartment was charged

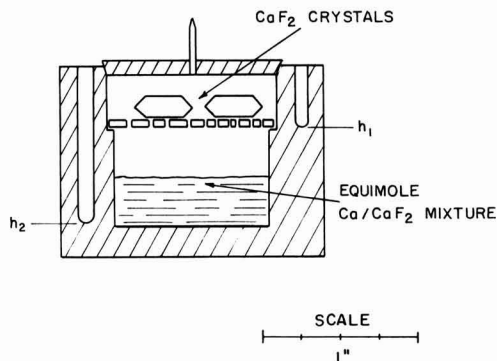


Fig. 1. Crucible assembly for high-temperature equilibrium.

¹ Research sponsored by the United States Atomic Energy Commission under contract with the Union Carbide Corporation.

² Present address: Division of Metallurgical Engineering, University of Washington, Seattle, Washington.

with a 2-3g approximately equimolar mixture of Ca pellets and CaF_2 powder. At the equilibration temperature, this mixture formed a saturated solution of CaF_2 in liquid Ca according to the phase diagram of Rogers, Tomlinson, and Richardson (3). The top compartment contained 2-5g of CaF_2 in the form of 2-8 mm thick platelets cleaved from a single crystal. The platelets were supported on a thin iron partition in which were drilled a number of small holes. The average composition of the combined systems varied in different runs from 0.2 to 0.5 mole fraction calcium, $N_{\text{Ca}} = \text{g atoms Ca} / (\text{g atoms Ca} + \text{moles CaF}_2)$. Several experiments were attempted with the partition removed and the CaF_2 crystals in contact with the Ca- CaF_2 mixture. However, these experiments resulted in erroneously high values for the solubility of Ca, due to pitting-type attack of CaF_2 crystals by the melt. This phenomenon is discussed further below.

The lid was fusion-welded to the crucible in an inert gas dry box. The crucible was evacuated through a tube in the lid to a pressure of $<10^{-5}$ mm Hg, and the tube was crimped and welded shut. The crucible was contained in the furnace in a closed Inconel tube under 2 atm pressure argon, and the temperature was controlled with two Pt/Pt-10% Rh couples in series, using a L&N Micromax controller. The temperature was measured at positions h_1 and h_2 (Fig. 1) using Pt/Pt-10% Rh thermocouples. The variation of either couple during a run was $<\pm 1^\circ\text{C}$. However, the measured temperature difference between h_1 and h_2 could not be reduced below $\pm 5^\circ\text{C}$ at temperatures between 1060° and 1260°C .

The time to establish equilibrium was determined from results of duplicate runs and from results obtained with crystals of varying thickness in a given run.

Microscopic evidence for true solid solubility at elevated temperature.—Quenched CaF_2 crystals were translucent, appearing gray or rose-brown in color. However, crystals which were in contact with the melt were green. Microscopic examination under transmitted light revealed the following structures shown in Fig. 2:

(a) Metallic particles ranging from 1 to 10μ diameter were uniformly distributed in the crystal matrix.

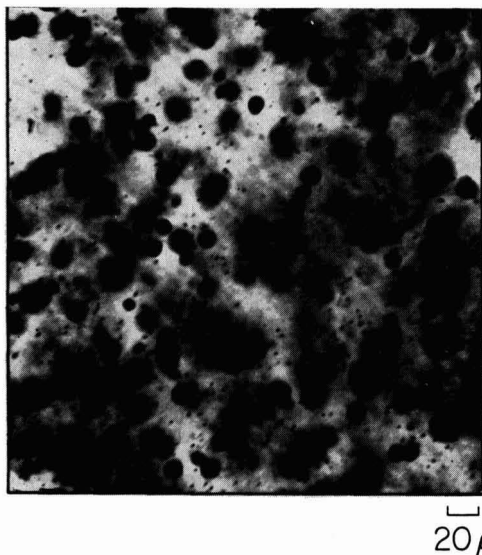


Fig. 2a. Structure of quenched CaF_2 crystals; Sample equilibrated through the gas phase.

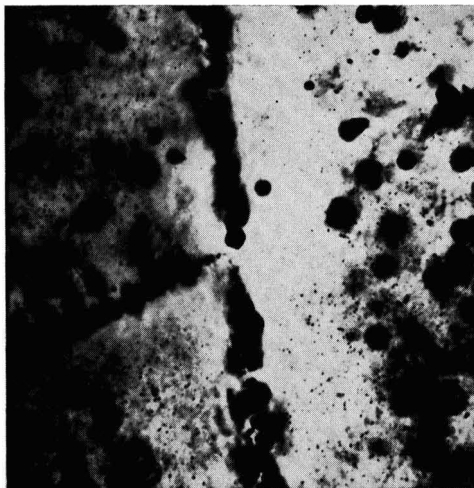


Fig. 2b. Sample equilibrated through the gas phase

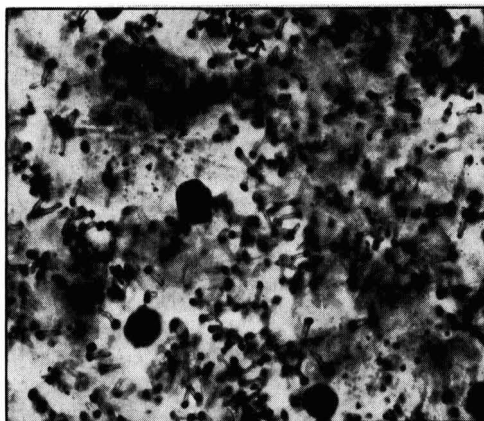


Fig. 2c. Sample in contact with the melt

The presence of submicroscopic colloidal particles was also indicated by the muddy appearance of the matrix.

(b) At certain locations in the crystal, presumably low-angle grain boundaries, the particle density was unusually high, while in immediately adjacent areas the particle density was low.

(c) Green crystals contained a larger amount of colloid as evidenced by lower transparency. In addition, a network of fine pits could be resolved at higher magnification.

The existence of isolated spherical particles in the single crystal matrix suggests that during quenching a true precipitation from saturated solid solution occurred, where the precipitating phase is a liquid. Areas of high particle density as shown in Fig. 2b are consistent with precipitation at preferential sites. However, for crystals in contact with the melt, dissolution of calcium in the crystal and dissolution of the crystal in the melt can occur simultaneously. Attack of the crystal presumably took place via the formation of small pits (Fig. 2c) which served to entrap excess calcium. The metallic content of green crystals was found to be about twice that of crystals equilibrated through the gas phase, and, in general, the results of

Table I. Solubility of calcium metal in solid CaF_2 between 1060° and 1265°C

Run No.	$t, ^\circ\text{C}$	$N_{\text{Ca}}(s) \times 100$	Annealing time, hr	Sample thickness, mm
13	1265	1.70	42	8.2
12	1215	1.55	86	8.6
11	1175	1.00	51	6.4
2	1145	0.60	22	2.0
6	1080	0.52	96	2.2
14	1090	0.44	113	4.6
5	1060	0.42	65	7.4

calcium analysis were less reproducible for green crystals.

Determination of excess calcium in quenched CaF_2 crystals.—Quenched crystals were ground to a fine powder, leached with distilled water, and the resulting solutions titrated against standard HCl and NaOH solutions. The amount of metallic calcium present was calculated from the measured basicity of the solutions on the reasonable assumption that, with the moderate quenching rate used, a negligible amount of calcium remained in supersaturated solid solution at room temperature.

No basicity was detected in crystals used in control experiments for which calcium was omitted from the crucible during high-temperature annealing. Crystals from the control experiments were transparent, uncolored, and free of any precipitate. Several additional sources of error were considered and evaluated as follows:

(a) Chromatographic analysis of the gas evolved from a sample during leaching revealed only hydrogen, and the calculated calcium content agreed to within 5% with results from the titration, thus ruling out significant contamination from soluble impurities (P, S, N, and O).

(b) Before grinding, quenched crystals were washed in distilled water. Titration of the wash water revealed less than 1% of the calcium present in the crystal, thus ruling out errors from calcium condensed on the crystal surface during quenching.

(c) The major possible source of error was found to be incomplete dissolution of colloidal calcium during leaching. The procedure adopted was to grind the crystal in a known volume of standard HCl solution, back titrate the mixture with NaOH, reacidify, regrind the mixture, and repeat the titration. After 5-10 grindings no subsequent calcium dissolution was detected.

Results are summarized in Table I. The partial and total phase diagrams for the system CaF_2 -Ca are shown in Fig. 3 and 4 which include most of the data of Rogers *et al.* (3).

Discussion

Comparison with previous studies of phase equilibria in the system CaF_2 -Ca.—The existence of solid

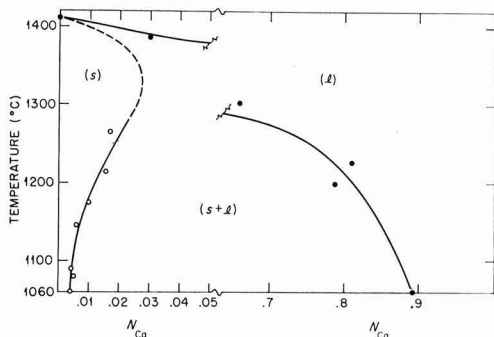


Fig. 3. Partial phase diagram of the system CaF_2 -Ca, incorporating data both from ref. (3), ●, and the present work, ○.

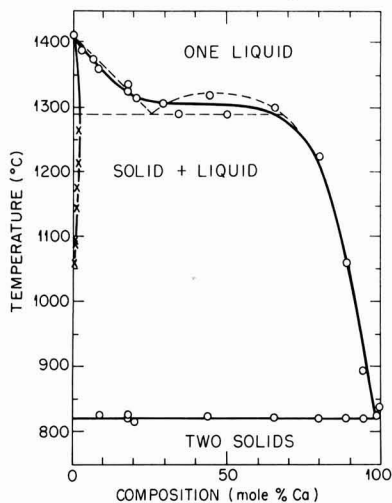


Fig. 4. Complete phase diagram of the system CaF_2 -Ca, showing absence of monotectic reaction and of liquid-liquid phase equilibria. — — —, R., T., R. (in error); — — —, Lichter and Bredig; ○, differential thermal analysis, R., T., R.; X, solubility, L and B.

subhalides (e.g., CaF) in alkaline earth metal-metal halide systems as reported by Wöhler and Rodewald (7) has not been confirmed by more recent investigations (3,8,9). In particular, the main features of the system CaF_2 -Ca were recently determined by Rogers *et al.* (3), and the results pertinent to the present discussion are given in Fig. 3, 4, and 5. These authors did not determine the solubility of calcium in solid CaF_2 ; however, their observations do not support the exceptionally high solubility previously reported by Mollwo (6). Mollwo's results are based on (a) optical absorp-

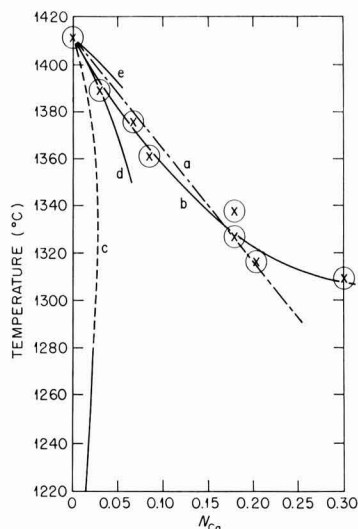


Fig. 5. Liquidus and solidus curves for system CaF_2 -Ca: a, experimental liquidus, after Rogers, Tomlinson, and Richardson (3); b, experimental liquidus proposed by Lichter and Bredig for data of ref. (3); c, solidus; d, ideal liquidus, $T = T_m - (2RT_m^2/\Delta H_m)(N_{\text{Ca}}(l) - N_{\text{Ca}}(s))$ for $\text{Ca} \rightarrow \text{Ca}^{++} + 2e^-$; e, ideal liquidus, $T = T_m - (RT_m^2/\Delta H_m)(N_{\text{Ca}}(l) - N_{\text{Ca}}(s))$ for $\text{Ca} + \text{Ca}^{++} \rightarrow \text{Ca}_2^{++}$. Note identity of curves b and d for $N_{\text{Ca}}(l) < 0.02$ and increasing positive deviation of b from d at higher metal concentrations.

tion measurements of samples annealed in calcium vapor at 450°–600°C and then quenched; (b) measurements at 600° and 800°C of the velocity of color centers produced by application of a strong electric field; and (c) measurements of pycnometric density of samples annealed in calcium vapor at ~1000° and ~1100°C and then quenched. These results are an order of magnitude greater than the results of the present work which are felt to be accurate to ±10%. This disagreement is difficult to explain without further experimental details of Mollwo's measurements. In particular, microscopic observations of quenched samples used in optical absorption and density measurements are lacking, and the absence of colloidal calcium in quenched samples is not confirmed.

It will be noticed that in our diagrams we have rejected the notion of the existence in this system of a monotectic reaction and consequently of a consolute or critical solution temperature. The opposite conclusion reached by Rogers, Tomlinson, and Richardson, namely, that between 1290° ± 5° and 1322° ± 10°C equilibria between two liquid phases exist is not supported by their experiments. The new interpretation of these data is necessary because no thermal effect at the alleged monotectic temperature of 1290° was obtained for any of the six compositions below 20 mole % Ca that were studied. Particularly on heating, the differential thermal analysis would have shown a monotectic reaction, if present, even more distinctly than the liquidus. That the sensitivity of the method used was satisfactory is attested to by the appearance of the corresponding eutectic effects even in these mixtures containing relatively little Ca metal which also has a lower heat of fusion than CaF₂. Furthermore, the thermal effects which Rogers, Tomlinson, and Richardson reported for three compositions within the range of the alleged liquid-liquid reaction, namely, 29, 45, and 65 mole % Ca cannot possibly have been caused by this reaction which is characterized by a very small enthalpy change (or, more correctly, a very small change in the heating or cooling rate) while the far greater enthalpy change of a monotectic reaction remained unrecorded in these three and six additional compositions mentioned above. There can be no doubt that actually all five of the observed thermal effects within the alleged liquid-liquid separation range involved solid CaF₂ (liquidus curve), with a scattering of ±12°C which is actually less than two thirds the scattering (±20°) of the three points between 75 and 95 mole % Ca. (One notes that the scattering increased greatly in going from the salt-rich to the metal-rich ranges of the phase diagram, namely, from ±2° to ±20°. This may be at least partly connected with a parallel increase in the tendency to phase segregation during the quenching operation carried out by Rogers *et al.* before each differential thermal analysis run.)

The results reported by Rogers *et al.* as "solubility" from another series of experiments designed to preserve the alleged liquid-liquid equilibria by quenching are subject to grave doubt because of the inherent faults of the method that were pointed out by the authors themselves as well as one of us (Bredig); thus, they cannot be included in the discussion (two of the experimental solubilities, those at 1303°C, show deviations of as much as 16 and 31%).

With the new interpretation, the CaF₂-Ca system represents the first metal-halide pair outside of the alkali metal systems (Cs-CsX and Rb-RbBr) to exhibit complete salt-metal miscibility in the liquid state, *i.e.*, absence of liquid-liquid phase equilibria. In comparison with the other calcium metal-halide systems, this is to be ascribed principally to the high melting point of the fluoride. However, the shape of the liquidus is characteristic of a large deviation from Raoult's law and of a more than incipient tendency toward formation of two liquid phases.

Analysis of freezing point depression of CaF₂ by calcium.—The finding of limited solubility of calcium metal in solid CaF₂ gives rise to a modification of the interpretation of the liquidus curve advanced by Rogers *et al.* (3). In the other CaX₂-Ca systems (X = Cl, Br, I), Dworkin, Bronstein, and Bredig (1, 9) have interpreted the observed melting point depression of CaX₂ by Ca and the electrical conductivity of dilute solutions in terms of the dissociation (ionization) of Ca metal in the highly ionized medium which the molten salt represents, *i.e.*, according to $\text{Ca} = \text{Ca}^{++} + 2e^-$. The electrons are thought of as anion- or color-centerlike species (2, 10-12). With increasing metal (or electron) concentration, the reaction $2e^- + 2\text{Ca}^{++} = (\text{Ca}_2)^{++}$ was assumed to progress toward the right, *i.e.*, the formation of a molecule ion resembling somewhat in electronic structure the (Cd₂)⁺⁺ and (Hg₂)⁺⁺ ions and especially the Na₂ molecules proposed earlier for the NaX-Na systems (2). If one assumes that in dilute solutions Ca dissolves in the liquid phase in a similar manner as in solid CaF₂, namely, according to $\text{Ca} = \text{Ca}^{++} + 2e^-$, with electrons substituting in "ideal" mixtures for F⁻ ions, one obtains for the activity of CaF₂ in both the solid and liquid phases

$$a_{\text{CaF}_2} = X_{\text{Ca}^{++}} \cdot X_{F^-} \quad [1]$$

where the Ca⁺⁺ cation fraction = $X_{\text{Ca}^{++}} = 1$ and the F⁻ anion fraction

$$X_{F^-} = \frac{n_{F^-}}{n_{F^-} + n_{e^-}} = \frac{2n_{\text{CaF}_2}}{2n_{\text{CaF}_2} + 2n_{\text{Ca}}} = N_{\text{CaF}_2}$$

Therefore

$$a_{\text{CaF}_2} = X_{F^-}^2 = N_{\text{CaF}_2}^2 \quad [2]$$

and the equation for the melting point depression becomes

$$T - T_m = \Delta T =$$

$$\frac{RT_m^2}{\Delta H_m} \cdot \ln \left[\frac{a_{\text{CaF}_2}^{(l)}}{a_{\text{CaF}_2}^{(s)}} \right] = \frac{RT_m^2}{\Delta H_m} \cdot 2 \ln \frac{N_{\text{CaF}_2}^{(l)}}{N_{\text{CaF}_2}^{(s)}} \quad [3]$$

Thus, the melting point depression, ΔT, is proportional to twice the difference in the logarithms of the mole fractions of CaF₂ in the liquid and solid phases. At low concentration of Ca, $\ln N_{\text{CaF}_2} = (N_{\text{CaF}_2} - 1) = -N_{\text{Ca}}$, and Eq. [3] can be written

$$\begin{aligned} \Delta T &= -\frac{2RT_m^2}{\Delta H_m} \left(N_{\text{Ca}}^{(l)} - N_{\text{Ca}}^{(s)} \right) \\ &= -\frac{4 \times (1684)^2}{7100} (\Delta N_{\text{Ca}}) = -1600 \cdot \Delta N_{\text{Ca}} \quad [4] \end{aligned}$$

Figure 5 shows that it is possible at temperatures near T_m, *i.e.*, at small concentrations of calcium metal, to reconcile the experimental results obtained for the liquidus by Rogers *et al.* (3) and the estimated solidus from the present work with this equation: At T approximating T_m, curve d, the ideal liquidus corresponding to $\text{Ca} = \text{Ca}^{++} + 2e^-$ and to

$$T = T_m - \frac{2RT_m^2}{\Delta H_m} \left(N_{\text{Ca}}^{(l)} - N_{\text{Ca}}^{(s)} \right) \quad [5]$$

with estimated N_{Ca}(s) from curve c, approximates curve b, the curve drawn by us through the experimental point from ref. (3). At higher metal concentrations in the liquid phase, there occurs strong positive deviation from Raoult's law as one might expect with limited miscibility in the liquid phase and/or increasing reaction according to



i.e., interaction and trapping of pairs of anion of F-centerlike electrons in the form of molecule ions.

Summary

1. Contrary to reports in the literature, solid CaF_2 , in equilibrium with the calcium vapor over a saturated solution of CaF_2 in liquid calcium metal, dissolves near 1330°C a maximum of approximately 2.7 mole % calcium metal.

2. The depression of the melting point of CaF_2 by low concentration of Ca can be interpreted in terms of a solidus as estimated from the measurements and of the known calorimetric heat of fusion, with the assumption that the solution mechanism in the solid is the same as in the dilute liquid phase, namely, $\text{Ca} \rightarrow \text{Ca}^{++} + 2e^-$ (F centerlike electrons). With increasing metal concentration, the dissolution of calcium metal in molten CaF_2 follows $\text{Ca} + \text{Ca}^{++} \rightarrow (\text{Ca}_2)^{++}$, or $2\text{Ca}^{++} + 2e^- \rightarrow (\text{Ca}_2)^{++}$ to an increasing degree. The ionization according to $\text{Ca} \rightarrow \text{Ca}^{++} + 2e^-$ is thus believed to be similar to that in the calcium metal solutions in the three other CaX_2 melts (X = Cl, Br, I) where such ionization is supported by electrical conductance data.

3. The CaF_2 -Ca system is the first metal-halide system outside of the alkali metal systems to exhibit complete metal-salt miscibility in the liquid state, i.e., absence of liquid-liquid phase equilibria.

Acknowledgment

The authors wish to express their thanks to Messrs. G. Goldberg and G. R. Wilson for chemical analyses and to Mr. T. E. Willmarth for the microphotographs.

Manuscript received April 20, 1964; revised manuscript received Dec. 8, 1964.

Any discussion of this paper will appear in a Discussion Section to be published in the December 1965 issue of the JOURNAL.

REFERENCES

1. A. S. Dworkin, H. R. Bronstein, and M. A. Bredig, *Discussion Faraday Soc.*, **32**, 188 (1962); M. A. Bredig, *J. Chem. Phys.*, **37**, 914 (1962).
2. H. R. Bronstein and M. A. Bredig, *J. Am. Chem. Soc.*, **80**, 2077 (1958); and *J. Phys. Chem.*, **65**, 1220 (1961); M. A. Bredig and H. R. Bronstein, *J. Phys. Chem.*, **64**, 64 (1960).
3. P. S. Rogers, J. W. Tomlinson, and R. D. Richardson, "Proceedings of the International Symposium on Physical Chemistry of Process Metallurgy," Pittsburgh 1959, G. R. St. Pierre, Editor, p. 909, Interscience Publishers, New York (1961).
4. B. F. Naylor, *J. Am. Chem. Soc.*, **67**, 150 (1945).
5. A solubility of 4% NaF in solid CaF_2 [D. M. Roy and Rustum Roy, *This Journal*, **111**, 420 (1964)] reconciles the depression of the melting point of CaF_2 by NaF as observed by Rogers et al. (3) with the actual heat of fusion, 7.1 kcal.
6. E. Mollwo, *Nachr. Ges. Wiss. Gottingen*, II, New Series, **1**, 79 (1934).
7. L. Wöhler and G. Rodewald, *Z. anorg. u. allgem. Chem.*, **61**, 54 (1909).
8. See, e.g. M. A. Bredig, "Mixtures of Metals with Molten Salts" in "Molten Salt Chemistry," Milton Blander, Editor, Interscience Publishers, New York (1964).
9. M. A. Bredig et al., To be published.
10. F. Seitz, *Revs. Modern Phys.*, **13**, 384 (1946); **26**, 7 (1954).
11. J. H. de Boer, *Rec. Trav. Chim. Pays-Bas*, **56**, 301 (1937).
12. K. S. Pitzer, *J. Am. Chem. Soc.*, **84**, 2025 (1962).

Some X-Ray and Thermoelectric Studies on Cubic Th_3X_4 Compounds

C. E. Price¹ and I. H. Warren

Department of Metallurgy, The University of British Columbia, Vancouver, British Columbia, Canada

ABSTRACT

Measurements of thermoelectric power and electrical conductivity have been made up to 950°C on Th_3P_4 , Th_3As_4 , Th_3Sb_4 , and $\text{Th}_3(\text{AsSb})_4$ solid solutions. Thermal conductivity data have been obtained near 30°C . X-ray and density measurements suggest that the compounds are stoichiometric.

A previous paper (1) indicated that Th_3As_4 may have interesting thermoelectric properties with a figure of merit comparable to the more widely investigated isostructural compound $\text{Ce}_3\text{-S}_4$. It was shown that compounds having either n- or p-type properties could be prepared, and that appreciable quantities of Fe, Co, Ni, CaS, and BaS could be taken into solution. This investigation was limited by the purity of the thorium available (99%) and the presence of ThO_2 as a major contaminant in the products. The present study, using three grades of thorium metal and an improved preparational technique, reports thermoelectric and x-ray data on Th_3P_4 , Th_3As_4 , Th_3Sb_4 , and $\text{Th}_3(\text{AsSb})_4$ solid solutions.

Experimental

Materials.—Three grades of thorium were used: 99.0% metal from Dominion Magnesium Limited, 99.9% metal from Lindsey Chemical Corporation, and 99.99+ % metal from Leytess Metal Corporation. All metals were received as fine powders; the Dominion and Leytess samples had been packed in sealed containers under an inert atmosphere. They were opened

and stored in an inert gas glove box. A typical analysis quoted by the suppliers for Leytess metal, in ppm, was: oxygen, 30; nitrogen, 20; hydrogen, 5; carbon, 20; aluminum, 5; copper, 10; iron, 25; and all others, ± 2 . Iron was also the main metallic contaminant in the other thorium powders. Arsenic and antimony of 99.999% purity were obtained from Consolidated Mining and Smelting Company. The 99.9% purity phosphorus was from the Fisher Scientific Company.

Preparation of compounds.—The compounds Th_3P_4 , Th_3As_4 , and Th_3Sb_4 were prepared by heating the constituents together in sealed and evacuated Vycor or quartz capsules. Quantities of 20g were made at a time, the elements being weighed to within 0.002g of that required stoichiometrically by the formula. The heating rates were critical for a too rapid increase in temperature led to a violent exothermic reaction which fragmented the capsules. The samples of phosphide, arsenide, and antimonide were heated over a period of 100 hr to 450° , 620° , and 900°C , respectively. For the arsenide it proved essential to maintain the temperature below 350°C for the first 30 hr. No attack of the containers was observed. The capsules were opened, and the products (fine gray powders) stored in the

¹ Present address: Mackay School of Mines, University of Nevada, Reno, Nevada.

glove box. Attempts to prepare a compound Th_3Bi_4 , isostructural to the known compound U_3Bi_4 , were unsuccessful.

Fabrication.—Cylindrical compacts 0.9 cm in diameter and 1-2 cm long were prepared by hot pressing with induction heating, and under a helium atmosphere. Graphite dies and plungers were used, loading taking place in the glove box. During the heating cycle a pressure of 5000 psi was maintained continuously. The heating rates were approximately $150^\circ/\text{min}$. Temperature measurement was by a W- W/26% Re thermocouple placed down a 0.3 cm hole drilled almost to the bottom of the upper plunger. In some instances a molybdenum sleeve was used to separate the sample from direct contact with the carbon of the die. When solid solutions were prepared the powders were mixed beforehand in a mortar. Prior to the measurement of properties, the outer layers of the samples were ground away.

Analyses.—X-ray measurements, using a diffractometer in conjunction with a Geiger counter and chart recorder, were made on the powders and compacts. The powders were imbedded in a flat surface of vacuum grease to prevent oxidation. For angles greater than about 22° it was possible to separate the two peaks of the α_1 - α_2 doublet in the $\text{CuK}\alpha$ radiation used. Less than about 2% of ThO_2 (or a second phase) could not be detected by this method, but from metallographic examination it was estimated, through comparison with contaminated samples, that 0.1% of ThO_2 would be visible readily. In contaminated samples ThO_2 occurred as small white particles. Representative compacts were chemically analyzed to determine the thorium-arsenic ratios and carbon contents. Analyses for dissolved oxygen were not made because of ease of atmospheric contamination.

Property measurement.—Densities were measured by immersion in CCl_4 . Thermal conductivity values (K) were obtained near room temperature by simultaneous absolute and comparative steady-state methods. Temperature gradients of near 10° , 20° , and 30°C were in turn maintained across the sample held under a vacuum of 10^{-5} mm Hg. Temperature measurements were made with copper-constantan thermocouples cleated into copper at each end of the sample. Indium amalgam was used to minimize thermal contact resistances (2). Agreement and reproducibility were to within 5%. Thermoelectric power (α) with reference to copper was determined from liquid nitrogen temperatures to near 1000°C *in vacuo*, using a 10° - $20^\circ\text{C}/\text{cm}$ temperature gradient. Electrical conductivity results (σ) of reproducibility to within 3% were obtained using stainless steel probes pressed against a side of the compact. These measurements have been described in more detail elsewhere (3).

Results and Discussion

The compacts which were all of a silver gray color tarnished very readily in air, dark surface films forming on antimonides and phosphides within 5 min. Although all measurements were done *in vacuo*, some exposure to air proved unavoidable during transfer and assembly. However, exposures of up to 1 hr appeared not to change the results. Samples placed clean and shiny in the apparatus showed a dark surface film after the high-temperature measurements. No reaction occurred with the copper end pieces. The materials were weakly diamagnetic.

Dense Th_3P_4 compacts could not be prepared, for on heating between 1200° and 1600°C the compound gradually decomposed giving the mono form. Th_3As_4 was stable up to 2050°C , densification started near 800°C and appeared to be complete by 1500°C . With Th_3Sb_4 a liquid phase appeared at about 1600°C , but dense compacts could be obtained at 1400°C .

X-ray measurements on the powders gave results, in $\text{A} \pm 0.0005$, of Th_3P_4 8.6530, Th_3As_4 8.8548, and

Table I. Thermoelectric data

Compact	Fabrication Time, min	Temp, $^\circ\text{C}$	α , $\mu\text{V}^\circ\text{C}^{-1}$	σ , ohm-cm^{-1}	K , $\text{cal cm}^{-1} \text{sec}^{-1} \text{C}^{-1}$	Density % theor.
Th_3P_4	15	1200	-223	1.5	0.0086	92
Th_3As_4	30	1900	-160	545	0.0130	100
Th_3Sb_4	15	1600	-52.5	3,370	0.0179	100

Th_3Sb_4 9.3659. These figures differ slightly from the solely reported data of 8.617, 8.843, and 9.372, respectively, summarized by Pearson (4). Attempts to vary the 3Th:4X ratio of arsenide and antimonide compacts failed; monocompound formation or anion deposition on the fabrication container occurred with all arsenide and antimonide compacts exhibiting the same lattice spacing. With Th_3P_4 compacts the lattice spacing appeared to vary in the range 8.630-8.654Å; however, our inability to get dense compacts free of ThP precludes any conclusions in this instance. In the isostructural compound $\text{Ce}_{3-x}\text{S}_4$, however, the lattice size was reported to vary only slightly from 8.6250Å ($x = 0$) to 8.6347Å ($x = 1/3$), but this led to a density drop from 5.68 to 5.18 gm cc^{-1} as x went from 0 to 1/3 (5). As, in the present study, the lattice spacing was constant and the measured densities of arsenide and antimonide were within 1% of that required for a stoichiometric structure, it seems probable that departures from the formula Th_3X_4 are very small or nonexistent in these compounds. Chemical analyses gave carbon contents of 0.02-0.04% and thorium-anion ratios within 5% of ideal.

Thermoelectric data near room temperature for compacts based on the 99.99% purity thorium are summarized in Table I. The variation of thermoelectric power (α) and electrical conductivity (σ) with temperature for these materials are shown in Fig. 1 and 2. Changes in pressing temperatures between 1400° and 2000°C could shift by up to 50°C the temperature at which a given value of α was obtained. Thus, in Fig. 1 the temperature axis may be moved $\pm 25^\circ\text{C}$. As before (1) the trend was for a higher room temperature α with an increased pressing temperature. The reported electrical conductivities (Table I) were the highest obtained, lower pressing temperatures giving in some instances values down to 25% of these figures. The possibility of carbon contamination or inhomogeneity was considered by progressively grinding layers off some samples and remeasuring but no property changes were found.

Data for arsenide and antimonide compacts made from the less pure thoriums are shown in Fig. 3 and 4. The compacts were fabricated as for the purest metal and again α was found to be slightly influenced by pressing temperature. The impure compacts tend to maintain a positive α to a much higher temperature and in the case of the arsenides give subsequently a smaller negative value. As the major metallic impur-

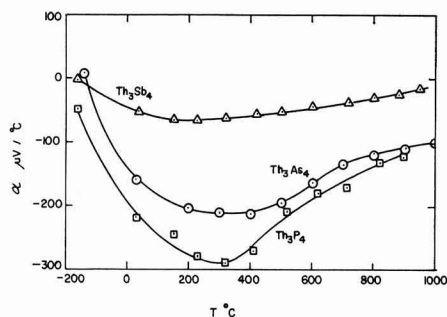


Fig. 1. Variation of thermoelectric power α with temperature for compacts based on the 99.99% purity thorium.

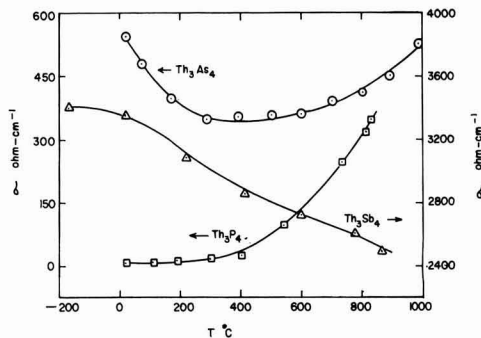


Fig. 2. Variation of electrical conductivity σ with temperature for compacts based on the 99.99% purity thorium.

ity in these compounds is iron it seems likely that the p-type behavior observed in these compounds is not intrinsic to the materials, but arises from the presence of iron and similar impurities providing acceptor levels at low temperatures. These impurity effects are very similar to those observed for metallic additions, nickel in particular, in the previous study.

One unexpected feature of this investigation concerned the behavior of Th_3As_4 compacts pressed in molybdenum lined dies, which were used to reduce the possibility of carbon contamination. Molybdenum diffused into samples pressed at $1800^\circ\text{--}1900^\circ\text{C}$ giving products which appeared to have partially melted. The properties of two specimens (using 99.99% metal) prepared in this way are shown in Fig. 5. One sample not only has a high p-type value near room temperature but, unlike any other compact studies here or previously (1), maintains a negative thermoelectric power

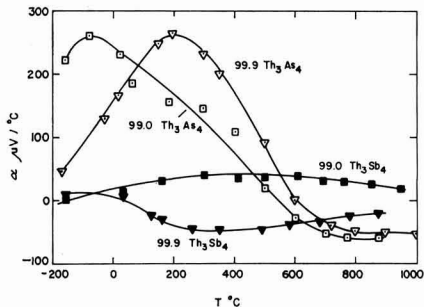


Fig. 3. Variation of thermoelectric power α with temperature for Th_3As_4 and Th_3Sb_4 compacts based on the 99.0 and 99.9% purity thorium.

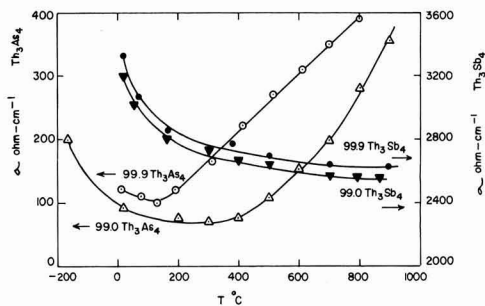


Fig. 4. Variation of electrical conductivity σ with temperature for Th_3As_4 and Th_3Sb_4 compacts based on the 99.0 and 99.9% purity thorium.

Table II. Room temperature x-ray and thermoelectric data

Compact Th_3As_4 , Th_3Sb_4 (proportion)	Lattice parameter A	\pm	$\mu\text{V}^\circ\text{C}^{-1}$ (ohm-cm) $^{-1}$	K , $\text{cal cm}^{-1} \text{sec}^{-1} \text{C}^{-1}$	Density, g cc^{-1}	
1.0	8.4383	0.0005	+170	270	9.51	
0.95	8.8638	0.0005	+203	120	9.55	
0.90	8.8613	0.0005	+53	93	9.52	
0.75	8.972	0.001	+36	260	0.0092	
0.50	9.10	0.02	-36	570	0.0098	
0.25	9.258	0.001	-40	950	0.0110	
0.10	9.3292	0.0005	-10	1430	0.0130	
0.05	9.3687	0.0005	-2	2010	0.0151	
—	1.0	9.3840	0.0005	+8	3300	0.0178

in excess of $200 \mu\text{V}/^\circ\text{C}$ from 500° to 1000°C . Chemical analysis of this sample showed 0.14 w/o (weight per cent) molybdenum; the x-ray pattern was unaltered from Th_3As_4 . In this instance, due to the size and shape of the samples, the electrical conductivities could only be measured approximately, but appeared to be between 150 and $450 (\text{ohm-cm})^{-1}$ over the temperature range.

The examination of the Th_3As_4 - Th_3Sb_4 solid solutions was undertaken using the 99.9% thorium metal which was plentifully available. In Table II room temperature x-ray and thermoelectric data are summarized. The lattice spacing of the middle alloys is only approximate for line broadening occurred. The compounds were all pressed between 1500° and 1600°C which was very near to the melting point for antimony rich alloys. Annealing compacts for 50 hr at 1400°C in *vacuo* had no effect on the properties. Figures 6 and 7 illustrate the variation of α and σ with temperature, intermediate properties occurring for those compounds not shown. The electrical conductivity peak with the 75% antimonide sample is not understood, but was reproduced on a second specimen. It appeared from these results that the arsenide rich compounds had the best thermoelectric properties, accordingly an alloy of composition $\text{Th}_3(0.9 \text{ As}, 0.1 \text{ Sb})_4$ was fab-

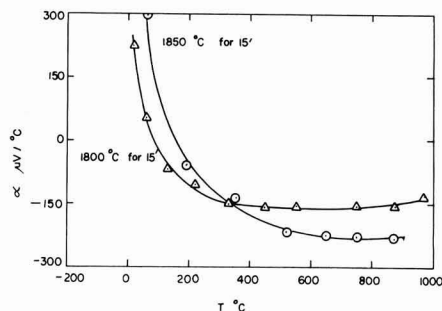


Fig. 5. Variation of thermoelectric power α with temperature for two molybdenum contaminated Th_3As_4 compacts, based on the 99.9% purity thorium.

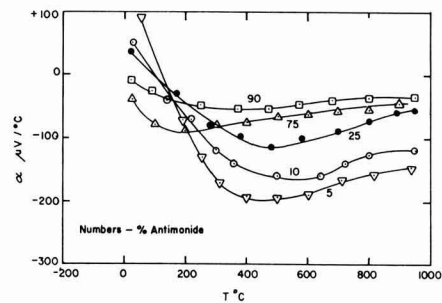


Fig. 6. Variation of thermoelectric power α with temperature for $\text{Th}_3(\text{AsSb})_4$ compacts, based on the 99.9% purity thorium.

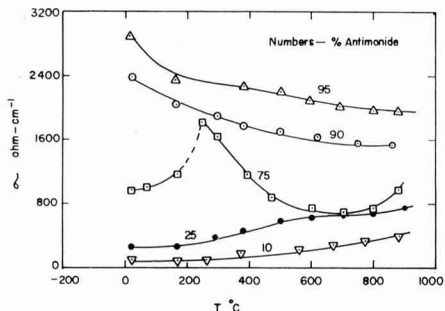


Fig. 7. Variation of electrical conductivity σ with temperature for $\text{Th}_3(\text{As-Sb})_4$ compacts, based on the 99.9% purity thorium.

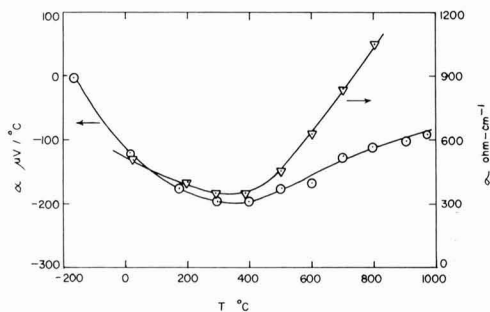


Fig. 8. Variation of thermoelectric power α and electrical conductivity σ with temperature for a $\text{Th}_3(0.9\text{As}, 0.1\text{Sb})_4$ compact based on the 99.99% purity thorium.

ricated using the 99.99% thorium metal. α and σ data for this compact (pressed for 30 min at 1550°C) are shown in Fig. 8.

These Th_3As_4 base compounds have possibilities as high-temperature n-type thermoelectrics. Exact figures of merit (Z) cannot be calculated but if, as in InAs and GeTe (6), K is assumed to halve between 30° and 800°C , then approximate values can be computed. The best Z obtained at 800°C is $0.5 \times 10^{-3} \text{ }^\circ\text{C}^{-1}$ for the $\text{Th}_3(\text{As}_{0.9}\text{Sb}_{0.1})_4$ of Fig. 8. The other materials studied give maximum figures of $0.1\text{--}0.4 \times 10^{-3} \text{ }^\circ\text{C}^{-1}$

up to 900°C . These values, which are almost certainly not the ultimate obtainable, are somewhat lower than the Z of $0.6 \times 10^{-3} \text{ }^\circ\text{C}^{-1}$ for InAs at 800°C and $0.9 \times 10^{-3} \text{ }^\circ\text{C}^{-1}$ for GeTe at 600°C (6).

Interpretation of the data obtained in this investigation is clearly restricted by the polycrystalline nature and limited purity of the compacts. They are conventional in that the electronegativity differences (7) $\text{Th}_{1.4}\text{P}_{2.1}$, As 2.0, Sb 1.8 are suitable for semi-conducting properties (8) and the increasing metallic behavior with temperature is in the correct order Sb-As-P. The fortuitous molybdenum contaminated samples show that n-type conductors of high thermoelectric power up to at least 1000°C can be produced. Phase diagrams of thorium-Group VB compounds are not available but the isostructural uranium compounds U_3Sb_4 (9) and U_3Bi_4 (10) break down below their melting point to give the mono compound. Reference to these diagrams and the observations here with the phosphide suggest that it will be difficult to take the investigation any further for zone refining will be inapplicable and single crystal growth techniques not straightforward.

Acknowledgment

The program was supported by a grant from the Canadian Uranium Research Foundation.

Manuscript received Aug. 23, 1964; revised manuscript received Feb. 15, 1965.

Any discussion of this paper will appear in a Discussion Section to be published in the December 1965 JOURNAL.

REFERENCES

1. I. H. Warren and C. E. Price, To be published.
2. A. D. Stuckes and A. P. Chasmar, *Proc. London Phys. Soc.*, p. 119 (1957).
3. I. H. Warren and C. E. Price, *Can. Met. Q.*, **3**, 183 (1964).
4. W. B. Pearson, "Lattice Spacings and Structures of Metals and Alloys," Pergamon Press, London (1958).
5. M. Cutler, R. L. Fitzpatrick, and J. F. Leavy, *J. Phys. Chem. Solids*, **24**, 319 (1963).
6. R. R. Heikes and R. W. Ure, Jr., "Thermoelectricity: Science and Engineering," pp. 429 and 435, Interscience Publishers, New York (1961).
7. W. Gordy and W. J. Orville Thomas, *J. Chem. Phys.*, **24**, 439 (1956).
8. C. H. L. Goodman, *J. Phys. Chem. Solids*, **6**, 305 (1958).
9. B. J. Beaudry and A. H. Daane, *AIME Trans.*, **215**, 199 (1959).
10. R. J. Teitel, *ibid.*, **215**, 131 (1959).

Some Considerations on the Use of Platinum Electrodes in Chloride Solutions

R. P. Frankenthal and H. W. Pickering¹

Edgar C. Bain Laboratory for Fundamental Research,

United States Steel Corporation, Research Center, Monroeville, Pennsylvania

ABSTRACT

As part of some studies on the passivity of iron-chromium alloys, experiments were performed to determine under which conditions platinum pre-electrolysis electrodes and auxiliary electrodes will dissolve anodically in chloride solutions and cause interference with subsequent measurements due to the cathodic redeposition on the alloy of the dissolved platinum. For these experiments potential-current relationships were measured and thin foils of the alloy were examined by transmission electron microscopy and by selected-area electron diffraction for the presence of deposited platinum. Even when the anolyte and catholyte were separated by a fine-porosity fritted disk during pre-electrolysis, platinum subsequently deposited on the working electrode. Platinum will also dissolve anodically from the auxiliary electrode when a net cathodic current flows at the working electrode; if the electrochemical measurements are not sufficiently fast, the dissolved platinum will diffuse to the working electrode and deposit on it. The presence of dissolved platinum can usually be detected electrochemically. However, an examination of the material under study by transmission electron microscopy and electron diffraction is the most certain means to determine whether platinum will re-deposit under the conditions of the experiment.

In the course of an investigation of the passivity of iron-chromium alloys, it was deemed necessary to investigate the effect of pre-electrolysis of the electrolyte solution. The need for pre-electrolysis in electrochemical studies has been well established, particularly by Bockris (1, 2). The usual procedure (3) is to perform the pre-electrolysis either between two electrodes of the metal under study or between two platinum electrodes and under conditions more stringent than those in the actual experiment, thereby, hopefully, eliminating the impurities that could affect the experiment.

In the work with iron-chromium alloys it was not possible to do the pre-electrolysis between two electrodes of this alloy, since at the current densities required for the pre-electrolysis the anode would assume a potential at which chromium is oxidized to dichromate ion; this ion would then interfere with the passivity experiment. It was, therefore, decided to use platinum electrodes. However, since some of the work was to be done in solutions containing NaCl and since it is well known (4-6) that a platinum anode will dissolve in a chloride medium to give either the chloroplatinite or the chloroplatinate ion, an investigation was conducted into the possible side effects of this anodic dissolution. From a combination of electrochemical measurements and observations by transmission electron microscopy, we have drawn certain conclusions concerning the use of platinum electrodes in chloride media.

Experimental

The working electrode for the electrochemical measurements and the foils for the electron microscope specimens were prepared from a laboratory vacuum melt of high purity Fe-24% Cr alloy. Cylindrical electrodes (1 in. high and ¼ in. in diameter) were machined with a threaded hole for electrical connection at one end. The material for the foils was cold rolled to 0.003 in. Immediately prior to use, the electrodes and the foils were electropolished in a mixture of glacial acetic acid and perchloric acid (5:1) at 35v, rinsed in reagent-grade methanol, dried, and immediately inserted into the cell. Electrical contact was made to the electrode by means of a brass screw that

was isolated from the environments by a Teflon sleeve. To obtain electrical contact with the foil, a thin platinum wire, covered by a glass sleeve, was spot-welded to one end of the foil. The opening at the weld area, as well as the weld, was sealed with polyethylene.

The studies were conducted in three solutions: 1N H₂SO₄, 1N H₂SO₄ + 0.1N NaCl, 1N H₂SO₄ + 0.01N NaCl. These were made from reagent grade chemicals and doubly distilled water with a conductivity of 3×10^{-7} mho-cm. Pre-electrolysis, when performed, was conducted for 24 hr at a current density of 15 ma/cm² between two platinum electrodes, each 10 cm² in area. Experiments were conducted with the anode and cathode in the same compartment and also with the electrode compartments separated by a fritted-glass disk (fine porosity). In the latter case, the electrolyte to be used in the passivity experiments was in the cathode compartment. All solutions were purged with prepurified helium before and during use.

The cell was constructed completely of Pyrex. Both water-wetted glass stopcocks and Teflon stopcocks were used. A Luggin capillary connected the cell to the reference electrode via a salt bridge. The auxiliary electrode was a platinum cylinder (40 mm diameter), concentric with the working electrode to insure uniform current distribution. The working electrode was inserted through a ball joint, so that the electrode could be properly placed with respect to the Luggin capillary. A hydrogen reference electrode was used when the electrolyte was H₂SO₄; a saturated calomel reference electrode was used when chloride was present in the solution. All potentials are reported relative to the normal hydrogen electrode (NHE). Prepurified helium was swept through the cell at all times. The potential-current curves were obtained with a Wenking potentiostat and a motor-driven potentiometer. The potential sweep rate was normally 100 or 200 mv/hr.

Bulk specimens and the foils were treated electrochemically in an identical manner, and the potential-current curves were always similar. The following polarization treatments were used:

1. Immersion at +0.475v vs. NHE (passive region, see Fig. 1); holding at this potential until the electrode was passive; sweeping the potential to -0.165v,

¹On leave until September 1965 at the Max Planck Institut für Physikalische Chemie, Göttingen, Germany.

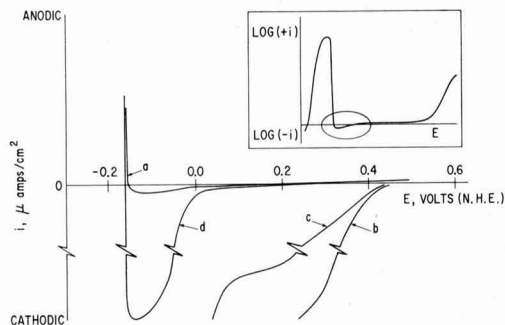


Fig. 1. Potential-current curves in the region of passivity and the Flade potential: (a) in 1N H_2SO_4 or in 1N $H_2SO_4 + 0.1N$ NaCl with no interference from platinum; (b) in presence of large quantities of dissolved platinum; (c) in presence of intermediate amounts of dissolved platinum; (d) in presence of traces of dissolved platinum. Inset shows the over-all passivity curve; the circled area shows the portion plotted in main part of figure.

at which potential the anodic current is increasing sharply as passivity decays.

2. Immersion at $-0.500v$ for 10 sec, at which potential hydrogen evolution proceeds vigorously, sudden switch to $+0.475v$, followed by the procedure outlined for treatment No. 1. This treatment should give an oxide-free surface prior to passivation.

3. Same as treatment No. 1, but potential is suddenly switched from $+0.475$ to $-0.165v$, instead of sweeping through this range.

When the foils reached the final potential, i.e., $-0.165v$, they were pulled from the cell with the potential still applied, rinsed with reagent-grade methanol, and dried. Some foils were examined immediately in the electron microscope; others were stored in a desiccator until they were examined. There was no effect due to storage. Each foil was examined by transmission electron microscopy in a Siemens Elmiskop. In addition, selected-area electron diffraction allowed examination of regions of specific interest.

Solutions were chemically analyzed for platinum by evaporating the solution to a very small volume and adding a few drops of stannous chloride. A brownish-black precipitate indicated the presence of platinum.

Results and Discussion

Table I summarizes the experimental conditions for the various experiments.

Figure 1 summarizes the electrochemical findings in the form of potential-current curves for the alloy under the different conditions in the region of passivity and of the Flade potential ($E \approx -0.2v$). Curve a is for the series of experiments a_1 and a_2 . In H_2SO_4 the potential-current relationship is essentially independent of pre-electrolysis, polarization sweep rate up to approximately 500 mv/hr, and polarization treatment. The cathodic loop has been explained by Edeleanu (7) and is due to hydrogen evolution prior to the breakdown of passivity. As soon as chloride is added to the solution, the other conditions become critical. In experiment a_2 , conditions were such that the po-

Table I. Summary of experimental conditions

Experimental series	Solution composition	Pre-electrolysis	Polarization sweep rate, mv/hr	Polarization treatment
a_1	1N H_2SO_4	Yes, No	100-500	1, 2, and 3
a_2	1N $H_2SO_4 + 0.1N$ NaCl	No	200	1
b	1N $H_2SO_4 + 0.1N$ NaCl	Yes	200	1
c	1N $H_2SO_4 + 0.1N$ NaCl	No	200	2
d	1N $H_2SO_4 + 0.01N$ NaCl	No	100	1

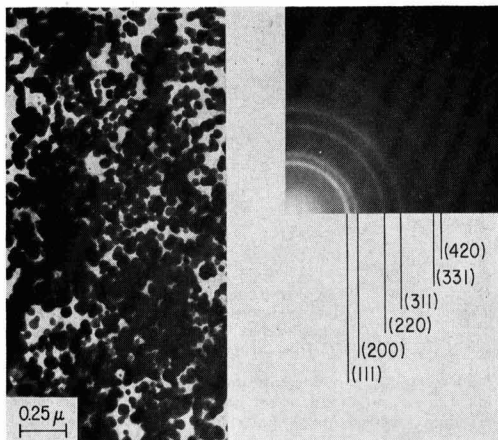


Fig. 2a. (Left) Transmission electron micrograph of platinum deposit at edge of foil after pre-electrolysis of chloride-containing solution between platinum electrodes. (b) (right) Selected-area electron diffraction pattern of area shown in (a) identifying the deposit as platinum.

tential-current curve was the same as for experiment a_1 , and the transmission electron micrographs of the foil showed no trace of platinum deposits.

In experiment b the same solution was used as in experiment a_2 , but it was first pre-electrolyzed between two platinum electrodes in the same compartment; the potential-current relationship is given by curve b. It is obvious that a different cathodic reaction is occurring and that it is occurring at potentials corresponding to a strong oxidizing agent. Chemical analysis of the solution revealed the presence of platinum. A transmission electron micrograph (Fig. 2a) of an area at the edge of a foil that had been subjected to a sweep through this potential range shows a heavy deposit, which has been identified as platinum by selected-area electron diffraction (Fig. 2b).

Experiment c in which the alloy surface was initially cathodically reduced (polarization treatment 2) resulted in curve c. The initial cathodic current is again due to platinum deposition; a limiting current is observed, indicating that the concentration of dissolved platinum is considerably less than for the case represented by curve "b". The transmission electron micrograph (Fig. 3) of a foil shows deposits of platinum. The further increase in the cathodic current after the limiting current is due to hydrogen evolution. This hydrogen evolution begins at a potential about 100 mv more positive than that observed for case a. This results from a lowering of the hydrogen

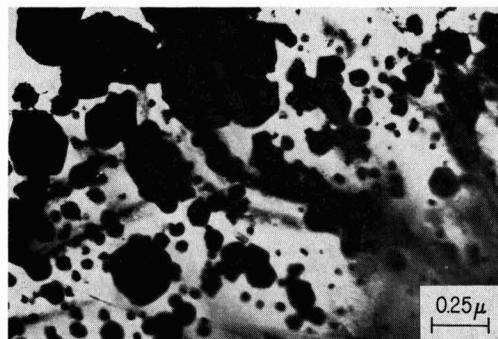


Fig. 3. Transmission electron micrograph of platinum deposit on a foil. Platinum dissolved from the auxiliary electrode during initial hydrogen evolution treatment to clean surface.

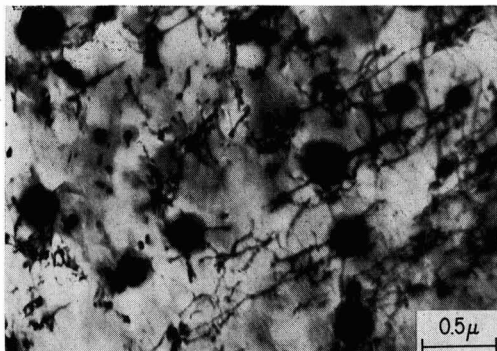


Fig. 4. Transmission electron micrograph of platinum deposit on a foil. Platinum dissolved from auxiliary electrode during potential sweep through cathodic loop. Lines in background are dislocations.

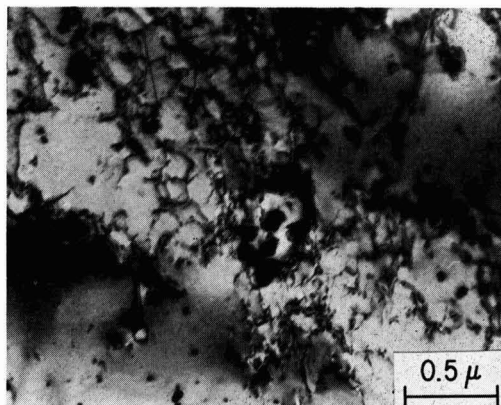


Fig. 5. Transmission electron micrograph showing deposit, which is presumably platinum, on foil exposed to H_2SO_4 . Solution had been pre-electrolyzed between two platinum electrodes for 24 hr at 15 ma/cm². Foil was subjected to polarization treatment No. 1.

overpotential by the platinum deposit. Sweeping through the same potential range with a platinum electrode, the beginning of hydrogen evolution also occurred at the potential shown in curve c.

The deposition of platinum was also observed in experiment d in which more stringent precautions were taken to avoid the anodic dissolution of platinum and its redeposition, but in which a slower polarization sweep rate was used. A potential-current curve similar to a was expected. Instead, the potential-current curve showed a sharply increased cathodic current in the loop, as shown in curve d. The cathodic loop began at about the same potential as for curve a. A transmission electron micrograph (Fig. 4) of the foil shows deposits of platinum. The platinum, undoubtedly, came from the auxiliary electrode during the sweep through the cathodic loop, during which time this electrode had a net anodic current imposed on it. Because of the slow potential sweep rate, the dissolved platinum had time to diffuse to the working electrode, to deposit and to depolarize the hydrogen-evolution reaction. Integrating the area under the time-current curve (potential varied linearly with time) of the cathodic loop, it is estimated that the maximum amount of platinum that could have been dissolved is equivalent to $\frac{1}{2}$ coulomb, assuming the complete absence of other anodic reactions such as chlorine evolution.

When the cathode and anode compartments were separated by a fine-porosity fritted disk during a 24-hr pre-electrolysis of a chloride-containing solution, sufficient dissolved platinum diffused through the disk to be detected qualitatively by chemical analysis. The presence of the dissolved platinum was also detected as a cathodic current when a platinum electrode was swept through the potential range from +0.5 to 0.0v in this solution. Although no foils were examined for this pre-electrolysis condition, the platinum undoubtedly would also have been found on them.

It has been determined that passivity curves in chloride solutions can best be measured by rapidly sweeping the sample through the desired potential range, a procedure which can lead to markedly distorted passivity curves (8), if the rate is too great, or by obtaining a point-by-point plot (polarization treatment No. 3), omitting regions in which the net current on the working electrode is cathodic; and by omitting pre-electrolysis and the initial cathodic reduction of air-formed oxide films. Work in H_2SO_4 showed no deleterious effects on the potential-current curves when pre-electrolysis and oxide reduction were omitted.

The authors are indebted to the reviewer for bringing to their attention the fact that platinum has been found to dissolve in H_2SO_4 (9). The dissolution of platinum by H_2SO_4 is also thought to have occurred

in this work since micrographs of foils treated in H_2SO_4 showed deposits which looked like platinum (Fig. 5). This foil had been subjected to polarization treatment No. 1 after pre-electrolysis of the H_2SO_4 solution. Additional evidence in the form of electron diffraction data must be obtained before it may be unequivocally stated that platinum dissolves in H_2SO_4 under the conditions of our experiments. In this regard it should be noted that the test conditions were considerably more severe in the work of Hirano *et al.* (9) than they were in the work reported here. In their work an anodic current of 2 amp was imposed on a platinum wire (area, 5 cm²) for 3 to 5 hr; analysis of the mercury cathode showed the presence of approximately 10 μ g of platinum. If the deposits, such as those in Fig. 5, are platinum, it was not evident from the potential-current curves indicating that electron microscopy is a more sensitive technique.

The cathodic deposition of platinum appears initially as random deposits (Fig. 4), which grow with continued deposition; for the case in which large quantities of platinum are in solution, the deposits eventually impinge upon one another (Fig. 2a) to cover significant portions of the working electrode surface.

Conclusions

Great caution must be exercised when platinum electrodes are used in chloride-containing media. It has been shown that, whenever a platinum electrode is subjected to an anodic current, some dissolution will occur; if the electrochemical measurements are not sufficiently fast, the dissolved platinum will diffuse to the working electrode and deposit on it. The presence of dissolved platinum can usually be detected electrochemically. However, an examination of the material under study by transmission electron microscopy and electron diffraction is the most certain means to determine whether platinum does deposit under the conditions of the experiment. It has been determined that passivity curves in chloride media can best be measured by rapidly sweeping the desired potential range or by obtaining a point-by-point plot, omitting regions in which the net current on the working electrode is cathodic and by omitting pre-electrolysis and the initial cathodic reduction of oxide films.

Acknowledgments

The authors wish to express their thanks to the following members of this Laboratory: Dr. S. S. Brenner for editorial discussions while writing this paper; Mr. G. W. Momeyer for the chemical analyses; and

Drs. L. S. Darken and R. A. Oriani for their continuing encouragement.

Manuscript received Aug. 24, 1964.

Any discussion of this paper will appear in a Discussion Section to be published in the December 1965 JOURNAL.

REFERENCES

1. J. O'M. Bockris and B. E. Conway, *Trans. Faraday Soc.*, **45**, 989 (1949).
2. J. O'M. Bockris, "Modern Aspects of Electrochemis-

- try," Vol. 1, p. 260, Butterworths Scientific Publications, London (1954).
3. J. O'M. Bockris, I. A. Ammar, and A. K. M. S. Huq, *J. Phys. Chem.*, **61**, 879 (1957).
 4. A. Shluigin and A. Frumkin, *Acta Physicochim. U.R.S.S.*, **3**, 791 (1935).
 5. B. Ershler, *ibid.*, **19**, 139 (1944).
 6. J. Llopis and A. Sancho, *This Journal*, **108**, 720 (1961).
 7. C. Edeleanu, *J. Iron Steel Inst.*, **188**, 122 (1953).
 8. N. D. Greene and R. B. Leonard, *Electrochim. Acta*, **9**, 45 (1964).
 9. S. Hirano, A. Mizuike, and M. Saheki, *Bunseki Kagaku*, **8**, 827 (1959); *CA*, **57**, 1965g (1962).

On the Equilibrium Properties of Single Crystalline Copper Electrodes

Leslie H. Jenkins and Ugo Bertocci

Solid State Division, Oak Ridge National Laboratory, Operated by Union Carbide Corporation for the United States Atomic Energy Commission, Oak Ridge, Tennessee

ABSTRACT

It is shown that, when true equilibrium conditions exist in the aqueous system studied, no single crystal orientation exposed to solution spontaneously changes with time. Also, under these conditions no differences in equilibrium potential can be measured between different orientations. Data are offered which suggest that some previous measurements possibly were not the result of equilibrium properties, but rather were produced by kinetic phenomena.

Previous studies to determine the equilibrium shapes of copper crystals exposed to aqueous solutions and/or to explore the possibility of the existence of thermodynamically more stable orientations have been reported. Getman (1) observed that in CuSO_4 solutions single crystalline copper exhibited an equilibrium potential about 3.5 mv greater than that of copper amalgam electrodes. Leidheiser and Gwathmey (2) reported that in acidic copper sulfate solutions copper single crystals with surfaces oriented (100) were anodic to the (111) orientation by approximately 7 mv in solutions exposed to the atmosphere. This difference dropped to ~ 2 mv in solutions from which air had been removed previously by boiling and which were under a hydrogen atmosphere. Annealing the crystals in hydrogen before exposure to air-saturated solutions caused the (111) to become anodic to the (100) by about 3 mv. However, Tragert and Robertson (3) concluded that only the (111) orientation was stable and capable of producing a reversible cell, and that in time all other orientations approached the (111) since they were metastable in CuSO_4 solutions. Since these and other published data are not in complete agreement, it seemed worthwhile to establish and attempt to understand, if possible, the reasons for disagreement.

Materials

Three different types of 99.999% pure copper single crystals were used. Coupons $\sim 10 \times 20 \times 1$ mm with the preferred orientation on the large 20×10 mm area were prepared in a manner described previously (4). Coin shaped crystals, 25 mm diameter \times 7 mm thick, were cut with an acid saw from larger single crystal cylindrical slugs which had been grown by a modified Bridgman technique. Spherical crystals ~ 12 mm in diameter also were grown by the latter technique. Copper sulfate solutions were prepared from reagent grade $\text{CuSO}_4 \cdot 5\text{H}_2\text{O}$ and H_2SO_4 . These solutions were prepared and maintained in a rack reservoir by methods previously described. All solutions reported in this study were 0.2M in CuSO_4 with pH adjusted to ~ 1 with sulfuric acid. Also, at the time of removal from the storage rack and admission to the systems of interest, the solutions, free of dissolved oxygen,

were under a hydrogen atmosphere and at equilibrium with copper metal.

Experimental Method

Following normal mechanical preparation (4), coupon crystals were electropolished in an acid copper phosphate bath, rinsed in dilute phosphoric acid, washed in distilled water, and dried in a jet of oxygen. They were then suspended from one of the four glass hooks of the insert thimble of the test cell, as shown in Fig. 1. The entire apparatus was attached to the reaction rack through the side-arm standard glass joints with o-ring seals. After repeated evacuation and filling with hydrogen, a heater was placed about the lower portion of the flask, and the crystals annealed at 450°C

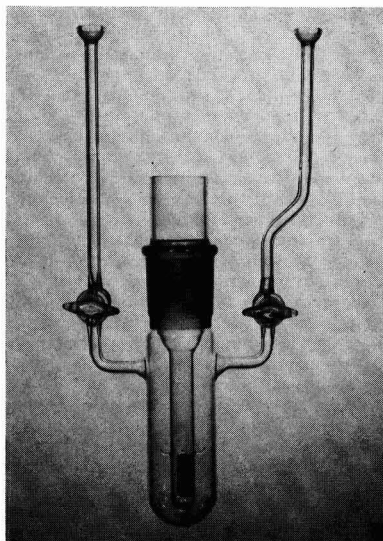


Fig. 1. Annealing cell for coupon crystals

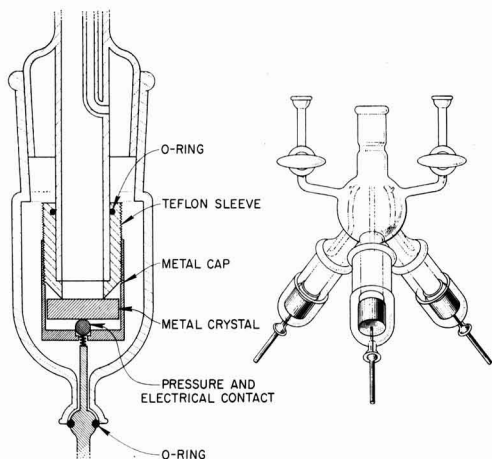


Fig. 2. Tripod cell permitting isolation of a single orientation

under H_2 for ~ 15 hr. When annealing had been completed and the crystals cooled to ambient temperature, the pre-equilibrated copper sulfate solution under a hydrogen atmosphere was admitted to the flask. The side-arm stopcocks were closed and the apparatus removed from the filling rack and immersed in a water bath at $25.04^\circ \pm 0.02^\circ C$. Periodic visual inspections could be made of the systems.

Cylindrical (coin shaped) crystals were first polished on a chemical polishing wheel to remove small surface irregularities introduced by the acid sawing process (5). The remainder of the polishing and washing procedure was identical to that given coupon crystals. After drying, the polished crystals were mounted on one of the three legs of a tripod cell in the manner shown in Fig. 2. A glass electrode which had been sealed vacuum-tight into a standard taper glass bushing with o-rings and epoxy resins was inserted in the standard taper joint at the top of the cell. Another entry port to the system, not shown in the illustration and hereafter referred to as the side port, was provided by a small standard taper joint located in the upper rear quadrant of the cell. A platinum wire sealed through the corresponding male member of the joint provided a means of electrical contact as well as a means of suspension of a polycrystalline 99.999% copper wire. When assembly was complete, this entire apparatus was also attached to the filling rack with o-ring seals at the standard joints on the side-arms of the cell. After repeated evacuations and filling with hydrogen, copper sulfate solution was admitted to the system and the side-arm stopcocks closed. Obviously, it was impossible to anneal the crystals. A constant temperature air bath, temperature $23.0^\circ \pm 0.1^\circ C$, was placed about the system and constant temperature maintained for the remainder of the experiment. Since the system was so massive, temperature fluctuations within the cell were small.

Potential differences between the glass electrodes and metal specimens were measured with a Beckman, model G, pH meter. Potentials between metal crystals were measured with a Cary, Model 31V, vibrating reed electrometer.

In all cases after experimentation was completed, the cells were opened quickly and the crystal hurriedly washed in distilled water, dried in a jet of oxygen, and examined with the optical microscope.

Experimental Results

Equilibrium Systems

Annealed crystals.—Four coupon crystals, oriented (100), (110), (111), and (321), respectively, were

suspended from the glass hooks of the insert thimble. Systems were exposed to the copper sulfate solution for periods of 1, 3, 7, and 17 weeks. Visual inspection of the crystals showed no detectable changes in surface topography on all samples during this time. In every case, after removal from the cell, absolutely no evidence of change in surface structure could be observed microscopically. In one instance, rather than filling the flask to a level such that all samples were entirely immersed, as was normally done, only enough solution was admitted to cover half of each coupon. Upon opening, it was impossible to detect even where the solution level had been on these crystals. Also, determination of sample weights in two systems before and after exposure to solution showed no weight changes.

A spherical copper crystal¹ was suspended from a special insert thimble consisting of only one large vertical hook, annealed, and exposed to solution for two weeks in one case and four weeks in another. At the end of the indicated times no changes could be detected on any surface area in either case.

Nonannealed crystals.—To insure that the previous results were not due to the presence of undesired orientations on the edges of the coupon crystals, similar studies were conducted on cylindrical crystals in tripod cells since exposure to solution could be restricted to the orientation of interest. Coin shaped crystals with the large flat areas oriented (100), (110), and (111), respectively, were mounted one on each leg of the cell. After exposure to the copper sulfate solution at controlled temperature for periods varying from one week to four months, the cells were opened and the solution removed and saved for analysis. Examination of the crystal surfaces showed that in no case was there any detectable change in the surfaces exposed to the solutions.

Neither could a change be observed on any of these three orientations which in one system had been exposed to the solution for one year at ambient laboratory temperature, nor was any change in surface structure observed on a spherical crystal suspended from the glass electrode after a four months' exposure at controlled temperature of $23.0^\circ \pm 0.1^\circ C$.

Rest potentials.—The following observations were made only on nonannealed crystals in cells of the tripod type. It is difficult experimentally both to isolate an orientation and anneal the crystal, and it was judged to be unnecessary in this instance.

Immediately on admitting solution to the cells, a small initial potential difference (never exceeding 1.5 mv) could sometimes be measured between different orientations as well as a polycrystalline wire suspended through the side entry port. However, within 1 hr these differences had decreased to 0.2 mv, a value never exceeded during the remainder of the experiments and thought to be about the limit of experimental error in these systems. Since the magnitude and sign of both the initial and later potential differences varied from one orientation to another in different systems, they are not thought to be significant, and only one typical set of data are shown as system A, Table I.

Because the glass electrode had been subjected to vacuum treatment during preparation of the system, it usually required about 4 hr of exposure to solution before reliable results could be obtained. After that period a potential difference of ~ 300 mv was observed between the glass electrode and the copper crystals. The exact magnitude varied from one electrode and one system to another. Since aging and standardization of the electrode could not be accomplished after the vacuum treatment and prior to exposure to solutions, the absolute magnitude of the potentials observed is not significant. However, it is significant that other than the first few hours not only were no potential differences measured between crystals after one day or one year, but in every instance the potential measured

¹ Spherical 99.999% pure copper single crystals were kindly supplied by John V. Cathcart of this Laboratory.

Table I. Potential differences of various orientations

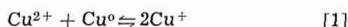
System	Potential of (100) mv vs. (111)		Time after solution admitted
	(110)	(111)	
(A)	0.75	0.62	0.1 hr
No O ₂ leak	0.09	-0.27	1.0 hr
No residual O ₂	0.02	-0.11	1.5 hr
(B)	2.01	1.66	0.1 hr
No O ₂ leak	2.26	2.01	1.0 hr
Slight residual O ₂	0.99	1.53	8.0 hr
	0.24	0.10	24.0 hr
	-0.10	0.14	48.0 hr
(C)	9.15	8.65	1 day
Constant O ₂ leak	7.42	7.70	5 day
Equivalent to a cor- rosion current of ~10 μa/cm ²	5.98	6.84	15 day
	4.96	4.64	30 day
	4.48	3.47	60 day
	3.88	2.61	90 day

between the glass electrode and the crystals also did not change with time.

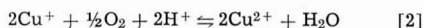
Nonequilibrium Systems

Since the experimental conditions described here were quite different from those of previous workers (1-3), it was understandable that the data were not in full agreement. However, a possible explanation of the cause(s) for disagreement was desirable. Fortunately, air inadvertently leaking slowly into a system under observation resulted in potential differences arising between electrodes and produced changes in surface topography which suggested a means of explaining these differences.

It has been shown (6) that surfaces being oxidized by oxygen dissolved in solution are attacked uniformly since the reaction rate is diffusion controlled. However, another reaction mechanism is possible in a system of copper metal exposed to a solution of its ions. If the system is originally at equilibrium, then the equilibrium constant of $\sim 10^{-6}$ is satisfied for the reaction



If air slowly leaks into the system at a point far removed from the metal, equilibrium is destroyed by the reaction



The equilibrium concentration of copper(I) ions can be restored only when copper metal is oxidized by copper(II) ions, as in reaction [1] proceeding to the right.

Controlled, constant leak rates in the systems could be obtained through faulty platinum-through-glass seals of the male standard joint at the side entry port. If a very limited reaction was desired, evacuation and

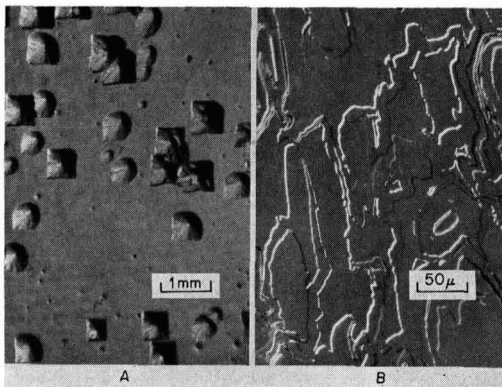


Fig. 3. Structures developed on surfaces after oxidation by cupric ions: (a) (100) surface; (b) (111) surface.

flushing with hydrogen was limited so that a trace of air was retained in the system. The following data were all obtained using tripod cells.

Figure 3 shows typical structures developed by cupric ion oxidation of the indicated surface. It is obvious that dissolution on the (100) and (111) occurred in highly restricted regions rather than uniformly over the entire surface. This phenomena was repeated in all systems at all reaction rates up to 30 μa/cm², the greatest rate studied. Facets developed on the (110) were more uniformly distributed, but their appearance and habit also were observed repeatedly in all systems not at equilibrium.

Table I records some typical potential differences measured in these systems. As previously stated, the first group of data in the table was collected from an experiment in which not only had the cell initially been well evacuated and flushed with hydrogen so that no residue of oxygen remained, but there was also no leak in the system. The experiment supplying the second group of data, System (B), had not been well evacuated and flushed so that a small residue of oxygen remained. However, there was no leak in the cell, and equilibrium was established within two days. Obviously the potential differences observed reflect the corrosion process occurring on the various orientations. Although the potentials are meaningful, when the system was opened and the surfaces examined the reaction generating the potentials had been so slight that surface changes could be detected only on the (100), and then only after extremely careful observation. Needless to say, no corrosion rate could be established since no detectable change in copper concentration occurred in solution.

System (C) in Table I had a constant leak of air into the system which resulted in a corrosion rate equivalent to approximately 10 μa/cm² geometric electrode area. The gradual decrease in potential differences reflects (among other things) changes in the crystal surfaces, for when the samples were removed after 111 days, very little of the original surface remained on any of the electrodes.

Discussion and Conclusions

The failure of all crystals (annealed or not; either coupon, spherical, or cylindrical) to develop facets spontaneously after exposure to oxygen-free copper sulfate solutions (initially at equilibrium with polycrystalline copper) for varying periods of time up to one year suggest that no crystal orientation is thermodynamically more stable than any other in the system studied. The data in Table I show that even small departures from equilibrium conditions generate a measurable and significant potential difference and suggest that, if at equilibrium a potential difference as little as ~1 mv existed between different orientations, facets of preferred orientation(s) would develop since mass transfer could occur.

Because equilibrium potentials were measured in a cell which did not permit annealing the crystals, it is probable that initial small potential differences sometimes observed between crystals was due primarily to the dissolution of oxide originally present on the electrode surface. Certainly in noncorroding systems no potential differences could be measured between unlike orientations or between the glass electrode and one orientation as compared with another. Therefore since any potential differences between orientations cannot be measured experimentally, and since spontaneous faceting does not occur over long periods of time, it is reasonable to conclude that no potential difference exists between different orientations under equilibrium conditions.

The nature of the pits developed on (100) surfaces and the formation of ledges on the (111), as well as the potential differences observed in cells containing dissolved oxygen, perhaps explain the variance of

these data with most of those in the literature. First of all, the physical dimensions of each leg of the tripod cell were equal, and geometric surface areas exposed to solution were the same for all crystals. It can be assumed then that over-all corrosion rates were equal in the legs of any one cell. The potential differences observed were not due to differences in corrosion rate, but reflect rather complex surface properties of the different crystals. These problems will be enlarged and treated in another paper.

None of the data discussed here was collected under conditions in which the corrosion current exceeded $30 \mu\text{A}/\text{cm}^2$. Many observations were made on systems reacting at rates $\sim 10 \mu\text{A}/\text{cm}^2$, but most data were obtained with rates of $0.5\text{--}3 \mu\text{A}/\text{cm}^2$. In all cases significant differences in potential could be measured, even at the slowest rates. The magnitude of the differences was generally proportional to the difference in corrosion rates from one system to another, and although the significance is not clear, the (100) was usually anodic with respect to the (111) and (110) in all corroding systems.

In summary, it has been shown that two conditions must be fulfilled before true equilibrium exists in a solution of copper sulfate exposed to copper metal: (A) No dissolved oxygen can be present or corrosion will occur as shown in Eq. [1] and [2]. (B) Even if no dissolved oxygen is present, the solution must be pre-equilibrated with copper metal before immersion of the test electrode, or reaction [1] will occur until equilibrium is established. It must be emphasized again that dissolution due to the latter cause is not appreciable for the equilibrium concentration of copper(I) ions in solutions of copper (II) ions at unit activity is $\sim 10^{-3}\text{M}$. Finally, although not discussed here previously, Miller and Lawless (7) have shown that the pH of such systems is a factor in establishing equilibrium as defined by Eq. [1]. Their results need not be described at length, but clearly they demonstrate that, even in deaerated CuSO_4 solutions at all pH values above ~ 3.2 , oxide films grew over the metal surfaces for periods of hours, and that in addition to the composition and growth forms of the films being complex,

it was reasonable to assume that little, if any, metal surface is free of oxide under such conditions. Therefore, whatever the final equilibrium state in these latter systems, it is reached slowly, accompanied by a decreased pH of the solution, and certainly must involve some consideration of the presence of an oxide film. Obviously, in such a system an initial potential difference between electrodes which decreased with time possibly could be due only to the complex processes occurring on the surface rather than to differences in thermodynamic states of crystal orientations.

Then at the moment of immersion of a test electrode true equilibrium exists only in solutions which are free of dissolved oxygen, which have been pre-equilibrated with copper metal, and which exhibit a pH less than about 3.2. While the equilibrium results reported here were obtained under these conditions, the authors are unaware of any previous reports on the single crystal Cu-aqueous copper sulfate system in which all three requirements were satisfied. Therefore, it is possible that many previous measurements of others reporting crystallographic differences in equilibrium potentials were obtained from systems originally removed from equilibrium, and the potential differences observed were due to kinetic rather than thermodynamic phenomena.

Manuscript received Oct. 21, 1964; revised manuscript received Jan. 30, 1965.

Any discussion of this paper will appear in a Discussion Section to be published in the December 1965 JOURNAL.

REFERENCES

1. F. Getman, *J. Phys. Chem.*, **34**, 1454 (1930).
2. H. Leidheiser, Jr., and A. T. Gwathmey, *Trans. Electrochem. Soc.*, **91**, 97 (1947).
3. W. E. Tragert and W. D. Robertson, *This Journal*, **102**, 86 (1955).
4. L. H. Jenkins and J. O. Stiegler, *ibid.*, **109**, 467 (1962).
5. F. W. Young, Jr., and T. R. Wilson, *Rev. Sci. Inst.*, **32**, 559 (1961).
6. L. H. Jenkins, *This Journal*, **107**, 371 (1960).
7. G. T. Miller, Jr., and K. R. Lawless, *ibid.*, **106**, 854 (1959).

Studies of the Electrochemical Kinetics of Indium

II. System Indium + Indium Sulfate at Higher C.D.

V. Markovac and B. Lovrecek

*Institute of Electrochemistry and Electrochemical Technology,
Faculty of Technology, University of Zagreb, Zagreb, Yugoslavia*

ABSTRACT

In a previous paper the kinetics of the deposition and dissolution of indium was studied by a galvanostatic method of single current pulses. At c.d. higher than $2.5 \times 10^{-3} \text{ amp}/\text{cm}^2$ a change in the mechanism of the deposition and dissolution of indium was observed. To study the phenomenon, the cathodic and anodic polarization in solutions of indium sulfate with pH 2.5, pH 1.56, and pH 1.0 was investigated as well as the deposition of hydrogen at cathodic polarization in equivalent sulfate solution without indium. After cathodic polarization at chosen c.d.'s, the polarographic investigation of the indium sulfate solution was done. Analysis of the experimental data obtained by cathodic polarization in indium sulfate solution at higher c.d. points to the reaction step $\text{In}^{3+} + 2e_0 \rightarrow \text{In}^{1+}$ as rate-determining. For anodic polarization one can conclude that a disproportionation reaction occurs with increasing c.d., and that the first anodic reaction step $\text{In}^0 - e_0 \rightarrow \text{In}^{1+}$ becomes rate-determining.

In a previous paper (1) the kinetics of deposition and dissolution of indium in sulfate solution was studied using a galvanostatic method of single square-wave pulses.

In that paper it was mentioned that experimental $\eta_A - \log_{10} i$ curves for c.d.'s higher than $2.5 \times 10^{-3} \text{ amp}/\text{cm}^2$ do not follow Tafel linear relation as found for the region of lower c.d.'s, but show reproducible

deviations. The phenomena indicate the existence of some other processes which interfere in the processes previously described (1) and point to changes in the mechanism of deposition and dissolution of indium at higher c.d.'s.

These phenomena were investigated by a slightly modified experimental method (1). The expressions

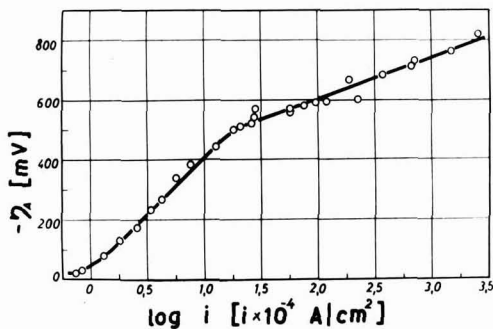


Fig. 1. $\eta_A - \log i$ curve for cathodic polarization. Electrolyte: 0.116N $\text{In}_2(\text{SO}_4)_3 + 0.5\text{N K}_2\text{SO}_4$, pH 2.5.

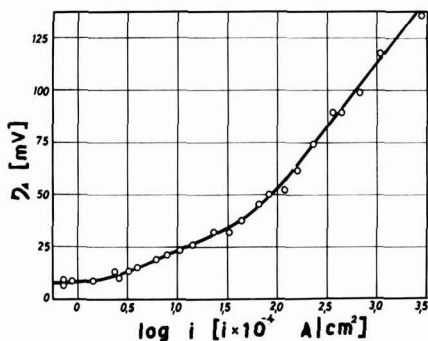


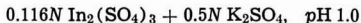
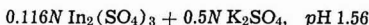
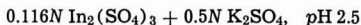
Fig. 2. $\eta_A - \log i$ curve for anodic polarization. Electrolyte: 0.116N $\text{In}_2(\text{SO}_4)_3 + 0.5\text{N K}_2\text{SO}_4$, pH 2.5.

for kinetics of "many steps" electrode reactions (2) were used.

Experimental

For cathodic and anodic polarization of indium (as 0.3% indium amalgam) with galvanostatic single pulses the same apparatus was used as described (1), with the exception that the electrolytical cell was placed in a wooden air thermostat provided with thermoregulator and ventilator that allows work at a constant temperature of $25^\circ \pm 1^\circ\text{C}$.

Polarization was carried out in the following electrolytes



Chemicals used were of analytical reagent grade and water was redistilled.

The experimental $\eta_t - t$ curves were obtained in the same way as previously described (1).

To test for the presence of ions of lower valency in the electrolyte after cathodic polarization, the electrolysis and polarography of indium sulfate solution were done in an analogous way as earlier (3).

Results

Activation overpotential-current density relationship.—The difference between the steady-state potential and the ohmic overpotential η_Ω represents the activation overpotential η_A (1).

When the values of activation overpotential (η_A) were plotted against the logarithms of c.d. ($\log_{10} i$), the curves (Fig. 1, 2) for cathodic and anodic polarization in 0.116N $\text{In}_2(\text{SO}_4)_3 + 0.5\text{N K}_2\text{SO}_4$ at pH 2.5 were ob-

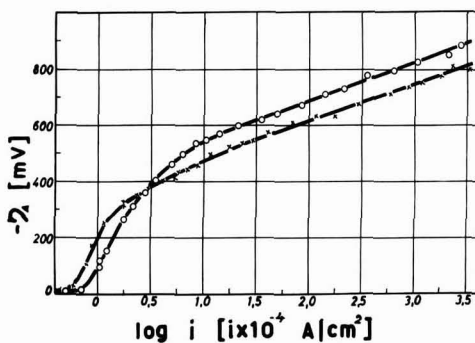


Fig. 3. $\eta_A - \log i$ curves for cathodic polarization. Electrolyte: 0.116N $\text{In}_2(\text{SO}_4)_3 + 0.5\text{N K}_2\text{SO}_4$; x, pH 1.0; O, pH 1.56.

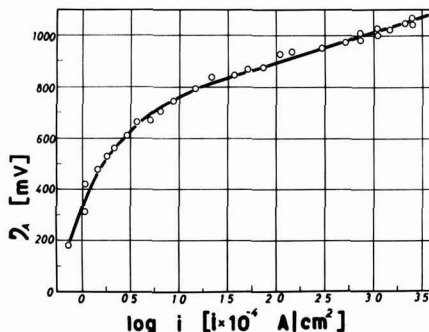


Fig. 4. $\eta_A - \log i$ curve for cathodic polarization. Electrolyte: 0.5N K_2SO_4 , pH 2.5.

tained. Both curves are linear in the c.d. ranges $2.5 \times 10^{-4} - 2.5 \times 10^{-3}$ amp/cm² and $8.5 \times 10^{-3} - 2.5 \times 10^{-1}$ amp/cm².

Figure 3 shows $\eta_A - \log i$ curves for cathodic polarization in 0.116N $\text{In}_2(\text{SO}_4)_3 + 0.5\text{N K}_2\text{SO}_4$ at pH 1.56 and pH 1.0, respectively. The curve corresponding to the solution with pH 1.56 is linear in the c.d. ranges $8.5 \times 10^{-5} - 2.5 \times 10^{-4}$ amp/cm² and $1.5 \times 10^{-3} - 3.0 \times 10^{-1}$ amp/cm² as is the curve in the solution with pH 1.0 in the c.d. ranges $7.0 \times 10^{-5} - 1.2 \times 10^{-4}$ amp/cm² and $1.5 \times 10^{-3} - 3.0 \times 10^{-1}$ amp/cm².

Figure 4 shows the $\eta_A - \log i$ curve for cathodic polarization in an electrolyte without indium (0.5N K_2SO_4 at pH 2.5). In the c.d. range $1.5 \times 10^{-3} - 2.5 \times 10^{-1}$ amp/cm² the experimental curve shows a marked linear relation with characteristics usual for the deposition of hydrogen. (Experimentally obtained parameters of Tafel-line are: $a = -0.666\text{v}$, $b = 0.114\text{v}$).

The linear parts of the experimental $\eta_A - \log_{10} i$ curves (Fig. 1, 2, 3, 4) that are in fact Tafel-lines are treated with a method earlier developed (2), using expressions for the slowest reaction step, i.e., the rate-determining step.

$$\frac{\partial \log i_-}{\partial V} = -\frac{zF}{2.303 RT} (n_c^* - \alpha) \quad [1]$$

$$\frac{\partial \log i_+}{\partial V} = \frac{zF}{2.303 RT} (n_a^* - 1 + \alpha) \quad [2]$$

Since the left sides of Eq. [1] and [2] represent the slopes of the experimental Tafel-lines, it was possible to obtain from the experimental data n_c^* , n_a^* , and α .¹

¹ n_c^* and n_a^* being the ordinal numbers of the slowest reaction step for the cathodic and anodic polarization (small integer), α the transfer coefficient ($0 < \alpha < 1$), and z the number of electrons involved in the slowest reaction step.

Table I. Kinetic parameters for cathodic polarization

Electrolyte	pH	Range of c.d., amp/cm ²	$\partial \log_{10} i_{\text{c}}$ - #		
			∂V	$\alpha\#$	$n_e^* z$
0.116N In ₂ (SO ₄) ₃ + 0.5N K ₂ SO ₄	2.5	2.5 × 10 ⁻⁴ to 2.5 × 10 ⁻³	2.87	0.834	1 1
		8.5 × 10 ⁻³ to 2.5 × 10 ⁻¹	6.11	0.823	1 2
0.116N In ₂ (SO ₄) ₃ + 0.5N K ₂ SO ₄	1.56	8.5 × 10 ⁻⁵ to 2.5 × 10 ⁻⁴	1.44	0.917	1 1
		1.5 × 10 ⁻³ to 3.0 × 10 ⁻¹	7.20	0.792	1 2
0.116N In ₂ (SO ₄) ₃ + 0.5N K ₂ SO ₄	1.0	7.0 × 10 ⁻⁵ to 1.2 × 10 ⁻⁴	1.24	0.929	1 1
		1.5 × 10 ⁻³ to 3.0 × 10 ⁻¹	7.84	0.773	1 2
0.5N K ₂ SO ₄	2.5	1.5 × 10 ⁻³ to 2.5 × 10 ⁻¹	8.74	0.494	1 1

Mean values derived from 2-7 complete experimental curves.

Table II. Kinetic parameters for anodic polarization

Electrolyte	pH	Range of c.d., amp/cm ²	$\partial \log_{10} i_{\text{a}}$ - #		
			∂V	$\alpha\#$	$n_a^* z$
0.116N In ₂ (SO ₄) ₃ + 0.5N K ₂ SO ₄	2.5	2.5 × 10 ⁻⁴ to 2.5 × 10 ⁻³	48.0	0.803	3 1
		8.5 × 10 ⁻³ to 2.5 × 10 ⁻¹	14.99	0.869	1 1

Mean values derived from 4-7 complete experimental curves.

Results of the calculations are presented in Table I and Table II.

Polarographic investigations.—Figure 5 shows polarograms obtained before and after cathodic polarization of indium in sulfate electrolyte and a polarogram obtained in the corresponding sulfate electrolyte without indium. As it is seen (Fig. 5) there is no experimental curve with an anodic wave. Consequently after cathodic polarization it is not possible to prove the existence of ions of lower valency by polarography.

Discussion

Ohmic Overpotential

When the experimental values of the ohmic overpotential were plotted against the values of the cur-

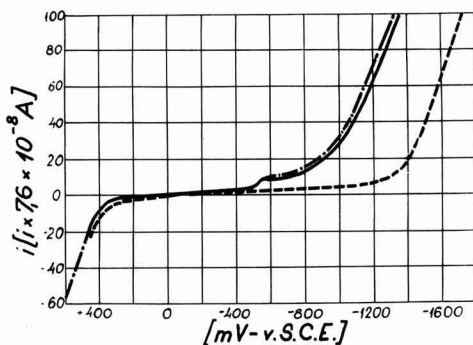


Fig. 5. Polarograms for electrolyte: 0.116N In₂(SO₄)₃ + 0.5N K₂SO₄, pH 2.5: —, before electrolysis; - - -, after electrolysis ($i_c = 71.9$ ma/cm², $t = 10$ min); - · - · - electrolyte without indium.

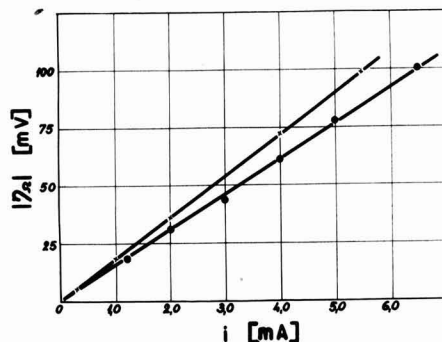
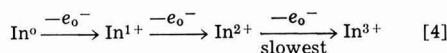
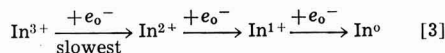


Fig. 6. $\eta_{\text{A}} - i$ curves for electrolyte: 0.116N In₂(SO₄)₃ + 0.5N K₂SO₄; x, pH 1.56; o, pH 1.0.

rent i , the linear relation was obtained with slope representing the resistance R (Fig. 6). The resistance R calculated on the ground of expression of Mattsson and Bockris (4) is in good accordance with values determined experimentally (Table III).

Activation Overpotential-Logarithms of Current Density Curves

For the electrochemical deposition and dissolution of indium in the region of lower c.d.'s (Fig. 1, 2, Table I, II) it was found that the first step was the slowest one in the cathodic reaction and that the third step was the slowest one in the anodic reaction (1).



If the c.d. is increased over 2.5×10^{-3} amp/cm², $\eta_{\text{A}} - \log_{10} i$ curves do not follow earlier relations either at cathodic or at anodic polarization.

Cathodic curve at higher c.d.'s.—The curve for cathodic polarization shows a transition in the range of c.d.'s $2.5 \times 10^{-3} - 8.5 \times 10^{-3}$ amp/cm², but in the range of higher c.d.'s there exists again a linear relation with another slope (Fig. 1). Such an experimental fact points to the change in the mechanism of indium deposition at higher c.d.'s. To explain the significance of the linear part of the experimental $\eta_{\text{A}} - \log_{10} i$ curve at higher c.d.'s we have to consider the processes that might occur under given circumstances.

It might be assumed that the first step of the overall reaction, Eq. [3], at higher c.d.'s is so much accelerated that the over-all reaction is controlled eventually by the second or third cathodic step. The assumption is questionable because the linear part of the experimental curve has a slope that shows according to Eq. [1] that the first cathodic reaction step is the slowest one (Table I). Furthermore, after the cathodic polarization at chosen c.d.'s it was not possible to find oxidizable intermediates by polarography, i.e., we did not succeed in recording the anodic wave (Fig. 5).²

² In an earlier investigation (3) it was possible to register ions of lower valency by polarography after anodic polarization.

Table III. Resistance calculated and experimentally determined for 0.116N In₂(SO₄)₃ + 0.5N K₂SO₄ at various pH values

pH	$R_{\text{calc.}}$	$R_{\text{exp.}}$
1.56	17.7	18.0
1.0	15.3	15.4

For corresponding data for electrolyte of pH 2.5 see ref. (1).

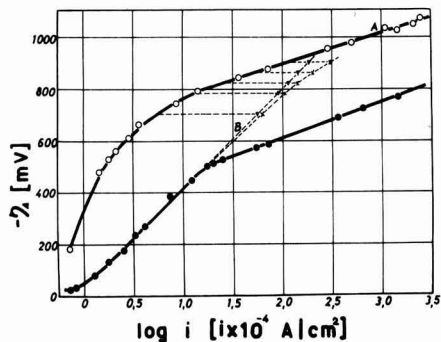


Fig. 7. ●, cathodic $\eta_A - \log_{10} i$ curve for electrolyte: 0.116N $\text{In}_2(\text{SO}_4)_3 + 0.5N \text{K}_2\text{SO}_4$, pH 2.5. ○, Cathodic $\eta_A - \log_{10} i$ curve for electrolyte: 0.5N K_2SO_4 , pH 2.5. ▽, Selected points at the lengthened linear part of curve of deposition of indium. x, Curve constructed by addition A and B.

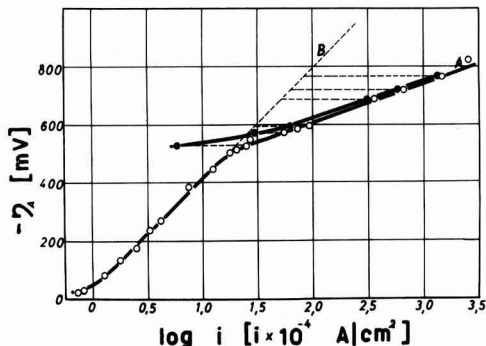
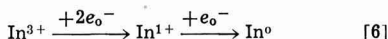
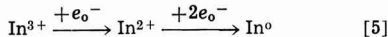


Fig. 8. ○, cathodic $\eta_A - \log_{10} i$ curve for electrolyte: 0.116N $\text{In}_2(\text{SO}_4)_3 + 0.5N \text{K}_2\text{SO}_4$, pH 2.5. ●, Curve constructed by subtraction A and B.

According to other authors (5) it might be assumed that the deposition of hydrogen may influence the experimental curve at increased c.d.'s and low pH values. Actually, our experimental results (Fig. 3) show some changes with decreasing pH, although the general shape and characteristic slopes remain the same. To find the magnitude of the influence that hydrogen deposition might have at higher c.d.'s on the experimental $\eta_A - \log_{10} i$ curve, a parallel cathodic polarization was carried out using an equivalent electrolyte without indium. The curve obtained in such a way shows over a wide range a typical Tafel linear relation for hydrogen deposition as often reported in the literature.

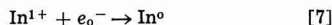
To compare experimental $\eta_A - \log_{10} i$ curves at cathodic polarization in the presence and absence of indium, we applied the following procedure (Fig. 7). The linear part of the curve in the presence of indium at lower c.d.'s was lengthened, and at that part of the curve random points of c.d.'s were added to those of hydrogen discharge at the same overpotentials. In such a case, the constructed and experimental curve would coincide if the discharge of hydrogen is a simultaneous and parallel process to the deposition of indium at higher c.d.'s. However, this is obviously not the case (Fig. 7) and indicates that at higher c.d.'s some changes occur in the kinetics of deposition of indium itself, although under such conditions some deposition of hydrogen might be expected.

Let us therefore consider again the possible reaction steps of the over-all electrochemical process of deposition. There is no reason not to accept the possibility of the fusion of any two of the three possible reaction steps [3], especially in the range of higher c.d.'s; i.e., the deposition of indium might proceed as follows:



Reaction [5] would hardly be possible because either the second cathodic step should be the slowest, or the linear part of the experimental curve at lower c.d.'s (Fig. 1) should have the same slope at higher c.d.'s too. However, the slope at higher c.d.'s does not show according to Eq. [1] that the second reaction step is the slowest one. It follows that only the reaction [6] may be considered as the possible ones.

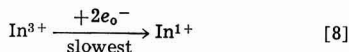
Considering reaction [6], from the slope of the experimental curve at higher c.d.'s it can be calculated that the first cathodic reaction step is the slowest one (Table I). In addition, the reaction step



was fast enough at lower c.d.'s too, and it would hardly be possible that the over-all reaction is influenced by it. In support of this is the fact that after cathodic polarization at chosen c.d.'s it was not possible to register oxidizable ions of lower valency by polarography.

On the basis of the shape of the experimental curve (Fig. 1) and earlier considerations it follows, that going from lower c.d.'s to higher ones, a change in the mechanism of the deposition of indium occurs. One mechanism is predominant at lower c.d.'s and the other at higher c.d.'s, while in the region between both processes are possible. The difference between the total experimental c.d. and the partial current of the interfering process is the c.d. to be used for the rate-determining process in the given range. Applying this principle in the higher c.d. range by subtracting the c.d. values of the lengthened Tafel-line (representing the rate-determining process at lower c.d.'s) from the c.d. values of the experimental curve at the same overpotential, one obtains a curve representing the rate-determining reaction step at higher c.d.'s. That curve differs very little from the experimental one in the range of higher c.d.'s (Fig. 8). From the slope of the constructed curve and Eq. [1] can be calculated that the first step is the slowest one of the over-all reaction [6]. All the mentioned facts and qualitative considerations point to the possibility of a reaction involving two electrons and one ion of In^{3+} at higher c.d.'s. Increasing the density of electrons at the cathode increases the probability of the simultaneous reaction of two electrons and one ion of In^{3+} , especially at higher concentrations of In^{3+} (concentration of the electrolyte) and low concentrations of In^{2+} . (In^{2+} was a product of the slowest reaction step at lower c.d.'s, and because of the faster subsequent reaction steps this ion would hardly be found near the cathode).

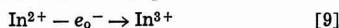
From these facts it can be concluded that the reaction



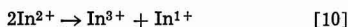
is the slowest step in the cathodic polarization of indium in sulfate solutions at higher c.d.'s.

Anodic curve at higher c.d.'s.—At higher c.d.'s the experimental $\eta_A - \log_{10} i$ curve of the anodic polarization of indium does not follow the original Tafel linear relation. It changes slope. In the range of c.d.'s $8.5 \times 10^{-3} - 2.5 \times 10^{-1}$ amp/cm² it follows again a linear relation but with a different slope. The slope of this second part of the curve shows according to Eq. [2] that the first anodic step is now the slowest one

in the over-all electrochemical dissolution of indium (Eq. [4], Table II). That change in the mechanism of the dissolution of indium is possible to explain in following way: As the reaction step



is the slowest one at lower c.d.'s, the ions of lower valency are accumulated as proved by polarography (3). By the accumulation of the ions less stable than In^{2+} there is the general possibility (6, 7) that they are removed by a disproportionation reaction as for instance

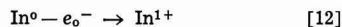


An increase of c.d. increases the concentration of In^{2+} and therefore the disproportionation reaction [10] is accelerated. With such an accelerated disproportionation, the third step of the over-all electrochemical reaction of dissolution [4] has less and less influence. In addition, with the process accelerated according to reaction [10], other disproportionation reactions may be assumed, as of the type



In favor of reaction [11] are earlier observations (3) when small crystals of indium were found in electrolyte after anodic polarization.

Considering accelerated disproportionation reactions [10] and [11], it can be assumed that the over-all anodic reaction [4] is really controlled by the first reaction step



at higher c.d.'s as proved by the slope of experimental curve (Fig. 2, Table II).

Manuscript received June 9, 1964; revised manuscript received Feb. 1, 1965.

Any discussion of this paper will appear in a Discussion Section to be published in the December 1965 JOURNAL.

REFERENCES

1. B. Lovrecek and V. Markovac, *This Journal*, **109**, 727 (1962).
2. B. Lovrecek, *J. Phys. Chem.*, **63**, 1795 (1959).
3. Lj. Duić, Z. Kovac, and B. Lovrecek, *Croat. Chem. Acta*, **32**, 213 (1960).
4. E. Mattsson and J. O'M. Bockris, *Trans. Faraday Soc.*, **55**, 1586 (1959).
5. W. Kangro and Fr. Weingärtner, *Z. Elektrochem.*, **58**, 505 (1954).
6. J. Heyrovsky, *Discussion Faraday Soc. Electrode Processes*, 212 (1947).
7. K. J. Vetter and G. Manecke, *Z. Physik. Chem.*, **195**, 337 (1950).

Technical Notes



Preparation of Transition Metal Oxide-Metal Electrodes

Richard L. Every

Central Research Division, Continental Oil Company, Ponca City, Oklahoma

Recent interest has been evidenced in the formation of oxides on transition metals for various purposes. Electrodes of NiO on Ni are used in batteries (1) and fuel cells (2). Tantalum oxide on tantalum is used for electron emission (3), as an electrolytic rectifier (4), and for electrolytic capacitors (5-7). Titanium oxide on titanium has also been used as a capacitor (8). Oxides are used to protect the transition metals from corrosion and erosion (9, 10). Transition metal oxides have been used in catalysis (11) and electrochemistry (12-26). Various other workers have conducted miscellaneous studies of oxides on the transition metals, i.e., Mo (27), W (28), Nb (29, 30), Nb and Zr (31), Zr (32), Ta (33), Ni (34-36), Pt (37-47), Pt and Pd (48), Pd (49, 50), Rh and Ir (51), Nb, Th, W, U, and Co (52), and Nb, U, V, Ti, Zr, and Ta (53).

The present study is concerned with the fabrication of metal oxide-metal electrodes of ZrO_2 , $\alpha\text{-Nb}_2\text{O}_5$, Nb_2O_5 (penta), Rh_2O_3 , PdO , HfO_2 , $\beta\text{-Ta}_2\text{O}_5$, Ta_2O_5 (penta), and PtO on their respective parent metals. (The α , β , and penta are ASTM designations.) The electrochemical characteristics of these electrodes are being studied and will be reported at a later date.

Experimental

All electrodes were about $0.038 \times 1.3 \times 3.8$ cm. About two-thirds of the electrode (about 6.5 cm^2 of metal) was oxidized. The oxides formed were identified either by x-ray or electron diffraction.

The electrode metals were designated "commercially pure" by the manufacturer. All metals except platinum were abraded with fine emery cloth prior to each oxidation. X-ray diffraction patterns verified the removal of residual oxides with this treatment. The plat-

inum electrode was preheated to redness for several seconds in order to remove residual oxides before depositing the platinum black (54). The oxides and the methods of formation are listed in Table I.

Many unsuccessful attempts were made to form the transition metal oxides before trying the general method of using the molten oxidizing salts with and without electrolysis. The exact temperature of the molten salt is apparently not critical in the formation of the oxide. As seen in Table I, typical temperature conditions range from 360° to 420°C . However, the use of electrolysis is important in the formation and growth of certain of the oxides.

To accomplish electrolysis, dry cell batteries were used in series with an ammeter and a rheostat. The current densities given in Table I represent maxima as controlled with the rheostat. The ability to maintain these maxima was limited. In each electrolysis the current density could be controlled for about 1 min before it slowly decayed to a minimum value. Using fresh batteries and established oxide films, these minimum current values could be repeated; this proved that the current decay was due to formation of the oxide film and was not due to the current drain on the battery.

Discussion

Films identified as the oxides were formed on Ta, Rh, and Hf without electrolysis. The thickness of the oxide films was increased with prolonged exposure to the molten salts. Upon microscopic examination of the films, the surface of the electrodes appeared slightly etched. Surprisingly, Ta was oxidized in molten KClO_3 after only 30 min while it was apparently not oxidized after 3 hr in molten KNO_3 .

Table I. Method of preparation of metal-metal oxide electrodes

Oxide	Condition	Appearance
ZrO ₂	Anode in 400°C KNO ₃ for 5 min with 6v. No current control.	Dark gray
α-Nb ₂ O ₅ (high temp)	Anode in 360°-400°C KNO ₃ or KClO ₃ with 180v and current density controlled at a maximum of 31 ma/cm ² .	White
Nb ₂ O ₅ (penta)	Anode in 360°-400°C KNO ₃ or KClO ₃ for 5 min with 90v and current density controlled at a maximum of 31 ma/cm ² . Electrode was then boiled in 96% H ₂ SO ₄ .	Silvery-gray
Rh ₂ O ₃	Placed in 400°C KNO ₃ or KClO ₃ for 12 hr.	Dull
PdO	Anode in 400°C KNO ₃ for 2 hr with 6v. No current control.	Gray
HfO ₂	Placed in 400°C KNO ₃ or KClO ₃ for 1 hr.	Blue
Ta ₂ O ₅ (penta)	Anode in 420°C KClO ₃ for less than 5 min with 6-60v and current density controlled at a maximum of 2.3-23 ma/cm ² .	Yellow and blue-green
β-Ta ₂ O ₅	Placed in 380°C KClO ₃ for 30 min.	Dark blue
	Anode in 400°C KNO ₃ or KClO ₃ with 90v for 1 min. No current control.	Gray
PtO	Pt black (54) electrode placed in O ₂ atmosphere at temperatures exceeding 465°C for several hours.	Black below 500°C; gray above 500°C.

Merely dipping the electrodes of Zr, Nb, and Pd into molten salt was not sufficient to form enough oxide for identification; however, the color of the Nb electrode did change to blue. This blue Nb had a few weak x-ray lines in common with Nb₂O₅ (ASTM Powder Diffraction File Card No. 5-0352), but the evidence was inconclusive.

The ZrO₂ formed in 400°C KNO₃ with 6v was a thick, gray coating and could be removed only with extreme difficulty. However, when Zr was made the anode in molten KClO₃ with 6v for 5 min, a white coating formed which flaked off and left a blue, deeply etched, and relatively oxide-free Zr surface.

The α-Nb₂O₅ (high temperature) formed as a thick, white adherent powder which could be scraped from the electrode with difficulty. The fact that it formed at 360°-400°C is a little surprising since the transition to the α structure is given as 1095°C (55). The electrical energy used to make this electrode may explain the unexpected appearance of the high-temperature form.

A somewhat less adherent gray coating with flecks of white was formed on Nb when the applied voltage was dropped from 180 to 90v. This coating was dissolved by placing it in hot H₂SO₄ for about 2 hr; this resulted in an etched Nb₂O₅ (penta) surface. The α-Nb₂O₅ was also dissolved by a similar treatment, but the resulting surface was severely eroded.

Niobium was also subjected to electrolysis in molten salts with 6 to 45v. The electrode color changed from blue to amber to gray as the voltage was increased. A study of the diffraction patterns indicated some Nb₂O₅ (penta) might have been present, but positive identification was doubtful.

Diffraction d-spacing values for Rh₂O₃ are not available from the ASTM data file. However, we were able to obtain 6 coincident peaks on comparison of x-ray diffraction patterns from commercial anhydrous Rh₂O₃ powder (Alfa Inorganic Inc.) and our own oxidation product.

When Pd was made the anode in 400°C KClO₃ with 6v, a heavy froth in the electrolyte forced the experiment to stop at the end of 5 min. A thick black coating had formed and was identified as PdO. The PdO formed in KNO₃ with 6v was a thick, gray adherent

coating at the end of 2 hr. No problems with froth were experienced in KNO₃.

The forms of Ta₂O₅ are many, and as in the case of Nb₂O₅ the positive identification of any given structure is elusive. Ta₂O₅ (penta) (ASTM Card No. 7-231) was identified as the result of electrolysis in KClO₃ with 6v at a maximum current density (c.d.) of 2.3 ma/cm² and again with 60v at a maximum of 23 c.d. units. These thick adherent coatings were yellow and bluish-green to violet, respectively. Little success was realized in trying to form Ta₂O₅ (penta) with electrolysis in KNO₃. Some highly colored oxides were formed with various treatments, but identification was not positive.

β-Ta₂O₅ (ASTM Card No. 8-255) apparently may be fabricated in a number of ways. Thin films of this type were the result of heating Ta to redness in work preliminary to this study and also resulted from exposing Ta to molten KClO₃ for about 30 min. The β form was also obtained with electrolysis in both molten salts with 90v for about 1 min. This was an extremely adherent, thick gray coating. Under a microscope, it was found that scratches on the Ta surface had been smoothed over by the gray coating.

Mixed oxides of PtO₂ and PtO were identified spectrophotometrically from adherent films which were formed when Pt was placed in molten salts with and without electrolysis (56).

ASTM diffraction d-spacing values are also not available for PtO. It had been reported (57) that PtO should have the same structure as PdO. We found 7 coincident x-ray diffraction peaks on comparing our platinum oxide with ASTM data on PdO, and have therefore tentatively identified our product as PtO. The PtO made by exposing Pt black to O₂ at high temperatures is more tightly adherent than the original Pt black, but is still easy to remove by scraping.

Manuscript received Nov. 30, 1964; revised manuscript received Jan. 22, 1965.

Any discussion of this paper will appear in a Discussion Section to be published in the December 1965 JOURNAL.

REFERENCES

- G. W. D. Briggs, E. Jones, and W. F. K. Wynne-Jones, *Trans. Faraday Soc.*, **51**, 1433 (1955).
- F. T. Bacon, *Nature*, **186**, 589 (1960).
- E. K. Smith, U. S. Pat. 2,565,004 (1951).
- G. P. Zharikov, *Uch. Zap., Azerb. Gos. Univ., Ser. Fiz.-Mat. i Khim. Nauk*, **1962**(3), 43 (1962); *Via C.A.* 60:2417h.
- G. J. Kahan, U. S. Pat. 2,775,553 (1956).
- M. J. Bolton and A. F. Torrisi, U. S. Pat. 2,785,116 (1957).
- J. Burnham, U. S. Pat. 2,871,425 (1959).
- E. Wainer, U. S. Pat. 2,874,102 (1959).
- U. R. Evans and J. Stockdale, *J. Chem. Soc.*, **1929**, 2651.
- E. A. Gulbransen, *Ind. Eng. Chem.*, **41**, 1385 (1949).
- D. A. Dowden, N. Mackenzie, and B. M. W. Trapnell, *Adv. in Cat.*, **IX**, 65 (1957).
- M. Breiter, K. Hoffmann, and C. A. Knorr, *Z. Elektrochem.*, **61**, 1168 (1957).
- H. A. Johansen, G. B. Adams, Jr., and P. Van Ryselberghe, *This Journal*, **104**, 339 (1957).
- P. Van Ryselberghe and H. A. Johansen, *ibid.*, **106**, 355 (1959).
- B. E. Conway and P. L. Bourgault, *Can. J. Chem.*, **37**, 292 (1959).
- A. V. Byalobzheskii and V. D. Val'kov, *Doklady Akad. Nauk S.S.S.R.*, **134**, 121 (1960).
- A. Kozawa, *Bull. Chem. Soc. Japan*, **35**, 1051 (1962).
- D. M. Mohilner, W. J. Argersinger, Jr., and R. N. Adams, *Anal. Chim. Acta*, **27**, 194 (1962).
- S. Uneri, *Commun. Fac. Sci. Univ. Ankara, Ser. B*, **10**, 7 (1962).
- L. Lederer and N. D. Greene, *Electrochim. Acta*, **8**, 883 (1963).
- M. W. Breiter, *ibid.*, **8**, 973 (1963).
- S. Shibata, *Bull. Chem. Soc. Japan*, **36**, 525 (1963).

23. N. G. Bardina, *Zh. Fiz. Khim.*, **37**, 2688 (1963); *Via C. A.* **60**: 10203a.
24. J. J. Lingane and P. J. Lingane, *J. Electroanal. Chem.*, **5**, 411 (1963).
25. S. W. Feldberg, C. G. Enke, and C. E. Bricker, *This Journal*, **110**, 826 (1963).
26. J. S. Mayell and S. H. Langer, *ibid.*, **111**, 438 (1964).
27. H. A. Liebhafsky, *J. Appl. Phys.*, **17**, 901 (1946).
28. R. W. Schmidt, *Kolloid Zeits.*, **102**, 15 (1943).
29. J. V. Cathcart, J. J. Campbell, and G. P. Smith, *This Journal*, **105**, 442 (1958).
30. D. W. Aylmore, S. J. Gregg, and W. B. Jepson, *ibid.*, **107**, 495 (1960).
31. R. E. Salomon, G. B. Adams, and W. M. Graven, *ibid.*, **110**, 1163 (1963).
32. N. G. Bardina and P. D. Lukovtsev, *Z. Fiz. Khim.*, **37**, 57 (1963).
33. J. V. Cathcart, R. Bakish, and D. R. Norton, *This Journal*, **107**, 668 (1960).
34. H. K. Embaby and A. A. Moussa, *J. Chem. Soc.*, **1958**, 4027.
35. J. S. Anderson and D. F. Klemperer, *Proc. Roy. Soc.*, **258A**, 350 (1960).
36. A. U. MacRae, *Appl. Phys. Letters*, **2**, 88 (1963).
37. M. Becker and M. Breiter, *Z. Elektrochem.*, **60**, 1080 (1956).
38. F. C. Anson and J. J. Lingane, *J. Am. Chem. Soc.*, **79**, 4901 (1957).
39. H. A. Laitinen and C. G. Enke, *This Journal*, **107**, 773 (1960).
40. K. Nagel and H. Dietz, *Electrochim. Acta*, **4**, 1 (1961).
41. *Ibid.*, **4**, 141 (1961).
42. W. Boeld and M. Breiter, *ibid.*, **5**, 145 (1961).
43. F. C. Anson, *Anal. Chem.*, **33**, 934 (1961).
44. F. C. Anson and D. M. King, *ibid.*, **34**, 362 (1962).
45. D. G. Peters and J. J. Lingane, *J. Electroanal. Chem.*, **4**, 193 (1962).
46. A. I. Brodskii and V. A. Lunenok, *Burmakina, Doklady Akad. Nauk S.S.S.R.*, **151**, 1358 (1963).
47. V. E. Petrakovich, *Z. Analit. Khim.*, **18**, 1161 (1963).
48. J. K. Lee, R. N. Adams, and C. E. Bricker, *Anal. Chim. Acta*, **17**, 321 (1957).
49. D. Inman, *Nature*, **194**, 279 (1962).
50. Y. A. Mazitov, K. I. Rozenal, and V. I. Veselovskii, *Z. Fiz. Khim.*, **38**, 151 (1964); *Via C. A.* **60**: 11616b.
51. W. Boeld and M. Breiter, *Electrochim. Acta*, **5**, 169 (1961).
52. D. W. Aylmore, S. J. Gregg, and W. B. Jepson, *This Journal*, **106**, 1010 (1959).
53. J. S. L. Leach, *ibid.*, **110**, 680 (1963).
54. O. F. Steinbach and C. V. King, "Experiments in Physical Chemistry," p. 143, American Book Co., New York (1950).
55. F. Holtzberg, A. Reisman, M. Berry, and M. Berkenblit, *J. Am. Chem. Soc.*, **79**, 2039 (1957).
56. R. L. Every and R. L. Grimsley, *J. Electroanal. Chem.*, in press.
57. W. J. Moore and L. Pauling, *J. Am. Chem. Soc.*, **63**, 1392 (1941).

Cobalt Phthalocyanine as a Fuel Cell Cathode

Raymond Jasinski

Tyco Laboratories, Incorporated, Waltham, Massachusetts

One of the necessary characteristics of an oxygen electrode is that it chemisorb oxygen without degradation of the catalytically active surface. Reversible absorption has been observed in aqueous solution for some metal chelates, e.g., bis (salicylal) ethylene diamine cobalt (II), heme, and cobalt (II) histidine (1). The possible application of these soluble compounds as fuel cell cathode catalysts would lead to a complicated engineering system, even if the oxygen-exchange kinetics were favorable.

A number of insoluble metal chelates will also chemisorb oxygen; the most chemically stable of these are the metal porphyrins and the metal phthalocyanines. The molecules are square planar complexes (2) with the metal atom symmetrically surrounded by four nitrogen atoms. These nitrogen atoms are each members of ring systems, which in turn are connected by carbon atoms (porphyrins) or nitrogen atoms (phthalocyanines). The details of crystal structure, chemical properties, and methods of preparation have been summarized recently (3).

A number of these compounds are insoluble in most common solvents, acid (8M H₂SO₄) and base (7N KOH). Concentrated sulfuric acid is required to solvate cobalt and copper phthalocyanine (CoPc, CuPc). CuPc is reported to be stable to thermal decomposition at 500°C. No decomposition of CoPc has been observed at 120°C under oxygen. Further stability can be achieved by partially chlorinating the compound or by polymerization (4).

Copper phthalocyanines (CuPc) have been reported to be active catalysts for hydrogen reactions such as o-p conversion and H₂-D₂ exchange (5-7). More relevant to the present work are the properties of copper and cobalt phthalocyanines as oxidation catalysts. For example, both compounds have been used in the air oxidation of mercaptan sulfur to disulfides for the "sweetening" of petroleum products (3,8). A preliminary appraisal of CoPc as a fuel cell cathode catalyst has been discussed in a recent note (9). In the present paper, CoPc is more fully evaluated in a

practical electrode configuration, and its catalytic activity is compared to that of other known catalysts measured under identical experimental conditions.

Experimental

IR-free voltage measurements were made with the interrupter technique, employing a transistorized sine wave commutator (10). The test H₂/O₂ fuel cells had end-plates machined from Teflon; a Teflon O ring was employed to prevent uncontrolled evaporation of water. The use of Teflon components obviates problems which could arise from the oxidation and/or corrosion of metal end-plates.

A platinum wire imbedded in the end-plates served as the electrical lead. The contribution of the Pt wires to catalytic activity was found to be negligible; thus the electrodes were the only electrochemically active materials in the system.

An electrolyte of 35% KOH, immobilized in an asbestos membrane, was used. The anodes, 5 cm² disks, consisted of 9 mg Pt/cm² plastic-bonded to a nickel screen (American Cyanamid Corporation).

The cell temperature was 80°C unless otherwise noted. A thermocouple was placed in one of the Teflon plates and positioned above the cathode.

Only total cell voltages were measured since it was difficult to insert a probe into the test set-up described. Platinum cathodes were therefore run in the same cell to establish a point of reference. Data for H₂/O₂ cells are apparently self-consistent to ± 0.015v, as the reproducibility of the cell performances indicates. The flow rate of oxygen was adjusted to remove the water produced by the cell reaction; the hydrogen was "dead-ended." Both gas pressures were kept at 2.08 atm (16 psig).

In previous work (9) a cathode had been used which consisted of a porous nickel plaque onto which a coating of CoPc had been slurried. These structures were effective electrodes only if O₂ was passed through the CoPc coating. Impregnating porous plaques was difficult because of the limited solubility of CoPc in com-

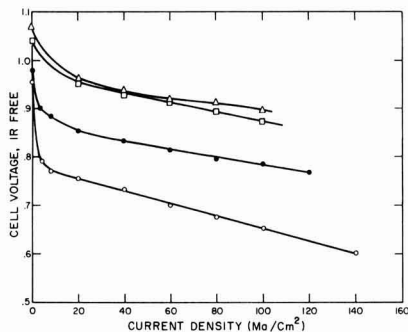


Fig. 1. Performances of H_2/O_2 fuel cells operating at $80^\circ C$ with an electrolyte of 35% KOH, and a platinum black anode (9 mg/cm^2). The cathodes are: 9 mg/cm^2 platinum (\square); 40 mg/cm^2 silver (Δ); 14 mg/cm^2 CoPc (\bullet); and 20 mg/cm^2 acetylene black (\circ).

mon solvents. A more suitable electrode structure was formed by Teflon-bonding a mixture of 0.072 g of CoPc and 0.048 g of acetylene black to a 5 cm^2 nickel screen disk. Acetylene black cathodes were also prepared by Teflon-bonding 0.12 g to nickel screen.

This method of electrode preparation is relatively independent of the particular material employed as the catalyst and has been used to investigate a variety of nonconductive metal chelates. After the electrode has been "activated" in the manner described below, a cell resistance of 0.022 ohm was obtained. This may be compared to a cell resistance of 0.018 ohm obtained for Teflon bonded platinum electrodes in the same cell. No attempt was made to reduce further the internal resistance.

Cobalt phthalocyanine, supplied by the National Aniline Division of Allied Chemical Corporation, was 99% pure and was used without further treatment.

Results

The chemical stability of CoPc under conditions approximating fuel cell operation was evaluated as follows. A sample was placed in 35% KOH and heated to $75^\circ C$. No discoloration of the liquid was noted. A second sample was placed in 30% H_2O_2 . Again no discoloration occurred, although gas evolution was noted. Similar experiments with iron phthalocyanine resulted in considerable decomposition of the chelate, particularly in the presence of hydrogen peroxide.

Electrode activation.—The initial performance of CoPc cathodes was generally low, e.g., 80 ma/cm^2 at 0.70 v . However, it was found that if the cathode were polarized to H_2 evolution potentials, subsequent operation improved, e.g., 80 ma/cm^2 at 0.81 v . No decrease in output was noted after 10 hr of operation. The maximum performance which could be obtained is that shown in Fig. 1. The increase in electrochemical activity is accompanied by a change in appearance of the electrode. On dismantling the cell, it is found that the color of the catalyst mixture had changed from red-violet to brown-black. "Activation" also lowers the internal resistance of the cell. Typically, the resistance decreased from 0.05 to 0.02 ohm .

That this pretreatment is not a temporary charging effect is indicated by a comparison of the quantity of charge passed during activation with that passed on subsequent fuel cell operation. Activation is accomplished with 600 ma/cm^2 (3 amp), flowing for 2 min (0.05 amp-hr). Typically, the cell was then operated at 100 ma/cm^2 for 10 hr (5.0 amp-hr). This difference in charge of 10^2 can best be explained by postulating a permanent alteration in the structure of the catalyst.

Since activation was carried out at a current density of 600 ma/cm^2 , significant IR heating occurred. Thus,

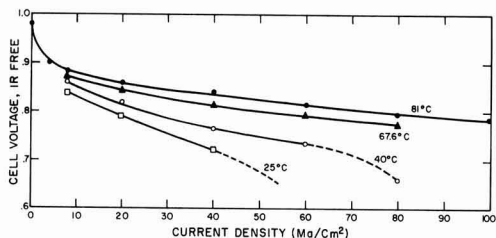


Fig. 2. Temperature dependence of the performance of H_2/O_2 fuel cells employing a CoPc cathode. The cell was operated with an electrolyte of 35% KOH and a platinum anode.

the presence of oxygen and the generation of H_2 in the cathode cavity suggest at least five possible activation mechanisms: (i) the effect is electrochemical; (ii) the effect is thermal; (iii) the effect involves heat and O_2 ; (iv) the effect involves heat and H_2 ; (v) the effect involves an alteration of the physical structure of the electrode. e.g., wetting characteristics.

Temperature measurements, made with the thermocouple placed above the cathode compartment, indicated that the cell temperature never rose above $90^\circ C$. Since heat transfer through Teflon is low, most probably the temperature at the electrode surface was somewhat higher during the current density flow of 600 ma/cm^2 . To insure an adequate evaluation of the effect of temperature, the electrode was first heated to $350^\circ C$ under argon before use in a cell. Since this did not activate the electrode, heating alone is not sufficient. Second, the electrode was heated in a hydrogen atmosphere up to $340^\circ C$. A number of inactive electrodes resulted, although the electrode had changed color to brown-black and the internal resistance was lowered. Therefore, mechanism (iv), IR heating plus H_2 , is not the explanation. It should be noted that heating the electrode in H_2 at a higher temperature ($370^\circ C$) did provide active cathodes. Activation under these conditions is presumed to be an alternate mechanism. Third, a cell was polarized so that O_2 was evolved at the CoPc electrode. Activation did not occur. Finally, activation was not noted for the acetylene black or the platinum black electrodes, indicating that the effect represented an alteration of CoPc.

Apparently the effect is electrochemical, indeed, an "arrest" in the time-potential curve is observed at a cell voltage of approximately 1 v . This occurs when activating the CoPc electrodes but not the acetylene black. The "arrest" was noted for only CoPc electrodes which were inactive initially, i.e., those not activated by gaseous H_2 at $370^\circ C$. It is not possible with this limited data to offer a detailed description of the mechanism by which the electrochemically altered CoPc improves cathode performance.

Cell performance.—The performance of the CoPc cathode in a H_2/O_2 cell is compared in Fig. 1 to that for acetylene black, platinum black, and silver (40 mg/cm^2). At a constant current density of 100 ma/cm^2 the cells performed as follows: CoPc cathode $0.79 \pm 0.015 \text{ v}$, acetylene black 0.65 v , platinum black and silver 0.87 v . Thus, it is apparent that CoPc functions as an oxygen electrode catalyst, although its performance is 0.08 v poorer than that obtained with platinum black. This difference could be slightly greater if an equal loading, 15 mg/cm^2 , of platinum were used. On the basis of relative cost, however, the use of CoPc becomes more favorable.

Cell performance as a function of temperature is summarized in Fig. 2. Some output is obtained at room temperature so that a fuel cell employing this catalyst could be considered as self-starting. An increase in temperature results in an increase in performance. The

temperature of 80°C was arbitrarily chosen as the operating point.

Discussion

It has been possible to form an oxygen electrode with a metal chelate, cobalt phthalocyanine, as the active catalyst. Sufficient electrical conductivity was achieved by mechanically blending the chelate with acetylene black. A stable electrode structure was formed by Teflon-bonding the mixture to a metal screen. Since a supported electrolyte was also used, no difficulty was noted due to variations in electrode uniformity across the face of the screen.

The electrochemistry (e.g., activation, pretreatments) of the chelate compounds is different from that experienced with metal and oxide catalysts. The "activation" treatment, found with cobalt phthalocyanine, (which resulted in an increase in cell voltage of 0.1v at 100 ma/cm²) was without noticeable effect when applied to acetylene black, platinum, and silver.

The activation step is a reductive procedure; chemical testing indicated the absence of free cobalt or cobalt oxide. A recent paper (7) on the activation of hydrogen by copper phthalocyanine has indicated three types of catalytically active sites: (a) the chelated metal atom, (b) unpaired electrons arising during heat treatments, (c) unpaired π electrons formed by the opening of double bonds. Furthermore, it is indicated that the hydrogen reaction rates are enhanced by catalyst polymerization due to an increase in the density and stability of unpaired electrons. It is possible that the electrochemical treatment induced polymerization and/or increased the density of unpaired electrons. It is also possible that Co(II) was reduced to Co(I). However, phthalocyanine complexes of monovalent metal atoms are generally unstable. A more rigorous explanation for this effect cannot be made until the mechanism for oxygen reduction is determined.

The current densities sustained with H₂/O₂ cells were sufficiently high (60-120 ma/cm²), to be considered for application in practical fuel cell systems. The H₂/O₂ cell voltage is about 0.1v lower than can be obtained at present with either platinum or silver catalysts. Some metal phthalocyanines are relatively inexpensive and are employed commercially as dyes; for example, the copper compound is available at approximately \$1.10/lb.

Acknowledgment

The author wishes to acknowledge the support of the Air Force Cambridge Research Laboratories under Contract AF 19 (628)-2845.

Manuscript received Sept. 22, 1964; revised manuscript received Jan. 18, 1965.

Any discussion of this paper will appear in a Discussion Section to be published in the December 1965 JOURNAL.

REFERENCES

1. J. C. Bailar, "Chemistry of the Coordination Compounds," p. 45, Reinhold Publishing Corp., New York (1956).
2. G. T. Byrne, R. P. Linstead, and A. R. Lowe, *J. Chem. Soc.*, **1934**, 4017.
3. F. Moser and A. Thomas, "Phthalocyanine Compounds," Reinhold Publishing Co., New York (1963).
4. M. Dahlen, *Ind. Eng. Chem.*, **31**, 839 (1939).
5. M. Calvin, E. Cockbain, and M. Polanyi, *Trans. Faraday Soc.*, **32**, 1436 (1936).
6. M. Calvin, D. Eley, and M. Polanyi, *ibid.*, **32**, 1443 (1936).
7. D. Eley and G. Acres, *ibid.*, **60**, 1157 (1964).
8. W. Gleim and P. Urban, U. S. Pat. 2,882,224 (1959).
9. R. Jasinski, *Nature*, **201**, 1212 (1964).
10. G. Pollnow and R. Kay, *This Journal*, **109**, 648 (1962).

Effect of Oxide Hydration on Surface Potential of Oxidized P-Type Silicon

A. B. Kuper¹ and E. H. Nicollion

Bell Telephone Laboratories, Incorporated, Murray Hill, New Jersey

The n-type tendency of silicon surfaces under thick oxide has been known since the first work of Atalla, Tannenbaum, and Scheibner (1). In the present paper experimental evidence is presented showing that an important cause of this tendency is hydration of the oxide and that the effect is reversible. Temperature-humidity history is thus important in establishing the silicon surface potential of passivated structures. This effect has practical significance for oxidized silicon device performance and reliability.

Atalla *et al.* (1) showed that fast (close to the interface) donor-type states were present and observed the n-type surface tendency on diodes oxidized after diffusion. Sah (2) reported the n-type tendency on diodes where oxidation was done before diffusion. Kahng (3) used high pressure steam oxidation after diffusion and also found n-type surfaces. Edagawa *et al.* (4) found the n-type tendency using grown junction silicon diodes oxidized in wet O₂, dry O₂, wet N₂, and wet H₂.

Water is expected to be present in silica films grown in steam or after exposure to steam as shown by Ligenza and Spitzer (5, 6) who studied the exchange of oxygen between silica and steam and by Moulson

and Roberts (7) who observed infrared absorption due to water in silica.

Diodes in the present work were conventional n⁺p planar junctions with no metal contacts. Oxidation preceded diffusion. Preoxidation cleaning was similar to that used by Atalla *et al.* (1).

Planar diodes 3.6 x 10⁻⁴ cm² in area, approximately 8 mils in diameter, were made by diffusion of phosphorus into chemically polished (Appendix A) boron-doped pulled crystal silicon. Resistivities from 0.5 to 5 ohm-cm were used. To make the diodes, the silicon was given a final boiling nitric acid, boiling water cleaning (Appendix B) and oxidized in atmospheric pressure steam (Appendix C) at 1050°C for 1 hr, which formed 6000Å of oxide. Photoresist masking was used and holes were etched in the oxide. Phosphorus doped layers 4 μ deep with a sheet resistance of 50 ohm/sq were then formed in the etched areas by pre-diffusion at 740°C for 40 min followed after glass removal by 1 hr at 1230°C in dry nitrogen - 10% oxygen. Diodes in this "dehydrated" state had reverse dark currents in the nanoampere range. Diode reverse current results were qualitatively the same when the oxide was grown in dry oxygen.

Diodes then oxidized in unpressurized steam at 1050°C with consequent "hydration" of the oxide had

¹ Currently on leave of absence at Case Institute of Technology, Cleveland, Ohio.

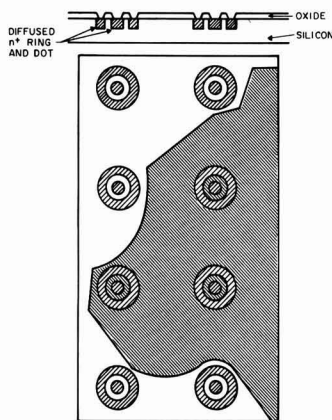


Fig. 1. Extent of n-channel under oxide after steaming ring and dot diodes 2 hr at 408°C. Silicon is 0.5 ohm-cm p-type. Shaded region indicates extent of channel measured by diode photoresponse. Outside diameter of devices is 15 mils, and center to center distance is 50 mils.

channel saturation currents in the milliamperage range. If diodes were then heated for about 1 hr at 1000°C in dry ambient, reverse currents were reduced to the nanoamp range again. Dry air, oxygen, nitrogen, and argon as well as vacuum were found to be suitable for drying.

The channel that resulted when the oxide was hydrated was shown to be n-type extending over the p-region by measuring diode photoresponse using a small chopped light spot. The extent of one channel resulting from steaming a set of ring and dot diodes at 408°C for 2 hr is shown in Fig. 1. Here, hydration was stopped before the entire surface was inverted. The oxide was of uniform thickness. This patchy inversion (also suggested the spread of data in Fig. 2) suggests that localized conditions at the oxide-air or oxide-silicon interface may control the rate of inversion.

If the oxide were completely etched off in concentrated HF and the sample then rinsed thoroughly and dried, no channel was present, as has been reported (1). Results are summarized in Fig. 2. Hydrogen at 400°C also produced channels, in agreement with Blum *et al.* (8), but longer exposure time than with steam was required to produce a channel of the same strength. Exposure to other gases at 400°C did not produce channels as shown in Table I.

Reversible channeling was also seen by means of measurements of the diode capacity. In the dehydrated state for the case of 0.5 ohm-cm p-type there was negligible excess capacity. In the hydrated state, the presence of a channel was clearly indicated by excess capacity at low bias. This excess capacity went to zero at about the same reverse voltage at which the reverse current saturated.

Five ohm-cm p-type ($N_a = 2.5 \times 10^{15} \text{ cm}^{-3}$) silicon remained slightly inverted at the surface after 1000°C baking in dry nitrogen for 2 hr while 0.5 ohm-cm ($4 \times 10^{16} \text{ cm}^{-3}$) did not, suggesting that there was an effective donor concentration of the order of 10^{11} cm^{-2} in this experiment.

At 800°C, the current-voltage characteristic of the dehydrated state was found to reach equilibrium from the hydrated state in less than 1 min. Likewise, the heavily channelled state could be achieved at 1050°C in steam in less than 1 min. Reverse currents of diodes in the dehydrated state changed slowly when given wet-dry cycling at low temperatures as shown for 300°C in Fig. 3. Data of this kind generally indicated that hydration proceeded somewhat faster

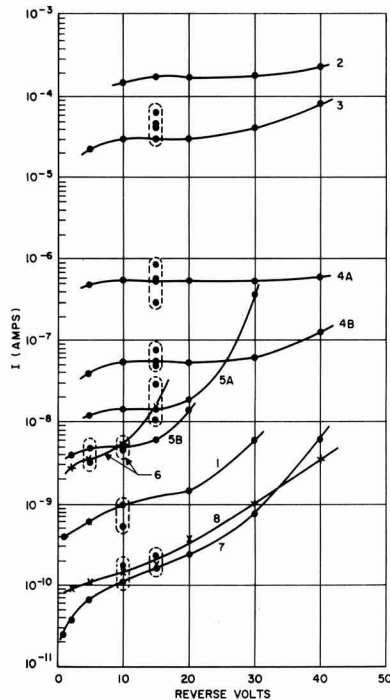


Fig. 2. Summary of reverse current vs. voltage on planar diodes from one diffused slab of 0.5 ohm-cm boron doped pulled crystal silicon. Each curve represents a group of diodes. Vertical dashed line indicates the spread of current data. A and B refer to regions of a piece which showed a distinct grouping of currents after baking. Curve 1, initial state after phosphorus diffusion; curve 2, oxidized in 1 atm steam pressure at 1050°C for 1 hr after 1. Oxide over junction is approximately 8000Å thick; curve 3, baked 5 min in air at 460°C after curve 2; curve 4, baked 30 min in dry argon at 700°C after curve 2; curve 5, baked 30 min in dry argon at 750°C after curve 2; curve 6, baked 30 min in dry argon at 800°C after curve 2; curve 7, baked 1 hr in dry nitrogen at 1000°C after curve 2; curve 8, oxide etched off in concentrated HF after curve 2, dry nitrogen ambient. The "soft" characteristic of curves 5 and 6 is a typical result of heating an unclean sample and is not regarded as significant for this experiment.

than dehydration at the same temperature. Estimated relaxation times (time for reverse current to decrease by a factor 10) for baking temperatures between 200° and 700°C were consistent in many cases with the known rate of diffusion of water through silica glass (7).

The effect of water on diode reverse current observed in the present experiments is similar, except for longer relaxation times, to the effect of humidity at room temperature on diodes that have not been thickly oxidized. This suggests that the observed effects are due to water or a water-related species largely concentrated at the silicon-oxide interface.

To test this model, hydrated oxide was progres-

Table I. n⁺p (1.5 ohm-cm) Planar diode aging

Aging temp, °C	Exposure time, hr	Gas at 1 atm	Saturation current, μa
390	64	Room air	No channel
390	64	Dry N ₂	No channel
390	4	Dry CO ₂	No channel
390	64	Dry He	No channel
390	17	Dry H ₂	0.5
406	0.16	H ₂ O	16
406	0.5	H ₂ O	40
390	3.5	H ₂ O	2000

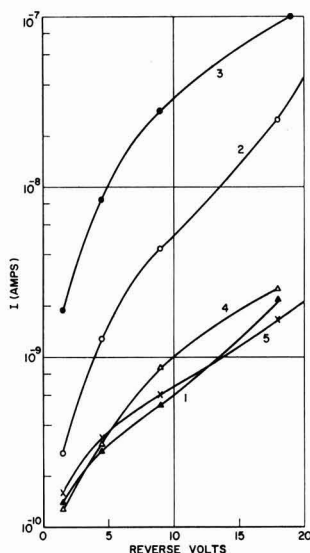


Fig. 3. Diode reverse characteristics. Low-temperature steam and bake cycle of a diode starting in the dehydrated state. The p-region resistivity is 0.5 ohm-cm. Oxide over junction is approximately 6000Å thick. Curve 1, start; curve 2, After 30 min in atmospheric pressure steam-oxygen mixture at 300°C; curve 3, after 52 min more as in curve 2; curve 4, after 40 min bake in air at 300°C after curve 3; curve 5, after 60 min more as in curve 4.

sively etched off a channeled diode and the zero-bias capacity was measured. The result in Fig. 4 shows that the surface of the 0.5 ohm-cm silicon remained inverted until only a few hundred angstroms of hydrated oxide remained. (Oxide thickness less than 1000Å was obtained by controlled etching and checked by dielectric breakdown.) Figure 4 shows that a substantial number of ionized donors from hydration were in the oxide within 600Å of the silicon. The charge may be confined even closer because disappearance of the channel beginning at a thickness of 600Å may be a spurious result due to the fact that such thin oxide probably contains pinholes, and/or that states at the oxide-air interface become important.

The experiments suggest that hydration effects in steam depend on a water species acting as a donor localized on the oxide side of the oxide-silicon interface.

Manuscript received Jan 6, 1965. This paper was presented at the Washington Meeting, Oct. 11-15, 1964.

Any discussion of this paper will appear in a Discussion Section to be published in the December 1965 JOURNAL.

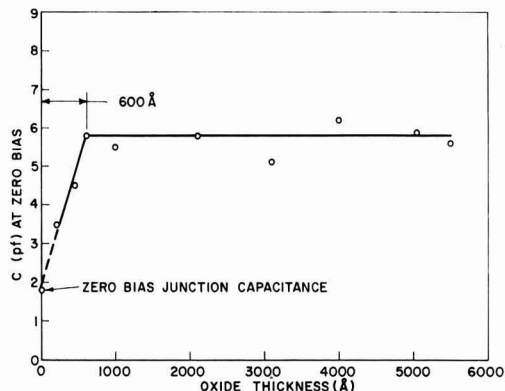


Fig. 4. Total zero bias capacitance of one channeled 0.5 ohm-cm diode measured at 100 kc as a function of oxide thickness on the inverted surface. Oxide thickness is measured by matching color to a standard whose thickness is known by ellipsometer measurement and is verified for each point by measuring the dielectric breakdown voltage of oxide on the slab.

REFERENCES

1. M. M. Atalla, E. Tannenbaum, and E. J. Scheibner, *Bell Sys. Tech. J.*, **38**, 749 (1959).
2. C. T. Sah, *Proc. IRE*, **49**, 1623 (1961).
3. D. Kahng and M. M. Atalla, "Silicon-Silicon Dioxide Field Induced Surface Devices," IRE-AIEE Solid State Device Research Conference, Pittsburgh, Pa. (1960).
4. H. Edagawa, Y. Morita, S. Maekawa, and Y. Inuishi, *J. Phys. Soc. Japan*, **17**, 1190 (1962).
5. J. R. Ligenza and W. G. Spitzer, *J. Phys. Chem. Solids*, **14**, 131 (1960).
6. W. G. Spitzer and J. R. Ligenza, *ibid.*, **17**, 196 (1961).
7. A. J. Moulson and J. P. Roberts, *Nature*, **182**, 200 (1958); and T. Drury, G. J. Roberts, and J. P. Roberts, Sixth International Congress Glass, Washington, D. C. (1962).
8. J. Blum, R. Warwick, H. M. Pollack, and M. Genser, *This Journal*, **111**, 58C (1964) Abstract No. 55.
9. R. Lieberman, W. R. Bracht, D. L. Klein, *ibid.*, **111**, 62C (1964).

APPENDIX

(A) *Silicon surface preparation.*—(111) orientation silicon sawed into 0.020 in. slices. Both sides lapped with 12μ aluminum oxide to thickness of 0.0095 in. Diode side polished with 0.3μ aluminum oxide to 0.0085 in. Slice cleaned of grit by copper displacement (9). Both sides etched with 19:1 HNO₃:HF in rotating cup. Final thickness 0.0045 in.

(B) *Cleaning before oxidation.*—Degrease. 2 min in HF, 20 min in deionized water recirculator at 80°C; 15 min in HNO₃ at 80°C; 20 min in deionized water at 80°C again.

(C) *Steam oxidation* is done in an all-quartz system. Water is from recirculating deionizer and 0.2μ filter system in which conductivity is monitored at 0.05 μmho/cm.

The Minimum in Molar Conductance of CdCl₂ in Water-Methanol

D. O. Johnston

Department of Chemistry, David Lipscomb College, Nashville, Tennessee

and P. A. D. de Maine

Department of Chemistry, University of California, Santa Barbara, California

Molar conductances of CdCl₂ in methanol (1) and in ethanol (2,3) have been measured. Golben and Dawson (3) proposed that in ethanol CdCl₂ dissociates in the most dilute range as a uni-univalent electrolyte. For CdI₂ in methanol (4,5) conductance values show a maximum, but no maxima have been reported for

the chlorides. Hartley and Raikes (6) have reported the ionic mobilities of Cd⁺⁺, Cl⁻, and other ions in methanol.

Conductance minima have been reported for methanol-water systems containing KCl, KOH, NH₄Cl, or HCl (7). The minima for the KCl and KOH systems

Table I. Molar conductance values for CdCl₂ in methanol-water at 5°, 20°, and 45°C

Salt concn., M/L	Water concentration in moles/liter																			
	0.000	0.001	0.005	0.010	0.400	1.010	1.510	2.020	3.030	3.550	4.060	4.570	5.090	5.660	6.200	7.680	9.240	12.89	15.51	20.74
@ 5°																				
0.0005	52.70	52.70	52.69	52.81	52.64	52.15	51.46	49.91	49.06	50.15	50.08	50.26	50.97	51.84	54.01	55.03	56.58			
0.0010	45.25	45.59	45.59	45.76	45.89	45.80	45.58	45.10	44.86	44.81	44.28	43.74	43.87	43.94	43.90	44.43	44.63	46.55	47.58	49.90
0.0015	41.50	41.64	41.50	42.23	42.03	41.95	41.89	42.29	41.88	41.97	41.19	40.99	41.08	40.89	41.13	41.31	41.35	42.82	44.37	46.06
0.0020	38.31	38.04			38.69			38.62			38.99		38.90		38.07			39.79		44.67
0.0040	31.07	31.39			31.84			33.21			33.63		33.52		33.46			34.37		37.98
0.0100	22.65	22.57			23.14			24.32			25.61		26.06		26.38			27.84		29.83
@ 20°																				
0.0005	63.53	63.53	63.53	63.51	63.43	63.47	63.37	63.47	63.28	64.30	63.46	63.17	64.41	65.40	65.40	66.81	69.21	74.41	78.00	84.28
0.0010	52.72	53.40	53.17	53.63	54.00	54.85	55.28	55.42	55.76	56.16	56.10	56.00	56.72	56.87	57.09	58.57	59.56	63.99	67.02	73.46
0.0015	47.87	47.69	47.65	48.61	48.73	49.43	50.14	51.14	51.66	52.23	51.93	51.86	52.47	52.60	53.24	54.06	55.17	58.98	62.56	68.13
0.0020	43.62	43.55			44.61			46.65			49.33		49.33		50.41			54.93		65.30
0.0040	34.79	35.10			36.20			39.15			41.55		41.93		42.64			47.20		55.41
0.0100	25.13	25.03			25.78			28.27			30.93		31.90		32.85			37.54		43.55
@ 45°																				
0.0005	76.36	77.39	76.87	77.67	78.95	81.60	82.61	84.00	85.60	88.80	86.93	87.11	90.49	91.06	92.80	96.13	101.7	113.4	121.8	140.0
0.0010	61.45	62.03	61.74	62.65	64.18	67.04	69.08	70.48	72.63	74.62	75.85	76.63	78.40	79.01	80.15	83.64	86.8	97.1	105.9	121.2
0.0015	55.22	54.70	54.47	55.96	56.93	59.19	61.38	63.44	66.56	68.25	68.72	69.54	71.41	71.73	73.29	76.71	79.4	89.4	96.8	111.6
0.0020	49.09	49.07			51.90			57.33			64.56		65.85		69.75			82.9		107.0
0.0040	38.16	38.70			40.58			46.23			52.66		54.46		57.25			70.3		89.1
0.0100	27.49	27.42			28.63			32.84			38.09		40.12		42.28			54.6		69.6

* As this table is traversed to the right, the CdCl₂ concentration increases by 3% because of the nonideality of water-methanol.

occur between 40 and 60 mole % water which coincide with maxima in the viscosity. At 25°C water-methanol mixtures show a maximum in viscosity at 73 mole % water (8). The pronounced conductance minimum at 5°C for HCl-methanol-water at 20 mole % water has been ascribed by Gurney (9) to partial suppression of proton jumps by the water molecules capturing protons from methonium ions since the methonium ion has a proton level higher than that of the hydronium ion. As the water concentration is increased, the conductance increases because of proton jumps between water molecules.

Experimental

General techniques of preparing solutions and measuring resistances with a General Radio Company Impedance Bridge (Type 1650A) at 5°, 20°, and 45°C have been described elsewhere (1,10). The Fisher Spectrograde methanol had a specific conductivity of 9×10^{-7} ohms⁻¹ cm at 20°C. The anhydrous Fisher Certified Reagent CdCl₂ assayed 99.1% CdCl₂, and chloride analysis showed a maximum deviation of 0.52% from stoichiometry. The water, distilled in an all-glass apparatus, had a specific conductivity of 3.5×10^{-6} ohms⁻¹ cm at 20°C.

In Table I concentrations of CdCl₂ and water are given. In calculation of CdCl₂ concentrations solvent densities reported by Mikhail and Kimel (8) were used. The solutions were stable for at least 24 hr. Resistance measurements on 29 duplicate samples in the area of the minimum showed that resistances could be measured reproducibly to within 1%.

Results

For constant CdCl₂ concentrations the molar conductances of CdCl₂-water-methanol systems decrease with an increase in water concentration to about 4.5M (17 mole %) (Table I). Conductances then increase for higher water concentrations. This effect was observed for CdCl₂ concentrations from 0.005 to 0.0015M at 5°, and 0.0005M at 20°C, but was not noted for salt concentrations equal to or greater than 0.0005M at 45°C. Table I contains some of the data which illustrate these statements. Concentrations near 9M in water are required to achieve the conductance value obtained in anhydrous methanol at 5°C.

Discussion

If water complexing with the salt is important, the high local dipole moment of the water molecules should enhance and not decrease ionization. It appears that solvolysis products may be important in producing the

minimum. At 5°C the minimum for the CdCl₂-water-methanol system occurs between 16 and 18 mole % water, while for HCl-water-methanol the minimum is at 20 mole % water. Decreased mobility of the Cd species formed by hydrolysis together with diminished proton jumps would account for a decrease in conductance as water is added to the system. The increase at higher water concentrations would result from increased ionization of the salt and from increased proton jumps.

However, the lack of a conductance minimum at 45°C and at higher salt concentrations indicates that besides solvolysis there may be other important effects such as basic solvent structure. Viscosity studies (1,8) indicate that water increases structure in a solution more than methanol. Increased solvent structure might offer sufficient resistance to ions to effect a conductance decrease until ionization effects offset the structural resistance. Then conductance increases with higher water concentrations. At 45°C water would not add a sufficient increase in structure to counteract the greater production of ions.

Acknowledgments

This research was supported by a grant from the Petroleum Research Fund, administered by the American Chemical Society. D.O.J. is appreciative of the National Defense Education Act Fellowship.

Manuscript received Oct. 9, 1964. This paper was taken from the Ph.D. thesis of one of the authors (D.O.J.), University of Mississippi, 1963.

Any discussion of this paper will appear in a Discussion Section to be published in the December 1965 JOURNAL.

REFERENCES

1. D. O. Johnston and P. A. D. de Maine, *J. Chem. Eng. Data*, **8**, 586 (1963).
2. M. Golben, Thesis, University of Kentucky (1960).
3. M. Golben and L. R. Dawson, *J. Phys. Chem.*, **64**, 37 (1960).
4. S. I. Sklyarenko, I. V. Smirnov, and M. G. Zhukova, *Zhur. Fiz. Khim.*, **26**, 1125 (1952).
5. V. S. Galinker, *Ukrain. Khim. Zhur.*, **20**, 626 (1954).
6. H. Hartley and H. R. Raikes, *Trans. Faraday Soc.*, **23**, 393 (1927).
7. T. Erdey-Gruz, E. Kugler, and A. Reich, *Magyar Kem. Folyoirat*, **63**, 242 (1957).
8. S. Z. Mikhail and W. R. Kimel, *J. Chem. Eng. Data*, **6**, 533 (1961).
9. R. W. Gurney, "Ionic Processes in Solution," pp. 75-8, 224-6, McGraw-Hill Book Co., New York (1953).
10. D. O. Johnston and P. A. D. de Maine, To be published.

Observation of Active Areas in Thin Films of Palladium

Steve Eisner

Materials Research Section, The Martin Company, Denver, Colorado

Active centers in catalysts have been attributed by other investigators to emergent dislocations (1, 2), and point defects (2). Other kinds of crystal imperfections may also function as active centers, such as stacking faults, sessile dislocations, and impurity atoms.

The palladium-hydrogen system was chosen for the further study of active catalytic centers because of the large amount of hydrogen sorbed (from 1000 to 3000 times the metal volume) by palladium at room temperature. Exposure of palladium to hydrogen yields an expansion of the palladium lattice of 0.2Å, i.e., from 3.8Å to 4.0Å (3).

Experimental Methods

Films on thin transparent substrates.—Thin films were deposited in a vacuum chamber by vapor deposition of palladium on microscope cover glasses and on Mylar substrates. The glass substrate had previously been cleaned by glow discharge to provide adherent coatings.

The average thickness of the palladium deposit was measured by weight changes on known areas of substrate. Specimens having an average thickness of 570Å were chosen for the hydrogen experiments.

Before they were exposed to hydrogen, the coatings showed no palladium hydride lines in the x-ray diffraction pattern.

Films on iron crucibles.—Thin films were deposited on the outside of previously polished Arco iron analytical crucibles. The crucibles were then set up over a Unitron microscope so that changes in the surface films could be photographed as hydrogen diffused through the crucible and combined with the palladium.

The crucibles were filled with a 4% solution of H_2SO_4 containing As_2O_3 as a poisoning agent. A current of 1 amp/in.² was passed through the electrolyte, the crucible being cathodic. Diffusion of hydrogen through the crucible to the palladium film on the underside was clearly evident in 2 hr by the formation of the rosettes on the film.

The relative rate of hydrogen sorption and desorption in both types of experiments was recorded by two methods: (a) by measuring the change in intensity of the palladium hydride x-ray diffraction lines during and after exposure to hydrogen; (b) by measuring the change in light transmitted through the glass substrate specimens during and after exposure to hydrogen.

Discussion

Changes in thin films on glass and Mylar substrates.—Hydrogen was passed over thin palladium films on Mylar and on glass. The formation of a palladium hydride was indicated by the curling of the palladium-coated Mylar, showing expansion of the films. Glass-based films crinkled as the film expanded with the formation of palladium hydride (Fig. 1).

Crinkling started from microscopically observable points or lines on the surface. With only 300X magnification, defect areas rather than individual defects were seen. Circular crinkle patterns developed around point areas and elliptical crinkle patterns around active line areas. Increase in the diameters of the circles or ellipses means that the hydrogen gas entered through the hydride phase or through the palladium at a highly stressed edge of the crinkled area.

When the hydrogen was shut off, visible uncrinkling began after a few minutes (Fig. 2). This continued until all crinkling disappeared.

More photographs (Fig. 3) were taken when the palladium film was exposed to hydrogen again, after

the cycle of crinkling and uncrinkling shown in Fig. 1 and 2. Comparison of Fig. 1g and 3e shows that new active centers have been formed. Since no impurities have been added to the film, it is assumed that the new active areas are due to the cold work created by the crinkling process. [Recent work (2) has shown the relationship of cold work to catalysis in the case of ortho-para hydrogen conversion by nickel catalysts.]

After several cycles of crinkling and uncrinkling, the crinkling film changed its appearance from sharp-ridge crinkles to deformed or splayed-out crinkles, and occasional cracks also developed. This cracking, after frequent mechanical cycling, is reminiscent of fatigue cracking phenomena in metals.

Changes in films on iron substrates.—The effect of diffusing hydrogen by electrolysis for 2 hr through

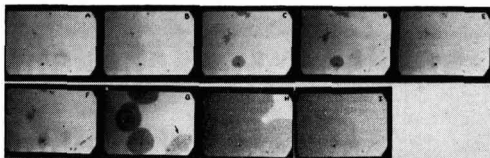


Fig. 1. (a through i). Approximately 160X micrographs taken 3 sec apart. Hydrogen gas was flowed over a palladium film evaporated on glass. Rosettes of crinkled area formed. When the flow was stopped (Fig. 1c) the rosettes disappeared. The flow was restarted again (Fig. 1e), and the rosettes grew until the entire surface was covered. It is interesting to note that active centers may be both in the form of points and lines (arrow).

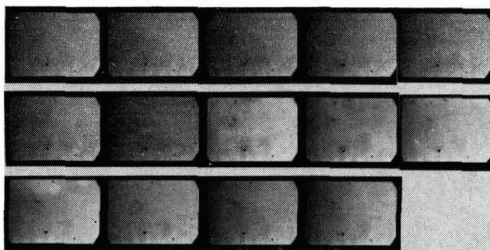


Fig. 2. Stream of hydrogen was stopped, and the crinkled surface was photographed every 3 sec. Uncrinkling was much slower than crinkling.

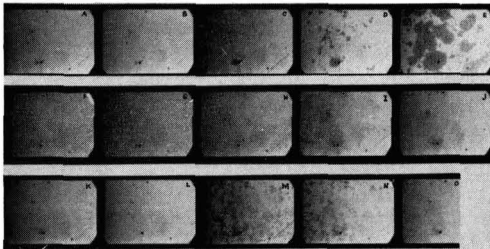


Fig. 3. (a through i). The flow of hydrogen was restarted. Figures 3c, 3d, and 3e show that new active centers are in evidence. These were generated by the cold work of the previous crinkling process. These centers are assumed to be crystal imperfections such as emergent dislocations or stacking faults. After several cycles of hydrogen pickup and release, the crinkles seem to lose their sharpness.



Fig. 4. Rosettes were formed on 500Å-thick palladium evaporated on an iron crucible which was hydrogen charged from the inside. Magnification 700X.



Fig. 5. Rosette shown in Fig. 4 deformed after a few hours. Magnification 700X.

polished Armco iron crucibles was the creation of individual rosettes on the palladium film deposited on the outside of the crucibles (Fig. 4). The rosettes did not disappear with time as did the crinkles in palladium films on glass. Instead, the rosettes deformed (Fig. 5) and cracked (Fig. 6) within 24 hr.

Changes in x-ray diffraction line intensity.—The rapid increase and slow decay of x-ray diffraction line intensity (Fig. 7) for the palladium hydride lines can be related to the rapid crinkling and slow uncrinkling of the palladium film shown in Fig. 1 and 2. The rate of change in diffraction line intensity can also be related to the microcinematographs taken of the crinkling and uncrinkling phenomena. Saturation of the palladium film with hydrogen is indicated by the constant intensity level of the palladium hydride line (Fig. 7).

Densitometer readings.—Similar evidence was given by densitometer readings as light was transmitted

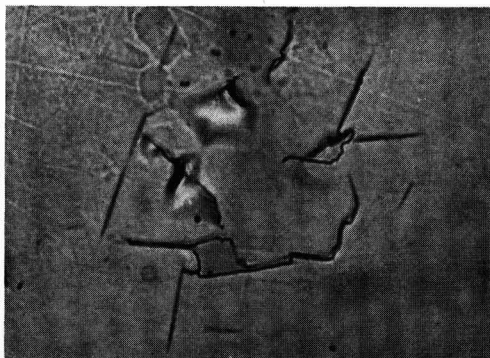


Fig. 6. Rosette shown in Fig. 5 and Fig. 6 cracked within 24 hr. Magnification approximately 800X.

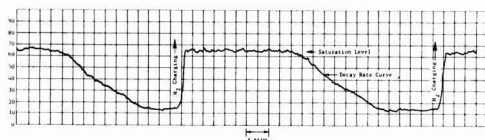


Fig. 7. Intensity of a single palladium hydride line changes with sorption and desorption of hydrogen. The sorption is quite rapid; the desorption is slow.

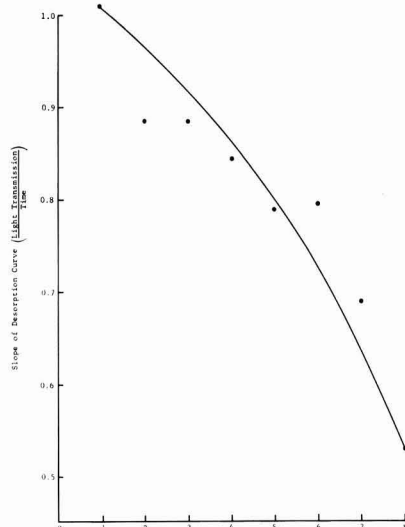


Fig. 8. Slope of the hydrogen desorption curve as measured by densitometry tends to decay with the number of charging cycles.

through the thin palladium film during hydrogen sorption crinkling and desorption uncrinkling. The desorption curves have a smaller slope with each succeeding cycle of hydrogenation. The slopes of the desorption curves were obtained from the densitometer recordings.

The slopes of the desorption curves were measured from 0.1 to 1.0 min after hydrogen saturation of the palladium film, the curve being relatively straight during this time.

These slopes, when plotted against the number of hydrogenation cycles (Fig. 8), show a gradual decrease. This decrease in hydrogen escape from a thin palladium film with an increasing degree of cold work due to crinkling indicates that hydrogen traps are

formed by cold work. Such an assumption is not out of line with metallurgical investigations that show it is more difficult for hydrogen to diffuse through hard steels than through soft steels (4).

X-ray diffraction studies showed the rapid increase of palladium hydride line intensity under hydrogen exposure, but the slow decrease in this intensity after exposure. Visual confirmation was provided also in the rapid crinkling and slow uncrinkling of the palladium film by means of microcinematographs. Eventual saturation of the palladium film with hydrogen is indicated by the constant-intensity level of the palladium hydride line. The decrease of hydrogen escape shows that hydrogen traps are formed by cold work.

Conclusions

The following conclusions apply:

1. The active areas of the hydrogen-palladium thin film systems (as evidenced by mechanical crinkling) are due to impurities and/or crystal imperfections.
2. New active areas are created by cold working (due to crinkling) of thin palladium films. This indicates that the creation or interaction of dislocations is important in forming active areas.

3. Hydrogen traps are created by cold work in palladium thin films as shown by decay curves of palladium hydride lines in the x-ray diffraction pattern after repeated hydrogen exposure. Densitometer readings through the palladium film also support this conclusion.

Acknowledgment

This work was initiated at the Boeing Company.

Manuscript received Dec. 18, 1964. This paper was prepared for delivery before the San Francisco Meeting, May 9-14, 1965.

Any discussion of this paper will appear in a Discussion Section to be published in the December 1965 JOURNAL.

REFERENCES

1. I. Uhara, S. Yanagimoto, K. Tani, and G. Adachi, *Nature*, **192**, 867 (1961).
2. I. Uhara, S. Kishimoto, T. Hikino, Y. Kageyama, H. Hamada, and Y. Numoto, *J. Phys. Chem.*, **67**, 996 (1963).
3. J. N. Andrews and A. R. Ubbelohde, *Proc. Roy. Soc.*, **A253**, 6 (1959).
4. U. V. Bhat and H. K. Lloyd, *Iron and Steel*, p. 451 (November, 1950).

Brief Communications



Recrystallization of Thin Films of Germanium and Silicon

S. Nielsen

Ministry of Aviation, Royal Radar Establishment, Great Malvern, Worcestershire, England

Recent work on thin alloy zone crystallization processes (1) has suggested the possibility of recrystallizing thin films of semiconductors. We report here some progress in recrystallizing films of silicon and germanium deposited on insulating substrates and comment on some of the difficulties experienced with these processes.

Recrystallization has been attempted by forming a thin liquid alloy zone in the film and driving this zone across the film using a temperature gradient. For example a layer of germanium 1μ thick was evaporated onto a sapphire substrate at room temperature and a stripe of aluminum, 100μ wide, evaporated on top of the germanium layer. The layer was then subjected to a temperature gradient for 8 hr by placing the sapphire on a molybdenum strip heater in a vacuum system at 10^{-5} Torr. Thermocouples on the heater in-

dicated a gradient of $150^\circ\text{C}/\text{cm}$ across the 100μ wide aluminum-germanium alloy zone and a zone temperature of $650^\circ\text{C} \pm 10\%$. Under these conditions the zone did not move (Fig. 1), but certain regions of the film adjacent to the zone (appearing white in Fig. 1) had recrystallized. The crystallite size in these regions is $\sim 0.05\mu$ (Fig. 2) compared to $\sim 100\text{A}$ before recrystallization. The crystallites showed no preferred orientation with respect to the substrate or zone and were confirmed as silicon by x-ray microprobe analysis. Larger gradients and longer times did not significantly increase the area recrystallized.

Silicon films, 1μ thick, deposited on sapphire by reduction of trichlorosilane also showed recrystallized regions (Fig. 3) when treated in the same way. Figure 3 shows a region near an aluminum zone, which had



Fig. 1. Polycrystalline germanium film and aluminum alloy zone on sapphire substrate after heating for 8 hr in a temperature gradient of $150^\circ\text{C}/\text{cm}$.

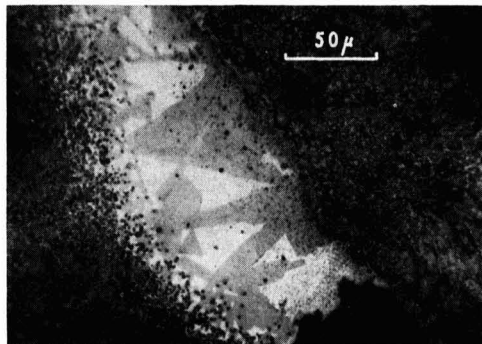


Fig. 2. Recrystallized region near aluminum alloy zone shown in Fig. 1.



Fig. 3. Recrystallized region of a polycrystalline silicon film on sapphire.

been subjected to a temperature gradient of $100^{\circ}\text{C}/\text{cm}$ at a zone temperature of 1000°C .

Zones of gold or tin alloys were used with germanium and silicon layers with various temperature gradients, but no zone movement was observed. In all cases the gold or tin diffused rapidly away from the zone, but produced no recrystallization. Attempts were also made to drive the gold or tin zones using an electric current (2); this produced very irregular movement of alloy, but again gave no recrystallization.

Experiments on the epitaxial deposition through thin liquid alloy layers (3) showed that epitaxy is possible through gold or tin alloy layers but not

through aluminum layers. We attributed this to a coherent oxide skin over the surface of the aluminum alloy, the alloy then not being able to accept silicon from the vapor. We think that the recrystallization observed with aluminum zones in the above experiments is due to the removal of oxide from grain boundaries enabling the alloy to interact with the silicon crystallites. The gold or tin alloys do not remove this oxide and hence diffuse along grain boundaries without affecting the crystallites.

We conclude therefore that considerable recrystallization of silicon or germanium films by thin alloy zone crystallization processes is possible, but that difficulties are to be expected over the zone movement. These difficulties are probably enhanced by oxide contamination and must be overcome either by use of an oxide getter or perhaps by use of very steep temperature gradients such as is possible with electron beam processes.

Acknowledgment

This paper is published by permission of the Controller H. M. Stationery Office.

Manuscript received Jan. 22, 1965.

Any discussion of this paper will appear in a Discussion Section to be published in the December 1965 JOURNAL.

REFERENCES

1. D. T. J. Hurle, J. B. Mullin, and E. R. Pike, *Solid State Communications*, **2**, 201 (1964).
2. D. T. J. Hurle, J. B. Mullin, and E. R. Pike, *Phil. Mag.*, **9**, 473 (1964).
3. J. D. Filby and S. Nielsen, *This Journal*, **112**, 535 (1965).

Low-Temperature Epitaxy of Silicon by Sublimation onto Thin Alloy Layers

J. D. Filby and S. Nielsen

Ministry of Aviation, Royal Radar Establishment, Great Malvern, Worcestershire, England

The work of, for example, Carman *et al.* (1) on the regrowth of silicon from a silicon-gold eutectic, of Wagner and Ellis (2) on their V.L.S. process, and of Hurle *et al.* (3) on thin alloy zone crystallization processes, suggested that it would be possible to epitax silicon at low temperatures by evaporation onto a thin alloy layer. Results from recent experiments indicate that this is true, epitaxy of silicon having been obtained as low as 300°C .

The apparatus used is illustrated in Fig. 1. Silicon was sublimed from the source by heating it to 1300°C using induction heating. The substrate was heated by

radiation from the source. The substrate temperature and the deposition rate were determined by the source-to-substrate distance and varied from 1100°C and $5 \mu/\text{hr}$ to 500°C and $\frac{1}{2} \mu/\text{hr}$. The substrate temperature was calibrated against the source temperature and source-substrate distance by using thermocouples in a blank run. At the start of each run the source temperature was determined with an optical pyrometer and the substrate temperature derived from it. This substrate temperature may be in error by $\pm 50^{\circ}\text{C}$. The apparatus was pumped by a 10 l/sec ion pump which maintained a pressure of 5×10^{-8} Torr during the sublimation.

The substrate used in these experiments was a (111) silicon wafer which had been mechanically polished, degreased, and freed from oxide in HF. Before putting the substrate in the apparatus, a layer of metal 1-10 μ thick was evaporated over part of the surface, the surface being near room temperature during the evaporation. The metal then alloyed with the silicon substrate to form a thin liquid layer at the deposition temperatures. Layers of gold, silver, copper, indium, and tin were alloyed in this way. After deposition, the layers were examined before and after removal of the alloy layer, and after bevel and vertical sectioning and etching, using optical microscopy and electron diffraction techniques.

The results from these experiments indicated that epitaxial silicon could be prepared by deposition through the liquid alloy layer. However, certain difficulties were experienced. First, the alloy layer showed a tendency to break up, the area covered by it

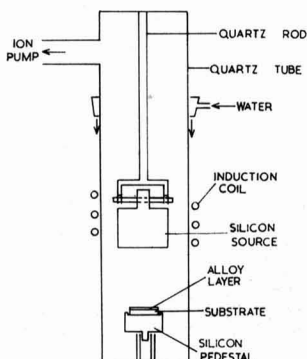


Fig. 1. Schematic diagram of sublimation apparatus

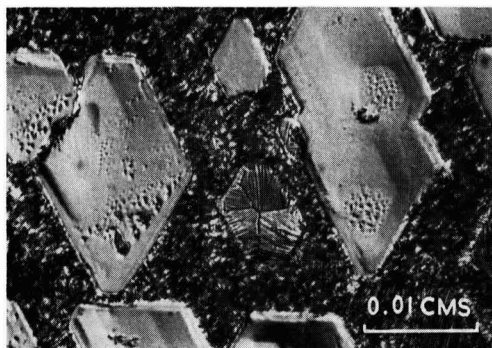


Fig. 2. Cellular silicon growth obtained under a gold alloy layer

depending on the constituents used and on the temperature. With gold alloy layers, for example, the layer broke up into droplets of 10-100 μ diameter at temperatures above 1000°C. If radial temperature gradients were present, these droplets moved across the surface. At lower temperatures the droplet size increased, and at 700°C or lower the layer was substantially stable. Second, the silicon deposit underneath the alloy layers was often irregular. Figure 2 shows an example of this; a gold alloy layer has been removed and an irregular cellular type of growth revealed. This type of growth was observed under gold, silver, indium, and tin, but not copper alloys. The surface area of cells varied with the alloy and with the deposition temperature from 100 μ^2 to 0.5 mm 2 . Sections through layers showing cellular growth also often revealed droplets of alloy trapped at the interface. We attribute this cellular growth to an irregular alloying caused by impurity on the substrate surface.

A polycrystalline deposit was observed on the surface of aluminum alloy layers; this we attribute to

silicon depositing onto a coherent skin of oxide on the surface of the alloy.

Etching studies showed that the silicon deposited in the cells was usually more perfect than that deposited between them. A stacking fault density of 10 6 /cm 2 within the cells was typical. An exception was the case of gold where no stacking faults were observed in the grown material unless a substrate with a heavily oxidized surface was used. For copper, where cellular growth was not observed, stacking fault densities of 10 3 /cm 2 were obtained underneath alloy globules and in their immediate surroundings. We think that the stacking fault density is related to the oxygen concentration in the alloy.

One advantage of the sublimation process is that the temperature gradient through the alloy layer is such that the temperature of the alloy vapor interface is higher than that of the alloy substrate interface, the significance of this having been stressed recently by the authors (4).

So far our work has shown that epitaxial growth of silicon on silicon can be obtained at 850°, 800°, 500°, 400°, and 300°C using silver, copper, tin, gold, and indium alloys, respectively.

Acknowledgment

This paper is published by permission of the Controller, H. M. Stationery Office.

Manuscript received Jan. 22, 1965.

Any discussion of this paper will appear in a Discussion Section to be published in the December 1965 JOURNAL.

REFERENCES

1. J. N. Carman, P. E. Stello, and C. A. Bittman, *J. Appl. Phys.*, **25**, 543 (1954).
2. R. S. Wagner and W. C. Ellis, *Appl. Phys. Letters*, **4**, 89 (1964).
3. D. T. J. Hurlle, J. B. Mullin, and E. R. Pike, *Solid State Communic.*, **2**, 201 (1964).
4. J. D. Filby, S. Nielsen, and G. J. Rich, C.V.D. Conference on Electronic Materials, Birmingham, England, 1964.

Microampere Multiple Constant Current Power Supply

Joseph B. Story¹ and Robert D. Wales

Materials Sciences Laboratory, Lockheed Missiles and Space Company, Palo Alto, California

A number of the more interesting anodic oxide thin films can be grown to potentials exceeding 100v. If it is desired to carry out this growth at a constant cur-

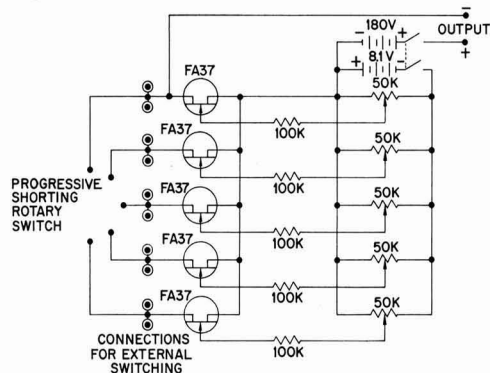


Fig. 1. Field effect transistor constant current power supply

rent, there is a problem in obtaining a suitable constant current source. The simple unit that is used for many purposes involves the use of a very large resistance in series with the cell, and a correspondingly high voltage across the combination. This makes the change in voltage across the cell small compared with the total and results in a correspondingly small change in the current. The voltage required for this apparatus is inconveniently large for use in thin film studies.

One solution to this problem has been presented by one of the authors (1), who utilized the properties of a photomultiplier tube. It has now been found that a supply with smaller drift can be constructed using one or more field effect transistors in parallel (each individually adjustable). In addition, this arrangement offers the possibility of switching rapidly through a series of constant currents by using the transistors in various combinations. This rapid switching has been used by one of the authors (2) in investigating the mechanism of anodic germanium oxide film formation.

A circuit diagram of the power supply is shown in Fig. 1. The most critical factor involved is the stability of the biasing potential. For this purpose, six Mallory RM-42R mercury batteries (1.35v each) were used in series. It appears that a partial discharge of the batteries increases the stability. The FA 37 field effect transistors were of Amelco manufacture. Beckman

¹ Present address: University of Arkansas, Graduate Institute of Technology, Fayetteville, Arkansas.

precision potentiometers (50K) were used for adjusting the biasing potential.

Each of the FA 37 transistors is useful for currents up to 75 μa . The paralleling of transistors permits proportionately higher currents. It should also be possible to increase the current range by the selection of a different field effect transistor.

After a warm-up of 1½ hr, the drift over a period of 6 hr was 0.6% for currents up to 75 μa for one transistor. During this time there was usually a period of several hours during which the drift was about 0.01%. When

the load is varied such that the voltage across it varies from zero to 100v, the current drops by 3.6%, 2.3%, and 1.8% for initial currents of 25 μa , 50 μa , and 75 μa , respectively.

Manuscript received Jan. 7, 1965.

Any discussion of this paper will appear in a Discussion Section to be published in the December 1965 JOURNAL.

REFERENCES

1. R. D. Wales, *This Journal*, **110**, 946 (1963).
2. J. B. Story, To be published.

Errata

On page 417 of the April 1965 issue of the Journal in the paper by Joseph B. Kushner "Relationship between Deposit Thickness and Current Density during the Early Stages of Electrodeposition," Eq. [8a], [9a], and [10a] should read

$$T_1 (I_1)^{3p/2} = T_2 (I_2)^{3p/2} = \text{constant} \quad [8a]$$

$$t_1 (I_1)^{(3p+2)/2} = a \text{ constant} \quad [9a]$$

$$T_1/T_2 = t_1/t_2^{3p/(3p+2)} \quad [10a]$$

Manuscripts and Abstracts for Fall 1965 Meeting

Papers are being solicited for the Fall Meeting of the Society, to be held at the Statler-Hilton Hotel in Buffalo, N. Y., October 10, 11, 12, 13, and 14, 1965. Technical sessions probably will be scheduled on: Batteries (including Symposia on Charging Characteristics of Batteries and Characteristics of Electrodes during Charging), Corrosion, Electrodeposition (including Symposium on Thin Film Technology), Electronics-Semiconductors, Electrothermics and Metallurgy (including a Symposium on Zirconium and Its Alloys).

To be considered for this meeting, **triplicate copies of the usual 75-word abstract, as well as of an extended abstract of 500-1000 words** (see notice on page 121C of this issue), must be received at The Electrochemical Society, 30 East 42 St., New York, N. Y., 10017, *not later than May 17, 1965*. (Papers solely sponsored by the Corrosion Division **do not** require an extended abstract.) *Please indicate on 75-word abstract for which Division's symposium the paper is to be scheduled, and underline the name of the author who will present the paper.* No paper will be placed on the program unless one of the authors, or a qualified person designated by the authors, has agreed to present it in person. Clearance for presentation of a paper at the meeting should be obtained before the abstract is submitted. An author who wishes his paper considered for publication in the JOURNAL or ELECTROCHEMICAL TECHNOLOGY should send triplicate copies of the manuscript to the Managing Editor of the appropriate publication 30 East 42 St., New York, N. Y., 10017. Concerning papers to be published in the JOURNAL, see notice on per page charge on page 122C of this issue.

Presentation of a paper at a technical meeting of the Society does not guarantee publication in the JOURNAL or ELECTROCHEMICAL TECHNOLOGY. However, all papers so presented become the property of The Electrochemical Society, and may not be published elsewhere, either in whole or in part, unless permission for release is requested of and granted by the Editor. Papers already published elsewhere, or submitted for publication elsewhere, are not acceptable for oral presentation except on invitation by a Divisional program Chairman.

FUTURE MEETINGS OF The Electrochemical Society



★ ★ ★

San Francisco, Calif., May 9, 10, 11, 12, and 13, 1965

Headquarters at the Sheraton Palace

Sessions will be scheduled on Electric Insulation, Electronics (including Luminescence and Semiconductors and a Symposium on Optical Masers), Electro-Organic (including a Symposium on Industrial Organic Chemistry and a Symposium on Elucidation of Electro-Organic Electrode Processes jointly with the Theoretical Electrochemistry Division), Electrothermics and Metallurgy (including joint Symposium on Molten Salts jointly with the Theoretical Electrochemistry Division and, also, a Symposium on Strengthening Mechanisms in Nonmetallics), Industrial Electrolytic (including a Symposium on Electrolytic Diaphragms and Battery Separators jointly with the Battery Division and, also, a Symposium on the Production of Chlorine without Caustics)

★ ★ ★

Buffalo, N. Y., October 10, 11, 12, 13, and 14, 1965

Headquarters at the Statler-Hilton Hotel

Sessions probably will be scheduled on Batteries (including symposia on Charging Characteristics of Batteries and Characteristics of Electrodes during Charging), Corrosion, Electrodeposition (including Symposium on Thin Film Technology), Electronics—Semiconductors, Electrothermics & Metallurgy (including a Symposium on Zirconium and its Alloys)

★ ★ ★

Cleveland, Ohio, May 1, 2, 3, 4, and 5, 1966

Headquarters at the Sheraton-Cleveland Hotel

★ ★ ★

Philadelphia, Pa., October 9, 10, 11, 12, and 13, 1966

Headquarters at the Sheraton Hotel

★ ★ ★

Dallas, Texas, May 7, 8, 9, 10, and 11, 1967

Headquarters at the Hilton Hotel

★ ★ ★

Papers are now being solicited for the meeting to be held in Buffalo, N. Y., October 10, 11, 12, 13, and 14, 1965. Triplicate copies of the usual 75-word abstract, as well as of an extended abstract of 500-1000 words (see notice on following page), are due at The Electrochemical Society, 30 East 42 St., New York, N. Y. 10017, *not later than May 17, 1965 in order to be included in the program.* (Papers sponsored solely by the Corrosion Division do not require an extended abstract.) *Please indicate on 75-word abstract for which Division's symposium the paper is to be scheduled, and underline the name of the author who will present the paper.* No paper will be placed on the program unless one of the authors, or a qualified person designated by the authors, has agreed to present it in person. Clearance for presentation of a paper at the meeting should be obtained before the abstract is submitted. An author who wishes his paper considered for publication in the JOURNAL OF ELECTROCHEMICAL TECHNOLOGY should send triplicate copies of the manuscript to the Managing Editor of the appropriate publication, 30 East 42 St., New York, N. Y., 10017. Concerning papers to be published in the JOURNAL, see notice on per page charge on page 122C of the issue.

Presentation of a paper at a technical meeting of the Society does not guarantee publication in the JOURNAL or in ELECTROCHEMICAL TECHNOLOGY. However, all papers so presented become the property of The Electrochemical Society, and may not be published elsewhere, either in whole or in part, unless permission for release is requested of and granted by the Editor. Papers already published elsewhere, or submitted for publication elsewhere, are not acceptable for oral presentation except on invitation by a Divisional program Chairman.

Extended Abstract Book Publication Program for the Society's 1965 Fall Meeting in Buffalo, N. Y.

The Board of Directors has provided that the National Office shall assist Divisions with the mechanics of publishing Extended Abstracts for sessions involving 15 or more papers at our National Meetings.

The Divisions will handle the technical editing of the abstracts following which the Society Office will arrange for the printing and distribution of the books, thus relieving Division representatives of this responsibility. Each Division program will be the subject of a separate Extended Abstract Book. Papers sponsored solely by the Corrosion Division do not require an extended abstract.

This means that each author who submits a paper for presentation at our meeting should do three things:

- 1—Submit *three* copies of the usual 75-word abstract of the paper for publication in the printed program of the meeting;
- 2—Simultaneously submit *three* copies of an extended abstract of the paper of 500-1000 words; and
- 3—Send the 75-word abstract and the 500-1000-word extended abstract to Society Headquarters, 30 East 42 St., New York, N. Y., 10017, not later than May 17, 1965.

The Extended Abstract Books will be published by photo-offset reproduction from *typewritten copy submitted by the author*. Special care should therefore be given to the following typing instructions so as to establish uniformity in printing:

- 1—Abstracts are to be 500-1000 words in length.
- 2—Use white bond paper, size 8½ x 11 inches.
- 3—Abstracts should be typed SINGLE space.
- 4—Use 1¼ inch margins at the top and bottom and at the sides of each page.
- 5—All copy, including figures, symbols, and corrections, should be in black ink.
- 6—Figures should be pasted in within the typing dimensions indicated. Captions should be typed not wider than figure dimensions and pasted in proper place in the abstract. Figure captions should appear at bottom of figure. Table titles should appear at top of tables.
- 7—Wherever possible, avoid use of halftones.
- 8—Title of paper should be in capital letters. Author(s) name and affiliation should be typed immediately below. It is not necessary in the heading or body to designate paper as "Extended Abstract," or quote the Divisional Symposium involved.
- 9—Mail to Society Headquarters *unfolded*.

Members and JOURNAL subscribers will receive notice of Extended Abstracts Books to be scheduled for publication. The notices will be accompanied by order blanks for the copies desired. Orders should be submitted with remittance. The advance orders will be necessary for estimating numbers of books to be printed and will be mailed to purchasers prior to the Buffalo meeting. Some extra copies will be available at the meeting but the advance-paid order is the only way to be assured of getting copies.



1965 Gordon Research Conferences

The Gordon Research Conferences in New Hampshire for 1965 will be held from June 14 to September 3 at Colby Junior College, New London; New Hampton School, New Hampton; Kimball Union Academy, Meriden; Tilton School, Tilton, and Proctor Academy, Andover.

Meetings are held in the morning and in the evening, Monday through Friday, with the exception of Friday evening.

Requests for attendance at the conferences, or for additional information, should be addressed to W. George Parks, Director, Gordon Research Conferences, University of Rhode Island, Kingston, R. I. From June 14 to September 3, 1965 mail for the office of the Director should be addressed to Colby College, New London, N. H.

The following portions of the program are of interest to ECS members.

Hydrocarbon Chemistry

June 14-18, 1965
Colby Junior College
New London, N. H.

T. J. Hardwick, Chairman
L. Friedman, Vice-Chairman

June 14

- P. Gardner—Thermochemical and Base Catalyzed Isomerization
R. Srinivasan—Photochemical Isomerization

June 15

- J. Grosmanin—Radiation-Induced Oxidation of Hydrocarbons
K. Gollnick—Photosensitized Oxidation of Hydrocarbons
R. Cvetanovic—Reaction of Oxygen Atoms with Hydrocarbons

June 16

- J. Calvert—Stability of Free Radicals in the Gas Phase

- P. Skell—Stereochemistry of Free Radicals
L. Friedman—Chairman, Invited Papers

June 17

- H. M. Frey—Reactions of Methylene
I. Dvoretzky—Reactivity of Methylene Towards Hydrocarbon Substrates
G. B. Kistiakowsky—Shock Tube Experiments on Hydrocarbon Oxidation

June 18

- R. A. Benkesser—Metallation of Organic Compounds

Physical Metallurgy

July 19-23, 1965

Kimball Union Academy
Meriden, N. H.
D. N. Beshers, Chairman
W. W. Mullins, Vice-Chairman

Interaction of Imperfections

July 19-23

- L. A. Girifalco—The Theory of Point Defects in Stress Fields
A. Sosin—The Interaction of Dislocations with Point Defects Introduced by Radiation Damage
H. A. Wriedt—Effect of Lattice Defects on the Solution of N in α -Fe
C. L. Bauer—Stress-Induced Pipe Diffusion of Substitutional Impurities
R. W. Balluffi—Dislocation Sources and Sinks for Vacancies
R. H. Chambers—Suppression of Dislocation Relaxations by Point-Defect-Dislocation Interactions
R. Bullough—Theory of Strain Aging
C. S. Hartley—Strain Aging in Ta
G. S. Baker—Interaction of Interstitial Impurities with Dislocations in Ta and W

- G. Alefeld—Thermal Activation of Dislocations with Emphasis on Materials with High Peierls Stresses
T. Jossang—Energies of Dislocation Configurations
I. L. Dillamore—Stacking Fault Energy in Aluminum

Corrosion

August 9-13, 1965
Colby Junior College
New London, N. H.

W. W. Smeltzer, Chairman
M. J. Pryor, Vice-Chairman

Correlations of Reactant Transport With Properties of the Corrosion Product and Metal Substrate

August 9

J. Wagner, Jr., Discussion Leader

- K. L. Moazed—Oxide Nucleation Studies with Field Electron Emission Microscope
K. R. Lawless—Recent Studies on the Early Stages of the Low Pressure Oxidation of Copper and Nickel
E. A. Gulbransen, Discussion Leader
J. V. Cathcart—Influence of Paths of Easy Diffusion in Oxide Films on Oxidation Kinetics
M. A. Heine, P. R. Sperry, and M. J. Pryor—Dielectric Properties of Thermal Oxide Films on Aluminum and Its Alloys

August 10

H. H. Uhlig, Discussion Leader

- A. T. Fromhold, Jr.—Redistribution of Electric Charge in the Metal-Oxide System during Growth for Several Emission and Transport Mechanisms
M. J. Dignam—The Growth of Oxide Films under the Influence of High Electrostatic Fields

Page Charge Adopted for the JOURNAL

Increased costs of publication have made it necessary for The Electrochemical Society to institute a per page charge for publication in the JOURNAL.

At the Meeting of the Board of Directors held in New York on September 29, 1963 a charge of \$35.00 per printed page was established by the Board of Directors, on recom-

mendation of the Publication and Finance Committees, for papers published in the JOURNAL. This action becomes effective for papers received after February 1, 1964.

A 10% reduction in the page charge will apply to papers authored by one or more members of The Electrochemical Society and/or by one or more employees of Patron or

Sustaining Members of the Society.

Papers are accepted for publication on the basis of merit by established practices of review. Acceptance of future papers for publication will not be dependent on payment of this invoice. Where funds are not available for payment of this charge it will be waived by The Electrochemical Society.

- E. L. Koehler, Discussion Leader
 V. Nivoko and H. H. Uhlig—Logarithmic Oxidation Kinetics of Zinc
 D. P. Seraphim—Electron and Ion Transport through Silicon Dioxide Films on Silicon

August 11

- B. Cox, Discussion Leader
 R. E. Pawel—Oxygen Solution in Tantalum and Niobium during Oxidation at Low Temperatures
 D. L. Douglass and J. Van Landuyt—The Oxidation of Titanium and Zirconium: An Electron Microscopy Study of Oxides Formed in the Thin Film Range
 M. J. Pryor, Discussion Leader
 P. Kofstad—Low-Pressure High-Temperature of Niobium and Tantalum
 J. P. Pemsler—High Temperature Oxidation Kinetics of Zirconium and Hafnium

August 12

- J. V. Laukonis, Discussion Leader
 W. E. Boggs and A. J. Pignocco—Oxidation of High Purity Iron: Kinetics and Structures
 E. A. Gulbransen—Structural Aspects of Localized Corrosion Processes on Iron in Oxygen and Water Vapor

J. B. Berkowitz-Mattuck,
 Discussion Leader

- M. Kahlweit—Internal Oxidation of Alloys
 D. Caplan—Effect of Cold Work on the Oxidation of Iron and Iron-Chromium Alloys

August 13

- W. W. Smeltzer, Discussion Leader
 C. T. Fujii—The Reaction of Iron-Chromium Alloys with Carbon Dioxide at High Temperatures
 A. U. Seybolt—Oxidation-Nitridation of Chromium Base Alloys

Chemistry and Physics of Solids

August 16-20

Kimball Union Academy
 Meriden, N. H.

M. Lax, Chairman
 B. Mozer, Vice-Chairman

Physical Properties of Disordered Systems

August 16

- N. F. Mott—Behavior of a Fermi Electron Gas in a Disordered Lattice
 H. Fritsche—Impurity Interaction Effects in Semiconductors
 B. Halperin—Impurity Band Tails in the High Density Limit

August 17

- V. Jaccarino—Magnetic Localized States: Experimental Aspects

- H. Suhl—Magnetic Localized States: Theory
 M. Klein—Statistical Properties of Dilute Magnetic Alloys in Noble Metals

August 18

- H. Cusack—Present Status of Liquid Metals: Experiment
 A. D. Pearson—Transport and Fluorescence Anomalies in the Glassy State
 T. J. Rowland—Magnetic Resonance in Metallic Solid Solutions

August 19

- J. Rayne—Experimental Evidence Concerning the Band Structure of Disordered Alloys
 J. Friedel—Electronic Properties of Alloys
 J. Langer—Vibrational Properties of Disordered Lattices

August 20

- I. M. Lifshitz—On the Structure of the Energy Spectrum of Disordered Systems
 Speaker and Subjects to be announced.

Section News

Boston Section

The forty-seventh meeting of the Boston Section was held on Tuesday, February 23, 1965 at the M.I.T. Faculty Club in Cambridge, Mass. After dinner, Prof. Ali Javan, Dept. of Physics, M.I.T., Cambridge, Mass., presented an excellent lecture on "Spectroscopic Applications of Gas Lasers to Some Problems in Physical Chemistry." He first discussed some of the experimental difficulties in using gas lasers, such as parallelism of mirrors and resonance characteristics of atomic and cell systems. The frequency stability of current gas lasers is of the order of $1:10^{13}$ for short times and $1:10^{10}$ for long times. This stability permits observation of the beat frequency from two lasers containing different isotopes of neon.

High resolution I.R. spectroscopy is possible with many different types of gas lasers as sources. The limitations of wavelength control is partially overcome by use of the Zeeman effect. In addition, the absorption peak of the sample can be changed by use of the Stark effect, so that in practice nearly any band can be studied with a 10^3 improvement in resolution over conventional I.R. methods.

M. D. Banus
 Secretary

South Texas Section

The South Texas Section of the Society met in Houston on February 23, 1965. The meeting was held at

the Houston Engineering and Scientific Society Building.

The speaker was Mr. Donald M. Taylor, Public Information Officer for Project Mohole. Mr. Taylor pointed out how little is known about the earth's geologic history and that the purpose of Project Mohole is to obtain fundamental data for the earth sciences. Six holes are going to be drilled. The deepest of these will be located near Hawaii. The total cost of this project will be about 40 cents per taxpayer. This is about the same as the cost of launching one satellite.

Mr. Taylor's talk was preceded by a social hour and dinner. Ten members and one guest attended the meeting.

R. C. Ayers, Jr.,
 Secretary-Treasurer

News Item

Rare Volumes of the ECS Available

Mr. A. Kenneth Graham has informed the National Office of the availability for sale of a set of bound volumes of the TRANSACTIONS of the AMERICAN ELECTROCHEMICAL SOCIETY covering the period 1902-1930, and the TRANSACTIONS and the JOURNAL OF THE ELECTROCHEMICAL SOCIETY, 1931-1949. There are also four bound copies of the 10-year indexes for 1902-1941.

These volumes are in excellent condition. Anyone interested may contact Mr. Graham at, Graham, Savage & Associates, Inc., 475 York Road, Jenkintown, Pa., 19046.

Personals

D. Thomas Ferrell, Jr., has been appointed to the newly created post of technical coordinator of The Electric Storage Battery Co., Philadelphia, Pa., it was announced.

Dr. Ferrell, who has been assistant director of engineering for ESB's Industrial Division, will have his office in the company's headquarters at 2 Penn Center Plaza, Philadelphia. Dr. Ferrell will assist in the continuing improvement and advancement of the company's research, development, and engineering efforts involving products, processes, and raw materials.

Walter J. Hamer, Chief, Electrochemistry Section, Electricity Division, National Bureau of Standards, recently was awarded a Gold Medal by the Bureau. The medal was awarded to Dr. Hamer for "continued distinguished service to gov-

ernment and industry, exemplified by authorship and leadership in the field of electrochemistry."

Dr. Hamer joined the Bureau staff in 1935 and became Chief of the Electrochemistry Section in 1950. He is the author of NBS Monograph "Standard Cells-Their Construction, Maintenance, and Characteristics."

Edwin C. Rinker has been elected to the board of directors of Sel-Rex Corp., Nutley, N. J., it has been announced recently. The new director, who is also vice-president and technical director of Sel-Rex, has been associated with the company for the past 18 years. Mr. Rinker has been active in the field of precious metal electroplating for 36 years.

Sprague Electric Co. as a research chemist in the research and engi-



Stanley F. Bubriski

Calendar of Events

Other Organizations

The 7th International Congress on Glass, sponsored by the International Commission on Glass, Bruxelles, Belgique, will be held during June 28 to July 3, 1965.

The 10th Annual Session of the Appalachian Underground Corrosion Short Course, sponsored by the West Virginia University, will be held on the University campus, Morgantown, W. Va., June 8-10, 1965.

Obituary

Stanley W. Bubriski

Among the victims of the February 8, 1965 airline tragedy over New York City was Stanley W. Bubriski an executive in the Sprague Electric Co., North Adams, Mass.

Mr. Bubriski was a native of Massachusetts and received his bachelor of science degree in chemistry in 1943 from the University of Massachusetts. Following distinguished service in the U.S. Army, he began his career in the employ of the Nickel Cadmium Battery Corp. as a research chemist. He held this position from 1948 to 1950. At that time he joined the International Nickel Co. and was employed there in a similar capacity until 1952. In February of that year he joined the

neering department. In 1955 he was made a senior engineer in the research and engineering department where he worked predominantly on the electrochemical processes associated with tantalum foil electrolytic capacitors. In 1957 he was appointed section head in charge of the electrolytic capacitor evaluation and performance laboratory. During this period he was author of several basic papers on tantalum electrolytic and in 1958 he was awarded a U.S. Patent for his development of a new type of electrolytic capacitor designed to circumvent many of the basic problems associated with electrolyte losses. In 1963 he became a senior product specialist for electrolytic capacitors in the field engineering department. He served on several EIA engineering committees and most recently was chairman of the P 2.4 committee for electrolytic capacitors.

Mr. Bubriski was a member of the American Association for the Advancement of Science, the American Chemical Society, Sigma Xi and Adelpia, honorary scientific research fraternities, and Alpha Phi Fraternity. He was an active member of The Electrochemical Society.

Mr. Bubriski was equally active in community affairs being chairman of the board of trustees of the First Congregational Church of Williamstown and a former trustee of the University of Massachusetts Alumni Association. He was a former President of the Williamstown Boys'

Chemical or Electrical Engineer

Experienced in storage battery manufacturing Southwest U. S. area. Mail details of education, experience, and personal background to Box A 304, c/o The Electrochemical Society, Inc., 30 East 42 St., New York, N. Y., 10017.

Club, a former member of the Williamstown Rotary Club, and a former member of the Williams Faculty Club.

He is survived by his wife, Mrs. Dagmar E. Bubriski, and four children.

Announcements from Publishers

"Failure Mechanisms in Ferroelectric and Nonlinear Dielectrics," Report AD 605 795N, * \$3.00.

"Study of Comprehensive Failure Theory," Report AD 608 365N, * \$6.00.

"Failure Mechanisms in Silicon Semiconductors," Report AD 608 456N, * \$3.00.

"Corrosion of Metals in Tropical Environments, Part 6—Aluminum and Magnesium," Report AD 609 618N, * 50 cents.

"The Diffusion of Nonvolatile Metallic Elements in Graphite," Report UCRL-7324N, * \$1.50.

"Electropolishing the Rare Earth Metals," Report IS-1036N, * \$1.00.

"Thermoelectric Power Modules," Report AD 600 365N, * \$2.75.

"High-Temperature Thermoelectric Research," Report AD 609 051N, * \$7.00.

"Rotary, Deployable Space Solar Power Supply," Report N64-32821N, * \$2.25.

(Continued on page 126C)

December 1965 Discussion Section

A Discussion Section, covering papers published in the January-June 1965 JOURNALS, is scheduled for publication in the December 1965 issue. Any discussion which did not reach the Editor in time for the June 1965 Discussion Section will be included in the December 1965 issue.

Those who plan to contribute remarks for this Discussion Section should submit their comments or questions in triplicate to the Managing Editor of the JOURNAL, 30 East 42 St., New York, N. Y., 10017, not later than September 1, 1965. All discussion will be forwarded to the author(s) for reply before being printed in the JOURNAL.

Buffalo, N. Y. Meeting Symposia

Battery Symposium Plans

The Battery Division of the Society is planning symposia on "Charging Characteristics of Batteries" and on "Characteristics of Electrodes During Charging" for the 1965 Fall Meeting in Buffalo, N. Y., October 10-14, 1965. General sessions are also planned.

Triplicate copies of the usual 75-word abstract, as well as of an extended abstract of 500-1000 words (see notice p. 121C of this issue) should be sent to The Electrochemical Society, 30 East 42 St., New York, N. Y., 10017, or to Mr. T. J. Hennigan, Goddard Space Flight Center, Code 636-2, Greenbelt, Md., 20771, *not later than May 17, 1965.*

Corrosion Symposia Plans

General Sessions

Inasmuch as the symposia this year are rather specific in nature it is both anticipated and hoped that more papers than usual will be submitted for the general sessions. Authors who have material for a paper which does not fit in with one of the symposia are urged to submit it for the general session.

Any inquiries or suggestions regarding these sessions should be addressed to the Divisional Chairman, Ernest L. Koehler, Continental Can Co., 7622 S. Racine Ave., Chicago, Ill., 60620.

For all papers at any of the Division's sessions, three copies of an abstract of 75-words or less must be received at The Electrochemical Society, 30 East 42 St., New York, N. Y., 10017, by May 17, 1965.

The Corrosion Division does not require extended abstracts.

Symposium on Corrosion Inhibition of Organic Compounds

Announcement is made by Chairman Ernest L. Koehler of the Corrosion Division that symposia plans for the 1965 Fall Meeting of the Society include "Corrosion Inhibition of Organic Compounds." Symposium Chairman is Dr. Z. A. Foroulis, Esso Research & Engineering Co., P.O. Box 101, Florham Park, N.J.

Papers are now solicited for presentation at this symposium. Contributions concerning the mechanism of corrosion inhibition by organic compounds and, in particular, the effects of their chemical and structural characteristics on adsorption and the kinetics of corrosion reactions are particularly suitable. Papers concerning both mercury and solid metals are invited.

To be considered for this meeting, triplicate copies of the usual 75-word abstract should be sent to The Electrochemical Society, 30 East 42 St., New York, N. Y., 10017, *not later than May 17, 1965.*

Inquiries and suggestions should be sent to the Symposium Chairman. Anyone considering submitting a paper for this symposium, should notify him as soon as possible.

Symposium on Microbiological Corrosion

The Corrosion Division is planning a symposium on "Microbiological Corrosion" for the 1965 Fall Meeting of the Society. There has been a considerable amount of effort in this field during the last few years in a number of laboratories. It is hoped that, with the work accomplished, it will be possible to appraise some of the theories and propositions that have been advanced to explain the relationship between microbial growth and corrosion. Papers reporting advances in the field are now being solicited.

To be considered for this meeting, triplicate copies of the usual 75-word abstract should be sent to The Electrochemical Society, 30 East 42 St., New York, N. Y., 10017, *not later than May 17, 1965.*

Inquiries on the technical content of the symposium or expressions of willingness to participate should be directed to Dr. R. T. Foley, Chemistry Dept., The American University, Washington, D.C., 20016.

Symposium on Corrosion in Nonaqueous Media

The Corrosion Division is planning a Symposium on "Corrosion in Nonaqueous Media" for the 1965 Fall Meeting of The Society.

"Corrosion in Nonaqueous Media" is to be considered as inclusive of research in organic and inorganic solvents, molten salts, and gas systems. Papers which may relate properties of the corrosion products to corrosion performance or to the corrosion mechanism are especially, but not exclusively, desired.

Suitable papers are solicited for the Symposium. Three copies of the usual 75-word abstract must be received at The Electrochemical Society, 30 East 42 St., New York, N. Y., 10017, *not later than May 17, 1965.*

Inquiries and suggestions should be sent to the Symposium Chairman, Sheldon Evans, Rocketdyne D/991-356, 6633 Canoga Ave., Canoga Park, Calif., 91304. Anyone considering submitting a paper for the symposium should so notify the Chairman.

Electrodeposition Symposium Plans

The Electrodeposition Division of the Society is planning a symposium on "Thin Film Technology" for the 1965 Fall Meeting to be held in Buffalo, N. Y., October 10-14, 1965. Papers are solicited in both basic and applied areas. Communications and inquiries should be addressed to Dr.

I. W. Wolf, Ampex Corp., 401 Broadway-Ms 3-21, Redwood City, Calif.

Triplicate copies of the usual 75-word abstract as well as of an extended abstract of 500-1000 words (see notice p. 121C of this issue) should be sent to The Electrochemical Society, 30 East 42 St., New York, N. Y., 10017, *not later than May 17, 1965.*

Electrothermics and Metallurgy Symposium Plans

General Session

A general symposium on subjects that come within the scope of activity of the Electrothermics and Metallurgy Division is being organized by the Division as part of its 1965 Fall Meeting of the Society to be held in Buffalo, N. Y., October 10-14, 1965

To assist potential contributions to decide whether their papers fall within the field of interest of the Division, the following paragraph from the Division's tentative statement of scope has been reproduced as follows:

In general, the purpose of the Division is to aid and encourage the advancement of electrochemical science and industry concerned with specialty materials and processes.

As specific examples of fields in which the Division has maintained interest and activity, there may be cited: Materials such as refractory metals and compounds, intermetallics, graphite, fused salts, and rare earths metals; Equipment for the utilization of electrical energy and materials synthesis; Processes using arcs, vacua, plasma, and electron and ion beams; and Phenomena such as melting, vaporization, reaction, sintering, diffusion or oxidation occurring at high-temperatures, high pressures or involving high temperature materials.

Papers of both the fundamental and applied nature are welcomed.

Triplicate copies of the usual 75-word abstract as well as an extended abstract of 500-1000 words must be received at The Electrochemical Society, 30 East 42 St., New York, N. Y., 10017, *not later than May 17, 1965.* Inquiries may be sent to W. E. Kuhn, Chairman, Electrothermics and Metallurgy Division, c/o Spindletop Research, Iron Works Pike, Lexington, Ky.

Symposium on Zirconium and Its Alloys

A Symposium on Zirconium and Its Alloys is being organized by the Electrothermics and Metallurgy Division as part of the 1965 Fall Meeting of The Electrochemical Society to be held in Buffalo, N. Y., October 10-14, 1965.

Sessions will be held on: Mechanisms of Corrosion and Oxidation Processes; Mechanisms of Hydrogen Pickup; Deformation and Fracture; Transformation and Diffusion; and Irradiation Effects.

Papers should consider the fundamental nature of the processes involved.

Symposium Co-Chairmen are: E. C. W. Perryman, Chemistry and Metallurgy Div., Atomic Energy of Canada Ltd., Chalk River, Ont., Canada and J. P. Pemsler, Ledgemont Lab., Kennecott Copper Corp., 128 Spring St., Lexington, Mass., 02173.

Triplicate copies of the usual 75-word abstract, as well as an extended abstract of 500-1000 words must be received at Society Headquarters, 30 East 42 St., New York, N. Y., 10017, not later than May 17, 1965.

Publication of papers from this Symposium is planned.

Authors are therefore requested to submit three copies of each manuscript to Dr. W. W. Smeltzer, Dept. of Metallurgical Engineering,

McMaster University, Hamilton, Ont., Canada, as soon as is possible, prior to presentation of the paper at the National Meeting of the Society.

Panel Discussion on Zirconium

For the Symposium, "Zirconium and Its Alloys" being organized by the Electrothermics and Metallurgy Division as part of the 1965 Fall Meeting in Buffalo, a Panel Discussion will be held on "Factors Affecting the Lifetime of Zirconium Components in Nuclear Reactors."

This panel discussion is being led by international experts in the field. The panel will consist of the following participants: H. Mogard, Aktieolaget; R. W. Nichols, Culcheth Labs., United Kingdom Atomic Energy Authority; H. H. Klepfer, Vallecitos Atomic Lab., General Electric Co.; and U. Rosler, Reactor Development Div., Siemens-Schuckertwerks, AG.

The presiding Chairman for the panel discussion is W. B. Lewis, Atomic Energy of Canada Ltd., Chalk River, Ont., Canada.

"Progress in Superalloys," Report N64-31001N,* 50 cents.

"Cellular Aluminum," Report N64-28313N,* \$1.00.

"Solidification Behavior of Aluminum Alloys," Report AD 607 916N,* \$4.00.

"Refractory Metal Sheet Alloys," Report AD 608 164N,* 50 cents.

"Nickel-Titanium Alloys," Report OTR-102N.* 50 cents.

"Processing Refractory Metal Foil," Report AD 607 683N,* \$6.00.

"Extrusion of TZM Alloys," Report AD 607 682N,* \$4.00.

"Stamping Sintered Aluminum Sheet," Report TT-64-51260N,* \$1.00.

* Order from Office of Technical Services, U. S. Department of Commerce, Springfield, Va., 22151.

(Continued from page 124C)

"Research and Development Program of Thermionic Conversion of Heat to Electricity, Vol. I," Report AD 605 389N,* \$5.00.

"Characteristics of Separators for Alkaline Silver Oxide Zinc Secondary Batteries," Report AD 447 301N,* \$4.00.

"Energy Storage for Automotive Use," Report BNL-7447N,* \$1.00.

"Thermoelectric Materials and Fabrication," Report OTR-110N,* 50 cents.

"Effect of Hydrogen Content on the Mechanical Properties of Ti6Al-4V Bar at -423°F," Report AD 604 054N,* \$1.00.

"Irradiation Effects on Structural Materials," Report HW-81334N Part 2,* \$4.00.

"Bibliography on the Measurement of Bulk Resistivity of Semiconductor Materials for Electron Devices," Technical Note 232, 60 cents. (Order from the Superintendent of Documents, U.S. Government Printing Office, Washington, D.C. 20402)

"Evaluation of Several Oxidation-Resistant Coatings," Report N64-28332N,* \$2.00.

"Reactivity of Titanium with Oxygen," Report N64-27509N,* \$2.75.

"Electrolytic Removal of Oxygen from Sodium," Report AD 608 042N,* \$3.00.

"Electronic Properties of Aromatic Compounds," Report AD 607 660N,* \$2.00.

"Physics of Semiconductors and Metals," Report TT-64-51031N,* \$3.00.

Position Available

Chemist or engineer experienced in solid electrolytic capacitors to collaborate in translation and adaption of articles and books. Indicate conditions and background to: *Box A 306, c/o The Electrochemical Society, Inc., 30 East 42 St., New York, N.Y. 10017.*

Buffalo Program Issue

The complete program of the Buffalo, N. Y., Meeting of the Society will appear in the August 1965, Vol. 112, No. 8 issue of the JOURNAL.

Advertiser's Index

Bell Telephone Laboratories, Inc. 116C

Great Lakes Carbon Corp., Graphite Products Div. ... Cover 2

The Kendall Co. 113C

E. H. Sargent & Co. 119C

Stackpole Carbon Co. 120C

John Wiley & Sons, Inc. 118C

ATTENTION, MEMBERS AND SUBSCRIBERS

Whenever you write to The Electrochemical Society about your membership or subscription, please include your Magazine address label to ensure prompt service.

ATTACH Change of Address LABEL

HERE

To change your address, please give us five weeks' advance notice. Place magazine address label here. Print your NEW address below. If you have any question about your subscription or membership, place your magazine label here and clip this form to your letter.

Mail to the Circulation Department, The Electrochemical Society, Inc., 30 East 42 St., New York, N. Y., 10017.

name _____

address _____

city _____ state _____ zip code _____

The Electrochemical Society

Patron Members

- Aluminum Co. of Canada, Ltd.,
Montreal, Que., Canada
- The Dow Chemical Co.,
Chemical Dept., Midland, Mich.
Metals Dept., Midland, Mich.
- International Nickel Co., Inc.,
New York, N. Y.
- General Electric Co.
Capacitor Dept., Hudson Falls, N. Y.
Chemical Laboratory, Knolls Atomic
Power Laboratory, Schenectady, N. Y.
Chemical and Materials Engineering Lab-
oratory, Advanced Technology Labora-
tories, Schenectady, N. Y.
- Chemistry Research Dept., Schenectady,
N. Y.
- Direct Energy Conversion Operation, West
Lynn, Mass.
- Lamp Division, Cleveland, Ohio
- Materials & Processes Laboratory, Large
Steam Turbine-Generator Dept., Sche-
nectady, N. Y.
- Metallurgy and Ceramics Research Dept.,
Schenectady, N. Y.
- Olin Mathieson Chemical Corp.,
Chemicals Div., Research Dept., New
Haven, Conn.
- Union Carbide Corp.
Divisions:
Carbon Products Div., New York, N. Y.
Consumer Products Div., New York, N. Y.
- Westinghouse Electric Corp.
Electronic Tube Div., Elmira, N. Y.
Lamp Div., Bloomfield, N. J.
Molecular Electronics Div., Elkridge, Md.
Research Laboratories, Pittsburgh, Pa.
Semiconductor Div., Youngwood, Pa.

Sustaining Members

- Air Reduction Co., Inc., New York, N. Y.
- Allen-Bradley Co., Milwaukee, Wis.
- Allied Chemical Corp.
General Chemicals Div., Morristown, N. J.
- Alloy Steel Products Co., Inc., Linden, N. J.
- Aluminum Co. of America,
New Kensington, Pa.
- American Metal Climax, Inc.,
New York, N. Y.
- American Potash & Chemical Corp.,
Los Angeles, Calif.
- American Smelting and Refining Co.,
South Plainfield, N. J.
- American Zinc Co. of Illinois,
East St. Louis, Ill.
- American Zinc, Lead & Smelting Co.,
St. Louis, Mo.
- M. Ames Chemical Works, Inc.,
Glen Falls, N. Y.
- Ampex Corp., Redwood City, Calif.
- Armco Steel Corp., Middletown, Ohio
- Basic Inc., Bettsville, Ohio
- Bell Telephone Laboratories, Inc.,
New York, N. Y. (2 memberships)
- Bethlehem Steel Co., Bethlehem, Pa.
(2 memberships)
- Boeing Co., Seattle, Wash.
- Burgess Battery Co., Freeport, Ill.
(2 memberships)
- Burndy Corp., Norwalk, Conn.
- Canadian Industries Ltd., Montreal,
Que., Canada
- Carborundum Co., Niagara Falls, N. Y.
- Chrysler Corp., Detroit, Mich.
- Consolidated Mining & Smelting Co. of
Canada, Ltd., Trail, B. C., Canada
(2 memberships)
- Continental Can Co., Inc., Chicago, Ill.
- Corning Glass Works, Corning, N. Y.
- Diamond Alkali Co., Painesville, Ohio
- Wilbur B. Driver Co., Newark, N. J.
(2 memberships)
- E. I. du Pont de Nemours & Co., Inc.,
Wilmington, Del.
- Eagle-Pitcher Co., Chemical and Metals Div.,
Joplin, Mo.
- Eastman Kodak Co., Rochester, N. Y.
- Eltra Corp.,
Prestolite Div., Toledo, Ohio
- C&D Batteries, Conshohocken, Pa.
- Electric Storage Battery Co.,
Philadelphia, Pa. (2 memberships)
- Engelhard Industries, Inc., Newark, N. J.
(2 memberships)
- The Eppley Laboratory, Inc., Newport, R. I.
- Exmet Corp., Bridgeport, Conn.
- Fairchild Semiconductor Corp., Palo Alto,
Calif.
- FMC Corp.
Inorganic Chemical Div., Buffalo, N. Y.
Chlor-Alkali Div., South Charleston, W. Va.
- Foote Mineral Co., Exton, Pa.
- Ford Motor Co., Dearborn, Mich.
- General Motors Corp.
Allison Div., Indianapolis, Ind.
Delco-Remy Div., Anderson, Ind.
Research Laboratories, Warren, Mich.
- General Telephone & Electronics
Laboratories Inc., Bayside, N. Y.
(2 memberships)
- Globe-Union, Inc., Milwaukee, Wis.
- B. F. Goodrich Chemical Co.,
Cleveland, Ohio
- Gould-National Batteries, Inc.,
Minneapolis, Minn.
- Great Lakes Carbon Corp., New York, N. Y.
- Hanson-Van Winkle-Munning Co.
Matawan, N. J. (2 memberships)

(Sustaining Members con'd)

- Harshaw Chemical Co., Cleveland, Ohio
(2 memberships)
- Hercules Powder Co., Wilmington, Del.
- Hill Cross Co., Inc., West New York, N. J.
- Hoffman Electronics Corp., Semiconductor
Div., El Monte, Calif.
- Honeywell Inc., Minneapolis, Minn.
- Hooker Chemical Corp., Niagara
Falls, N. Y. (3 memberships)
- HP Associates, Palo Alto, Calif.
- Hughes Research Laboratories, Div. of
Hughes Aircraft Co., Malibu, Calif.
- International Business Machines Corp.,
New York, N. Y.
- International Minerals & Chemical
Corp., Skokie, Ill.
- International Resistance Co., Philadelphia,
Pa.
- ITT Federal Laboratories, Div. of
International Telephone & Telegraph
Corp., Nutley, N. J.
- Jones & Laughlin Steel Corp.,
Pittsburgh, Pa.
- K. W. Battery Co., Skokie, Ill.
- Kaiser Aluminum & Chemical Corp.
Div. of Chemical Research,
Permanente, Calif.
- Div. of Metallurgical Research,
Spokane, Wash.
- Kawecki Chemical Co., Boyertown, Pa.
- Kennecott Copper Corp., New York, N. Y.
- Leesona Moos Laboratories, Div. of Leesona
Corp., Jamaica, N. Y.
- Arthur D. Little, Inc.,
Cambridge, Mass.
- Lockheed Aircraft Corp.,
Missiles & Space Div., Sunnyvale, Calif.
- Mallinckrodt Chemical Works, St. Louis, Mo.
- P. R. Mallory & Co., Indianapolis, Ind.
- Melpar, Inc., Falls Church, Va.
- Metal Pumping Services
Cleveland, Ohio
- Miles Chemical Co., Div. of Miles
Laboratories, Inc., Elkhart, Ind.
- Monsanto Chemical Co., St. Louis, Mo.
- M&T Chemicals Inc., Detroit, Mich.
- National Cash Register Co., Dayton, Ohio
- National Lead Co., New York, N. Y.
- National Steel Corp., Weirton, W. Va.
- North American Aviation, Inc.,
El Segundo, Calif.
- Northern Electric Co., Montreal, Que.,
Canada
- Norton Co., Worcester, Mass
- Owens-Illinois Glass Co., Toledo, Ohio
- Pennsalt Chemicals Corp.,
Philadelphia, Pa.
- Phelps Dodge Refining Corp., Maspeth, N. Y.
- Philco Corp., Research Div., Blue Bell, Pa.
- Philips Laboratories, Inc.,
Briarcliff Manor, N. Y.
- Pittsburgh Plate Glass Co., Chemical Div.,
Pittsburgh, Pa.
- Potash Co. of America,
Carlsbad, N. Mex.
- Radio Corp. of America
Electronic Components and Devices,
Lancaster, Pa.
Tube Div., Harrison, N. J.
RCA Victor Record Div., Indianapolis,
Ind.
- Raytheon Co., Waltham, Mass.
- Republic Foil Inc., Danbury, Conn.
- Reynolds Metals Co., Richmond, Va.
- Shawinigan Chemicals Ltd., Montreal, Que.,
Canada
- Socony Mobil Oil Co., Inc.,
Dallas, Texas
- Speer Carbon Co.
International Graphite & Electrode
Div., St. Marys, Pa.
- Sprague Electric Co., North Adams, Mass.
- Stackpole Carbon Co., St. Marys, Pa.
- Stauffer Chemical Co., Dobbs Ferry, N. Y.
- Texas Instruments, Inc., Dallas, Texas
Metals and Controls Corp.,
Attleboro, Mass.
- 3M Company, St. Paul, Minn.
- Titanium Metals Corp. of America,
Henderson, Nev.
- Tyco Laboratories, Inc., Waltham, Mass.
- Udylite Corp., Detroit, Mich.
(4 memberships)
- United States Borax & Chemical Corp.,
Los Angeles, Calif.
- United States Steel Corp., Pittsburgh, Pa.
- Univac, Div. of Sperry Rand Corp.,
New York, N. Y.
- Universal-Cyclops Steel Corp.,
Bridgeville, Pa.
- Upjohn Co., Kalamazoo, Mich.
- Western Electric Co., Inc., Chicago, Ill.
- Wyandotte Chemicals Corp.,
Wyandotte, Mich.
- Yardney Electric Corp., New York, N. Y.